FINAL REPORT

Addressing the Impacts of Climate Change on U.S. Army Alaska with Decision Support Tools Developed Through Field Work and Modeling

SERDP Project RC-2110

FEBRUARY 2016

Dr. Thomas A. Douglas
U.S. Army Corps of Engineers Engineer Research and Development Center Cold Regions Research and Engineering Laboratory

SERDP
DOD ▪ EPA ▪ DOE

REPORT DOCUMENTATION PAGE

Form Approved
OMB No. 0704-0188

1. REPORT DATE *(DD-MM-YYYY)*	**2. REPORT TYPE**	**3. DATES COVERED** *(From - To)*
10-03-2015	Final Report	May 2011- March 2015

4. TITLE AND SUBTITLE
Addressing the impacts of climate change on U.S. Army Alaska [illegible] With decision support tools developed through field work and modeling

5a. CONTRACT NUMBER

5b. GRANT NUMBER
RC-2110

5c. PROGRAM ELEMENT NUMBER

6. AUTHOR(S)
Thomas A. Douglas, M. T. Jorgenson, D.N. Brown, C.A. Hiemstra, A.K. Liljedahl, C. Downer, N. Pradhan, S. Marchenko, S. Campbell, G. Senseman, K. Olson

5d. PROJECT NUMBER

5e. TASK NUMBER

5f. WORK UNIT NUMBER

7. PERFORMING ORGANIZATION NAME(S) AND ADDRESS(ES)
U.S. Army Cold Regions Research and Engineering Laboratory

8. PERFORMING ORGANIZATION REPORT NUMBER

9. SPONSORING / MONITORING AGENCY NAME(S) AND ADDRESS(ES)
Strategic Environmental Research and Development Program

10. SPONSOR/MONITOR'S ACRONYM(S)
SERDP

11. SPONSOR/MONITOR'S REPORT NUMBER(S)

12. DISTRIBUTION / AVAILABILITY STATEMENT
Approved for public release; distribution is unlimited

13. SUPPLEMENTARY NOTES

14. ABSTRACT
The U.S. Army is the largest DoD land user in Alaska overseeing 1.5 million acres of training range and cantonment lands. Some of the training ranges are inaccessible by road and planned infrastructure over the next 10 years will greatly expand the DoD's presence and capabilities in Alaska. The area is underlain by a complex mosaic of discontinuous permafrost and its presence (or absence) plays a major role in soil thermal, hydrologic, and vegetation regimes. A projected 1 to 3 ºC increase in mean annual air temperatures in the area between now and 2100 is expected to have major ramifications on ecosystem and hydrologic processes. To identify the potential impacts of climate warming on U.S. Army Alaska training lands and to provide land managers with scientifically based information to help them plan for a warmer future we conducted this four year study. We combined field measurements at a variety of spatial and temporal scales with thermal, hydrologic, and ecosystem transitions modeling efforts to be able to apply the point scale nature of our field measurements across a broader region. Our results were linked with a broad array of historical and projected meteorological and climatological information to develop a geospatial decision support system to help DoD manage their lands in a potentially warmer future.

15. SUBJECT TERMS
Permafrost; climate warming impacts on ecosystems; geospatial tools

16. SECURITY CLASSIFICATION OF:			**17. LIMITATION OF ABSTRACT**	**18. NUMBER OF PAGES**	**19a. NAME OF RESPONSIBLE PERSON**
a. REPORT Unclassified	**b. ABSTRACT** Unclassified	**c. THIS PAGE** Unclassified	None	182	Thomas A. Douglas
					19b. TELEPHONE NUMBER *(include area code)* 907-361-9555

Standard Form 298 (Rev. 8-98)
Prescribed by ANSI Std. Z39.18

TABLE OF CONTENTS

LIST OF TABLES

LIST OF FIGURES

LIST OF ACRONYMS

ACIA	Arctic Climate Impact Assessment
ADE	Alternating direction explicit
ADH	adaptive hydrology code
AHAP	Alaska High Altitude Photography
ANOVA	Analysis of variance
ARSC	Arctic Region Supercomputing Center
CHL	Coastal and Hydraulics Laboratory
CIR	Color InfraRed
CPCRW	Caribou-Poker creek Research Watersheds
CRREL	Cold Regions Research and Engineering Laboratory
CRU	Climate Research Unit
DEM	digital elevation model
dGPS	Digital Geographic Positioning system
DD	Degree days
DoD	Department of Defense
DTAW	Donnelly Training Area West
DTAE	Donnelly Training Area East
EL	Environmental Laboratory
ERDC	Engineer Research and Development Center
ERT	Electrical resistivity tomography
ET	Evapotranspiration
FDD	freezing degree-day
GCM	Global Circulation Models
GIPL	Geophysical Institute Permafrost Laboratory
GIS	Geographic information systems
GISMO	Geographic information supporting military operations
GSSHA	The Gridded Surface Subsurface Hydrologic Analysis
HMET	Hydrometeorological
IPCC	Intergovernmental Panel on Climate Change
JPARC	Joint Pacific Alaska Range Complex
LANDSAT	Land Remote Sensing Satellite
LCM	Land Change Modeler
LiDAR	Light Distance and Ranging
masl	meters above sea level
MAST	mean annual surface temperature
MADT	mean annual deep temperatures
MPI	Message Passing Interface
NASA	National Aeronautics and Space Administration
NCDC	National Climatic Data Center
NCSS	National Cooperative Soil Survey
NED	National Elevation Dataset
NIR	Near infrared
NOAA	National Oceanographic and Atmospheric Administration
NMDS	nonmetric multidimensional scaling
NRCS	Natural Resources Conservation Service

NWS	National Weather Service
OC	Organic carbon
OLT	Organic layer thickness
OpenMP	Open Multi-Processing
PRISM	Parameter-elevation Regressions on Independent Slopes Model
RCP	Representative Concentration Pathway
RES	Electrical Resistivity
RMS	Root Mean Squared (error)
SDSWCD	Salcha-Delta Soil and Water Conservation District
SIPRE	Snow, Ice, and Permafrost Research Establishment
SERDP	Strategic Environmental Research and Development Program
SNAP	Scenarios Network for Alaska Planning
SWE	Snow water equivalent
SWRI	Shortwave infrared
TDD	thawing degree-day
TFTA	Tanana Flats Training Area
TCN	Total Carbon-Nitrogen
TRADOC	U.S. Army Training and Doctrine Command
Tukey HSD	Tukey Honestly Significantly Different test
USACE	U.S. Army Corps of Engineers
USARAK	U.S. Army Alaska
USGS	United States Geological Survey
UTM	Universal Transverse Mercator (projection)
WMS	Web map service
YTA	Yukon Training Area
1-D	One Dimensional
2-D	Two Dimensional

KEYWORDS

Permafrost
Climate warming
Boreal biome ecology
Geophysics
Electrical Resistivity
Hydrologic modeling
Field measurements
Disturbance
Soil thermal regime
Climate warming
Ecosystem transitions
Decision support systems
Geographic Information Systems
Arctic and subarctic

ACKNOWLEDGEMENTS

This research project was large in scope and discipline and, from initiation to development of this Report it spanned five years. We wish to acknowledge the efforts of a group of Co-Investigators for this work: Dr. Chris Hiemstra, Dr. Seth Campbell, Marc Beede, Art Gelvin, and Stephanie Saari of the ERDC-Cold Regions Research and Engineering Laboratory; Dr. Anna Liljedahl and Dr. Sergei Marchenko of the University of Alaska Fairbanks; Torre Jorgenson of Alaska Ecoscience; Dr. Charles Downer, Nawa Pradhan, and Mark Wahl of the ERDC-Coastal and Hydraulics Laboratory; Cal Bagley, Gary Senseman, Keith Olson, Dan Rees, and Dejuan Tanner of Colorado State University; Dana Nossov of the University of Alaska Fairbanks; and Kelly Burks-Copes of the ERDC-Environmental Laboratory. Hiemstra, Campbell, Beede, Gelvin, Saari, Liljedahl, Jorgenson, and Nossov participated in the field measurements. The modeling was undertaken by Liljedahl and Marchenko (GIPL) and Downer, Pradhan, and Wahl (GSSHA). GIS mapping and development of the decision support tool (GISMO) was led by Bagley, Senseman, and Olson with help from Tanner. Rees oversaw helicopter logistics for access to the Tanana Flats field sites. The aforementioned constituted the main participants who were funded by SERDP to do the work.

Numerous scientific collaborators participated in field measurements, helped edit text, or provided related data or techniques. Stephen Newman of ERDC-CRREL oversaw the airborne LiDAR data acquisition which was funded by a companion project. We thank Amanda Barker, Maria Berkeland, Kevin Bjella, Helene Genet, Tiffany Gatesman, Art Gelvin, Sarah Hayes, Miriam Jones, Karen Jorgenson, Mark Lara, Heikki Lotvonen, Katie Nicolato, and Anna Wagner for their help with field measurements. We also acknowledge field assistance and writing/editing from Dr. Miriam Jones of the U.S. Geological Survey, Dr. Teresa Hollingsworth of the U.S. Department of Agriculture Forest Service and the University of Alaska Fairbanks, and Dr. Jon O'Donnell of the National Park Service. We also want to thank numerous additional people that worked with us in the field, in the lab, and by sharing content and ideas at various project and scientific meetings. These included undergraduate and graduate students, visiting CRREL personnel, and a variety of collaborators with similar scientific goals and interests.

We would like to acknowledge the following institutions and people for monetary, in kind, and collaborative support. The SERDP Resource Conservation and Climate Change Program Area: Program Manager Dr. John Hall and support staff. Gary Larsen and John Haddix of the U.S. Army Alaska Directorate of Public Works provided access to U.S. Army Alaska lands and guided us toward useful information that DoD could use in land management activities. Jeff Durham and Colin Barnard of the Salcha-Delta Soil and Water Conservation District in Delta Junction, Alaska provided field support and access to their myriad maps, surveys, and field measurements. The glaciology research group at the University of Alaska Fairbanks' Geophysical Institute provided a willing group of collaborators for the work in the Jarvis Glacier watershed. Drs.Ted Schuur (now at Northern Arizona University) and April Melvin of the University of Florida shared field measurements and site information. Drs. Michelle Walvoord and Fred Day-Lewis of the U.S. Geological Survey helped identify topical areas where their research and ours is complementary. Beth Astley of the U.S. Army Corps of Engineers Alaska District, a former CRREL Research Scientist, shared her field measurements and knowledge. Drs. Jeff Arnold and Kathleen White of the U.S. Army Corps of Engineers Institute of Water Resources supported us for a related project focused on carbon itemization on U.S. Army Alaska lands.

The project benefitted from measurements, data, and research time leveraged from companion projects funded by the U.S. Army Corps of Engineers Engineer Research and Development Center's Center Directed Research Program, the Changing Arctic Ecosystems Initiative of the U.S. Geological Survey's Ecosystem Mission Area through the Alaska Cooperative Fish and Wildlife Research Unit and the Institute of Arctic Biology at the University of Alaska Fairbanks, U.S. Army Alaska, and the U.S. National Science Foundation.

1. ABSTRACT

Objectives

The U.S. Army is the largest Department of Defense (DoD) land user in Alaska, overseeing 1.5 million acres of training range and cantonment lands. Some of the training ranges are inaccessible by road. Infrastructure planned over the next 10 years to address access issues will greatly expand the DoD's presence and capabilities in Alaska. The training ranges and cantonments are underlain by a complex mosaic of discontinuous permafrost and its presence (or absence) plays a major role in soil thermal, hydrologic, and vegetation regimes.

A projected 1 to 3 ºC increase in mean annual air temperatures in the area between now and 2100 is expected to have major ramifications on ecosystem and hydrologic processes and their potential feedbacks to climate-permafrost-ecologic interactions. Elucidating or predicting the response of permafrost or ecosystems to climate warming is complicated by many factors including variations in soil type, precipitation, surface and ground water hydrology, vegetation, slope, aspect, fire prevalence, and the thermal state of the permafrost. This project was conducted to identify the potential impacts of climate warming on U.S. Army Alaska training lands and to provide land managers with scientifically based information to help them plan for a warmer future. It combined field measurements at a variety of spatial and temporal scales with thermal, hydrologic, and ecosystem transitions modeling to translate/scale-up? the point-scale nature of our field measurements across a broader region. Results were linked with a broad array of historical and projected meteorological and climatological information to develop a geospatial decision support system to help DoD manage its lands in a potentially warmer future.

Technical Approach

This project included a variety of field measurements and the application of multiple modeling platforms to identify how, where, and at what rate climate warming could impact vegetation, soils, hydrology, and permafrost on interior Alaska DoD lands. Repeat imagery was synthesized with field measurements of vegetation, soil, geomorphic, geophysical, and hydrologic information. Wells and thermistors were installed to measure hydrologic and soil thermal parameters. Detailed ground surface survey, geophysical, and biophysical measurements were made across a variety of terrain types.

The University of Alaska Fairbanks Geophysical Institute Permafrost Laboratory (GIPL) soil and vegetation thermal model also was coupled to the U.S. Army Corps of Engineers Gridded Surface Subsurface Hydrologic Analysis (GSSHA) hydrogeologic model. The resulting software package was tested with measurements from a research watershed near Fairbanks to validate the ability to simulate streamflow in watersheds with a variety of permafrost coverage. This product will allow for the projection of how and where stream flows may change when permarost extent is modified by press climate change processes or by pulse disturbances.

The project results were synthesized with the most up to date climate projections for Alaska and ecosystem information on soils, hydrology, permafrost extent, fire history, and vegetation to develop a queriable geographic information systems decision support tool that has been delivered to U.S. Army Alaska training range managers. This support tool is called the Geographic Information Supporting Military Operations (GISMO).

Results

The project addressed five thematic areas. First, research focused on permafrost-hydrogeology relationships on the Tanana Flats lowlands. To support this, an array of wells were installed across a lake-fen system to understand the seasonality of surface and shallow subsurface hydrologic flow. Regionally, surface water and groundwater move northward from the Alaska Range across the training ranges to feed an extensive (i.e., hundreds of square kilometers) wetland system. Permafrost plays a major role in channeling flow across this landscape. Hydrologic connectivity occurred through surface and shallow subsurface flow paths across a lake and fen system on Tanana Flats. Some fen regions responded more dramatically to the same summer precipitation events and the difference in the response to precipitation is ascribed to varied amounts of seasonal thaw. Where subsurface channels and flow paths were increased by seasonal thaw the fen had more storage at that location and water levels were less responsive to precipitation. With a projected warmer climate and degradation of near surface permafrost it is likely that the lateral connectivity of flowpaths will increase ane flows across these fen systems will be reduced. Enhanced downward movement of flowpaths will lead to an overall drying of the landscape. This will alter ecosystem processes and feed back to hydrogeology and water use. The downward movement of surface waters and their warm thermal mass will also promote permafrost thaw.

Second, research assessed the vulnerability of permafrost to fire-initiated thaw on training ranges. Fire can rapidly change the soil and vegetation thermal regime that protects permafrost. Five fire scars were identified across a chronosequence from 1930 to 2010 that were investigated for the rate and patterns of permafrost and vegetation response to fire. Substantial permafrost thaw, ground surface collapse, and water impoundment followed burns in ice rich silty soils within a year. This led to thermokarst (ground surface subsidence) and changes in the ground thermal regime. These processes, in turn, fee back to additional warming of permafrost soils. Thermal modeling was used to better evaluate the relative effects of burn severity on the soil thermal regime. We also attempted to identify when vegetation succession and redevelopment of the ecosystem protection of permafrost would return to these terrains.

Third, research quantified how and where biophysical, geophysical, and airborne measurements could be used to map subsurface permafrost geomorphology. Due to the remote nature of many of the landscapes in transition in this region there is a need for capabilities to identify and track locations where permafrost degradation could be at risk of causing ecologic or hydrologic change. Electrical resistivity tomography (ERT) was determined to be a robust tool in mapping three dimensional permafrost features to depths of tens of meters. Strong relationships were detected between vegetation type, topography measured with differential global positioning system (dGPS) and light detection and ranging (LiDAR) measurements, and permafrost extent. These relationships indicate that remote sensing of vegetation characteristics and LiDAR could be useful for monitoring the surficial and seasonal thaw depth response of permafrost to fire, human disturbance, or climate warming. This is a potentially valuable tool because of the remote nature of many of the landscapes in the area and the overall lack of long term measurements.

The fourth subtask of this project was a modeling effort focused on combining two established modeling capabilities- one that simulates the soil thermal regime and freeze-thaw processes and the other a surface shallow subsurface hydrologicl tool- into a coupled permafrost hydrology model. Two teams worked to synchronize the models and permafrost soil and hydrology measurements from a long term study site were used to tune and apply the model to real world measurements. The model adequately reproduced real work hydrologic information and was able to account for the varied flow responses to precipitation events in watersheds

underlain by different amounts of permafrost. Fifth, this project used repeat imagery analyses of landscape change to identify ecosystem transitions across the landscape. Fire history and biophysical factors affecting ecosystem change were measured through photo-interpretation of 2000 systematically distributed points on a time-series (1949–1952, 1978–1980, 2006–2011) of geo-rectified imagery across interior Alaska Army training lands. Overall, 56.8% of the region had changes in ecotypes over the 55–62 year period and most of the changes resulted from increases in upland and lowland forest types with an accompanying decrease in upland and lowland scrub types, as post-fire succession led to late-successional stages.

Benefits

Knowledge of patterns and processes affecting ecosystems and development of signals of landscape change aids in ecological management of DoD lands by identifying which changes can be affected by land management activities such as fire or infrastructure development. Taken in total, the results from this study will help to identify how, where, and hopefully when ecological changes will occur in interior Alaska ecosystems. Our study sites are on the front lines of projected climate wamring and impacts on ecosystems due to Arctic amplification.

The primary benefit of this study for the DoD is scientifically based strategic installation planning capabilities that account for potential climate change impacts on training ranges. U.S. Army Alaska received a queriable web based geospatial decision support tool that provides a soil thermal modeling capability, a module to project future permafrost extent, historical and projected meteorologic information for all seasons, and a fire history database. For the U.S. Army Corps of Engineers, the GSSHA hydrologic model can now account for seasonal freeze-thaw processes and can be applied to permafrost and seasonally frozen terrains. The thermal and hydrologic model results are transferable to other locations such as Afghanistan, Korea and the northern conterminous United States.

The scientific community will benefit through new and novel data presented in peer-reviewed publications and Technical Reports. These results include field measurements and modeling applications focused on mapping permafrost bodies, modeling hydrologic flow, predicting the soil thermal response to climate warming, understanding post fire disturbance effects on permafrost, and tracking ecosystem transitions over time.

2. OBJECTIVE

U.S. Army Alaska (USARAK) is the largest Department of Defense (DoD) land user in Alaska and conducts all season training activities throughout its 1.5 million acre training areas in the Alaskan interior (Figure 1). Most of the impact ranges used by the Air Force in Alaska are located on Army lands and the Army and Air Force stage joint training exercises on Army lands. This region includes the three largest training ranges utilized by DoD in Alaska, the largest Army Post in Alaska (Fort Wainwright), the U.S. Ground Based Missile Defense Agency infrastructure at U.S. Army Fort Greely, Eielson Air Force Base, and the U.S. Army Corps of Engineers Chena Project site. Landowners and users managing lands in interior Alaska (Figure 2) are aware that the projected future climate in interior Alaska will lead to fundamental changes in ecosystem dynamics. Of utmost concern is predicting the response of permafrost to anticipated climate warming and understanding how (and where) changes in permafrost stability will affect hydrology, soils, and vegetation.

USARAK faces numerous challenges in managing their lands within the uncertainties of a projected warming climate and across the broad variety of landscape and ecosystem types they manage (Figure 3). Landscape and ecosystem change, whether driven by climate warming, permafrost thaw, human disturbance, or the boreal forest fire cycle, can have major ramifications on USARAK's ability to manage their lands and support warfighter training needs. Some examples: estimated recovery times for disturbance (as required in Environmental Impact Statements) are likely to become less predictive in a warmer future state. Threatened or endangered species management activities, not currently a major concern, could grow in locations where habitats become suitable (or unsuitable) for species' survival or competition. Difficulties may emerge in managing habitat for large mammals, particularly moose, for which there is great public interest, largely focused on access and availability for hunting. A growing need exists for carbon source and sink inventories as the first step in identifying and implementing effective climate change mitigation strategies. For example, Executive Order 13514, "Federal Leadership in Environmental, Energy, and Economic Performance" requires U.S. Government agencies to account for greenhouse gas emissions with the long-term goal of establishing emission-reduction targets. If U.S. Government agencies need to more adequately account for greenhouse gas emissions the wetland, permafrost, and ecosystem status of interior Alaska DoD lands provides major challenges. Many of the interior Alaska training areas are remote and are only accessible by air or seasonal ice roads. This means there are little long term measurements across the broad geographic expanse and limited information supporting efforts to identify how and where landscape change will occur on USARAK lands.

Based on over a decade working with USARAK training range managers and soldiers we understand the most rapid, easily deployable, and broadly applicable tools that can help USARAK manage their lands now is provided as geospatial information, built on scientific measurements, that supports management decisions. The most useable tools integrate climate projection results with the most up to date terrain and ecosystem information to provide past, current, and future perspectives on landscape processes. If/where these tools can provide insight into how and where ecosystem change and trajectories of change are most likely to occur in the future, they will be the most robust training range management decision support tools available.

Within these aforementioned needs to support training range activities in an uncertain future climatic regime the overarching objective of this project was to develop a transparent, collaborative decision support system fed by spatially-explicit ecosystem response information

(permafrost, hydrology, vegetation, soils, and climate projection) to provide DoD land and facilities managers tangible information to help make decisions regarding where, when, and how to develop future training and installation management plans. Our geographic information systems (GIS)-based approach uses critical landscape-change analyses, field surveys, and coupled hydrologic-thermal modeling based on projected climate change outcomes to generate ecosystem response parameters (permafrost extent, the soil thermal regime, and fire histories) over the historical record and projected to the year 2100.

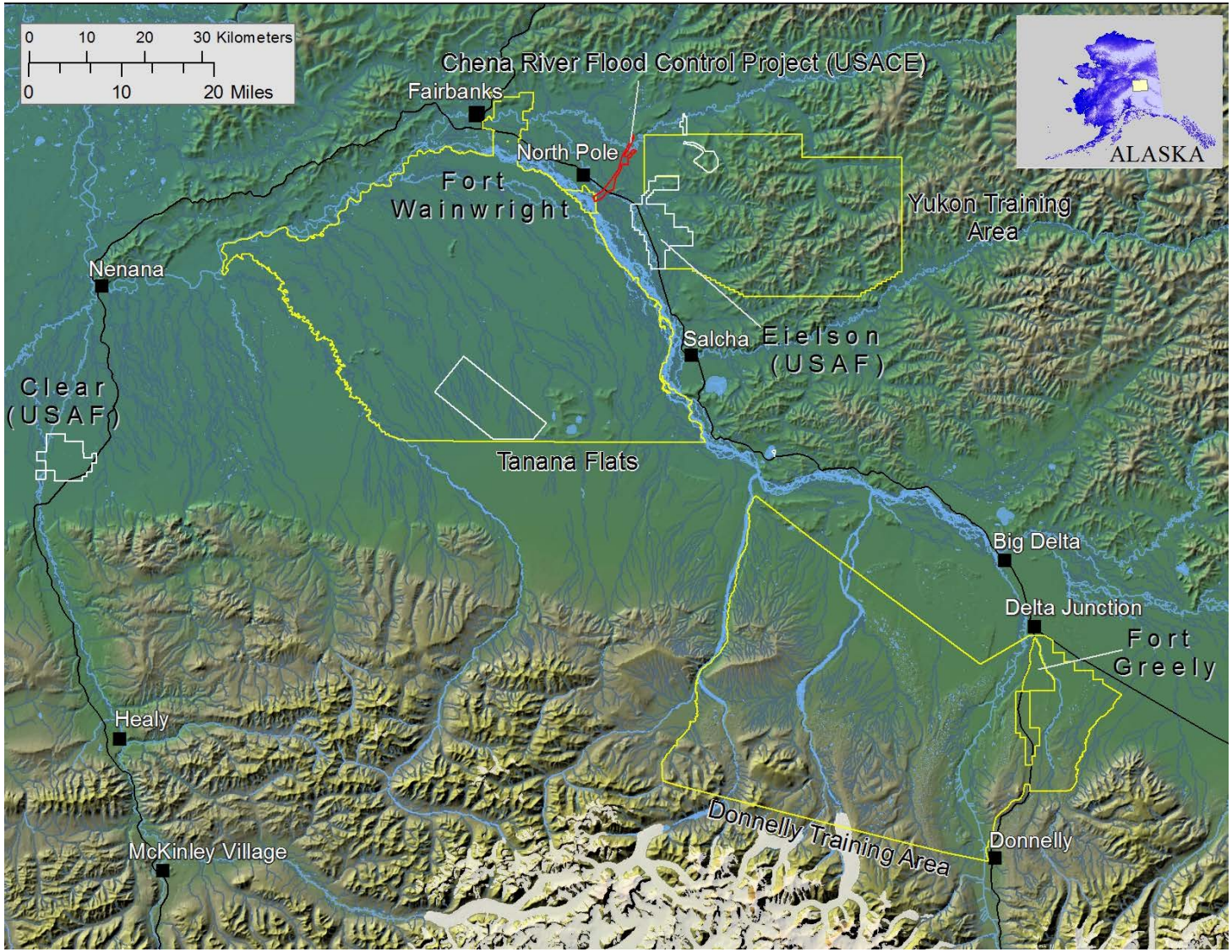

Figure 1. A terrain elevation map of interior Alaska with boundaries for the major Department of Defense facilities. U.S. Army cantonments and training lands (yellow outline), Air Force facilities (white outline) and U.S. Army Corps of Engineers project land (red outline) are identified.

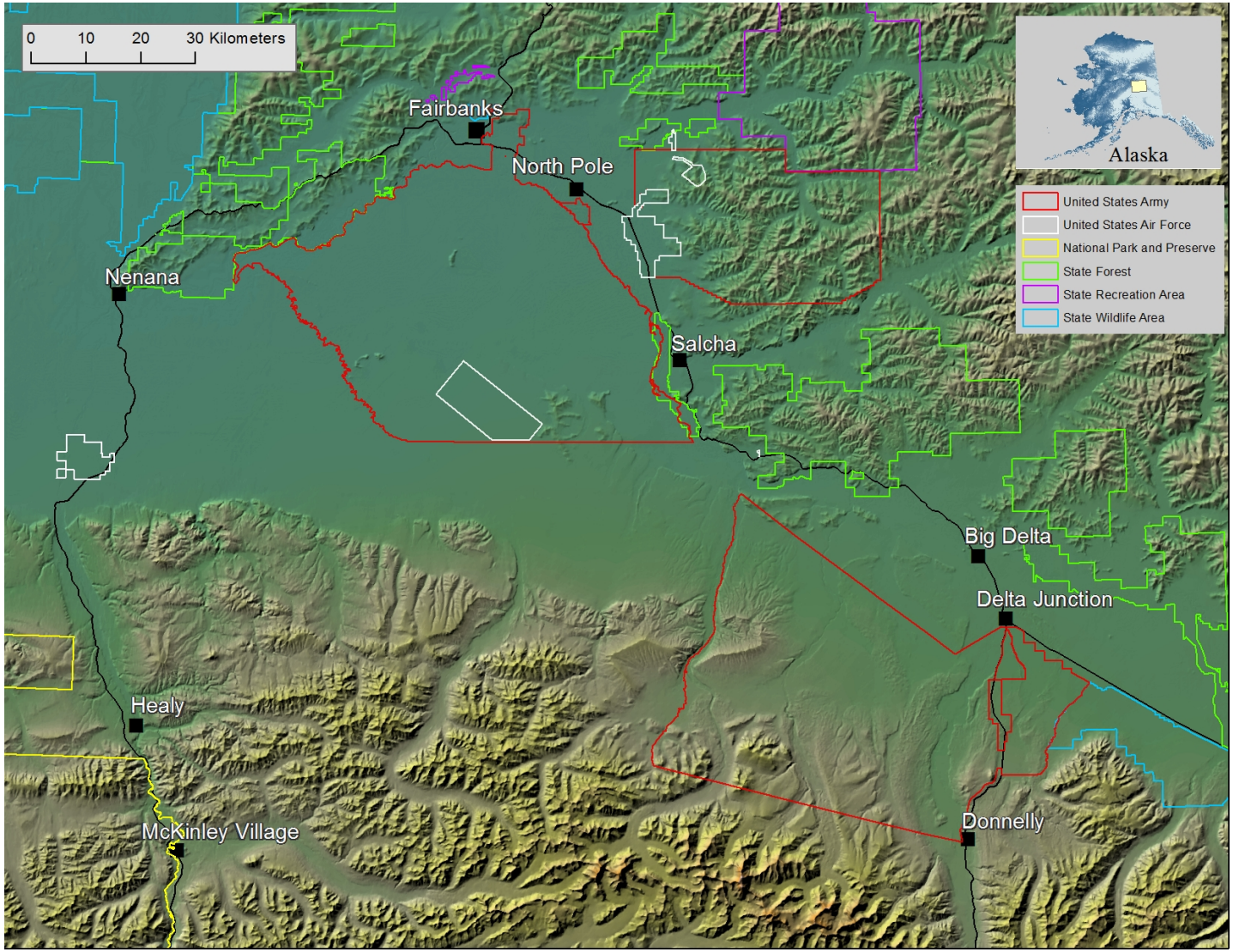

Figure 2.A terrain elevation map of interior Alaska with boundaries for the major Federal and State land managers.

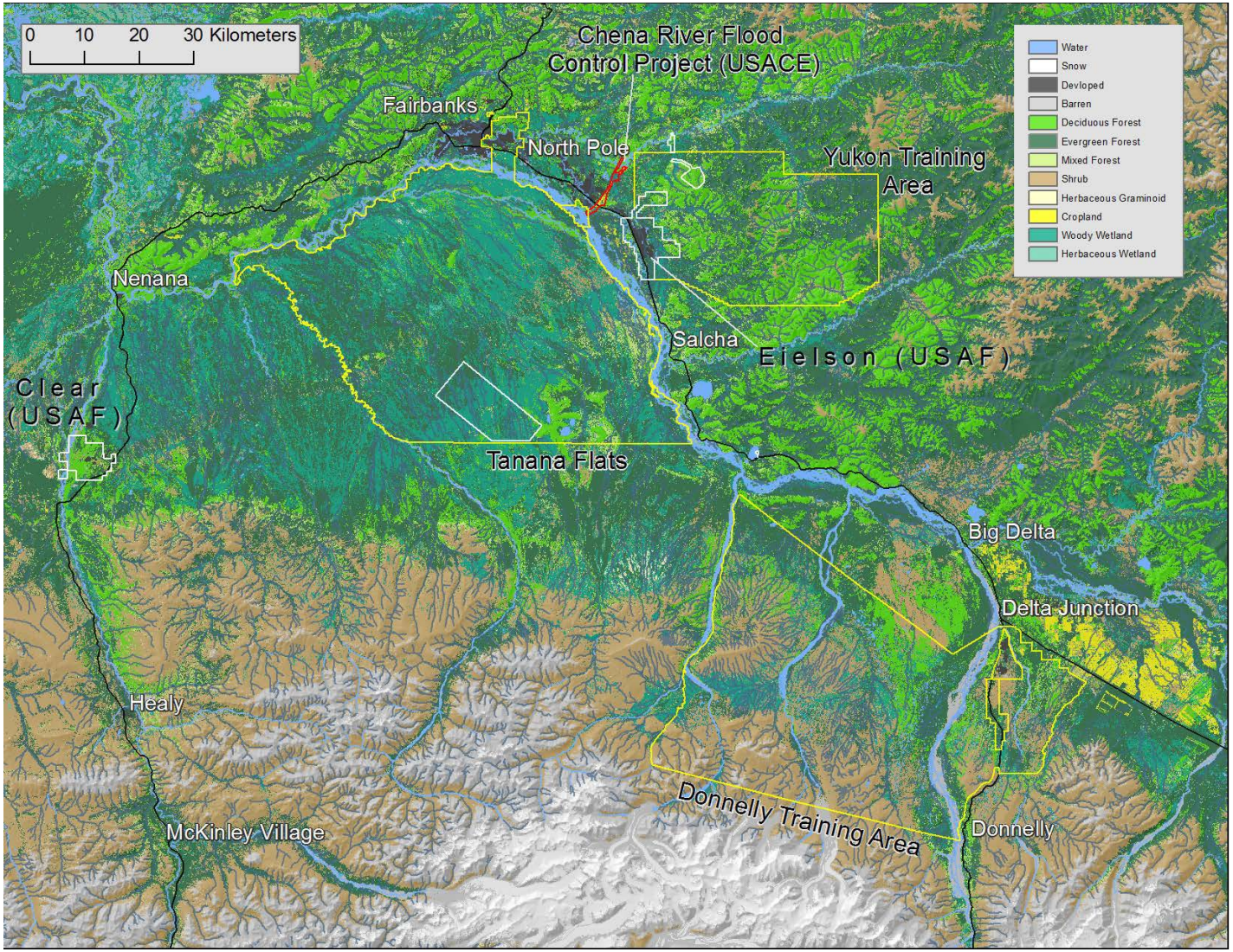

Figure 3. Predominant land cover classes for the Tanana Flats and surrounding areas of interior Alaska from the Alaska 2001 National Land Cover Database(Homer et al., 2007) include evergreen (34%) and deciduous (12%) forest, shrubland (24%), woody wetland (13%), and barren (7%). Percentages are calculated from DoD-owned lands within the visible domain. U.S. Army Corps of Engineers project lands are outlined in red, Army lands are delineated by yellow, and Air Force lands are marked by white.

Our research, driven by a fundamental desire to assist the U.S. Army in Alaska in planning and adapting for climate change, was designed to address the four Research Needs outlined in the SERDP Statement of Need SISON-11-01 as follows:

1) We conducted field measurements and collected time series repeat imagery in upland and lowland landscapes to determine where and what terrains are most susceptible for rapid or unpredictable changes with climate warming or land use activities.

2) To reduce the uncertainty in future ecosystem projections we integrated existing cryospheric components (permafrost, snow, and the vegetation and soil thermal regime) with hydrologic and vegetation succession/ecosystem modeling capabilities. This enhanced our ability to predict how and where fires or other disturbance stressors could affect ecosystem dynamics and to help identify favorable locations to site roads, buildings, and other infrastructure. Our efforts also can be used to support carbon itemization efforts on DoD lands, a topic that gained interest within the Federal Government and DoD after our project was started.

3) We developed a spatially-explicit decision support system to assist the DoD in training and land use management decision-making for interior Alaska by integrating the likely ecosystem responses to climate change and non-climate anthropogenic impacts into day-to-day training activities. The GIS-based tool "Geographic Information Supporting Military Operations" (GISMO) was developed by synthesizing field measurements, repeat imagery analyses, and the most up to date climate projection and thermal modeling information. The tool is designed to help identify challenges for training, management, and infrastructure activities given projected ecosystem changes in response to climate warming scenarios in the area projected to the year 2100. We also include historical meteorologic and fire area information to support a user-queriable change detection module in GISMO.

4) Our decision support tool can be used to minimize the effects of non-climate related anthropogenic stressors on ecosystem processes. Examples include changes in land use activities; infrastructure development such as roads, trails, buildings, berms, and prescribed burns; and the effects of natural and human caused fires on landscape ecology. By linking soils, vegetation, fire, and projected permafrost extent information together a user is able to identify where corridors or areas for infrastructure are least likely to affect (or be affected by) changing terrain properties.

Our project was comprised of five main research objectives. The results from the research objectives were assembled into the content that was used to develop the project's main transition product- a GIS based decision support system for land management. The research objectives are introduced below. Throughout this Report these same five technical areas are presented as separate topics and outcomes.

2.1 Permafrost-hydrogeology relationships on the Tanana Flats lowlands

The presence or absence of permafrost can greatly affect surface, shallow subsurface, and groundwater hydrology. Due to the extremely low gradient terrains in permafrost lowlands like Tanana Flats (<1 meter of elevation change per kilometer) there could be marked changes in the future hydrogeologic regime where permafrost degrades or where thermokarst (ground subsidence following degradation of ice rich permafrost) occurs. Since permafrost can channel or

support surface and subsurface flows its presence can dramatically affect hydrology (Douglas et al., 2013). Degradation of ice-rich permafrost may have particularly strong ecological impacts due to the effects of thaw settlement and subsequent water impoundment. The presence of surface water can substantially increase surface energy gains, raise the temperature of underlying soil, and thaw permafrost. This hydrologic shift can cause a positive feedback to permafrost degradation and changes in vegetation composition and ecosystem function. Lowland forests on ice-rich soils may become wetland or aquatic systems as a result of thaw settlement, with associated changes in vegetation, productivity, and nutrient cycling. These ecological changes can lead to feedbacks whereby forests initially transition into lowlands in which water ponds but they can eventually dry out (when permafrost thaws) and alter the forest succession trajectory. As such, the hydrogeologic landscape response to thermokarst is not consistent or easily predictable.

The hydrogeologic response to permafrost degradation is most likely quantifiable in late summer when the seasonally thawed ("active") layer is at its greatest downward vertical extent. This is when lateral surface and shallow subsurface hydrologic flows are at their maximum. The seemingly opposite responses of wetland systems to permafrost degradation (i.e. wetting and impoundment in some areas initially but eventually draining and drying in others) are difficult to predict but they can have major ramifications on ecosystem services and hydrology. The objective of this part of the project was to undertake a multiyear surface hydrogeology investigation across connected bog, lake, and fen systems on Tanana Flats to discern what role permafrost, and in particular seasonal thaw of the active layer, plays in regulating flows. For this part of the research project the goal was to identify how and where surface water hydrology was associated with seasonal thaw and permafrost extent. Two hypotheses framed this research.

Hypothesis 1: The fens, which are not underlain by permafrost but are focused through channels surrounded by (i.e. constrained by) permafrost, will experience a change in hydrologic connectivity across their reach as the summer season progresses and the active layer expands downward. If and where seasonal thaw allows surface water and shallow subsurface water to leave the main fen channel system through lateral losses or interaction with deeper flow paths these losses will be identifiable through analysis of nested hydraulic pressure dataloggers. The discharge regime in late summer will provide insight into how the projected future loss of permafrost in the area will lead to changes in surface water and shallow subsurface water flows.

Hypothesis 2: The response of fens to large summer rain events will change over the course of the summer season as a deeper thawed soil column is exposed by seasonal thaw. This will be manifest in a comparison of fen hydraulic head measurements following precipitation events across a broad (10s of km) spatial area.

2.2 Vulnerability of permafrost to fire-initiated thaw in interior Alaska

In the boreal biome fire is the most important disturbance in terms of ecological and social impacts (Viereck, 1973; Kasischke et al., 2000a; Wurtz et al., 2006; Turetsky et al., 2010). Interior Alaska is currently experiencing a climate warming trend associated with earlier snowmelt, drought, increased convection and lightning, and larger more severe wildfires (Kasischke et al. 2010; Wendler et al. 2011; Wolken et al. 2011). These changes need to be accounted for when assessing and mitigating risk for DoD training range fire management activities (live fire exercises, prescribed burns, optimization of the application of limited fire fighting resources, revegetation folllwing disturbance, and managing forest fuels). In a projected warmer climate there is greater risk that DoD training or land management activities will result

in large wildfires escaping DoD lands and causing loss of property or life. Three large wildland fires on training ranges since 2012 (i.e. since the project was initiated) are evidence of the challenges facing fire management on DoD lands in Alaska. One fire was started by live fire with pyrotechnics (Stewart Creek, in the Yukon Training Area uplands) and the other fires were initiated by prescribed burns that grew out of control (both in the roadless portion of Donnelly Training Area West lowlands). The three fires burned 180,000 acres of land, cost $44M to fight, and forced people to evacuate from their homes.

USARAK has a limited fire suppression and fuel management budget and the broad and remote expanse of the training range land areas thay manage make it extremely difficult to prioritize and apply fire management actions. Prescribed burns and natural fires on interior Alaska DoD lands could result in severe burning that: 1) triggers smoldering and ground smoke events that disrupt training activities, and 2) drastically alter vegetation, permafrost, and hydrogeology with a potentially global feedback on the carbon cycle and its climate forcing greenhouse gas inventories (Douglas et al., 2014; Turetsky et al., 2011; 2014).

In recent years the increased intensity of boreal fires has led to greater consumption of the protective moss layer resulting in enhanced permafrost thaw (Jorgenson et al., 2010). Moss cover, coupled with thicker organic soils (0.5 to >3m), in black spruce stands, are more protected against permafrost thaw than birch forests with no moss cover and little organic soil (Osterkamp et al., 2000). The surface organic material and soils in interior Alaska provide “ecosystem protection” against permafrost thaw (Shur and Jorgenson, 2007). Permafrost stability is intricately coupled with ground ice abundance, the soil thermal regime, vegetation succession, terrain physiography, and disturbance. If/when the surface organic material is disturbed (typically and dramatically by fire but also by human disturbance) the response to the change in thermal state can affect permafrost stability within months (Brown et al., 2015). The objective of this part of the research was to investigate how permafrost and the thermal state of the ground surface vegetation and soils respond to fires. By investigating the thermal response of permafrost to fire across a chronosequence of sites representing time since fire disturbance we could identify the rates and types of mechanisms related to fire, post-fire forest succession, and the soil thermal regime. Two hypotheses guided this research

Hypothesis 1: The initial (i.e. within 1-3 years) response of permafrost lowland landscapes to fire includes a measurable decrease in organic layer thickness, an increase in seasonal thaw depths, an increase in surface soil temperatures, and a change in the areal extent of thawed bogs. These processes lead to substantial permafrost thaw, ground surface collapse (thermokarst), and water impoundment in recently disturbed (burned) areas.

Hypothesis 2: Thermal model results simulating thaw depths following fire mimic field thermal measurements and can be used to predict the relationship between permafrost ice content, ecological disturbance, and thaw subsidence.

2.3 Biophysical, geophysical, and airborne measurements of permafrost geomorphology

Slope, aspect, soil type, permafrost extent, and disturbance history play major roles in controlling vegetation composition in the Alaskan boreal biome. Fire is the greatest ecologically important disturbance in the boreal biome but infrastructure development, particularly roads and large clearings, can greatly affect the vegetation and soil thermal regime. There is a need for remote sensing or ground based measurement capabilities that can “map” the presence or absence of permafrost and provide insight into how and where permafrost bodies can be expected to respond to disturbance. Of principal concern are transition zones where frozen and

thawed material meet. This is where the effects of permafrost thawing will be most pronounced because as the thaw front moves into previously frozen material subsidence, changes in hydrogeology, and soil and vegetation changes will be initiated. Identifying and predicting the response of permafrost to warming or disturbance requires accurate and detailed assessment of subsurface characteristics, predominantly permafrost extent. Infrastructure development and ecosystem modeling could both be supported by this type of research.

The objective of this aspect of the project was to identify sites that exhibited a range of times since fire disturbance and identify how and where permafrost, soil, and vegetation responded to the disturbance event. This research was also focused on applying some of the most recently available geophysical and airborne imagery analysis methods toward relating permafrost presence (or absence) to easily identifiable metrics (forest stand height, stand type, relative elevation, and ecotype) in an attempt to support remotely sensed applications of permafrost mapping.

Two hypotheses were addressed by this research.

Hypothesis 1: The response of permafrost to deep thawing and development of taliks (thawed regions that are deeper than the depth of the winter season freeze) or bogs is controlled by disturbance severity, organic layer thickness, and permafrost geomorphologic properties.

Hypothesis 2: The presence or absence of permafrost beneath lowland landscape features like bogs, thermokarst bodies, and islands of tree stands can be identified and mapped at the ~1 meter scale by combining field measurements, high resolution GPS measurements, and geophysical surveys. The complex relationships between thawed and frozen material, where permafrost degradation will occur, can be related to quantifiable surficial expressed biophysical measurements like relative elevation, vegetation, soil composition, and ecotype.

2.4 Permafrost hydrologic modeling in upland catchments

Projections of the long-term effects of climate warming on high latitude ecosystems require a coupled representation of the soil thermal state and local hydrogeologic dynamics. Modeling tools are needed to support efforts to identify how and where hydrologic flows will change in a warmer climate. Of particular need are tools linking the areal extent of permafrost in a watershed to the likely discharge in the watershed and a modeling capability to project changes in permafrost extent to changes in hydrology. This will support efforts to project how and where flow regimes in watersheds will respond to changing permafrost conditions. The work is particularly suited to upland terrains where discharge, seasonal flows, and hydrologic parameters are needed to support land management activities, to design infrastructure (like bridges, culverts and spillways) and to manage flows for hydropower or other water management needs.

The objective of this part of the project was to utilize the wealth of discharge and permafrost extent mapping information from the National Science Foundation supported Long Term Ecological Research Site at the Caribou-Poker Creek Research Watersheds (CPCRW) to develop the coupled soil thermal-hydrogeologic model. The watersheds are close in proximity, soils, vegetation, gradient, and geomorphology to the ungaged Yukon Training area uplands where USARAK training is ongoing. Results from the CPCRW focused modeling can be used to provide insight into how these watersheds may behave in a future warmer climate.

Two hypotheses were addressed by this research.

Hypothesis 1: A coupled framework explicitly simulating soil moisture effects of soil thermal conductivity and heat capacity and its effects on hydrological response can project how hydrologic flows in permafrost terrains will be altered in a warmer future climate. The

Geophysical Institute Permafrost Laboratory (GIPL) model can be coupled with the Gridded Surface Subsurface Hydrologic Analysis (GSSHA) model to add a permafrost heat transfer component to GSSHA that simulates soil temperature dynamics and the depth of seasonal freezing and thawing by numerically solving a 1D quasi-linear heat equation with phase change.

Hypothesis 2: Hydrologic-permafrost-soil thermal model results will simulate field measurements in catchments of varied permafrost extent. Specifically, warmer soils and decreased permafrost extent are associated with longer flow paths and a larger baseflow component while colder soils and increased permafrost extent lead to a more rapid stream response to precipitation events and a decrease in baseflow and storage.

2.5 Ecosystem transition modeling to identify landscape change

Ecosystems over large regions are highly diverse owing to gradients in environmental conditions and disturbance regimes and, as such, they can be expected to respond differently to climate warming. In the boreal biome a wide range of atmospheric, hydrogeologic, geomorphic, fire, biotic, and anthropogenic drivers can affect ecological patterns and processes that provide challenges for ecosystem subsistence resource management. The presence or absence of permafrost and the time since disturbance are two major drivers of ecosystem state changes and ecosystem trajectories.

One of the best ways to identify how and where diverse local-scale ecosystems (ecotypes) will respond to climate change or disturbance is to quantify ecosystem change over time and develop trajectories for how and where different ecotypes can be expected to respond to and evolve from disturbance. Repeat imagery analyses can be used to compile data on historical ecotype areal changes over the last 25–50 years. Based on the historical rates of change relative to time, state-transition models can be developed to project future changes in areal extent for the range of ecotypes represented. This can be applied across diverse ecosystems and a variety of biophysical characteristics by using a state-transition modeling approach incorporating a large number of historical observations of past rates of change (Jorgenson et al., 2015).

The objective of this part of the project was to identify and track terrain characteristics that can be measured remotely and in the field and to identify rates of change over a variety of upland and lowland landscape ecotypes. The areal extent included the major USARAK training ranges and their variety of ecotypes. The ecosystem transition trajectories can be projected into the future to identify how and where future climate warming will impact permafrost and landscape processes.

One principal hypothesis was addressed by this research.

Hypothesis 1: A time-series analysis, from 1950 to the present, of historical airphotos and recent satellite images can be used to identify and quantify changes in local-scale ecosystems (ecotypes) through photo-interpretation of points systematically distributed across a variety of ecotypes. Both rates of ecotype change and identification of the ecological drivers of change can be assessed through the photo interpretation.

2.6 Development of a GIS based geospatial decision support tool

Project results have been transitioned to potential end users through peer reviewed journal articles and Technical Reports, presentations to multidisciplinary scientific groups, and participation in presentations and meetings with a broad array of DoD, other Federal Government, and State of Alaska entities. Throughout the project we routinely met with potential land managers of USARAK and similar lands to identify what types of information, research

results, and tools they could use to help them manage lands now and in a warmer future state. We assembled the most up to date database of GIS layers for interior Alaska USARAK training lands. Digital elevation models (DEMs), USGS topography, wetlands, surface hydrology, soils, land cover, areas burned by fire, and roads and trails have been integrated into this tool. The most current and highest resolution permafrost maps for interior Alaska DoD lands were integrated into one layer. Locations of all major DoD impact areas, drop zones, cantonments, live fire ranges, and impact areas have also been included.

Results from this project and other project research team's thermal and permafrost modeling have been integrated as user-defined historical and projected information panels. The GIS tool allows the user to quantify differences, areas of change, and the layering of different database results to support query-based investigations of how and where projected climate warming will affect land management requirements. This set of layers comprises the foundation upon which project field and modeling results and end-user needs are integrated.

The objective of this part of the project was to develop a means of integrating all the project information, modeling outcomes, and scenario development into a management tool. The end-user we envisioned, and who helped us develop the tools, is the USARAK training land manager, ecologist, archaeologist, forester, fire scientist, infrastructure planner, or regulator. They need scientifically defensible datasets combining ecosystem, landscape, and training land information with historical and projected climate, permafrost, precipitation, meteorologic, and temperature information.

3. BACKGROUND

3.1 DoD in Alaska- regulatory and environmental drivers

The U.S. security posture is increasingly moving toward the Asia-Pacific region. Stationing personnel and equipment and training in Alaska, with equal air travel times to Southeast Asia, Europe and the Pacific Theater, provides "Operational maneuver from strategic distances" (U.S. Army Training and Doctrine Command (TRADOC) PAM 525-66). Alaska ranges offer wide open spaces with minimal encroachment or noise issues experienced at training ranges elsewhere. TRADOC PAM 525-66 states the Army should make decisions "enabled by advanced decision making tools, improved modeling and simulation tools, combined with more realistic training, practice, and experience… (to) further accelerate planning and execution on the future battlefield." Climate change is a new paradigm to incorporate into planning and execution activities, especially in Alaska. A wide variety of major infrastructure investments have been made in interior Alaska recently and more are planned. These projects must incorporate the most up to date scientific measurements to inform decisions on location, design, and adaptation to the presence and stability of permafrost and the potential vulnerability to thawing permafrost (U.S. Arctic Research Commission Permafrost Task Force (2003).

The "Department of Defense FY 2012 Climate Change Adaptation Roadmap" identifies requirements under October 2009 Executive Order 13514 "*Federal Leadership in Environmental, Energy and Economic Performance."* These include the need for Federal Agencies to evaluate climate change risks and vulnerabilities and to manage short and long term effects of climate change on mission and operations. Goals for implementation of the Adaptation Roadmap include the need to "utilize [a] robust decision making approach based on the best available science" and to "integrate climate change considerations into existing processes." The FY 2014 Climate Change Adaptation Roadmap identifies the effects of climate change as a "threat multiplier….. that will have real impacts on our military and the way it executes its missions." Permafrost thaw and changing precipitation patterns are the main phenomena of relevance that render DoD infrastructure and the training land mission in interior Alaska vulnerable, especially in light of projected climate warming.

The U.S. Army is the largest DoD land user in Alaska and conducts all season training throughout its 1.5 million acres of training areas in the interior, an area roughly the size of Delaware (Figure 1). Main DoD sites include the cantonments of U.S. Army Fort Wainwright, Eielson Air Force Base, U.S. Army Fort Greely, and three large training areas. Impact areas used by the Air Force are located on Army lands. Training and infrastructure are located in road accessible locations in the Yukon Training Area and Donnelly Training Area East and in vast lands only accessible by air or winter time ice roads on Tanana Flats and Donnelly Training Area West. Much of these lands are underlain by sporadic (discontinuous) permafrost and ground ice contents vary widely (Figure 4).

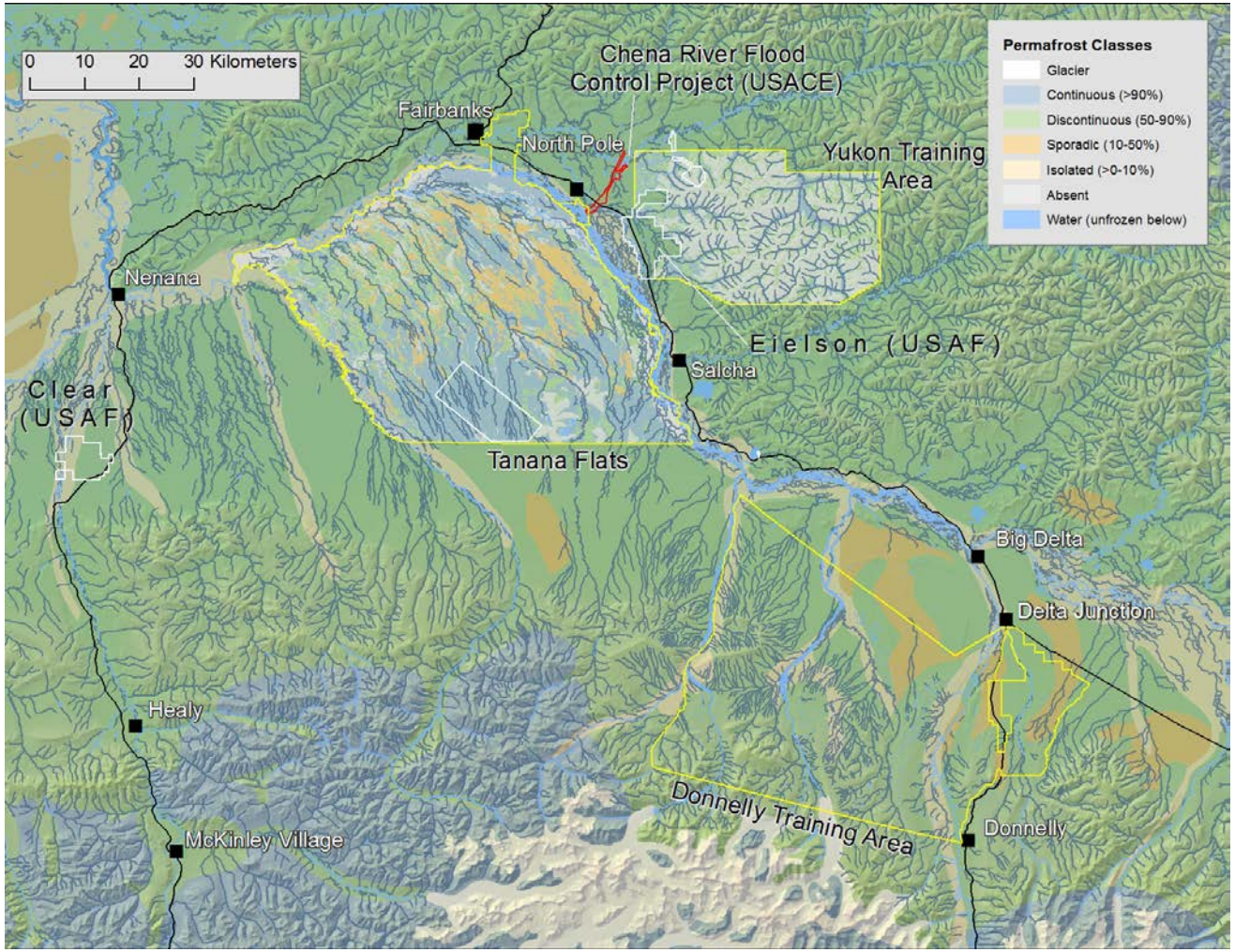

Figure 4. The extent and type of permafrost for interior Alaska DoD lands. U.S. Army Corps of Engineers project lands are outlined in red, Army lands are delineated by yellow, and Air Force lands are marked by white. Permafrost classes range from continuous to absent. Data sources for permafrost are varied with the majority from Jorgenson et al. (2008a) and from the fine scale maps of Tanana Flats and the Yukon Training area in Jorgenson et al. (1999). The spatial distribution of permafrost outside of the Tanana Flats and Yukon Training areas is not well mapped and is largely uncertain. Map from Douglas et al., 2014.

The Tanana Flats Training Area (TFTA; 650,000 acres) is comprised largely of lowlands underlain by a complex mosaic of ice rich permafrost and permafrost free land (Figure 5). Discontinuous permafrost exists within 0.5 to 4 m of the surface and is between 5 and 70 m thick (Hopkins et al., 1955; Anderson, 1970; Hamilton et al., 1983; Douglas et al., 2011). Open wetland corridors, thought to be permafrost free, are sharply bordered by birch and spruce forests underlain by permafrost. Abundant slumping of trees indicates recent and past permafrost degradation along the upland margins of Tanana Flats. This ecosystem is susceptible to major surface vegetation and permafrost changes with climate warming. There are currently no all season roads to TFTA but a $188M, 1 km bridge recently constructed over the Tanana River by the Alaska Railroad now provides year round access. The bridge is the first step in the Joint Pacific Alaska Range Complex (JPARC) Alaska training range modernization project- a major planned infrastructure development of $220 million in Army and Air Force facilities over the next 10 years.

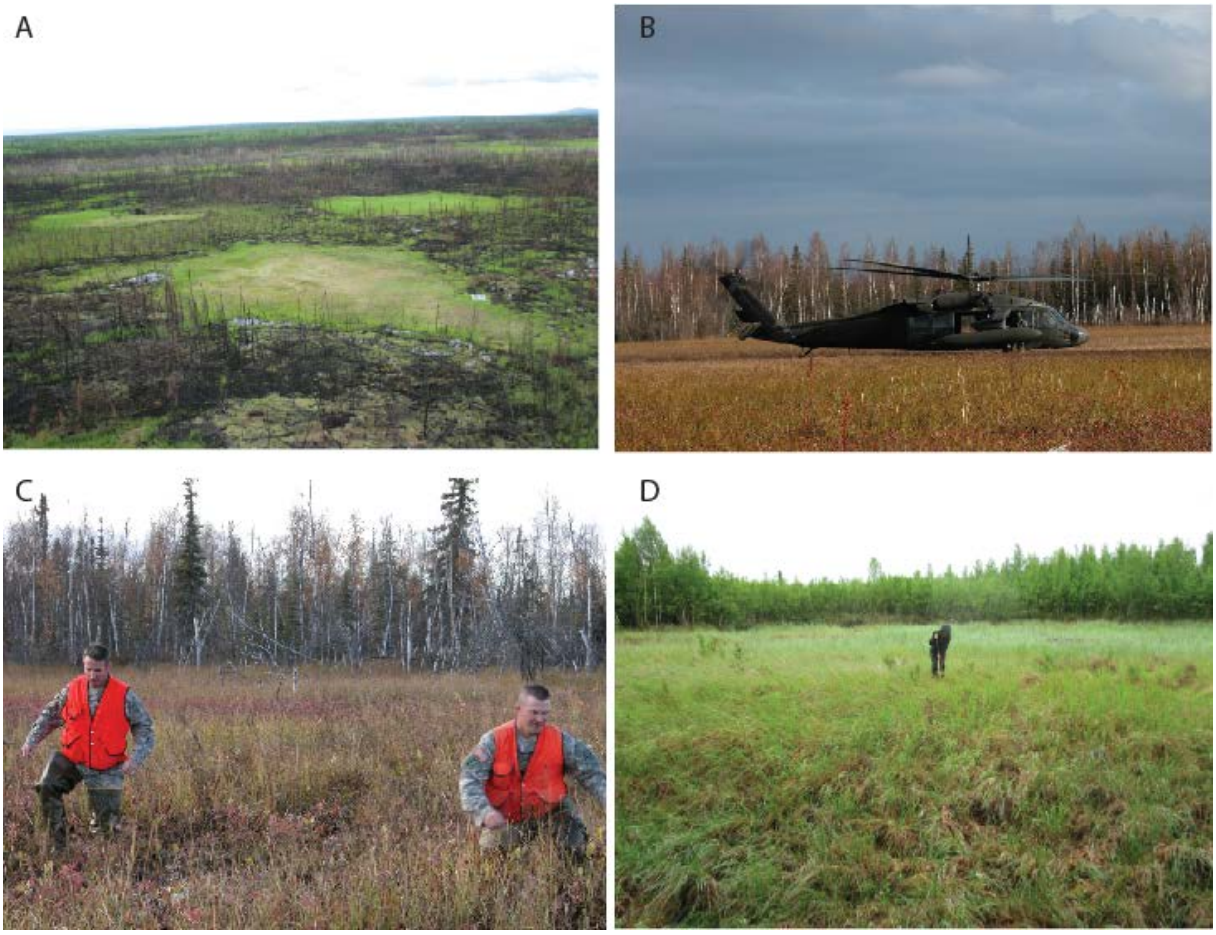

Figure 5. Photographs representing the vegetation typical of lowland ecosystems on the Tanana Flats Training Area. A) An overview of an area that burned in 2010 (site TF10). The green regions are locations where low lying fens are located. The brown and black standing dead trees are characteristic of burned spruce and birch. B) A view showing the fen to forest transition in an unburned location in the fall. C) A close up of the fen from C. D) The vegetation typical of a bog (site TF88). This area burned in 1988 and the dense forest in the background is typical of a vibrant birch forest.

Donnelly Training Area West (DTAW; 623,000 acres) contains upland landscapes (Figure 6) comprised of rocky moraines and thick loess deposits to the south and lowland landscapes resembling the TFTA in the north. Loess deposits in the northern DTAW are vulnerable to catastrophic collapse of ice-rich permafrost (Toniolo et al., 2009). There are currently no roads into this area but there are long term plans for the construction of 110 km of road and rail along the northeastern boundary of DTAW to link Fts. Wainwright and Greely. An additional 80 km of road to the north slopes of the Alaska Range is planned in the currently roadless DTAW to establish training areas on sparsely vegetated, rocky, high-elevation landscapes that resemble Afghanistan and the Middle East.

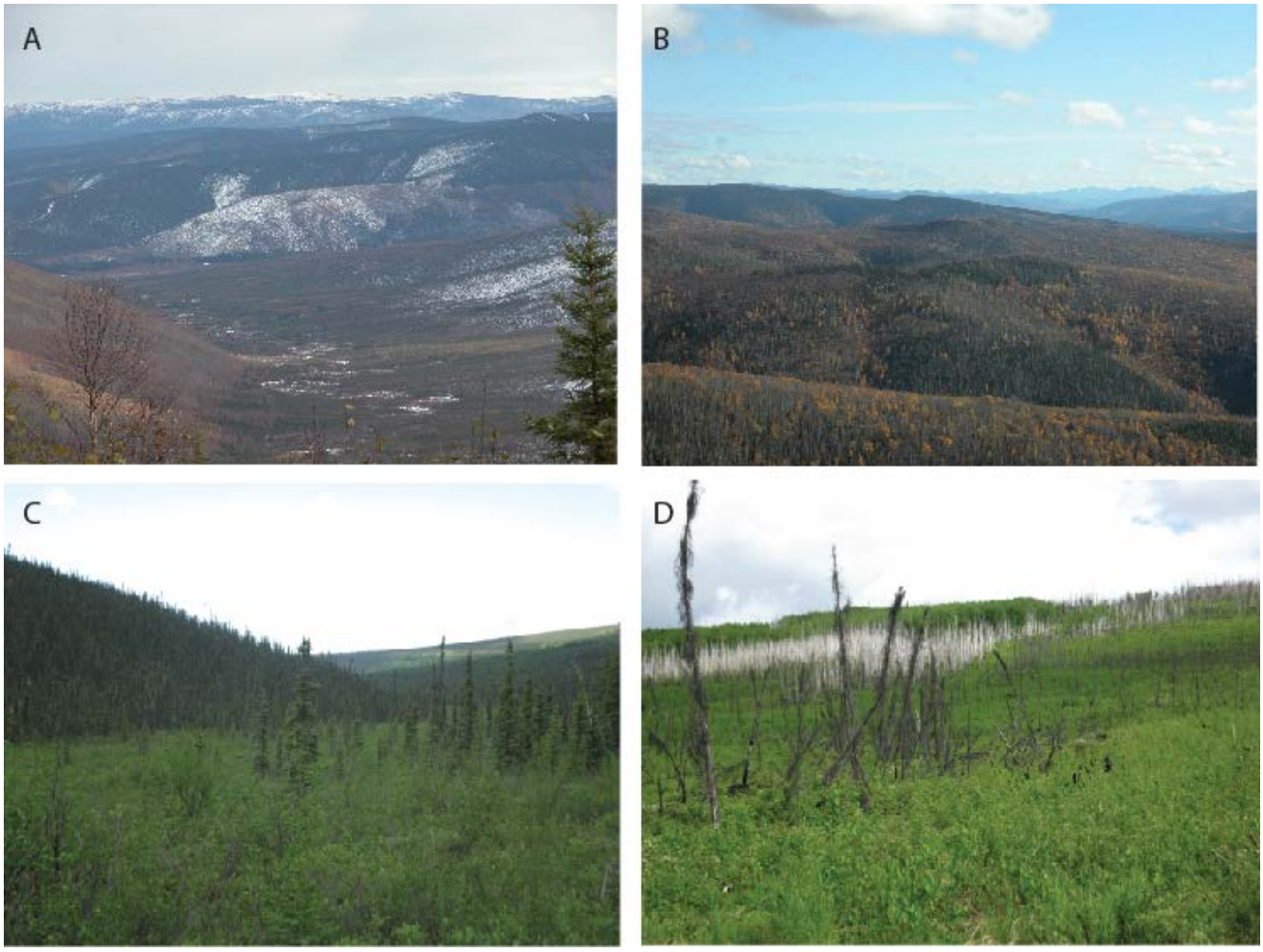

Figure 6. Photographs representing the vegetation typical of upland ecosystems found in the Yukon Training Area and in the Caribou-Poker Creeks research Watersheds (CPCRW). A) A winter view of the Stuart Creek impact area on Yukon Training Area showing the rolling hills and elevation gradients. B) A close up of the hills above Stuart Creek in late fall. C) A valley bottom underlain by discontinuous permafrost with a spruce forest at the CPCRW. D) A side hill in upland terrain that shows standing dead trees (white colored crowns) from a fire in 1999 in the CPCRW.

Donnelly Training Area East (DTAE; 65,000 acres) is immediately adjacent to Fort Greely cantonment and the U.S. Ground Based Midcourse Defense interceptor site. The area is comprised of upland and lowland landscapes underlain by glacial tills that contain sporadic discontinuous permafrost. In the past 10 years over $30 million has been spent to construct the Battle Area Complex/Combined Arms Collective Training Facility (BAX/CACTF) in DTAE. Over 30 km of road were upgraded and instrumented targets and buildings were constructed in a forested area underlain by sporadic permafrost. Local hydrogeology, linked to the agricultural town of Delta Junction to the north, is believed to be largely controlled by the presence (or absence) of permafrost.

The Yukon Training Area (YTA; 248,000 acres) is predominantly located in upland landscapes underlain by sporadic discontinuous permafrost generally underlying north facing slopes and valley bottoms (Osterkamp et al. 2000; Jorgenson et al. 2001a, b; Douglas et al., 2008). Vegetation is dominated by white spruce-birch-aspen forests. Soils are mostly rocky and well-drained with permafrost occurring only on north-facing slopes and in valley bottoms. YTA has an extensive network of gravel roads, some live fire training and target areas, and drop zones. The recently constructed Digital Multipurpose Training Range and a large area cleared of vegetation to expand Husky Drop Zone have experienced major surface perturbation due to permafrost thaw immediately following infrastructure construction.

Due to the increased access presented by the Alaska Railroad Bridge and the unique opportunities provided by interior Alaska training the DoD is proposing the Joint Pacific Alaska Range Complex (JPARC; Figure 7). The vast training areas in Alaska offer more realistic situations to test combat systems in a variety of environmental conditions. The proposed JPARC provides a training capability from interior Alaska to the Gulf of Alaska to integrate air, land, sea, space, and cyberspace components. Planned infrastructure represents Army, Air Force, Navy, Coast Guard, and the Special Forces and totals more than $220 million in investments over the next decade. Much of this infrastructure development will occur on remote lands that are currently not road accessible and are underlain by a complex mosaic of discontinuous permafrost. Remotely sensed measurements and geospatial tools are critical planning tools for this planned infrastructure.

Nine of the main JPARC projects are vulnerable to permafrost or hydrologic changes due to climate warming. Highlights include additional usage of the BAX/CACTF on DTA East (JPARC action #3), building and runway infrastructure to support unmanned aerial vehicles in lowlands (#6), enhanced vehicle access to DTAW (#7), a proposed road into TFTA (#8), construction of combat training complexes in multiple locations (#9), establishing staging base facilities in multiple locations (#10), and construction of precision airdrop zones in DTA West (#12).

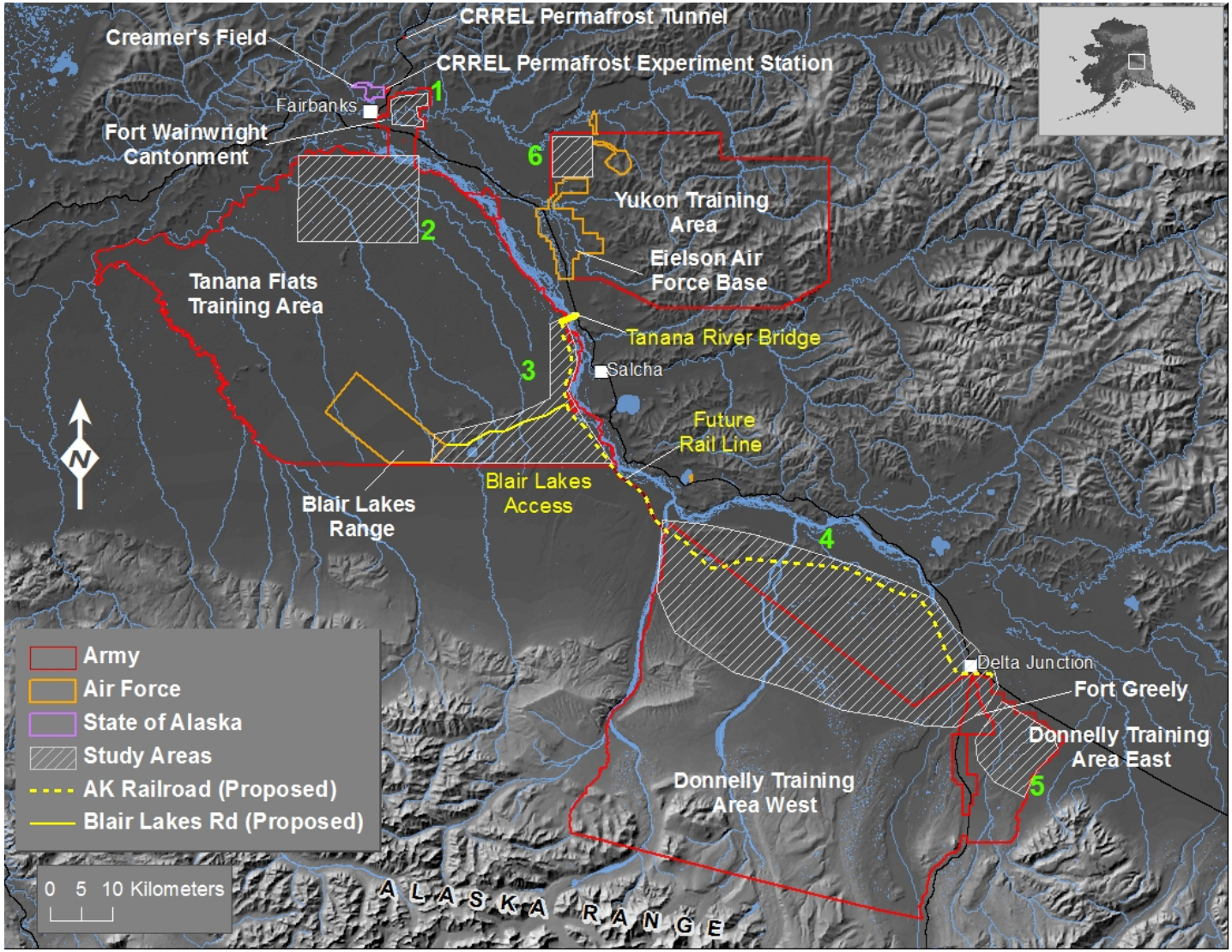

Figure 7.A terrain elevation map delineating Army, Air Force, and State of Alaska lands in interior Alaska with a focus on proposed JPARC infrastructure investments. The Alaska Railroad's recently constructed $185M Tanana River Bridge, the planned access road to the Air Force Blair Lakes site, and a future road and rail corridor to Fort Greely are denoted.

3.2 Past research/state of the science

The boreal forest biome, where interior Alaska DoD infrastructure is situated, is the largest terrestrial biome on Earth, extending roughly from 45º to 83º N, and consisting primarily of coniferous forests with thick organic soils. Much of the boreal biome is underlain by permafrost. Permafrost, defined as any substrate remaining below 0ºC for more than two consecutive years, can persist where mean annual air temperatures are as high as +2ºC. This is due to localized differences in the soil thermal regime, which is influenced by topography, slope, aspect, hydrology, winter snowfall, ground ice content, soil texture, plant cover, and fire history (Figure 8; Osterkamp and Romanovsky, 1999; Hinzman et al., 2003; Jorgenson and Osterkamp, 2005; Myers-Smith et al., 2008). Regional temperatures are not low enough to sustain permafrost everywhere (Schuur et al., 2008). Permafrost affects the vertical movement of water and nutrients through the soil column, so its presence can markedly affect surface soil and vegetation processes that are major aspects of the carbon cycle (Petrone et al., 2006, 2007; Walvoord and Striegl, 2007). Permafrost also provides major challenges to the siting and design of infrastructure.

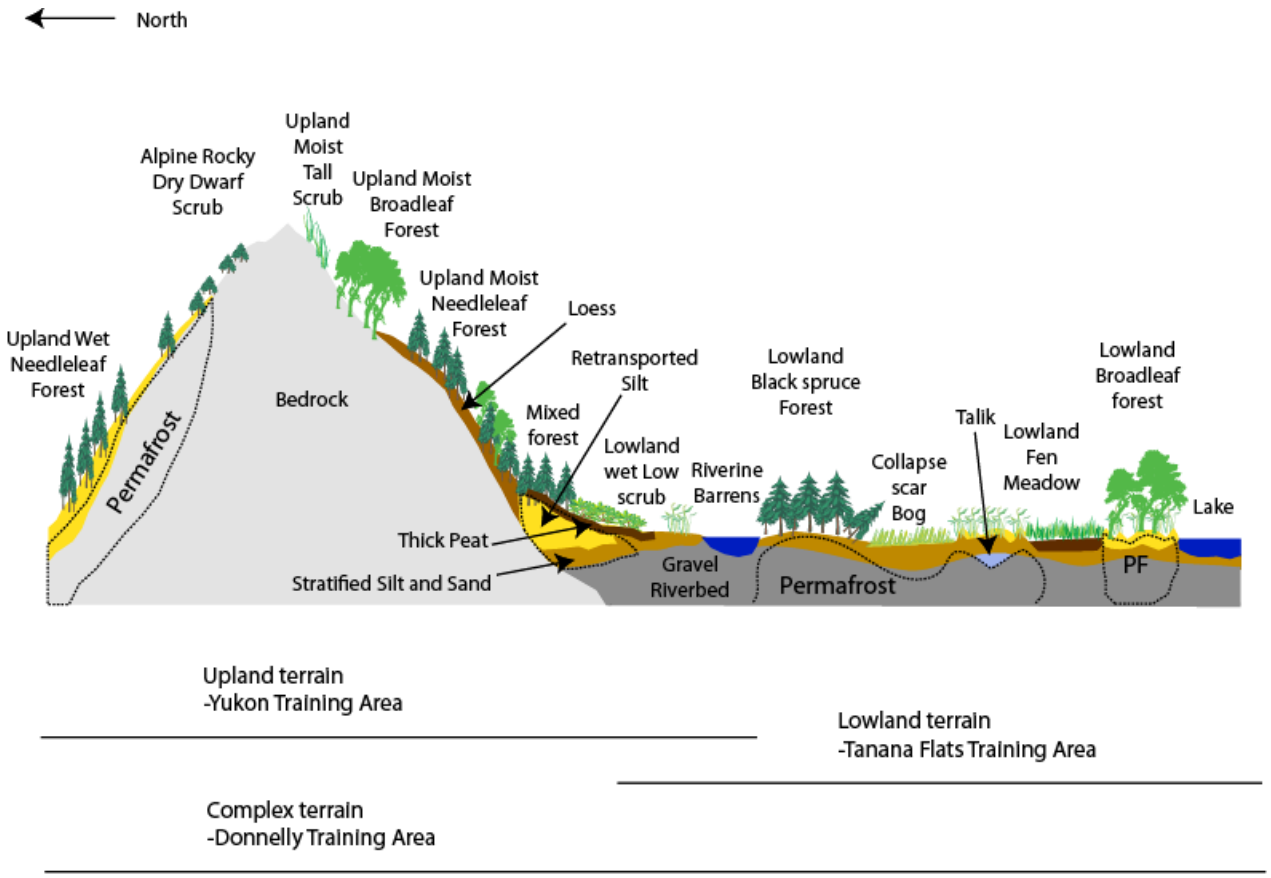

Figure 8. A cross section illustrating the physiographic variety of land forms, hydrologic features, and vegetation in interior Alaska and their relationship to permafrost. Adapted from Jorgenson et al., 2010 as published in Douglas et al., 2014.

Climate warming is expected to have pronounced effects on high latitude ecosystems, especially in locations underlain by relatively warm, discontinuous permafrost such as interior Alaska (Arctic Climate Impact Assessment, 2005; White et al., 2007). Large areas of interior Alaska permafrost now show signs of degradation (Racine and Walters, 1994; Jorgenson et al., 2001a; Osterkamp, 2007; Osterkamp et al., 2009) and these are expected to continue to degrade with further climate warming (Marchenko et al. 2008). Changes in permafrost distribution have dramatically affected ecosystems across the boreal and arctic regions through widespread drying in some regions (Riordan et al., 2006; Roach et al., 2011) and wetland expansion in others (Racine and Walters, 1991; 1994; Osterkamp and Jorgenson, 2006).

Interior Alaska winter snowpacks have been declining and more precipitation is falling as rain than in the recent past (Liston and Hiemstra, 2011). Warmer temperatures and an altered precipitation regime are expected to initiate permafrost degradation in many areas (Osterkamp and Romanovsky, 1999; Marchenko et al., 2008; Wolken et al., 2011) which could lead to a potentially thicker seasonally thawed (active) layer (Hinzman et al., 1991; 1998), the thawing of frozen soils, and the melting of massive ice bodies such as ground ice, ice wedges, and segregation ice (Osterkamp and Jorgenson, 2006). Climate-modulated changes in permafrost dynamics will provide a challenge in planning, designing, and operating Department of Defense (DoD) cantonments, facilities, and roads in interior Alaska. Changes in permafrost hydrogeology will also make fire and land management ecological decisions more difficult.

3.2.1 Permafrost hydrogeology

Increasing temperatures are expected to have pronounced effects on soil and water hydrogeologic processes in regions underlain by discontinuous permafrost (Osterkamp and Romanovsky, 1999). As the climate warms in both summer and winter, permafrost will continue its current warming trend (Romanovsky et al., 2012), the active layer will become thicker, the lower boundary of permafrost bodies will move upward and the areal extent of permafrost will decrease. These structural changes will affect components of the surface water and energy balances. As the active layer thickens there is greater storage capacity for soil moisture and lags are introduced into the hydrologic response times to precipitation events. When permafrost is close to the surface, the stream and river discharge peaks are higher and base flow is lower (i.e., streams are “flashier”). If permafrost degrades, connectivity between surface and subsurface water flow paths can increase (Walvoord et al., 2012). Depending on the hydraulic gradient, more infiltration of surface water or exfiltration of groundwater occurs when permafrost extent decreases. This has significant impacts at both large and small scales by reducing summer runoff and increasing the yearly proportion of winter runoff as deeper flow paths become a larger component of subsurface flows (Douglas et al., 2013).

Permafrost acts as a confining bed in the subsurface that reduces soil water storage capacity and restricts groundwater flow (Hinzman et al., 1991; 1998; Kane et al., 1991; Woo, 2000). The presence of permafrost can greatly affect the stream discharge response to storm activity (Carey and Quinton, 2005), the geochemistry of stream flow (Petrone et al., 2006; Bagard et al., 2011), and seasonal fluxes of nutrients like carbon and nitrogen out of northern watersheds (Carey, 2003; O’Donnell and Jones, 2006; Frey et al., 2007; 2009; Walvoord and Striegl, 2007; Cai et al., 2008a, b; O’Donnell et al., 2012a; Douglas et al., 2013).

Lowland landscapes are composed of a complex mosaic of forest, scrub, bog, fen, and open water bodies (Figure 5). They are underlain by sporadic bodies of ice-rich and ice-poor permafrost in gelisols predominately composed of organic material (Pergelic Cryofibrists and

Histic Pergelic Cryofibrists) or gravel, silt, and sand (Pergelic Cryochrepts; Brabets et al., 2000). The many open wetland corridors (floating vegetation mats and fens), thought to be permafrost free, are bordered by forests growing above permafrost or perched on top of well-drained gravel substrates. Lowlands comprise 42% of the boreal region in Alaska (574,000 square km), of which 13% is susceptible to collapse-scar bog formation (Jorgenson et al., 2001b). These bogs form when permafrost acts as an aquiclude (a low flow zone in the subsurface around which flow is channeled) or an aquitard (a zone with no subsurface flow) a few meters below the surface. If a talik penetrates deep enough the previously closed hydrological system can open up and increase contact with groundwater. In this case fens, wetlands with higher mineral and nutrient content, usually due to subsurface flow, can form. Racine and Walters (1994) suggest the large areas of fen wetlands are fed by groundwater discharge that moves northward from the Alaska Range to the south with permafrost acting as a confining layer channeling subsurface flow. Abundant slumping of trees indicate recent and past permafrost degradation along the upland margins of Tanana Flats.

The boreal region contains a heterogeneous distribution of lakes that are stable, increasing, or decreasing in areal extent. Lake stability is the result of heterogeneous permafrost, hydraulic gradients, and lake and catchment topography (Roach et al., 2011).Though they only cover ~2% of interior Alaska by area, lakes are an important component of the area's boreal ecosystems, wetlands, and their carbon cycle processes because of aquatic-terrestrial links between water bodies and the surrounding soil and vegetation. Nutrients, especially carbon and nitrogen, impact terrestrial ecosystems nearby, leading to enhanced lake productivity with increased run-off or permafrost thaw (Symstad et al., 2003; Ball et al., 2010).

The response of surface water features (rivers, lakes, streams, bogs, fens, other wetlands) to climate warming or other disturbance is not simple or uniform across the landscape (Roach et al., 2011; Rover et al., 2011). Watersheds underlain by permafrost exhibit an intense seasonality of flow paths, discharge, and stream water biogeochemistry (O'Donnell and Jones, 2006; Petrone et al., 2006; Walvoord and Striegl, 2007; Douglas et al., 2013; Barker et al., 2014). Time series remote sensing studies of the areal extent of thousands of lakes in arctic and sub-arctic Alaska have shown a general trend whereby lake area extents in the discontinuous permafrost zone tend to be decreasing, in some areas up to 31 percent of lake area coverage, while lake areal extents in the continuous permafrost zone are stable (Riordan et al., 2006). Lakes perched above continuous permafrost are believed to be more stable because they experience less vertical or horizontal drainage (Smith et al., 2005).

Fen, bog, and marsh systems, often linked hydrologically to lakes and ponds, also play major roles in nutrient cycling between aquatic and terrestrial ecosystems (Fan et al., 2013; Rober et al., 2014). Numerous studies at the Bonanza Creek Long-Term Ecological Research in interior Alaska have confirmed these results (e.g. Kane et al., 2010; Wyatt et al., 2010; Jones, et al, 2013). In the discontinuous permafrost zone, permafrost degradation may result in the partial or full disappearance of the permafrost aquiclude which can increase or decrease local hydraulic gradients depending on a variety of factors (Britton, 1957; Kane and Slaughter, 1973; Billings and Peterson, 1980; Woo, 1986; Jorgenson et al., 2001a; Yoshikawa and Hinzman, 2003). Fen systems are particularly sensitive to water table fluctuations (Roulet et al., 1992; Windsor et al., 1992). The fens on Tanana Flats provide a rich habitat for moose and serve as waterways for human access to what is otherwise inaccessible terrain. The fens are intimately coupled to the presence of permafrost along their reach and, as such, the flow regimes of the fens during the

summer season may yield insight into how and where surface hydrology in Tanana Flats is coupled with permafrost.

To support the research need of understanding the permafrost hydrogeology in lowland and upland terrains we undertook the subtasks “Permafrost-hydrogeology relationships on the Tanana Flats lowlands” and “Permafrost hydrologic modeling in upland catchments” to address hydrologic research questions in lowland and upland terrains, respectively.

3.2.2 Impacts of fire and other disturbance mechanisms on permafrost

Fire is a natural part of boreal forest ecosystem dynamics and can regenerate food sources for large mammals such as moose and decrease insect outbreaks. Historically, most fires were caused by lightning strikes. Today, humans cause the most individual fires but lightning-caused fires consume a greater extent of area burned (i.e. larger fires). Based on our analysis of lightning strike density information provided by the Alaska Fire Service, we determined that 40% of the number of fires since 1947 were caused by lightning which has an uneven distribution across the landscape (Douglas et al., 2014). Human activities, including accidents and prescribed burns, caused 47% of the fires, and the remaining 13% are attributed to a variety of other causes. Lightning strikes caused 57% of the area burned since 1947, while 26% were human caused, and 17% were attributed to other causes.

Over the period from 1947 to 2011, larger fires have occurred predominantly on lowlands, and the period from 2001 to 2011 experienced the largest area burned of any decade (Wendler et al., 2010), which also experienced an overall decrease in the number of fires per year compared to the 1970s and 1990s. These larger, more severe fires are generally associated with greater burn depths, higher carbon emissions, greater destruction of surface soils, enhanced permafrost degradation, and initiation of deciduous forests where the surface organic material burns down to mineral soils (O’Neill et al., 2002, 2003; Zhuang et al., 2003).

In interior Alaska the number of lightning derived fires has increased over time (Kasischke and Turetsky, 2006; Turetsky et al., 2010) and lightning strikes are more prevalent in upland terrain versus lowland terrain. As would be expected, lightning strikes predominantly occur in the summer months with June and July accounting for most of the lightning in a given year (Wendler et al., 2010). This is also the time when the potential for DoD live fire training caused fires is of greatest risk, particularly in impacts areas of the Stewart Creek and Tanana Flats Training Areas and Donnelly Training Area West.

Historically, black spruce forests are burned through stand-replacing fires every 70-130 years with an average return interval for the overall boreal forest of about 29-300 years (Yarie, 1981; Dyrness et al., 1986; Kasischke et al., 2000b). Fire frequency and severity depend largely on the climate (i.e., meteorology) and on human activities such as suppression and ignition (Burn, 1998). Recent increases in burn severity have led to changes in successional trajectories that break the legacy of black spruce regeneration and this has led to a shift toward deciduous forest (Johnstone et al., 2010). These ecological shifts are facilitated by the combustion of the moss understory and organic soil layer that increases the mineral soil seedbeds that favor deciduous recruitment (Chapin et al., 2000; Johnstone and Kasischke, 2005; Kasischke and Johnstone, 2005: Johnstone and Chapin, 2006). Furthermore, unlike moderately-burned stands, where the organic soil remains and spruce trees have higher recruitment success, severely burned stands favor faster-growing deciduous tree species which outcompete spruce trees because their taproots, absent in spruce, help buffer against moisture stress.

Black spruce ecosystems are often underlain by permafrost that is thermally protected by the moss groundcover, particularly where hummock-forming *Sphagnum* mosses are present (Turetsky et al., 2010; Nossov et al., 2013). The thick, organic layer in permafrost-impacted environments actively protects permafrost from thawing as part of the "ecosystem-protected permafrost" identified by Shur and Jorgenson (2007). The type of moss groundcover exerts an important control on the soil thermal regime since mosses with higher moisture content, such as *Sphagnum* mosses, protect the soil from warm summer temperatures better than feather mosses, which have a higher thermal conductivity (Yoshikawa et al., 2003). Since feather mosses are more likely to burn during fires, their presence or absence has a greater thermal impact on the thermal regime post fire. The depth of the active layer is largely dependent on the thermal conductivity of the soil which is a function of density, moisture content, and thermal phase. As a consequence, with increasing time since fire, and thus increasing forest succession, the landscape moves toward the "ecosystem protected" permafrost state. However, the immediate response of the vegetation and soil thermal regime and permafrost to fire starts the trajectory of whether the permafrost will respond to the fire or not.

In a study of post-fire soil climate dynamics near Delta Junction, Alaska, Harden et al. (2006) found that the coldest, wettest soils were accompanied by the thickest organic mats. They also report that with every centimeter of organic mat thickness the temperature at 5 cm depth was 0.5ºC cooler during the summer months. Model studies suggest that if an organic layer can remain >7-12 cm thick following wildfire, the impact of the fire on permafrost stability will be minimal (Yoshikawa et al., 2003). In fact, the largest driver of active layer thickness is the thermal conductivity of the organic layer, and as long as the organic thickness is not significantly altered, even with a decrease in surface albedo from the fire, the active layer is not significantly impacted. The importance of the organic layer and surface vegetation was also demonstrated by a study in which bulldozing of vegetation for fire lines showed more impact on active layer thickness than the severely burned black spruce during the 1971 Wickersham Dome fire. In this study the active layer was 161% deeper in the burned compared to the unburned forest (Viereck, 1982). Based on results from this and other studies it is apparent that within days to months following a high severity fire the thermal state of the ground can be changed enough to cause instant degradation of permafrost.

The degradation of ice-rich permafrost in lowland ecosystems may have particularly strong ecological impacts due to the effects of thaw settlement and subsequent water impoundment, a hydrologic shift that can cause a positive feedback to permafrost degradation and changes in vegetation composition and ecosystem function (Jorgenson and Osterkamp 2005, Jorgenson et al. 2010). Where ice volume exceeds the pore space of permafrost soils, thawing results in settlement of the ground surface. In flat lowland areas, the resulting thermokarst features usually impound water unless water can drain through coarse subsurface materials. The presence of surface water can substantially increase surface energy gains (Eugster et al. 2000), raise the temperature of underlying soil, and thaw permafrost (Jorgenson et al. 2010). Lowland forests on ice-rich soils may thus become wetland or aquatic systems as a result of thaw settlement, with associated changes in vegetation, productivity, nutrient cycling, and carbon storage (Camill et al. 2001, Jorgenson et al. 2001b, Myers-Smith et al. 2008).

The expansion of wetland ecosystems through thermokarst in boreal forest regions of discontinuous and sporadic permafrost has been attributed to interactions of climate and hydrology, as well as wildfire (Thie, 1974; Zoltai, 1993; Kuhry, 1994; Vitt et al., 1994; Camill and Clark, 2000; Jorgenson et al., 2001b; Myers-Smith et al., 2008). Wildfire is a widespread

disturbance influencing boreal forest ecosystems, and fire severity, frequency, and spatial extent of these fire scars may be increasing with climate change (Gillett et al. 2004, Kasischke et al. 2010). By combusting a portion of the surface organic layer, fire increases soil heat flux and may trigger permafrost degradation if enough of the organic layer is removed (Mackay 1995, Burn 1998, Yoshikawa et al. 2003, Viereck et al. 2008, Nossov et al. 2013). Deep and sustained permafrost degradation is associated with the development of a talik, a portion of the soil which remains unfrozen year-round. The unfrozen talik buffers remaining permafrost from freezing winter air temperatures and facilitates continued degradation (Osterkamp and Burn 2003). After fire, the re-accumulation of the surface organic layer may initiate permafrost recovery. Alternatively, changes in plant successional trajectories, hydrology, or climatic conditions may facilitate further degradation (Mackay, 1995; Shur and Jorgenson, 2007; Viereck et al. 2008; Johnstone et al., 2010; Jorgenson et al., 2010; Jafarov et al., 2013). Air temperature and snow cover are the principal physical controls over soil thermal regimes and permafrost degradation (Osterkamp and Romanovsky 1999, Zhang 2005). However, the texture of subsurface soils influences drainage and soil thermal properties, contributing to spatial variations in permafrost status and response to fire across the landscape (Johnson et al., 2011; 2013; Jorgenson et al., 2013a, b, Nossov et al., 2013; Pastick et al., 2014).

Considering the high frequency of wildfires and the potential for large shifts in boreal ecosystems from permafrost thaw, there is a need to better understand the sensitivity of permafrost to fire. To support the research need of understanding how time since fire can affect the thermal state of permafrost and vegetation in lowlands terrains on DoD training areas we undertook the subtask "Vulnerability of permafrost to fire-initiated thaw in interior Alaska." We focused on the effects of fire on permafrost within the Tanana Flats Training Area of interior Alaska, a landscape characterized by organic-rich, fine-grained soils associated with flat, abandoned floodplain deposits. We primarily relied on a chronosequence study design with fire scars from ~1930 to 2010 and utilized soil thermal modeling to further assess patterns in permafrost responses to varying soil and climatic conditions in lowland forests. Our main objectives were to: 1) compare vegetation and soil characteristics in fire scars of different ages; 2) assess the magnitude of permafrost thawing and thaw settlement; 3) document the effects of fire on soil temperatures; and 4) evaluate the soil vs. climatic controls over these responses through soil thermal modeling.

3.2.3 Identifying/mapping permafrost features

The upland and lowland terrains comprising the main interior Alaska training ranges are underlain by discontinuous permafrost that ranges from a few meters to over 50 m thick and is most commonly found on north facing slopes, in valley bottoms, and under poorly drained soils (Hopkins et al., 1955; Anderson, 1970; Hamilton et al., 1983; Jorgenson et al., 2001a, b; Douglas et al., 2008; Douglas et al., 2016).

The permafrost is typically tens of meters thick (Racine and Walters, 1994; Chacho et al., 1995; Jorgenson et al., 2008a). On the Tanana Flats, where permafrost is strongly associated with abandoned floodplain deposits with peat-rich, silty soils, ~50% of the area is in some stage of permafrost degradation (Jorgenson et al., 1999). In locations with taliks (zones of unfrozen material created as permafrost thaws in areas below the seasonally thawed active layer) the spatial extent of permafrost bodies is extremely difficult to measure or predict. The horizontal and vertical heterogeneity of permafrost distribution in the area prevents the establishment of any simple estimation of permafrost extent.

Permafrost stability is intricately coupled with ground ice abundance, the soil thermal regime, vegetation succession, terrain physiography, and disturbance. As a consequence, there is a need to correlate the response of permafrost to disturbance over both space and time. Of principal concern are transition zones where frozen and thawed material meet. This is where the effects of permafrost thawing will be most pronounced because as the thaw front moves into previously frozen material subsidence, changes in hydrogeology, and soil and vegetation changes can be initiated. Identifying and predicting the response of permafrost to warming or disturbance requires accurate and detailed assessment of subsurface characteristics, predominantly permafrost extent.

Geophysical techniques, particularly electrical resistivity tomography (ERT), have been used to map subsurface permafrost and to link terrain geomorphology to permafrost ice content (Lawson et al., 1996; Yoshikawa et al., 2006; Douglas et al., 2008; Lewkowicz et al., 2011; Hubbard et al., 2012; McClymont et al., 2013; Kneisel et al., 2014). Airborne resistivity has been used to map permafrost over large spatial extents but its application is limited due to high acquisition costs (Minsley et al., 2012). ERT works well in permafrost terrains because the electrical resistivity (in Ω–m) of an earth material (rock, unfrozen soil or frozen soil) is controlled by the mineralogy, porosity, moisture content, cation and anion concentration of pore moisture, temperature, and whether pore waters are frozen or thawed (Hauck and Kneisel, 2008). Resistivity (ρ) values of frozen soils are generally 10 to 1,000 times greater than unfrozen or brine-rich soils (Harada and Yoshikawa, 1996). When combined with topographic information like aerial imagery and light detection and ranging (LiDAR), ERT has been used to link permafrost distribution with terrain geomorphologic and cryospheric properties (Hubbard et al., 2012; Lewkowicz et al., 2011). This multidisciplinary research approach was well suited for application to the Tanana Flats Training Area to identify where and how permafrost bodies are present in the subsurface. Results from this part of the study could be used to develop standoff techniques for mapping permafrost in other locations.

To support the research need of mapping the extent of permafrost in lowlands terrains and in identifying what biophysical attributes could be used to map permafrost in the subsurface we undertook the subtask "Biophysical, geophysical, and airborne measurements of permafrost geomorphology."

3.3 Climate impacts on DoD activities and infrastructure in interior Alaska

Climate warming is expected to have pronounced effects on high latitude ecosystems, especially regions underlain by warm discontinuous permafrost such as the interior of Alaska (Arctic Climate Impact Assessment, 2005; White et al., 2007). Large areas of permafrost in interior Alaska have shown signs of degradation (Racine and Walters, 1994; Jorgenson et al., 2001) and this is expected to continue with further climate warming (Marchenko et al. 2008). These changes in permafrost distribution have dramatically affected ecosystems in interior Alaska through widespread drying in some regions and wetland expansion in others (Osterkamp and Jorgenson, 2006; Racine and Walter, 1994).

Climate projections for the 21st century indicate there could be a pronounced warming in the Arctic and sub-Arctic regions (Arctic Climate Impact Assessment (ACIA), 2004; Intergovernmental Panel on Climate Change (IPCC), 2007). This will significantly change the lateral and vertical distribution of permafrost in many areas of Alaska (Marchenko et al., 2008) which could lead to widespread thermokarst and talik development and potentially a thicker seasonally thawed (active) layer (Osterkamp and Jorgenson, 2006). Groundwater recharge,

runoff and water storage will be altered considerably, thereby increasing the role of subsurface flow in annual river runoff. This will change the seasonality of Alaskan river discharge by increasing its winter portion and, in some locations, may increase the total discharge as well (Peterson et al., 2002).These changes in permafrost and hydrologic dynamics will dramatically affect surface hydrological, soil and vegetation regimes which will have severe ramifications for how, where, and when the Department of Defense (DoD) can train in Alaska. The 2010 Quadrennial Defense Review Report mentions this threat to the DoD, stating "The Department is developing policies and plans to manage the effects of climate change on its operating environment, missions, and facilities."

Forecasting ecological responses to climate warming is complicated by soil type, precipitation, surface and ground water hydrology, vegetation, slope, aspect, fire prevalence, and the thermal state of permafrost. Currently, the DoD lacks effective land management tools that can estimate current and future relationships between changing ecological conditions and training load. This limits the DoD's ability to sustain or ecologically restore training resources, especially if climate warming is expected to fundamentally alter landscapes. Anticipated ecosystem changes in interior Alaska will likely have severe ramifications for how and where the DoD trains in Alaska over the next 20, 50 and 100 years. One of the best ways to identify how and where diverse local-scale ecosystems (ecotypes) will respond to climate change or disturbance is to quantify ecosystem change over time and develop trajectories for how and where different ecotypes respond to and evolve from disturbance.

To address this research need we undertook the subtask "Ecosystem transition modeling to identify landscape change." We used repeat imagery analyses to quantify, at the point scale, historical areal changes over the last 25–50 years across all interior Alaska Army training ranges.

4. MATERIALS AND METHODS

Introduction and Scope

The ultimate objective of this four year SERDP-funded project was to provide U.S. Army Alaska with scientifically defensible geospatial decision support tools to help them make sound land management and infrastructure development decisions. The project included a set of subtasks designed to identify missing research needs and to provide results that inform the GIS-based management tool. Some of our project subtask efforts included substantial field measurement efforts.

Due to the large spatial extent and heterogeneous nature of the vegetation, hydrogeology, and permafrost extent on USARAK training lands in interior Alaska we focused our field measurement efforts at locations where we could make impactful measurements in the relatively short timeframe allotted. Many of our permafrost biophysical and fire disturbance measurements were focused at sites on the roadless Tanana Flats that were near one another but provided a broad range of site conditions over a short area. Fen systems nearby were the sites of our focused surface hydrology measurements. We used historical hydrology measurements from the Caribou-Poker Creeks Research Watersheds (CPCRW) to refine and test the hydrogeologic modeling.

The overall project approach was to perform the five different field and modeling research efforts with the end goal of synthesizing the project results with a broad array of geospatial and climate projection information to develop the GIS based decision support system. Throughout the process we worked with USARAK land managers to ensure that what was developed for the GIS tool included information that they could use and would use. Here we provide the materials and methods information for the five different research subtasks.

4.1 Permafrost-hydrogeology relationships on the Tanana Flats lowlands

Groundwater levels and groundwater temperatures were measured in two fen systems and one lake on the Tanana Flats (Figure 9, Table 1). The deployed sensors/loggers included non-vented pressure transducers (HOBO U20 Fresh Water Level Data Logger 13 feet, U20-001-04, Onset Hobo Dataloggers), which were deployed inside a 5 cm diameter white PVC pipe. An additional sensor was hung from a nearby tree to obtain air pressure at some sites (Fen 1 Mid, Lake, and Fen 2 upper). We secured the logger to the top of the PVC pipe via a slack line for easy access. The sensors rested on top of a 3 cm diameter metal rod, which was secured deeper than the seasonal freeze-thaw depth (usually 2 m). Accordingly, the sensors were decoupled from any frost heave that the PVC pipe may have experienced. The sensors were between 1 and 1.5 m below the water level in the fall. Detailed surveys of the absolute water elevation were made at least once per year using a differential GPS system (dGPS). Wells were accessed via helicopter or snow machine.

Figure 10 includes photographs of the linked pond-fen system for which we measured water elevation in the wells in an effort to link the horizontal movement of surface-shallow subsurface-groundwater across Tanana Flats. The pond feeds the system by draining to the subsurface. Lateral flow through the shallow subsurface (believed to be controlled by permafrost channels) ends at the fen where the water is emitted to the surface. These pond and fen systems are critical habitats and a major component in the hydrology of the Tanana Flats ecosystem. Permafrost degradation is likely to allow for deeper flow paths and the loss of water from the shallow subsurface to the deeper subsurface. This could lead to drying of the fen ecosystem which would cause major ecological and habitat changes.

We measured water levels continuously from October, 2011 to October, 2014. To our knowledge this is the only lake-fen water level information ever continuously measured across an interior Alaska fen system. We accessed the sites two to three times per year to make manual water level dGPS measurements. These were used to develop a hydrologic model correcting the air pressure (measured at the sites and at the Fairbanks International Airport) to the water level pressures. Site specific hourly air pressure measurements were used, with the repeat high resolution GPS measurements of water level elevation at each site, to correct the hourly water level datalogger measurements for ambient air pressure changes. The computer program HOBOWare (Onset Computer Corporation, Bourne, Mass.) provides this correction and calculates water levels over time. Based on the measurement error for the z coordinate direction with the GPS (+/-5 cm) and the pressure transducer (+/-0.3 cm of water) we estimate the vertical water level elevation error to be +/- 6 cm. With the corrected water level values we could make a direct comparison of the water levels across the sites to assess how seasonal and spatial trends and responses to precipitation events yield insight into permafrost hydrogeology in these systems.

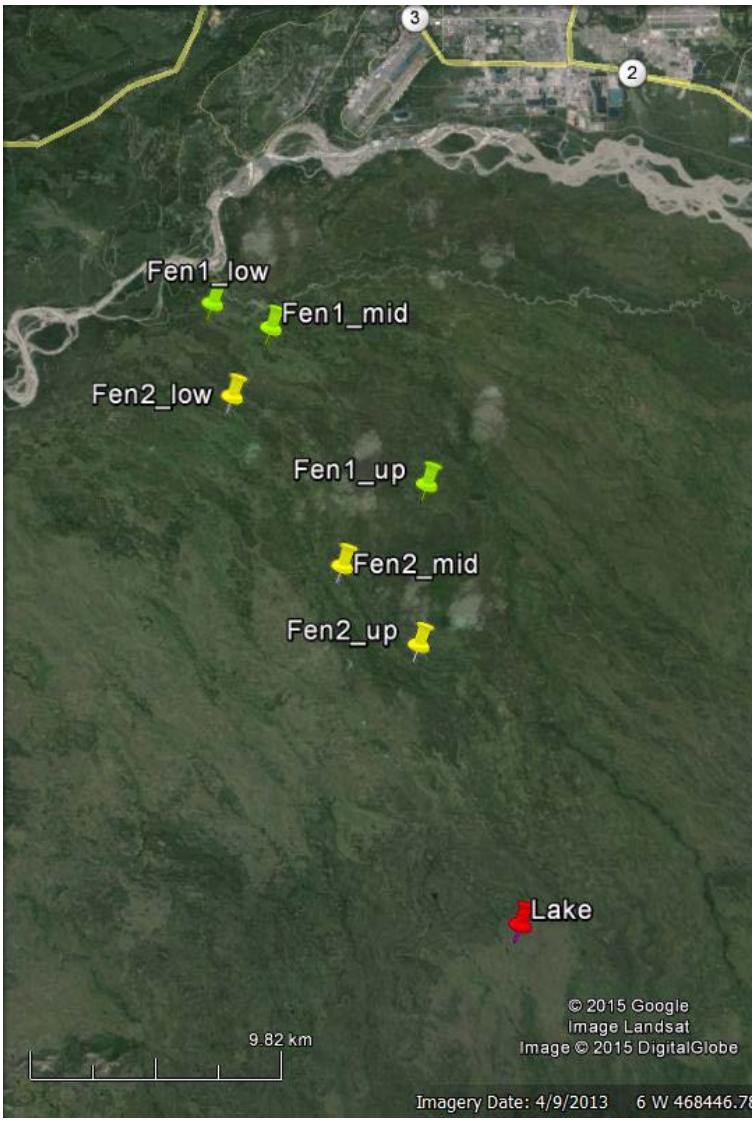

Figure 9. Locations of the groundwater monitoring wells in the two parallel fen systems (Fen 1 and 2) and the lake. Fen 1 and Fen 2 are separate fen systems but both are believed to be linked to the lake as the initial surface water source. Wells were installed at every marker location.

Table 1. Location information for water level monitoring sites on Tanana Flats and the elevation of the water surface in early October 2014 (the most recent time in which water levels were measured).

Site name	UTM easting	UTM northing	Water level 10/2/14 (masl)
Fen 1 lower	452009	7178760	ND
Fen 1 middle	454293	7177767	128.48
Fen 1 upper	460319	7171538	135.99
Fen 2 lower	452730	7175101	129.06
Fen 2 middle	456963	7168377	136.42
Fen 2 upper	459919	7165244	142.21
Lake	463740	7154229	162.58

UTM: Universal Transverse Mercator. All sites are in Zone 6.

masl: meters above sea level.

ND: not detected

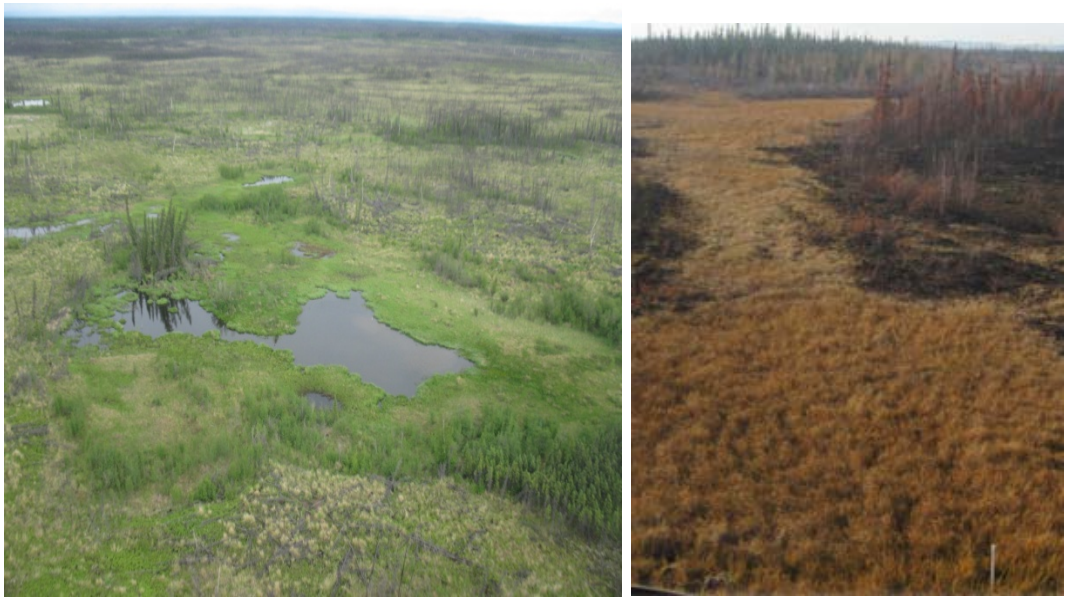

Figure 10. Left: the Lake where flow is initiated. A water level logger (not visible) is located in the middle of the lake. Right: The fen outlet (white stake in lower right, Fen 2 lower, where water level is measured.

4.2 Vulnerability of permafrost to fire-initiated thaw in interior Alaska

4.2.1 Study area and design

Our study area was within the northern portion of the Tanana River Valley (Tanana Flats) of interior Alaska. This physiographic region extends north from the foothills of the Alaska Range to the hills north of the Tanana River near Fairbanks (Figure 11; Van Cleve and Viereck, 1983). This area encompasses 15,000 square miles (3.8 million hectares). The Tanana Flats is situated in a large alluvial fan and abandoned floodplain complex, formed by the deposition of fluvial and glaciofluvial sediments from the Alaska Range. The history of channel migration, deposition, and permafrost dynamics creates a fine topographic relief within this landscape that is associated with differences in vegetation, permafrost, and hydrology (Jorgenson et al. 2001a). Forested areas typically occur on higher permafrost plateaus and bogs and fens occur on in thermokarst depressions. These relative elevations can shift with the formation or thawing of ice-rich permafrost.

Our field sites are comprised of five 200 to 300 m long transects located in the northern third of the Tanana Flats lowland south of Fairbanks, Alaska (Figure 11). Study sites were established in the forested portions of collapse-scar bog complexes in five fire scars (~1930s, 1975, 1988, 2001, and 2010). Fire years were ascertained from tree-ring dating, air photo and satellite imagery interpretation, and fire-perimeter maps from the Alaska Interagency Coordination Center.

The ~1930s, 1975, 1988, and 2001 sites had been visited numerous times over the previous years by members of the project team. Their slope, gradient, aspect, soil composition, and permafrost morphology were similar and, as such, they provided a set of comparable sites except for their time since fire. The 2010 fire occurred in similar terrain nearby in the year prior to study initiation. After some field and remote sensing survey measurements we identified the location of our 2010 field site to provide optimal comparison to the other fire scar locations. The average return interval for boreal forest wild fires ranges from 29 to 300 years (Yarie, 1981; Dyrness et al., 1986; Kasischke et al., 2000b). Based on numerous vegetation, soil, and permafrost degradation studies at the ~1930s site we identified that location as a control to which the subsequent fire scars could be compared (Jorgenson et al., 1999; 2001b).

Field sampling was conducted from May 2011 to October 2014. Within each fire scar, a 200–300 m transect was established that was oriented to cross both burned patches and thermokarst bogs and fens. Along each transect, three permanent intensive plots (5 x 10 m) were established in separate burn patches (separated by thermokarst bogs) for monitoring vegetation and soils. For vegetation, two addition extensive plots were established along each transect to increase sample size.

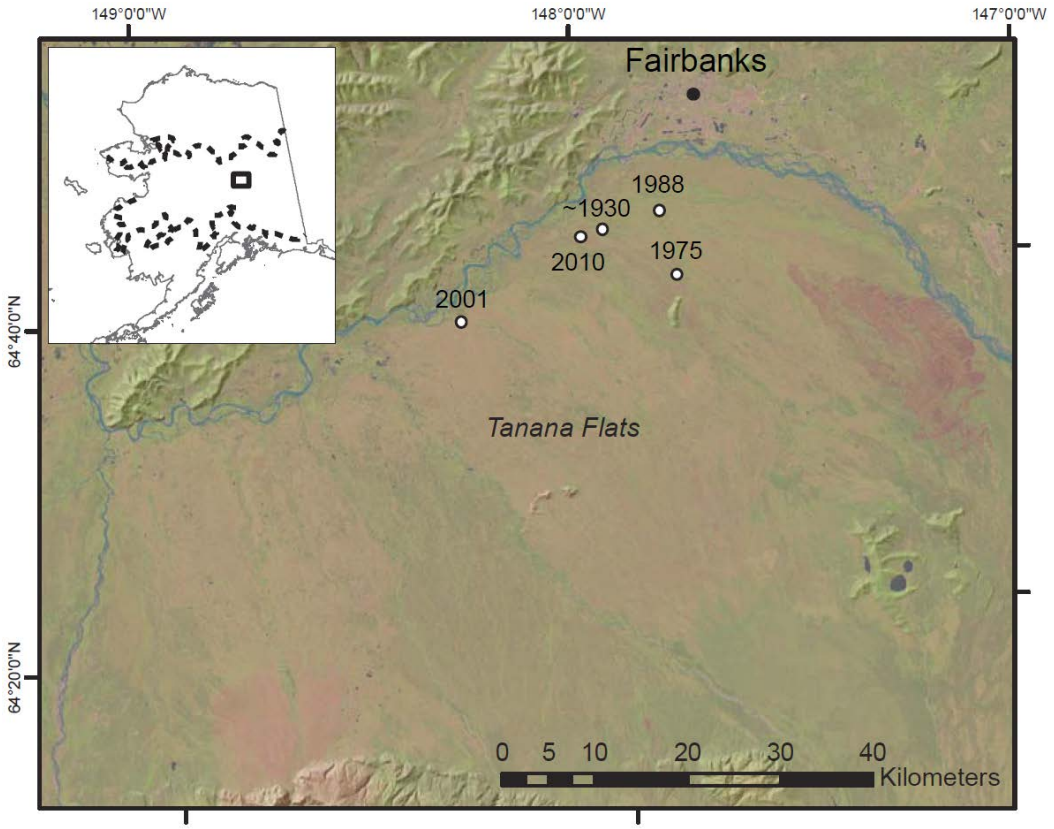

Figure 11. Map of the study sites (named by fire year) overlain on satellite image and digital elevation model, with inset showing location of the Tanana Flats study area within the discontinuous permafrost zone of Alaska (dashed lines; Jorgenson et al. 2008a). The Landsat 8 image (acquired June 18, 2013) is displayed as a color composite of bands 6 (SWIR), 5 (NIR), and 4 (red).

4.2.2 Vegetation

Vegetation percent cover was sampled in each plot using a point-sampling technique employing a 100-point grid to estimate percent cover of each plant species. Plant community composition was analyzed with nonmetric multidimensional scaling (NMDS), a multivariate ordination technique, using PC-ORD 6.0 (McCune and Grace 2002, McCune and Mefford 2011). The ordination axes represent the dominant patterns of species composition. Correlation analyses of the ordination axis scores with species and environmental data were conducted and presented as biplots, in which vector length and direction represent the strength and direction of the correlations. Data were assessed for normality and transformed prior to analysis.

4.2.3 Soil physical characteristics

At each permanent plot, soil plugs (8 cm diameter and up to 50 cm long cylindrical shaped cores extracted using a modified soil sampling augur) were extracted for unfrozen surface soils. Below this, frozen soils were cored to 3-4 m depths using a 7.5 cm diameter SIPRE (Snow, Ice, and Permafrost Research Establishment) corer. Soil stratigraphy was described according to Natural Resources Conservation Service (NRCS) methods. Coarse-fragment (>2 mm) percentage was visually estimated. Cryostructures were described using the system by French

and Shur (2010). Total organic carbon (OC) content (total carbon minus C-CO_3) was determined at the Colorado State University Soil, Water, and Plant Testing Lab using a LECO TruSpec CN combustion furnace (St. Joseph, Michigan) following methods of Nelson and Sommers (1996). Several samples were taken at distinctive breaks in peat stratigraphy for radiocarbon dating at the National Ocean Sciences Accelerator Mass Spectrometry Facility and Geochron Laboratories.

Volumetric soil samples were obtained approximately every ~20 cm and were weighed before and after oven-drying at 60°C for determination of moisture/ice content and bulk density. Volumetric soil moisture was calculated for each unfrozen stratigraphic layer and was weighted by the thickness of each layer to calculate the weighted mean volumetric water contents of the active layer in late summer. Volumetric ice content of the permafrost to 3 m depth was calculated using the same methods, and water-equivalent depth of moisture in permafrost was determined (Brown et al., 2015).

4.2.4 Thaw depths and thaw settlement

Thaw depths, ground surface elevations, and water surface elevations were measured at 1 m intervals along each transect. Thaw depth was measured in late August- early September using a metal probe. Elevations of the ground surface and of the water level of adjacent bogs were determined using high resolution dGPS and differential leveling.

Potential thaw settlement at each plot was calculated from thaw strain estimates for each layer of permafrost in the upper 3 m of soil, and represents the predicted vertical surface settlement following the thawing of existing permafrost to this depth (Crory, 1973; Pullman et al., 2007). For each permafrost layer:

$$T_l = (D_u - D_f)/ D_u \quad (1)$$

where T_l is thaw strain of the layer, D_u is the estimated dry density of the unfrozen soil (estimated using the average dry density of unfrozen samples of similar horizons and soil textures as the permafrost soil), and D_f is the measured dry density of permafrost soil.

Potential thaw settlement of a given layer (P_l) is calculated as:

$$P_l = T_l * t_l \quad (2)$$

where T_l is thaw strain of the layer and t_l is the thickness of the soil layer. The total potential thaw settlement at a site is the sum of the potential thaw settlement for each layer in the upper 3 m of the soil column.

Potential thaw settlement was subtracted from current surface elevations at the soil sampling sites to derive post-thaw surface elevations. The current and post-thaw elevations of the ground surface relative to the bog water level were calculated by differencing to infer the potential for water impoundment.

4.2.5 Soil thermal regimes

At each intensive plot, soil temperatures were recorded at two-hour intervals throughout the year using two-channel dataloggers (HoboProV2, Onset Corp.) with thermistor probes installed at 5 cm and 100 cm depths. Mean annual surface temperatures (MAST), mean annual deep temperatures (MADT), thawing degree-day sums (TDD), and freezing degree-day sums (FDD)

were calculated based on hydrological year (mid-September to mid-September), with hydrological years named by the calendar year of the end date. After assessing variables for normality and homoscedasticity, comparisons of thermal metrics between fire scars were conducted with one-way ANOVA (JMP 10.0.0, SAS 2012). Least square mean differences were calculated with Tukey HSD post hoc tests. Statistical significance was considered with $p < 0.05$.

4.2.6 Thermal modeling simulations

The Geophysical Institute Permafrost Laboratory (GIPL) thermal model was used to compare the sensitivity of permafrost to variations in organic layer thickness (OLT) and in relation to meteorological variables (Romanovsky and Osterkamp, 2000; Sergueev et al., 2003). The GIPL numerical transient model uses daily air temperature and snow depth forcing data and subsurface soil properties to simulate ground temperatures by solving nonlinear heat diffusion equations, taking into account the effects of unfrozen water during freezing and thawing. Climate data for the Fairbanks International Airport from 1930-2014 were used in the simulations (Alaska Climate Research Center 2014; Figure 13).

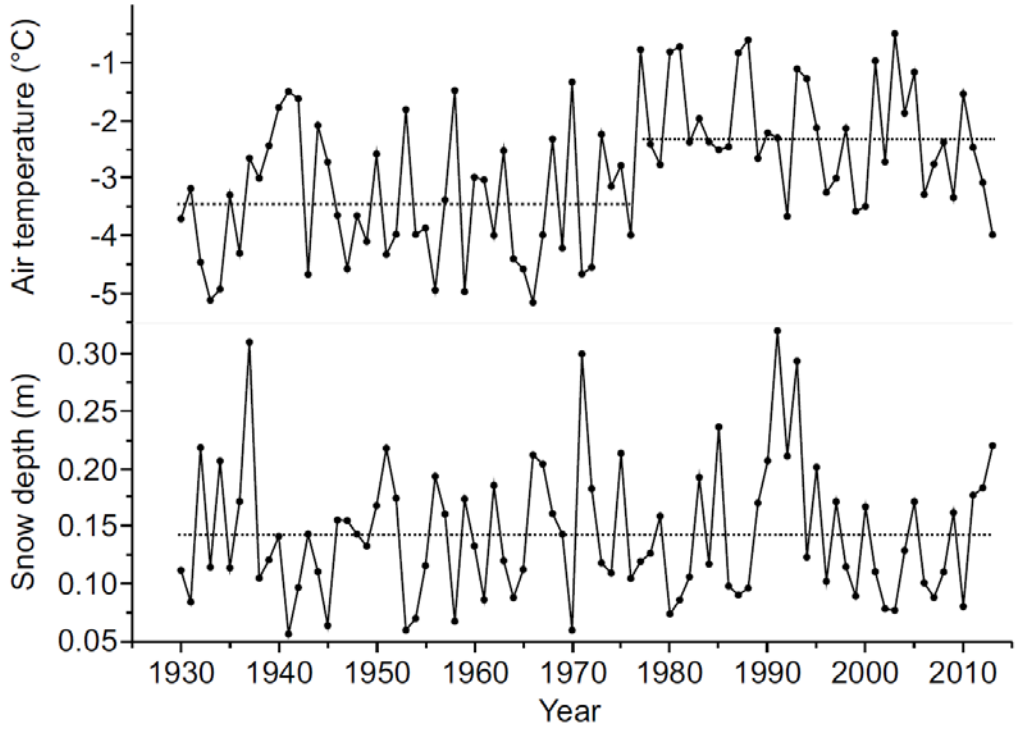

Figure 12.Mean annual air temperatures and snow depths at the Fairbanks International Airport, computed by hydrological year (October 1 – September 30) from 1930-2013 (Alaska Climate Research Center, 2014). Dotted lines indicate mean values over the specified time period.

The model was parameterized to reflect the observed stratigraphy and soil moisture profiles at a silt loam dominated field site (Table 2). The model was calibrated using the first half of the measured soil temperature record. Volumetric water content, thermal conductivity (frozen and unfrozen), heat capacity (frozen and unfrozen), and unfrozen water content curves for each soil layer were adjusted through the calibration process, and were within the range of expected values

by soil type (Farouki, 1981; Romanovsky and Osterkamp, 2000; O'Donnell et al., 2009; Jafarov et al., 2012, 2013). When soil temperature curves approximated measured values, the calibrated models were validated using the second half of measured temperature data. Modeled active layer depths were within 10% of measured values, and modeled mean annual temperatures were within 0.3˚C of the measured values.

Table 2. Subsurface soil parameters used in thermal model simulations for silt loam-dominated site with varying levels of organic layer thickness (OLT). Thickness, volumetric water content (VWC), thermal conductivity (W m^{-1} K^{-1}) of thawed (k_t) and frozen (k_f) soil, and heat capacity (J m^{-3} K^{-1}) of thawed (C_t) and frozen (C_f) soil are shown for each soil layer.

Soil layer	OLT=30 cm	OLT=15 cm	OLT=7 cm	OLT=0 cm	VWC	k_t/k_f	C_t/C_f (10^6)
Amorphous	0.3	0.15	0.07	0	0.2	0.20/0.60	2.6/2.2
Silt loam and organic	0.09	0.09	0.09	0.09	0.6	0.70/2.10	2.5/1.7
Silt loam	2.74	2.74	2.74	2.74	0.57	1.30/2.10	2.5/1.7
Sand and gravel	96.87	97.02	97.1	97.17	0.33	1.90/2.50	1.8/1.6

Simulations were run to model the effect of OLT on soil temperatures. The thicknesses of the unfrozen organic layer that were tested were 30 cm, 15 cm, 7 cm, and 0 cm, assuming the same thermal and moisture properties as in the model calibration. The models were run with a 30-year spin-up, in which climate forcing data from 1930 was repeated to allow the soil temperatures to stabilize prior to initiating simulations at time zero.

4.3 Biophysical, geophysical, and airborne measurements of permafrost geomorphology

4.3.1 Study Area

The ~8,000 km^2 Tanana Flats lowland is dominated by a combination of gravelly alluvial deposits extending northward from the northern slopes of the Alaska Range and abandoned floodplain deposits associated with the braided Tanana River (Walters et al., 1998; Jorgenson et al., 1999). The topography has extremely low elevational gradients (~1 m/km). Hydrology is affected by channelized surface flow in small streams, some surface and shallow subsurface flow across fen systems, and by areas with substantial groundwater discharge (Racine and Walters, 1994). The Tanana River, the largest tributary of the Yukon River, is a major physiographic barrier forming the boundary around the northern portion of the Tanana Flats lowland. Vegetation in the Tanana Flats lowland is a highly interspersed mixture of forest, scrub, bog, fen, and open water bodies (Jorgenson et al., 1999; 2001; Douglas et al., 2014). Forested regions are generally located on permafrost plateaus, while bogs and fens tend to be located in low lying areas that commonly form in thermokarst depressions. Long, linear fens with floating vegetation mats are associated with groundwater discharge and are generally free of subsurface permafrost (Racine and Walters, 1994; Racine et al. 1998). The fens are bordered by forests growing above permafrost or perched above well-drained sand and gravels. Sphagnum bogs are common in round thermokarst depressions within the forest patches and they are isolated from regional groundwater movement. The variable forest stands that cover the Tanana Flats lowland reflect differences in time since fire, permafrost extent, soil composition, and flood frequency (Jorgenson et al., 1999).

Bodies of discontinuous permafrost in the Tanana Flats lowland range from 0.5 to 12 m in vertical thickness (Racine and Walters, 1994), but sections up to 47 m thick have been documented (Chacho et al., 1995). Permafrost is abundant in areas with peat-rich fine-grained

soils. Volumetric ice contents in birch forests can reach greater than 50% (Osterkamp et al., 2000, Jorgenson et al., 2001a). Collapse-scar bogs are common in lowland black spruce forest regions where ice contents are typically closer to 20%. Where present, ice-rich and ice-poor permafrost gelisols are predominately composed of gravel, silt, and sand (Pergelic Cryochrepts) overlaid by organic material (Pergelic Cryofibrists and Histic Pergelic Cryofibrists; Brabets et al., 2000). In a 1990s study in the northern portion of Tanana Flats 17% of the area was unfrozen, 48% had stable permafrost, 31% was partially degraded, and 4% was totally degraded (Jorgenson et al., 1999). The permafrost in this area of the boreal biome is considered relatively 'warm' (mean annual temperatures of 0 to –3ºC) which makes it particularly sensitive to the effects of climate change (Jorgenson et al., 2001a).

The climate in interior Alaska is continental with a mean annual air temperature of -3.3ºC, typical mean summer temperatures of 20°C and mean winter temperatures of -20°C. Yearly extremes range from 38°C to -51°C (Jorgenson et al., 2001a). The mean annual precipitation is 28 cm (Wendler and Shulski, 2009), with a typical annual snow fall of 1.7 m (Jorgenson et al., 2001a). The snow pack represents 40-45% of the mean annual precipitation (Liston and Hiemstra, 2011).

4.3.2 Fieldwork

This study was designed to assess biophysical and permafrost characteristics across a chronosequence of time since wildfire. We focused our efforts at the same fire scars that were investigated for the vulnerability work (Section 4.2.1). These include fire scars from ~1930s, 1975, 1988, 2001, and 2010.

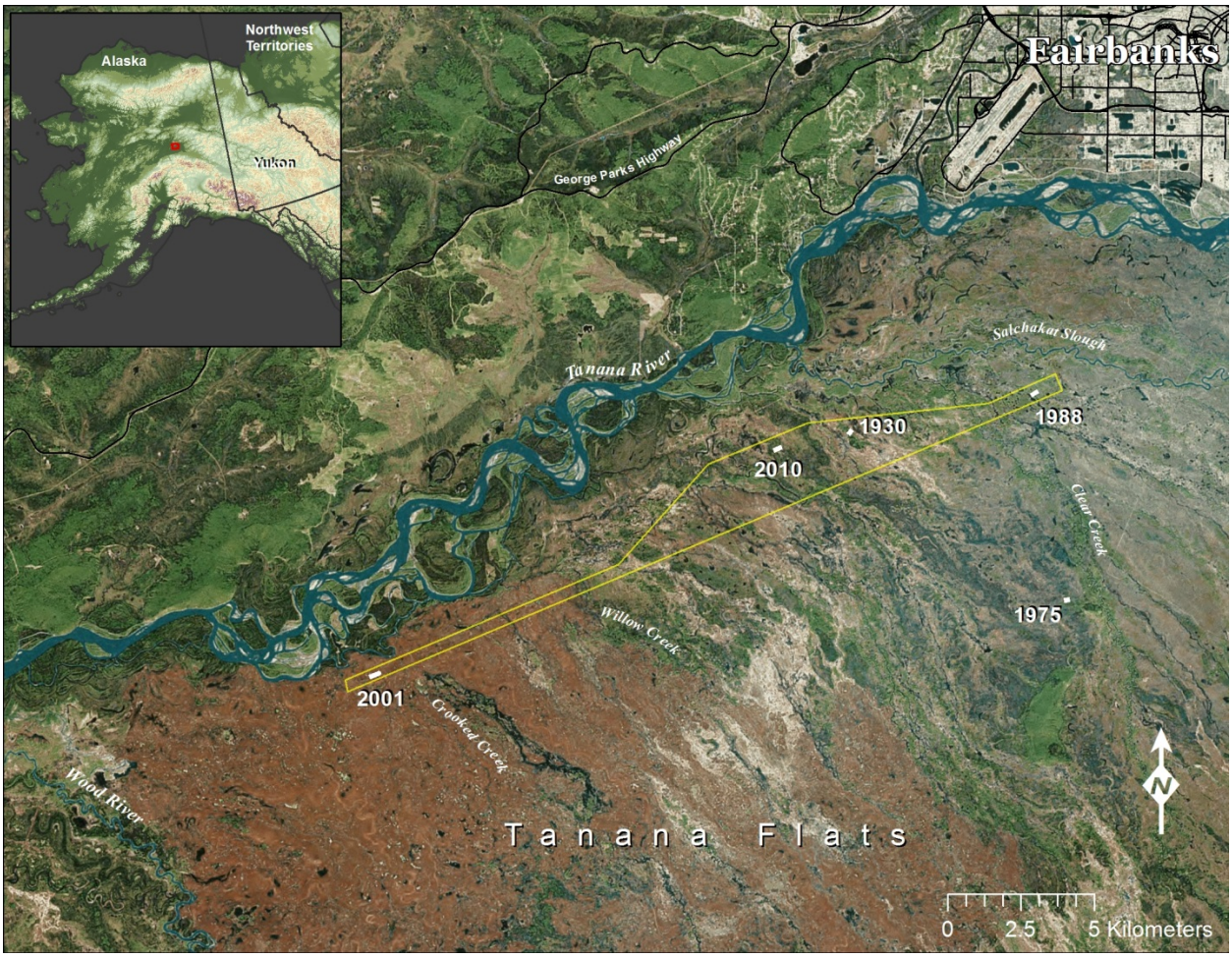

Figure 13. An aerial true color image of the northwestern portion of the Tanana Flats lowland near Fairbanks, Alaska. Locations of the five field locations, identified by the year of the fire that created the fire scar, are denoted. The yellowed line denotes the region within which airborne LiDAR was acquired in May, 2014.

The five remote sites were accessed by helicopter multiple times between the spring of 2011 and late fall 2014. In 2011 the transect end points were surveyed and 1 m wide trails were cleared of large woody vegetation to facilitate access for surveying and geophysical measurements. A summary of the location, transect length, and maximum and minimum elevations at each site is provided in Table 3. Maximum seasonal thaw depths were determined at 1 to 5 m intervals along each transect at the end of summer (late August to early October) from 2011 to 2014. We used a 1 cm diameter graduated metal rod ("frost probe") that extended to as much as 2.5 m in length. For each thaw depth measurement, the frost probe was pushed vertically into the ground to refusal to establish the distance between the ground surface and the ice-bonded base of the active layer/top of permafrost (Shiklomonov et al., 2013). If contact with permafrost was not made, the maximum observed depth of soft, unfrozen soil was recorded. In 2012 we made dGPS measurements at 1 m intervals along each transect to accurately survey the elevation, northing, and easting within 10 cm. Ground-surface elevations were also determined using differential leveling.

Table 3. Transect locations, distances, and elevation information.

	Site name (fire year)				
	1930	1975	1988	2001	2010
Transect start northing (UTM)	7177762	7171948	7179062	7169426	7177045
Transect start easting (UTM)	454293	461736	460639	438122	451616
Transect end northing (UTM)	7177614	7171934	7178923	7169304	7176954
Transect end easting (UTM)	454148	461520	460400	437820	451403
Transect distance (meters)	200	200	200	300	300
Maximum elevation along transect (meters) in 2012	128.91	139.781	132.43	123.518	128.169
Minimum elevation along transect (meters) in 2012	127.23	138.706	130.87	122.707	127.127
Number of elevation measurements	221	326	210	319	195

All four years of thaw depth measurements from the five sites and detailed information on the vegetation, soils, geomorphological characteristics, and permafrost composition are provided in Brown et al. (2015). The 2012 thaw depth measurements are presented here because they correspond with the same time the ERT surveys were performed. Some additional thaw depth measurements for 2013 or 2014, particularly maximum observed unfrozen depths, are provided for some sites to provide supporting data for surface zones lacking near-surface permafrost.

We used an 8 cm diameter SIPRE corer to extract 3 to 4 m long cores from multiple locations along each transect. Detailed cryostructural and stratigraphic information are provided in Brown et al. (2015) but our main focus for the core information here is to support whether permafrost is present or absent along the transects.

Vegetation types along segments of the transects were assigned ecotypes using the classification developed for the area by Jorgenson et al. (1999). We modified the system, however, by just using the vegetation terms (e.g., broadleaf forest) and dropped the physiography and moisture modifiers used in the ecotype terminology to simplify the analysis and presentation. In addition, we split the bogs into early- (sedge-sphagnum bog meadow) and late- successional (dwarf shrub-sphagnum bog) vegetation types to better differentiate young thawing margins from older bog centers.

4.3.3 Satellite and LiDAR imagery

Recent high-resolution satellite imagery was obtained for all of the sites, and the available images were selected based on their clarity and lack of cloud cover. All of the imagery used consisted of multispectral imagery (usually 2–4 m resolution) and a companion panchromatic image (~0.5–0.6 m). Using Erdas IMAGINE 2013, images were orthorectified, then pan-sharpened with the Hyperspherical Color Space (HCS) Resolution Merge to yield sub-meter detail. The 1930 and 2001 burn sites were collected by Geoeye1 on 5 May 2011. The 1975 and 1988 burn sites were obtained by WorldView-2 on 21 May 2010. The 2010 burn site contains imagery from the 21 May 2010 and 5 May 2011 images, representing pre- and post-fire conditions.

Airborne LiDAR imagery were collected from the 1930, 1988, 2001, and 2010 fire scars from May 9-11, 2014 by Quantum Spatial Incorporated (Anchorage, Alaska). A Leica (Wetzlar, Germany) ALS70 system (1064 nm) mounted in a Partenavia aircraft was used to acquire the imagery at an average pulse density of ≥25 pulses/m^2 at an altitude of 1,000 m. Position of the

aircraft was measured twice per second (2 Hz) by an onboard differential geographic positioning system (dGPS) unit, and aircraft attitude was measured 200 times per second (200 Hz) as pitch, roll and yaw (heading) from an onboard inertial measurement unit (IMU). To allow for post-processing correction and calibration, aircraft and sensor position and attitude data were indexed by GPS time. The measurement accuracy yielded a root mean square error (RMS) of ≤9.2 cm and yielded a spatial resolution of 0.25 m. The digital elevation model created from the LiDAR was hydro-flattened to correct for streams meeting a minimum width of 15 m and for water bodies ≥ 4,000 m^2 in area.

Hydro-flattening corrects for missing information due to absorption of the near infrared LiDAR signals by water. The hydro-flattening process eliminates artifacts in the digital terrain model caused by increased variability in ranges or dropouts in laser returns due to the low reflectivity of water. To address this, larger water bodies were flattened to a consistent water level. However, none of the water bodies present in our imagery (i.e., the areas including and around the transects at each site) were large enough to have been hydro-flattened.

4.3.4 Electrical resistance tomography

We used an Advanced Geosciences Incorporated (Austin, Texas) "SuperSting" R8 eight channel portable induced polarization galvanic earth resistivity meter for the ERT measurements. Similar arrays have proven exceptional in identifying permafrost in the continuous zone of the high Arctic (Fortier et al., 2008; Hubbard et al., 2012) and in discontinuous permafrost in the Yukon, Canada (Lewkowicz et al., 2011) and near Fairbanks (Osterkamp et al., 1980). Permafrost resistivity values have been established for the Fairbanks area in multiple studies. Resistivity values of 800 Ω-m were reported for syngenetic permafrost near Fairbanks at -5°C (Hoekstra and McNeill, 1973). Permafrost resistivity values of >600 Ω-m were reported as indicative of permafrost at the CRREL Farmer's Loop Permafrost Experimental Station (Douglas et al., 2008). Values of 600–10,000 Ω-m were measured at a pingo located 4 km west of the Permafrost Experimental Station (Yoshikawa et al., 2006). For the purposes of this study, resistivity values of 1,000 Ω-m or greater were indicative of permafrost.

Six cables, each with 14 take-out electrodes, were employed at 2- m spacings at four of the sites to achieve a maximum penetration depth into the subsurface of ~25 m. At the 1975 site, a 3-m spacing was used to provide a maximum penetration depth of ~35 m. The R8 control module was set up between electrodes 42 and 43. A dipole-dipole array was used for all measurements because it has been found to best represent spatial aspects of ice-rich terrain and to provide optimal horizontal resolution to detect vertical structures in permafrost terrains (Kneisel, 2006). Contact resistance was measured at each electrode prior to collecting any survey measurements for quality assurance and to check cable connectivity. When contact resistance values were higher than 2,000 Ω-m water, salt water was added to the electrode installation. Contact resistance was re-checked until adequate resistance was measured. Electrodes were typically 45 cm long but electrodes up to 3 m in length were used in areas with thick moss or vegetation mats. For the 2001 and 2010 sites there were regions of open water where contact resistance could not be established. To address this, ERT transects were measured along distances where adequate contact resistance was available. The survey proceeded when contact resistance was below 2,000 Ω-m for all electrodes along the 84 electrode line. Table 2 includes information on the location of the electrical resistivity transects and the electrode spacing configuration for the ERT transects.

Two-dimensional model interpretation was performed using RES2DINV (Geotomo Software, Penang, Malaysia), which performs smoothing and constrains inversion using finite difference forward modeling and quasi-Newton techniques (Loke and Barker, 1996; Loke et al., 2003). Using a least-squares inversion, convergence was tested by comparing the change in RMS quadratic error between two and five iterations, then three and five iterations, etc. When the RMS error reached 5%, convergence was achieved and further iterations would not significantly lower the RMS values.

4.3 Permafrost hydrologic modeling in upland catchments

We coupled two existing models (Figure 14): the physically-based and spatially-distributed Gridded Surface Subsurface Hydrologic Analysis (GSSHA) model and the spatially-distributed soil thermal regime model from the Geophysical Institute Permafrost Lab (GIPL; Marchenko et al., 2008). Adding thermal (cryospheric) aspects to GSSHA increased its applicability to cold regions locations. GSSHA simulates the hydrologic processes, soil moisture and snow depth information for GIPL. GIPL provides GSSHA with active layer depth and permafrost distribution. The confined bed (permafrost or seasonally frozen ground) is represented by reduced hydraulic conductivities in the GSSHA groundwater module. Input data requirements for GSSHA and GIPL include a digital elevation model, vegetation and soil maps, precipitation, air temperature, wind speed, vapor pressure and incoming shortwave radiation. The coupled model offers spatially distributed output in hourly to monthly resolution in ArcGIS.

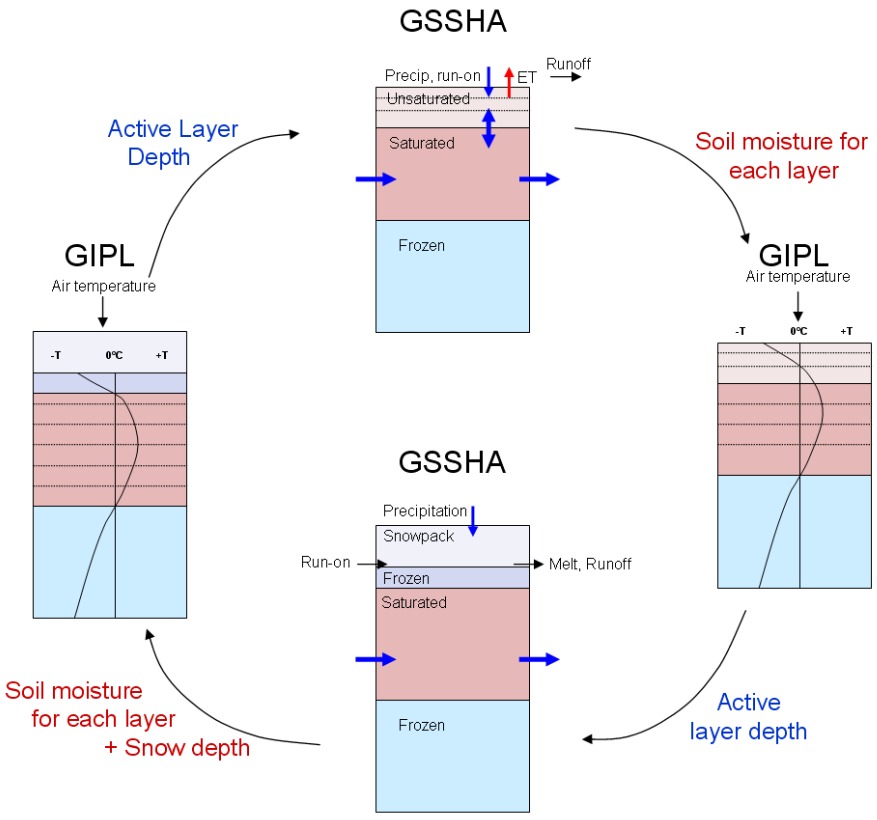

Figure 14. A flow chart identifying the interactions between major components in the coupled GSSHA and GIPL model.

The computational resources available at the Arctic Region Supercomputing Center (ARSC) at the University of Alaska Fairbanks and the USACE Engineer Research and Development Center's High Performance Computing Center were used to support this effort. Both GSSHA (Open Multi-Processing, OpenMP) and GIPL (Message Passing Interface, MPI) are parallel coded and are therefore computationally efficient. GIPL simulates 200 model years of 1000 temperature points per hour on 100 processors using a CRAY XT5 computer at the ARSC.

4.3.1 The GSSHA Hydrologic Model

GSSHA is a spatially explicit hydrologic model that simulates 2-D overland flow, 2-D groundwater flow, and 1-D flow in stream networks and includes evapotranspiration, infiltration, snow accumulation and snow melt. Additional simulation capabilities include artificial drainage and irrigation networks, wetlands hydraulics, and urban drainage hydrology. This is the first time GSSHA has been applied to a region affected by seasonally frozen ground or permafrost and adding GIPL components to GSSHA has strengthened the platform and expanded its applicability for other potential end users and project requirements.

4.3.2 The GIPL Permafrost Model

The Geophysical Institute Permafrost Laboratory (GIPL) model simulates soil temperature dynamics and the depth of seasonal freezing and thawing by numerically solving a 1D nonlinear heat equation with phase change. In this model the process of soil freezing/thawing occurs in accordance with the unfrozen water content curve and soil thermal properties, which are specific for each soil layer and for each geographical location. The finite difference numerical scheme (Alexiades and Solomon, 1993; Verdi, 1994) implemented in GIPL makes it possible to use coarse vertical resolution without loss of latent-heat effects in the phase transition zone, even under rapid or abrupt changes in the temperature fields.

The GIPL model captures physical processes essential for robust and appropriate modeling of permafrost dynamics in Alaska. Specifically, soil thermal properties are parameterized according to soil texture and organic matter. Additionally, GIPL includes thermal insulation of the snow cover and geothermal heating at the appropriately-selected depth. The GIPL model also incorporates an efficient algorithm to estimate soil thermal properties using in-situ temperature measurements in the active layer and in permafrost (Nicolsky et al., 2007). This simplifies model calibration for specific sites in Alaska. We selected the Caribou-Poker Creek Research watersheds.

4.4 Ecosystem transition modeling to identify landscape change

The study was designed to quantify ecotype (land cover) changes across three major military training areas Tanana Flats Training, Area Yukon Training Area, and Fort Greely that are situated within the Tanana-Kuskokwim Lowlands and Yukon -Tanana Uplands of central Alaska (Figure 15). The sampling used a photo-interpretation and point-intercept technique involving 20 grids (1.8 x 1.8 km) randomly selected from a set of 65 grids systematically distributed in 10-km intervals within the sampling domain, with a randomly assigned starting point. At each grid, a sub grid of 100 points was established at 200-m intervals, generating a total of 2,000 points for the study area.

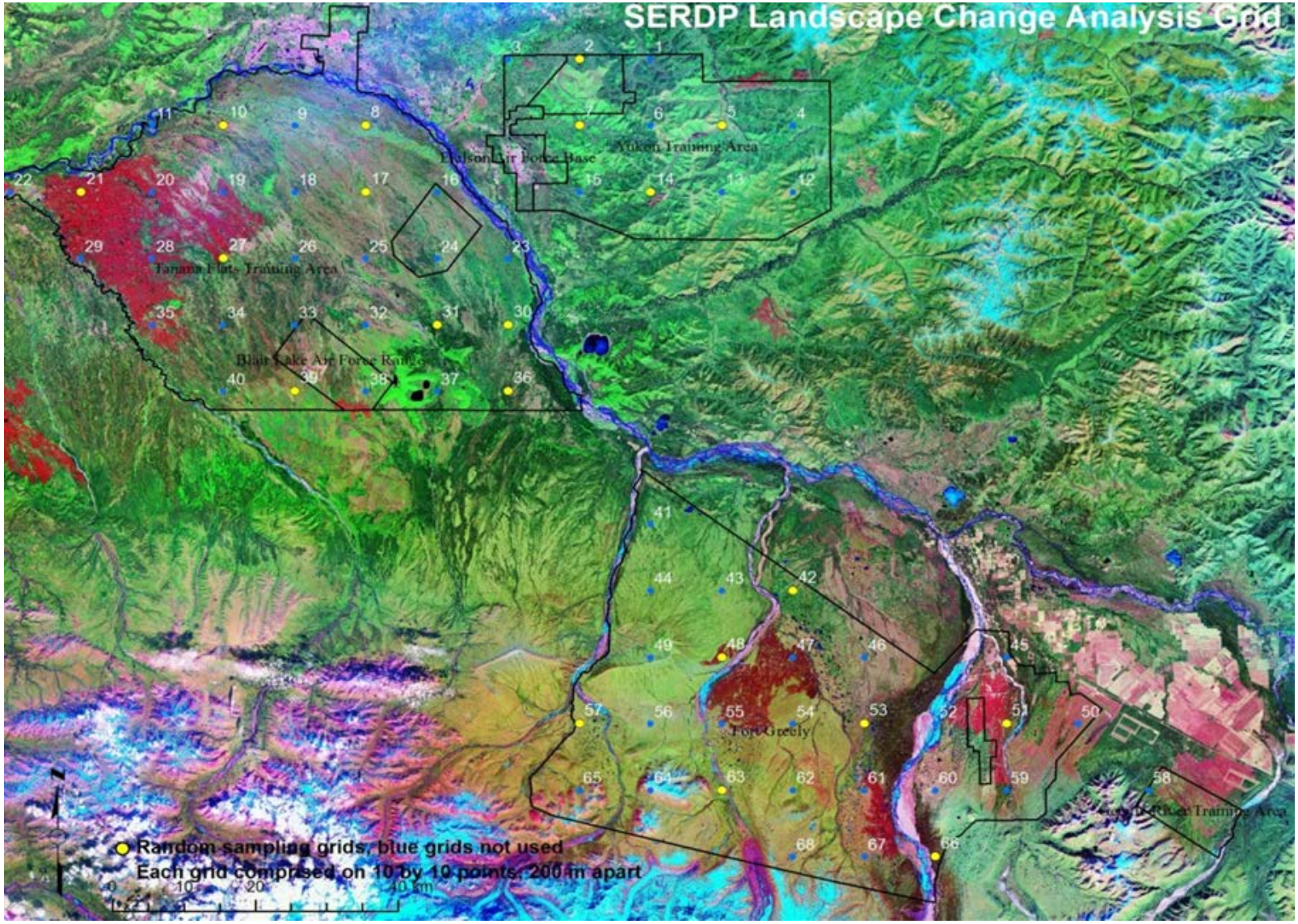

Figure 15. Sampling grid used for assessing landscape change within the Tanana Flats Training Area, Yukon Training Area, and Fort Greely. Blue and yellow circles denote the centers of the grid cells that comprise all interior Alaska DoD installation and training range lands. Yellow circles include a subset of locations where the landscape change measurements were focused.

4.5.1 Image Compilation and Georectification

Historical airphotos and recent satellite images were acquired for each of the grids for the time periods, 1949–1952, 1978–1980, and 2006–2011. For the 1949–1952 period, black and white airphotos (scale 1:40,000 to 1:50,000) were acquired from the USGS Earth Explorer web site and USGS scanned them at 14 micron for ~0.7 m pixel resolution. For the 1978–1980 period, the false color infrared (CIR) Alaska high altitude photography (AHAP) airphotos (scale ~1:63,000) were acquired from Earth Explorer at a high-resolution scan (25 micron) for ~1.7 m pixel resolution. For both the 1949–1952 and 1978–1980 time periods, orthomosaics (3.3 m and 2.5 m resolution, respectively) processed by the Alaska Satellite Facility were also utilized. For the recent satellite imagery, Quickbird (0.7 m pixel resolution), Nextview (1.2 m mosaic), Worldview (0.6 m), and IKONOS (1.0 m panchromatic-fused) images were acquired from the high-resolution image archives of the National Geospatial-Intelligence Agency by CRREL. Recent orthoimagery (0.6 m resolution) processed by the NRCS were also acquired through the Alaska Statewide Digital Mapping Initiative.

The raw imagery from the Yukon Training Area and Fort Greely was orthorectified using ERDAS Imagine software with the national elevation dataset (NED), and the raw imagery from the Tanana Flats Training Area was georeferenced using ArcMap. Control points (distinct terrain features) were obtained from a 1999 panchromatic, orthorectified air photo mosaic (Aerometrics, Anchorage, Alaska) for the Tanana Flats and Yukon Training Area, and from the Nextview orthorectified mosaics and other recent imagery available for Fort Greely. Camera model calibrations were used in rectifying the airphotos when this information was available. Otherwise, imagery was orthorectified or georeferenced primarily utilizing second order polynomial models. Geo-rectification errors for the 1949–1952 (RMS ranged from 0.1 to 3.5 m), 1978–1980 (RMS ranged from 0.2 to 3.7 m), 2006–2011 (RMS from 0.0 to 6.0) were small relative to the photo-interpretation sampling area (10 m for shrub and forest determinations).

4.5.2 Ecological Classification and Photo-Interpretation

The detection of change at each point involved photo-interpreting multiple terrain characteristics using established classifications (Table 4). We used the ecotype classification developed for Fort Wainwright (Jorgenson et al., 1999) and Fort Greely (Jorgenson et al., 2001a), which incorporated physiography, soil texture, moisture, and vegetation structure into the ecological classification. However, we simplified the classification by eliminating the soil textural designation for several classes. For the geomorphology (surficial geology, terrain units) classification, we used the system from the ecological land classifications for the military lands (Jorgenson et al., 1999; 2001a), which was modified from the terrain-unit classification of Kreig and Reger (1982). For permafrost/thermokarst conditions we modified the classification of Jorgenson and Osterkamp (2005). Thermokarst features were identified by their collapse form and vegetation and in areas without thermokarst permafrost presence or absence was interpreted through vegetation-landform association described in Jorgenson et al. (1999). For assigning ecological drivers to ecotype changes, we used the system developed by Jorgenson et al. (2015). To assign fire age, we used the fire history maps of the Alaska Interagency Coordination Center (http://afsmaps.blm.gov/imf/imf.jsp?site=firehistory) for fires since 1980; for older fires we used changes in fire scars between image dates to roughly estimate fire year. Even with more recent fire perimeters in the fire history database we needed photo-interpretation to establish whether a site was burned or not within the perimeter.

For photo-interpretation, the terrain classification was conducted onscreen at ~1:2,000 scale using the center of cross-hair created with the GIS for the sampling point (example in Figure 16). For shrub and forest types, the ecotype was based on a 10 m diameter circle because the classification is based on canopy cover, and for meadow/tundra types the interpretation was done for the cross-hairs because classification does not depend on shrub/forest canopy percentages. If more than one ecotype was evident within the circle, the ecotype encompassing the cross-hair was used. For thermokarst features, the classification was done at the cross-hair. We first interpreted the most recent imagery and proceeded to earlier imagery.

For the early black and white photography the image quality was poor, consequently, we were only able to differentiate large structural changes in vegetation and relied on ecotype interpretations from later imagery. Changes in the early airphotos were assigned only when there were distinct changes, thus biasing the sampling toward no change. The main photo-interpreter was able to apply experience gained in ecological land classification and mapping at Fort Wainwright, Yukon Training Area, and Fort Greely (Jorgenson et al., 1999; 2000; 2001a).

Table 4. Coding system used for classifying landscape change.

Code	Combined Ecotypes	Code	Permafrost/Thermokarst Status	Code	ChangeType
ARDB	Alpine Rocky Dry Barrens	US	Unfrozen Stable	N	None
ARDDS	Alpine Rocky Dry Dwarf Scrub	UL	Unfrozen Likely	LF	Landslides/fans
ARMLS	Alpine Rocky Moist Low Scrub	PL	Permafrost Likely	RE	River erosion
AWLS	Alpine Wet Low Scrub	PS	Permafrost Stable	RD	River deposition
AWM	Alpine Wet Meadow	DTL	Deep Thermokarst Lake	CE	Coastal erosion
AWTM	Alpine Wet Tussock Meadow	STL	Shallow Thermokarst Lake	CD	Coastal deposition
HDB	Human Disturbed Barrens	GTL	Glacial Thermokarst Lake	TK	Thermokarst
HDS	Human Disturbed Scrub	GL	Glacial Thermokarst	LD	Lake drainage
WL	Water-Lakes	TB	Thermokarst Basin	SD	Soil drainage
PFM	Lacustrine Fen Meadow (palustrine)	TLB	Thermokarst-lake Basin	DM	Drainage & migration
PMM	Lacustrine Moist Meadow	TSK	Thaw Sink	DMS	Drying/moisture Stress
LDSB	Lowland Dwarf Scrub Bog	TF	Thermokarst Fen	GM	Glacier melting
LFM	Lowland Fen Meadow	TB	Thermokarst Bog	AL	Acidification-leaching
LFS	Lowland Fen Scrub	THS	Thermokarst Shore Bog	PS	Primary succession
LGMLS	Lowland Gravelly Moist Low Scrub	TSL	Thaw Slump	PFS	Post-fire succession
LGMTS	Lowland Gravelly Moist Tall Scrub	DS	Detachment Slide	DSI	Dominance shift/infilling
LGDBF	Lowland Gravelly Dry Broadleaf Forest	CP	Collapsed Pingo	PME	Plant migration/expansion
LGDMF	Lowland Gravelly Dry Mixed Forest	BS	Beaded Stream	PAE	Paludification-early
LGNF	Lowland Gravelly Needleleaf Forest	TEG	Thermal Erosion Gully	PAL	Paludification-late
LLSD	Lowland Low Scrub Fire-Disturbed	TWT	Thermokarst Water Track	H	Human development
LMBF	Lowland Moist Broadleaf Forest	CBS	Collapse-block Shore	Hc	Clearings
LMM	Lowland Moist Meadow	BL	Block Landslide	Ht	Trails
LMMF	Lowland Moist Mixed Forest	TTP	Thermokarst Troughs and Pits	Hf	Fill/Roads
LMTS	Lowland Moist Tall Scrub	TP	Thermokarst Pits	He	Excavations
LTSB	Lowland Tussock Scrub Bog	CTM	Conical Thermokarst Mounds	Ha	Agriculture
LWLS	Lowland Wet Low Scrub	ITM	Irregular Thermokarst Mounds	F	Fire
LWTS	Lowland Wet Tall Scrub	SH	Sink Holes	FTK	Fire and Thermokarst
LWBF	Lowland Wet Broadleaf Forest				
LWMF	Lowland Wet Mixed Forest				
LWNF	Lowland Wet Needleleaf Forest				
WR	Water-River	**Codes**	**Geomorphic Unit**	**Code**	**Fire Range**
RGB	Riverine Gravelly Barrens	Nn	Metamorphic-noncarbonate	FireYrRct=>1980 or afterImageYrMid	
RGDDS	Riverine Gravelly Dry Dwarf Scrub	Ch	Hillslope Colluvium	FireYrMid=1950-1986, or after ImageYrOld	
RGDM	Riverine Gravelly Dry Meadow	Elu	Upland Loess	FireYrOld=<1950: assigned	
RGLTS	Riverine Gravelly Low and Tall Scrub	Elui	Upland Loess, ice-rich (yedoma)		~1920 if early-mid succession,
RGDBF	Riverine Gravelly Dry Broadleaf Forest	Fmri	Meander Inactive Channel Deposits		<1900 if late succession
RGDMF	Riverine Gravelly Dry Mixed Forest	Fmoi	Meander Inactive Overbank Dep		
RGNF	Riverine Gravelly Needleleaf Forest	Fmob	Mean. Abandoned Overbank Dep	**Point Interpretation Protocol**	
RMBF	Riverine Moist Broadleaf Forest	Fbrag	Braided gravelly active channel	Use crosshari(+) for TK feature and veg type.	
RMMF	Riverine Moist Mixed Forest	Fboi	Braided Inactive Overbank Dep	Use 10-m diam circle for determining tall shrub,	
RMNF	Riverine Moist Needleleaf Forest	Fbob	Braided Abandoned Ovrbank Dep	and forest canopy cover (forest is >10%)	
RMLS	Riverine Moist Low Scrub	Fhl	Headwater Lowland Floodplain	If circle has two ecotypes, chose type	
RMTS	Riverine Moist Tall Scrub	Fhm	Headwater Mod. Steep Floodplain (2–6% slp)	under crosshair	
RWLS	Riverine Wet Low Scrub	Fhmo	Headwater Moderately Steep Overbank Dep.		
RMW	Riverine Wet Meadow	Gfo	Glaciofluvial Outwash	**Scale**	
UMM	Upland Moist Meadow	Ldm	Drained-lake basin	Interpreted at 1:2000 scale on screen	
UMTLS	Upland Moist Tall and Low Scrub	Fsl	"Lowland" Retransported deposits		
UMSD	Upland Moist Scrub - Disturbed	Of	Organic Fens		
UMBF	Upland Moist Broadleaf Forest	Ob	Bogs		
UMMF	Upland Moist Mixed Forest	Wrlg	Lower Perennial, glacial		
UMNF	Upland Moist Needleleaf Forest	Wldit	Deep Isolated Lake, Thaw		
URDM	Upland Rocky Dry Meadow	Wlsit	Shallow Isolated Lake, Thaw		
URDLS	Upland Rocky Dry Low Scrub	Wldm	Deep Lake, morainal		
URDBF	Upland Rocky Dry Broadleaf Forest				
UWNF	Upland Wet Needleleaf Forest				

Figure 16. An example of a time-series of imagery from 1949, 1978, and 2007 used for quantify landscape change. White cross-hairs are sampling points used for photo-interpretation.

To analyze landscape change we cross-tabulated ecotypes by year, change driver, and ecoregion. We also aggregated the points by grid so that the grid became the sample unit for assessing variability and testing for differences among years.

4.5.3 Accuracy Assessment

For accuracy assessment, we collected ground information for 128 sites at 10 grids (02, 07, 08, 10, 14, 21, 36, 51, 66, 69) during summer 2012. Information was collected on site and sampling (nine variables), topography (two), soil summary data from a shallow soil plug (eight), and vegetation type and dominant plant species (11). Ground and soil photographs were taken at each site. The data were sufficient to classify the ecotype for comparison with photo-interpreted classes. The field data were withheld until the photo-interpretation was complete to allow an unbiased estimate. To determine overall accuracy we developed a contingency table of field versus photo-interpreted ecotype classes.

4.6 Development of a GIS based geospatial decision support tool

The GISMO Decision Support System for U.S. Army Alaska (GISMO DSS AK) provides an interactive map interface to query and display information about ranges and training facilities. It is designed to optimize the display of climate and permafrost model datasets on top of a broad array of imagery and commonly utilized mapping layers like contours, roads, trails, waterbodies, and wetlands. It also includes military relevant landscape identifiers like training areas, military grid coordinates, impact areas, and ranges.

GISMO DSS AK is developed with HTML and Javascript. It is viewable from most web browsers, but has been optimized for Internet Explorer 9 and greater and Firefox 10 and greater, both of which are approved applications of the Army Gold Master desktop environment. The map interface utilizes a Javascript library called OpenLayers, which provides the functionality for geospatial layer definition and map navigation. The large majority of the data displayed in GISMO is sourced from local files, employing client-side rendering in the browser and, therefore, can operate offline with no connection to the Internet. The only data layer requiring the Internet is the satellite imagery, which connects to a Web Map Service (WMS) provided by Alaska Mapped.

The GISMO DSS AK includes two distinct map layer control tools: Location Info and Analysis tools. The Location Info tool employs an OpenLayers function that extracts attribute values from every visible vector feature at the selected location and generates a report. Raster layers in GISMO DSS AK were developed in a way that encodes the raster value within the 3-band (red, green, and blue) pixel color values. The Location Info tool extracts the color values from the selected pixel and decodes them into the actual raster value in the proper temperature, precipitation, or elevation units for the raster layer and adds this to the report for the selected location.

GISMO DSS AK includes an Analysis tool that can be used to calculate differences between climate or permafrost data from different time periods or climate modeling scenarios. The tool converts color values to raster values for each input layer just like the Location Info tool. Then it performs a raster difference or percent difference calculation using the actual raster values. The results are then encoded back into color values for rendering in the map. This entire process is done real time in the browser.

5. RESULTS AND DISCUSSION

5.1 Permafrost-hydrogeology relationships on the Tanana Flats lowlands

All sites experienced dramatic seasonal variation in water temperature, with minimal day-to-day changes (Table 5 and Figure 17). The warmest water temperatures were recorded in late August and early September, ranging from 4.3 (Fen 1 upper) to 13.4 ºC (Lake). At most sites the maximum yearly temperature was near 10 ºC. The coldest water temperatures were similar across all sites (from ~0 to 1.3 ºC). The early season increase in water temperatures was relatively rapid compared to the rate of cooling in the fall. Not accounting for the Fen 1 upper site, the cumulative degree-day (DD) temperature sum presented a larger variability between the years (within a site) than between sites, both in regards to annual and seasonal (summer) time periods (Table 6). The Fen 1 upper site was substantially colder than all other sites during the summer, which resulted in about half the amount of accumulated DD compared to the other sites.

Table 5. Minimum and maximum recorded hourly water surface elevation and temperature between late Sep 2012 and early October 2014.

	Fen 1 upper	Fen 2 lower	Fen 2 mid	Fen 2 upper	Lake	Fen 1 middle (Birch Island)
Minimum WL, masl	135.0	128.7	135.3	141.7	160.5	ND
Max WL, masl	136.3	129.3	136.7	142.5	163.0	ND
Difference, m	1.3	0.6	1.4	0.8	2.5	ND
Min WT, C	0.0	0.0	0.0	-0.1	-0.1	1.3
Max WT, C	4.3	11.2	10.2	11.0	13.4	8.7

Table 6. Cumulative degree-days (DD) based upon mean daily temperature for the hydrologic year and summer months.

	Hydrologic Year (Oct.-Sep.)			Summer (May-Sep.)		
	2011-2012	2012-2013	2013-2014	2012	2013	2014
Fen 1 upper	ND	467	344	362	418	351
Fen 2 lower	ND	1056	1499	957	822	1332
Fen 2 mid	ND	1134	1446	1216	884	1275
Fen 2 upper	ND	1297	1311	1112	1079	1209
Lake	ND	1356	1296	1467	1098	1180
Fen 1 middle (Birch Island)	ND	ND	1354	1142	ND	939

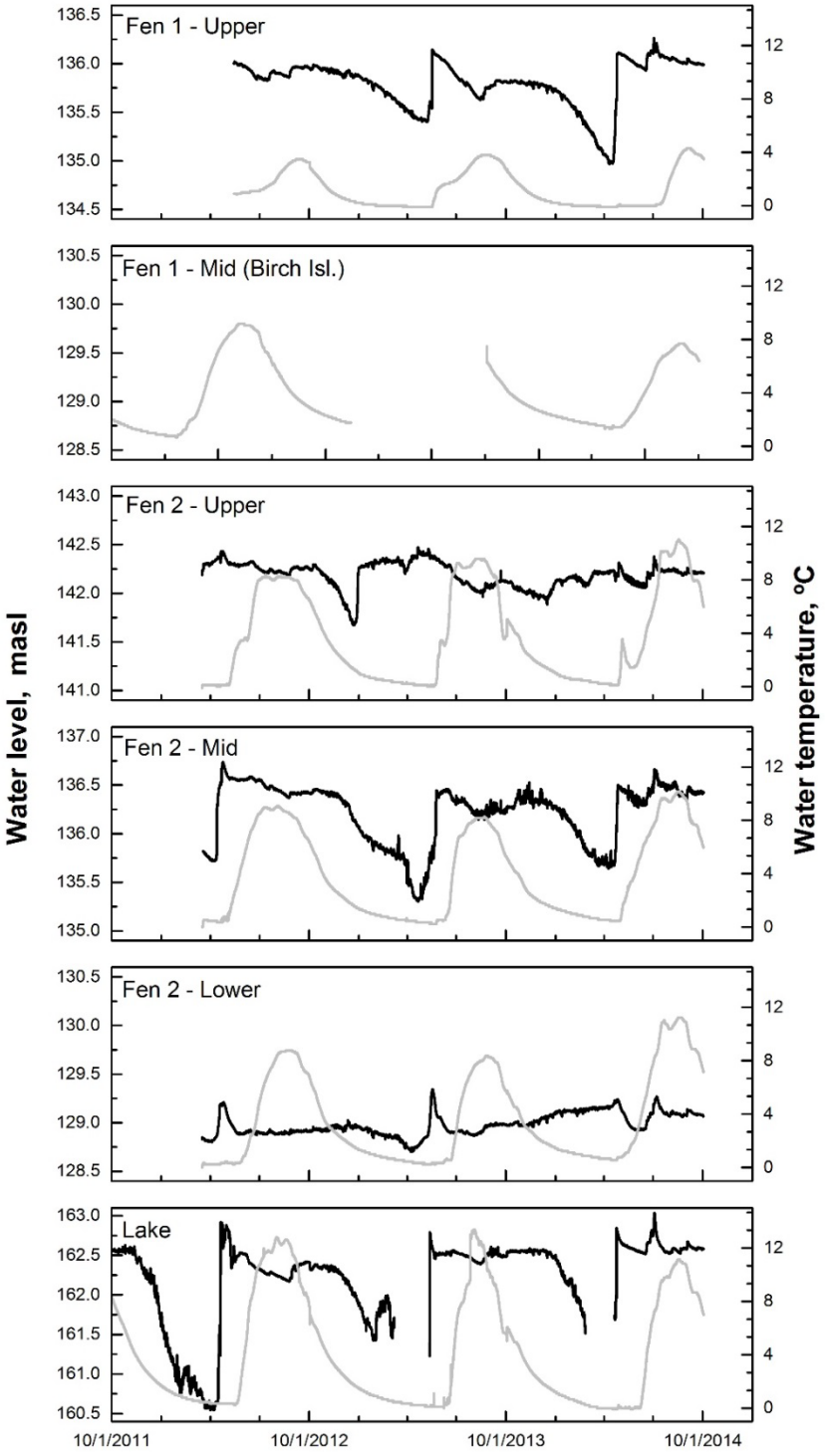

Figure 17. Measured (hourly) water levels (black) and water temperature (gray) in two parallel fens (Fen 1 and Fen 2) and at a groundwater-fed lake ~15 km south of the two fens. Each of the two fens had a sensor located at the head of the fen (upper) and further downstream. Apart from the bottom Lake graph, the y-axis represents an elevation range of 2 m.

At all sites for all years the peak water level elevations were measured immediately following spring melt. This is a time when the entire winter snow pack melts and that melt water runs off. It is also the time of the summer thaw season when there is the least amount of vertical seasonal thaw. There is little to no infiltration capacity in the soils and surface vegetation at this time. As such, there is little storage of the excess winter melt waters. Over the course of the summer, at all sites and for all years, the water levels slowly decreased from the peak spring melt elevations. This is likely a representation at the regional scale of seasonal thaw providing more vertical storage of surface waters.

By comparing the temperature and water level information over time at each site it is clear that the warmest water temperatures, in mid-summer for all years, are associated with the lowest water level elevations at all sites. This supports a conceptual model whereby the warmest waters, corresponding with the warmest soil temperatures of the summer season, are associated with the greatest downward percolation. The regional (i.e. 10s of km scale) areas these lake-fen systems represent are large enough that heterogeneous differences in soil type, vegetation, and even snow pack depth and water equivalence likely play roles in the hydrology but we do not have any of that information. A smaller scale study that includes side channels, soil termpature measurements, and snow pack measurements could close some of the uncertainty in our ability to compare processes at any given site to their regional context.

Seasonal variations in water levels were less coherent between the sites compared to the temperature data. The most dramatic seasonal variation was seen in the Fen 1 upper, Fen 2 Mid and Lake sites, while the variation was relatively dampened at the Fen 2 upper and lower sites (Figure 17). At the sites with the larger seasonal variation, we can see a steady and slow decrease in water level during late fall and winter, with a sudden and sharp increase during the snowmelt. The slow decrease we attribute to the slow lateral draining of water from the fen systems into the surrounding islands of birch and spruce that are underlain by permafrost. We suspect that later in the summer season the connectivity for flow paths and the areal extent of the flow paths themselves are increased and this leads to loss of water and loss of connectivity across the fen systems.

The early summer waters are cold and water levels are at their highest yearly values as there is little lateral drainage (loss) from the fens due to a thick layer of seasonally frozen surface soils. Water levels steadily decrease following the snowmelt peak and they remain relatively steady (within 0.5 m) during the summer months. Heavy rainfall in late June 2014 (Figure 18) caused a spike in mid-summer water levels at all sites. The response to this extreme precipitation event was greatest at the Lake site which we attribute to the lake-subsurface-fen flow paths being unable to transfer the water from the lake at the same rate at which it fell.

The most dramatic seasonal variation in water level was observed at the Lake (2.5 m), which was primarily due to the rapid decrease in winter. The Fen 2 lower represented the site with the least difference between low- and high water levels (0.64 m), which was primarily caused by the brief snowmelt period as the rest of the year presented a relatively steady water level. Late winter water levels (lowest of the year) were not consistently lower in a particular year for all sites. Late winter 2014 presented lower water levels than 2013 at the Fen 1 upper site, but the reverse was true at the Fen 2 Mid and lower sites. Summer 2014 had record high rainfall measured at the Fairbanks airport (Figure 18). Still, the late summer water levels were not significantly higher than in previous years.

Our measurements suggest that among all the sites, it is only the Fen 2 lower site that may be under the (buffering) influence of the Tanana River. The Fen 1 upper site experienced relatively

cold summer temperatures, which indicate a deeper pathway of the groundwater. The vertical change in water level or its seasonal response at a given site yields some insight into the hydrologically connected nature of the site. For example, the Fen 2 lower and Fen 2 upper sites had the least change in water level through the year and this suggests there is greater connectivity between this fen and its outlet or that this fen has less channelized flow through permafrost. However, in contrast Fen 2 middle and Fen 2 lower may have less lateral connectivity or more permafrost and thus the water levels in these locations respond more rapidly and more dramatically to seasonal controls.

Two hypotheses framed this part of our research: 1) that the fens would show a hydrologic response to seasonal thaw of the permafrost bodies that surround them laterally, and 2) that the hydrologic response to rain events would be lessened as summer progresses and seasonal thaw of the lateral soils around the fens could buffer flows through the fens. Our results suggest the two fen systems did not exhibit a strongly detectable seasonal response to flows that would have suggested a change in seasonal flowpaths through the summer thaw season. Further, without more detailed information on the drainage area and morphology that each water level site represents it would be difficult to quantify the rate or response of the fen water level sits to specific precipitation events or seasonal flow regimes. A challenge in ascertaining flow across the fens is the fact that they represent such low gradient terrains. For example, across a ~10 km lake to fen system the vertical change in gradient is only 30 meters. As such, the response time from precipitation event to a change in flow could be complicated by lateral channeling that we were not able to capture.

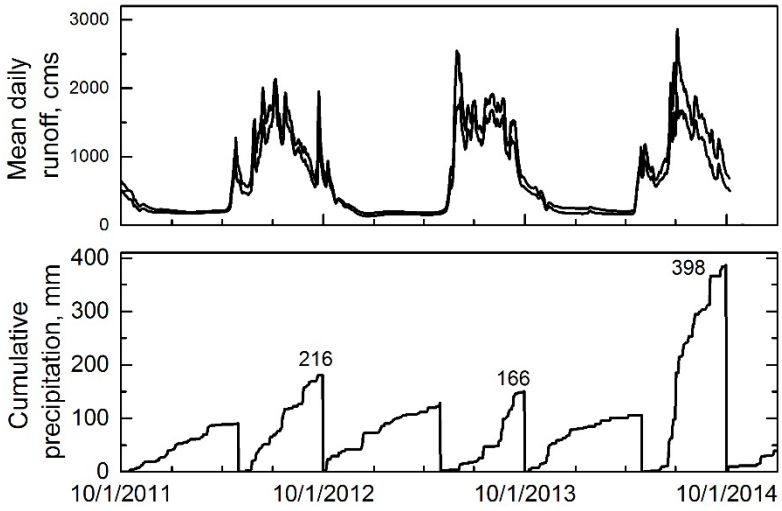

Figure 18. Mean daily runoff of the Tanana River near Fairbanks (top) and cumulative precipitation separated into winter (Oct-Apr) and summer (May-Sep) from Fairbanks International Airport. Noted are the total summer precipitation values in 2012, 2013 and 2014.

5.2 Vulnerability of permafrost to fire-initiated thaw in interior Alaska

5.2.1 Results

5.2.1.1 Vegetation

The clustering of plots by fire year in the NMDS ordination showed that vegetation composition was similar within each burn scar and different among burn scars (Figure 19). Forty-seven percent of the variation in plant community structure was represented by Axis 1 of the NMDS ordination, with Axis 2 accounting for 19%. Axis 1 had a strong negative correlation with black spruce (*Picea mariana*) cover (r = -0.86). In the oldest fire scar (~1930), the canopy was dominated by black-spruce and groundcover consisted primarily of feathermosses (*Hylocomnium splendens* and *Pleurozium schreberi*).

The vegetation canopy of the 1975 burn was a mixture of evergreen and deciduous trees consisting of black spruce, white spruce (*Picea glauca*), aspen (*Populus tremuloides*), and birch (*Betula neoalaskana*). Axis 2 was strongly correlated with birch cover (r = -0.90). The vegetation canopy of the 1988 burn was dominated by birch trees, and the groundcover was primarily leaf litter. The lack of trees and predominance of sedges (*Eriophorum vaginatum*, *Carex* spp), grasses (*Calamagrostis canadensis*), low shrubs (*Vaccinium uliginosum*), and colonizing mosses (*Ceratodon purpureus*) distinguished the early successional vegetation in the 2001 and 2010 fires from the others.

Axis 1 was correlated with stand age (r = -0.79), demonstrating that plant community composition varied along a gradient of time since fire, consistent with successional shifts in plant communities. Despite this correlation, plant species composition does not exhibit similar successional trajectories across all burns. The strong linear relationship between Axis 1 and soil moisture (r = 0.79) indicates that plant community composition is most reflective of this soil physical characteristic. The youngest sites with thawing permafrost had saturated silty soils (2010, 2001), compared to better drained surface organics at the ~1930 and 1988 fire scars and the sandy soils of the 1975 fire scar. Organic layer thickness (OLT) and thaw depth were not correlated with either ordination axis, indicating that the dominant patterns of plant community composition were not related to these variables.

5.2.1.2 Soil physical characteristics

Soil OLT, moisture, and texture are important properties affecting the thermal regimes of soils. OLT ranged from 0 – 260 cm across all sites. The soils at the 1930 and 1988 fires were similar in that they typically had thick peat layers greater than 1 m, with mean OLT of 89 cm and 176 cm, respectively (Figures 20 and 21). Mean organic carbon (OC) stocks in the upper 3 m of the soil profile were likewise greatest in the 1930 and 1988 fire scars (141 kg/m^2 and 125 kg/m^2) (Figure 21). In contrast, the soils in the 1975, 2001, and 2010 burns had thinner organic layers (7 cm, 14 cm, and 2 cm) and less organic carbon in the upper 3 m (18 kg/m^2, 52 kg/m^2, 55 kg/m^2).

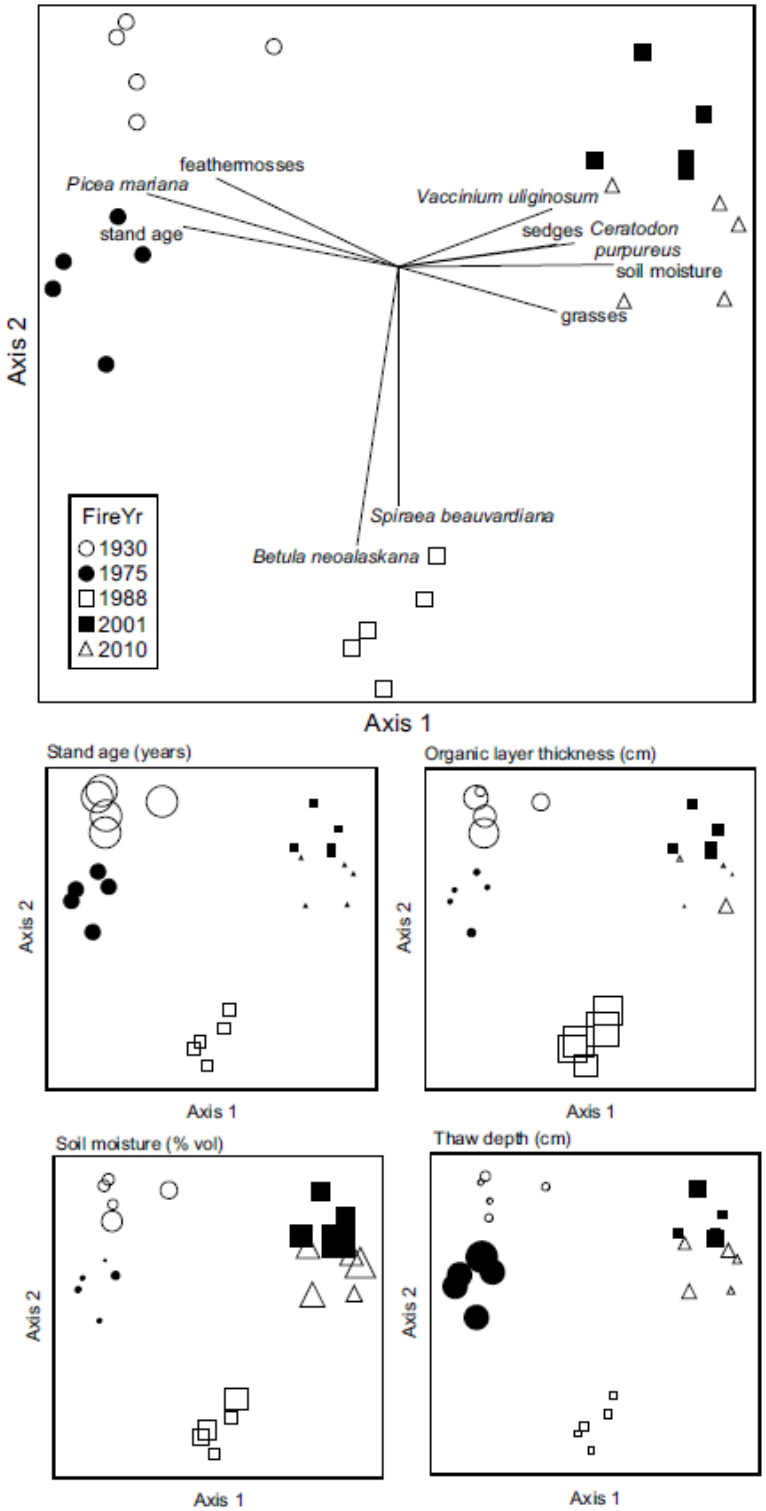

Figure 19. Nonmetric multidimensional scaling ordination of vegetation plots by fire year (upper large panel) and correlations of ordination axes with cover of plant species/functional type and site variables (lower small panels). The direction and length of a given vector represents the direction and strength of correlations. Symbols in the lower panels are scaled to individual site variables.

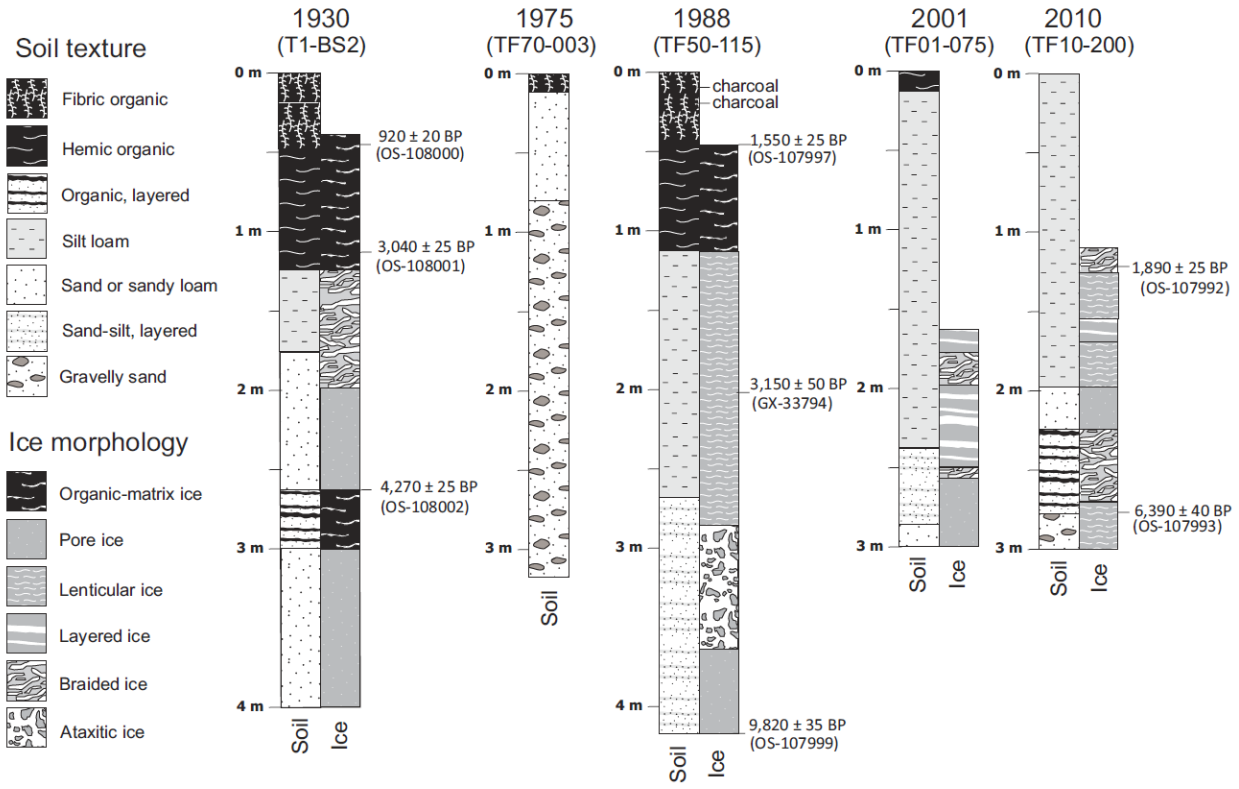

Figure 20. Soil texture, permafrost ice morphology, and radiocarbon dates with depth at one representative borehole from each fire scar. Site and radiocarbon sample IDs are in parentheses.

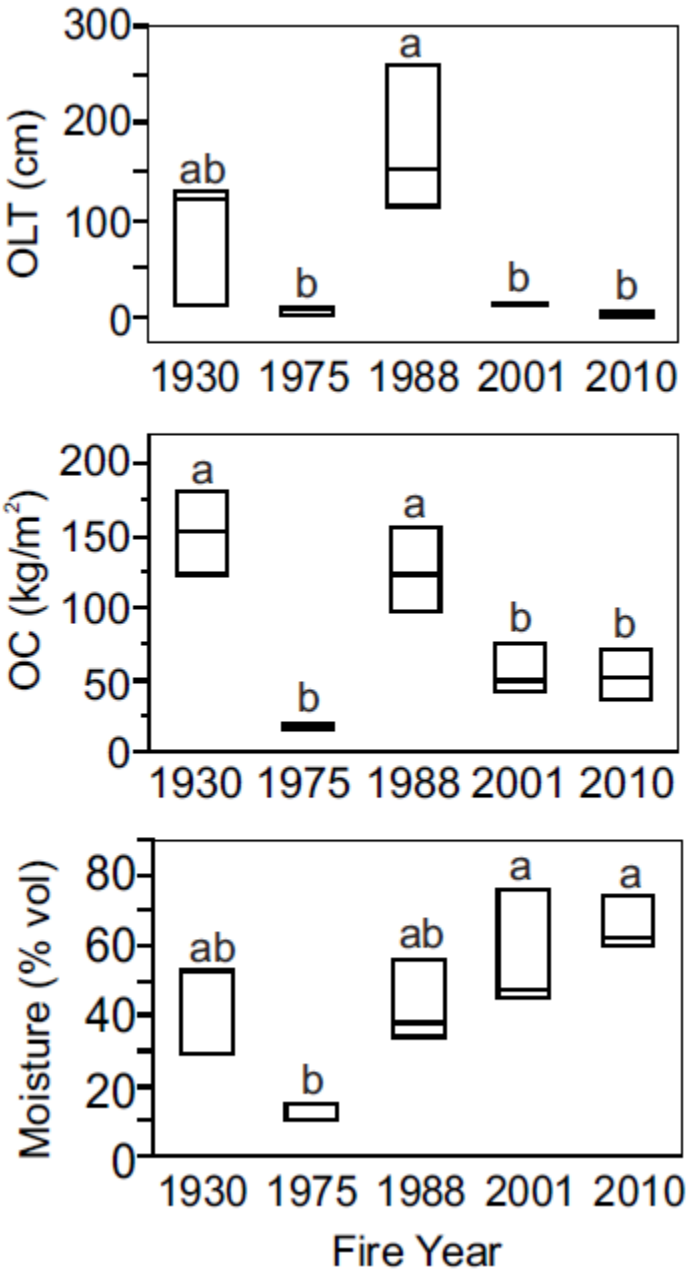

Figure 21. Box plots of organic layer thickness, organic carbon stocks (to 3 m depth), and active layer soil moisture by fire year (n = 14) with Tukey-Kramer post-hoc results of significant differences ($p < 0.05$) depicted by lettering.

Soil texture of the underlying mineral soil varied across fire scars (Figure 20). The upper mineral soils of the 2001 and 2010 fire scars were fine textured silt loams approximately 2 m thick, whereas the near-surface soils of the 1975 fire scar were typically sandy loams, sands, or thin layers of silt loams underlain by sandy soils, with gravels occurring at depths less than 1 m.

Mean soil volumetric moisture content of the active layer varied five-fold across fire scars (Figure 21). Mean soil moisture in the 1975 fire scar with sandy soils (13%) was significantly lower than in the in the 2001 and 2010 fire scars with silty soils (56%, 65%), and the 1930 and 1988 sites with thick peat had intermediate soil moisture (37%, 43%).

Soil stratigraphy descriptions revealed complex sediment deposition, organic accumulation, and permafrost histories that contributed to the large differences among sites. The 2001 and 2010 sites were similar in that they had a moderately thick eolian silt cap over fluvial interbedded silts, sands, and gravels. They had relatively thin surface organics with no evidence of herbaceous peat associated with previous thermokarst. The thick silt caps contributed to the prevalence of braided and layered ice morphologies within high ice contents in the frozen soils. In contrast, the 1930 and 1988 sites had thick peat with buried layers of herbaceous peat (*Menyanthes trifoliata*) indicative of past thermokarst fens. The ice-poor lenticular ice morphology at 1.1 to 2.8 m depth suggests that the 1988 fire thawed soils to 2.8 m. At the 1930 site, the basal hemic peat (116 cm depth) had an age of 3,040 ± 25 BP, and the fibric and hemic peat transition (48 cm depth) was dated at 920 ± 20 BP. In the 1988 burn, the base of the fibric peat layer (48 cm depth) was aged at 1,550 ± 25 BP. Large portions of these peat layers comprised the permafrost layer. Dates from the interbedded silt and sandy and gravelly sand layers (6,390 ± 40 and 9,820 ± 35 BP) indicate fluvial activity on the flats ended in early to mid-Holocene. The 1975 site was an outlier with eolian sand over fluvial sandy gravel. Overall the stratigraphy shows that abandoned floodplains have complex histories involving disparate fluvial environments ending at differing times, sand deposits developing near channels, eolian silt being deposited over wide areas after the end of fluvial activity, and complex histories of organic accumulation related to patchy thermokarst.

5.2.1.3 Thaw depths and thaw settlement

Mean thaw depths in late summer of 2012 were relatively shallow in the 1930 (57 cm) and 1988 (52 cm) fire scars compared to the 2001 (119 cm) and 2010 fire scars (119 cm), and in the 1975 fire scar, no permafrost was found in the upper 2.5 m or 3 m of soil (Figures 20 and 22). Permafrost was absent within the ~2.5 m depth of probing within the collapse-scar bogs.

Mean ice content of permafrost within the upper 3 m of soil ranged from 55 to 79 % vol. The equivalent depth of water contained in the ice at the 1930 and 1988 sites were nearly double those of the 2001 and 2010 fire scars, in part due to the shallower permafrost table. For both the 1930 and 1988 fire scars, calculated potential thaw settlement from thawing of all the remaining permafrost in the upper 3 m was 0.9 m, two to four times greater than the potential thaw settlement at the 2001 and 2010 burns (0.4 m and 0.3 m, respectively; Figure 22). Some of the reduced potential thaw settlement in the recent burns can be attributed to the deeper thaw already having removed some of the excess ice. The measured surface elevations at the 1930 and 1988 boreholes were about twice as high above the water level of adjacent bogs than those of the 2001 and 2010 fires (+0.7 m and +0.8 m above water level compared to +0.3 m and +0.4 m, respectively; Figure 22). On average, predicted post-thaw elevations were below or equal to water level at the 1930, 1988, and 2001 burns, and was 0.1 m above water level at the 2010 burn, although active thaw settlement and water impoundment were observed at both of the recent burns. Overall, the data show that permafrost thaw in these lowlands can lower the ground

surface to approximately water level over most areas, with 77% of our plots predicted to collapse to water level or below.

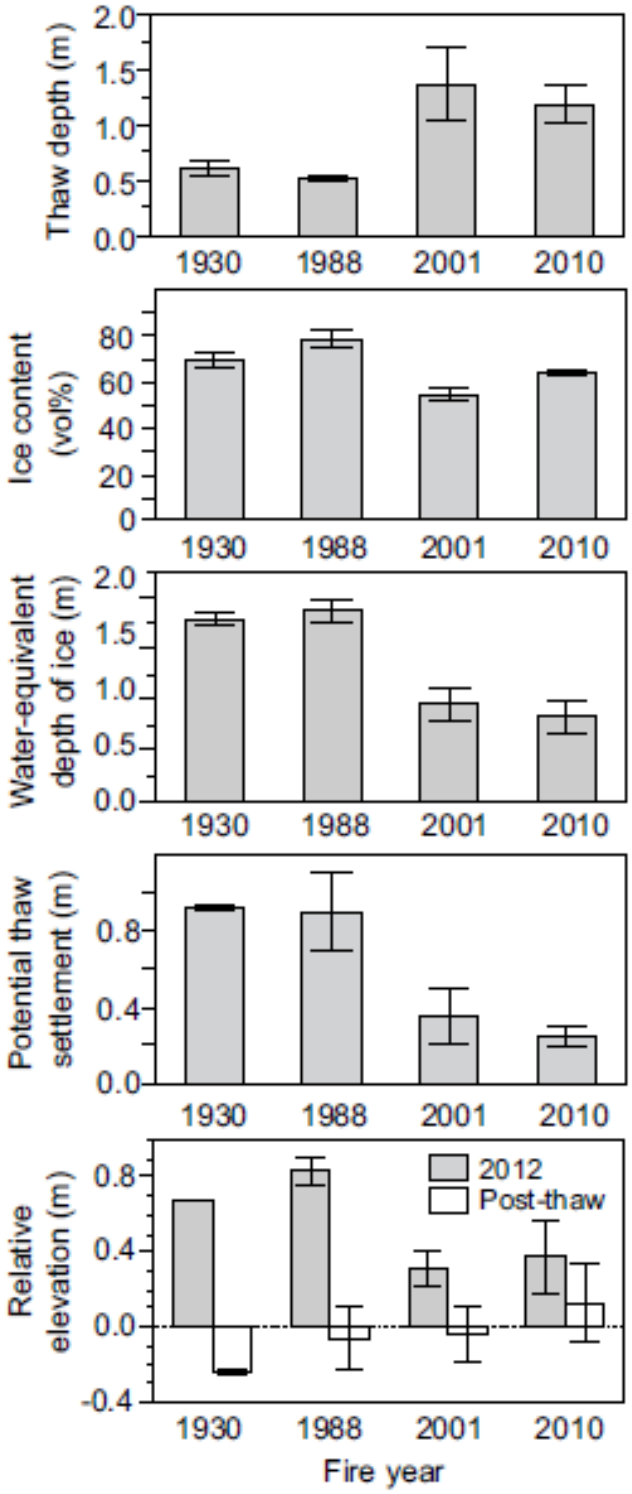

Figure 22. Thaw depth, permafrost ice content, water equivalent depth of ice in permafrost, potential thaw settlement, and elevation at time of sampling (2012) and predicted post-thaw elevation of the ground surface relative to the surface water level. Values represent means ± SE (n = 12). Permafrost characteristics and subsequent calculations of thaw settlement and relative elevation changes are based on the upper 3 m of the soil column.

Repeat measurements of surface elevations, thaw depths, minimum depths of unfrozen ground, and water levels were conducted along transects of burned forests and collapse-scar features. The elevation profile at the 2010 fire scar (Figure 23) shows the lowering of the permafrost table in the burned forest from 2011-2014 (mean = 1.04 m, max > 1.57 m), the thaw settlement of the ground surface (mean = 0.27 m, max = 0.54 m), and the water inundation of the forest margins from adjacent collapse-scar features (at transect locations ~ 0–10 m and ~70–80 m).

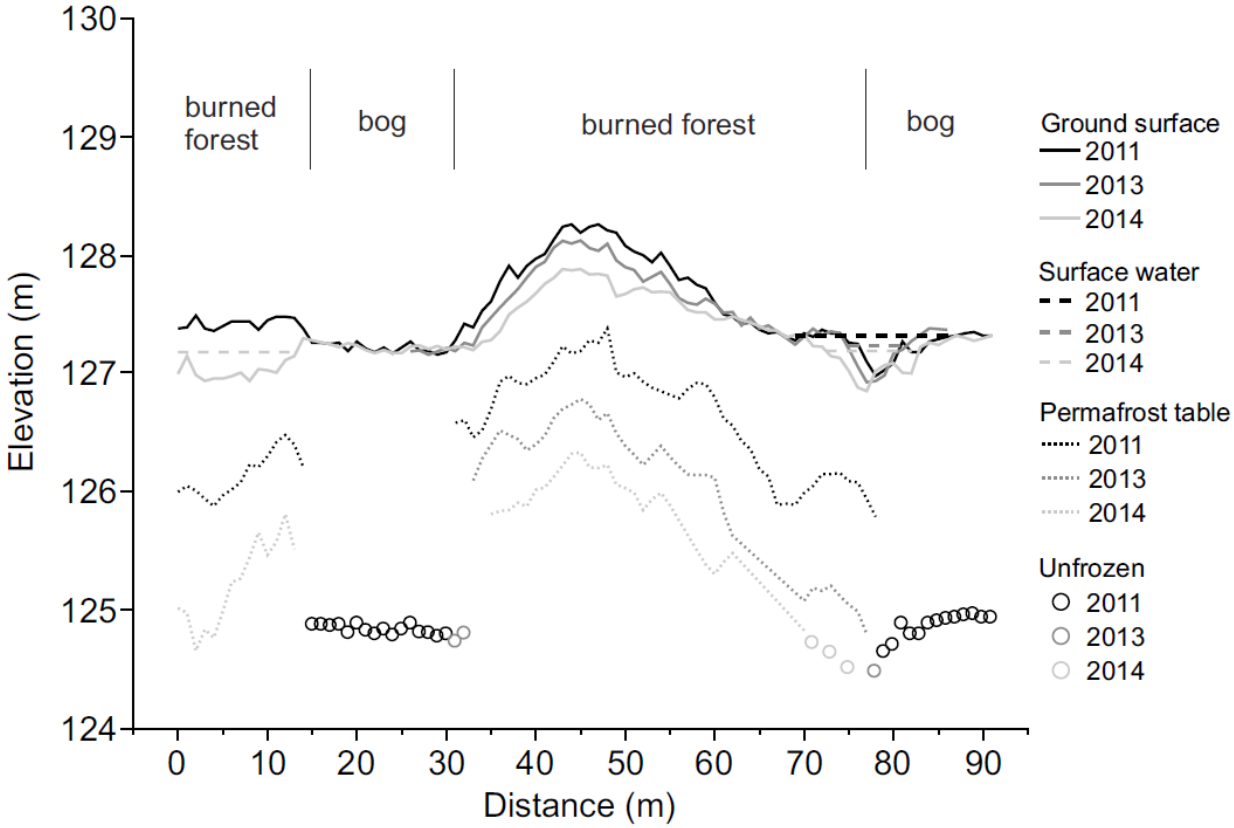

Figure 23. Cross-section of the 2010 fire transect through burned black spruce forest and collapse-scar bogs, showing the elevations (m) of the ground surface, surface water, permafrost table, and maximum observed depths of unfrozen ground in 2011, 2013, and 2014. Note that there is a data gap from 0-35 m for 2013. Another collapses car bog is present ~10 m before the beginning of the transect.

5.2.1.4 Observed soil thermal regimes

Mean annual surface temperatures (MAST) were generally higher in the most recent burns (Figure 24). In particular, the 2010 burn had the highest MAST (2.6˚C), whereas the 1975 burn had the lowest MAST (-0.6˚C). Mean annual deep temperatures (MADT, 1 m depth) were also higher in the most recent burns, though only the 2010 burn had MADT (0.6˚C) significantly warmer than the coldest sites, the 1930 and 1988 burns (-0.7˚C, for each). MADT was inversely correlated with OLT (n = 14, r = -0.73, r^2=0.54, *P* = 0.003), and was not correlated with active layer soil moisture (n = 14, r = 0.41, r^2=0.16, *P* = 0.151).

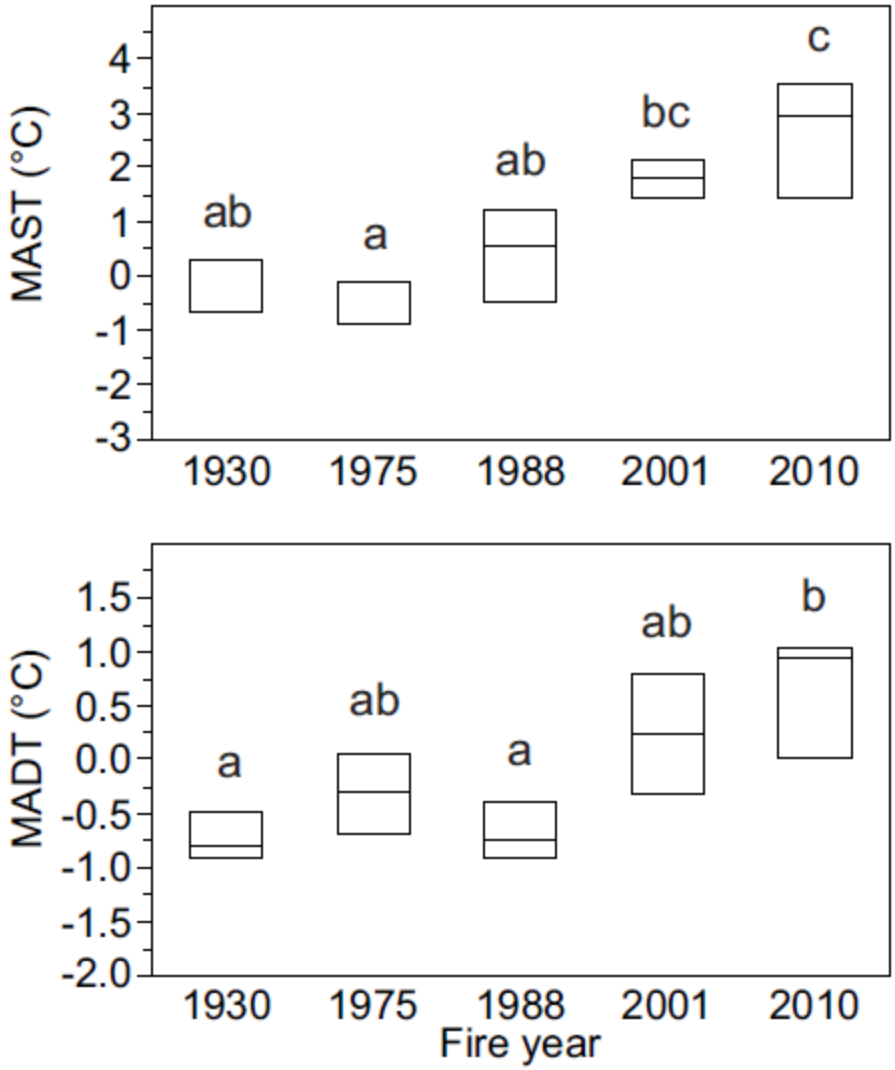

Figure 24. Box plots of MAST and MADT by fire year. Data are from hydrological year 2013 (n = 14). Tukey-Kramer HSD post hoc tests were conducted following one-way ANOVAs. Factors not connected by the same letter are significantly different ($p < 0.05$).

Surface thawing-degree days (TDD) were similar among fire scars (Figure 25). Surface freezing degree days (FDD) were lowest (coldest) in the oldest stands (1930 and 1975), and highest (warmest) in the youngest stands (2001 and 2010). At 1-m depth, mean FDD sums were generally higher in the two youngest stands. The 1930 and 1988 burns had 0 deep TDD. Mean deep TDD sums were highest in the 2010 and 1975 burns. The 1975 burn was unique in that it had both relatively high deep TDD and low deep FDD.

Seasonal soil temperature dynamics at 1-m depth were distinct at the 1975 burn, which exhibited the greatest seasonal fluctuation of soil temperature (Figure 26). These soils were the first to freeze in the winter and thawed rapidly in the summer. The 1930 and 1988 sites showed soil thermal patterns similar to each other, with soils remaining at or below 0˚C year-round and maximum permafrost temperatures from -0.3˚C to 0˚C. The 2001 and 2010 sites had similar thermal regimes. Within the 2001 fire scar, one site (OLT = 6 cm) showed the progressive thawing and warming of soil from 2011-2013, with winter soil temperatures constrained at 0˚C.

This observed warming trend was consistent with the thaw depth monitoring at this site, which showed increases in thaw depth from 99 cm to 179 cm between 2011 and 2013. At the other site in the 2001 fire scar (OLT = 13 cm), warm permafrost remained at 1-m depth, and thaw depths likewise were similar over the three years. In the 2010 fire scar, all three sites lacked permafrost at 1-m depth, and all exhibited increasing summer temperatures over the 2–3 year record. Winter soil temperatures at two of the three sites in the 2010 burn did not fall below 0˚C.

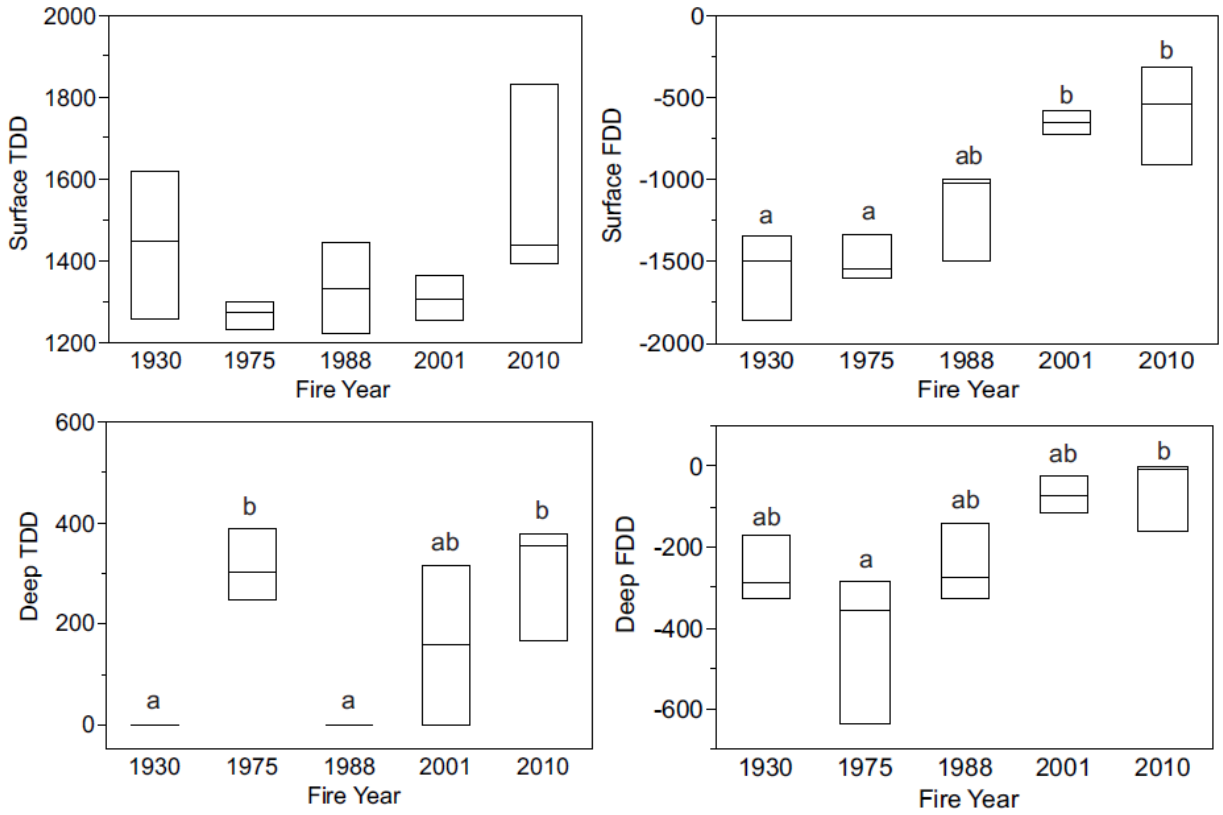

Figure 25. Box plots of surface and deep TDD and FDD by fire year. Data are from hydrological year 2013 (n = 14). Tukey-Kramer HSD post hoc tests were conducted following one-way ANOVAs. Significant differences ($p < 0.05$) are denoted by different letters.

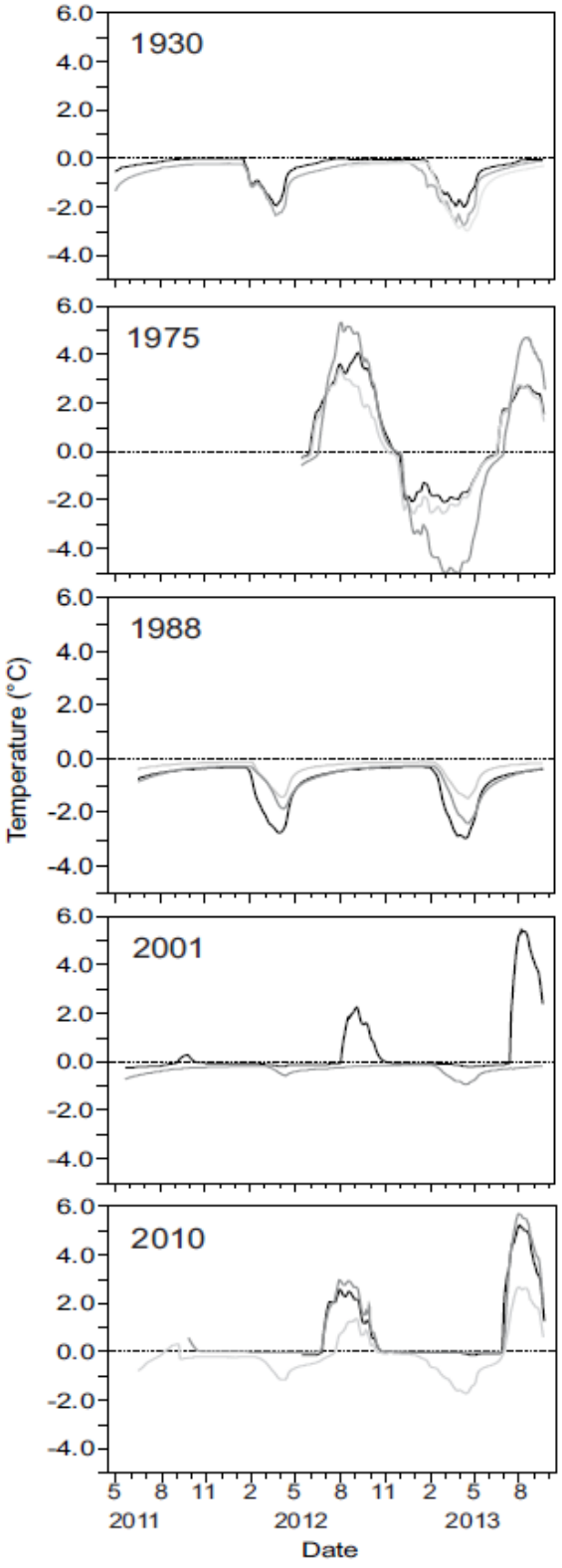

Figure 26. Measured daily soil temperatures at 1 m depth for all sites within each fire scar. The x-axis tick marks depict the first day of each month. The dotted reference line shows 0°C.

5.2.1.5 Thermal model simulations

Given the differences in the soil stratigraphy among sites and in the climate when the fires occurred, we used thermal modeling to better evaluate the effects of climate history (snow and air temperatures) on permafrost responses to fire. In the simulations, we varied OLT in the silty soil type and used actual climate forcing data over the 1930–2013 period.

Permafrost was stable in the simulations at the 30-cm and 15-cm OLT levels. At the 7 cm OLT level, permafrost thawed rapidly beginning in the 1970s, a talik formed in the 1980s, and the original permafrost table dropped to about 7.6 m. A brief period of permafrost aggradation occurred in the early 2000s, which subsequently reverted to an unfrozen talik in the 2010s. At the 0-cm OLT level, the permafrost table dropped below 10 m depth, although a thin layer of near-surface permafrost formed in the mid-1950s and disappeared in the early 1970s (1955-1972).

When comparing climatic periods, simulated thaw depths were deeper in the 1976–2013 period overall compared with the 1930–1975 period (Figure 27). Mean annual air temperature was significantly higher in the 1976–2013 period (-2.3ºC) relative to the previous 46 years (-3.4ºC) (t-ratio = 5.14, df = 82, P <0.0001), whereas mean annual snow depths were similar (t-ratio = 0.05, df = 82, P = 0.96). The permafrost dynamics in the simulations that exhibited talik formation appeared to be closely related to short-term weather patterns (Figures 27 and 28). Talik initiation began from 1976-1989, a period with relatively high air temperatures and average snow depths. Deepening thaw depths and extensive talik development occurred during 1990–1995, coincident with generally above average snow accumulation and relatively high air temperatures. Despite relatively high air temperature during 1996–2010, thaw depths decreased and the partial refreezing of taliks occurred in conjunction with low snow depths. During 2011–2013, the thawing of the upper newly-aggraded permafrost above taliks and the initiation of new taliks in some sites corresponded with increased snow accumulation, despite relatively low air temperatures. These observations suggest that changes in either air temperature or snow accumulation or both can significantly influence permafrost stability.

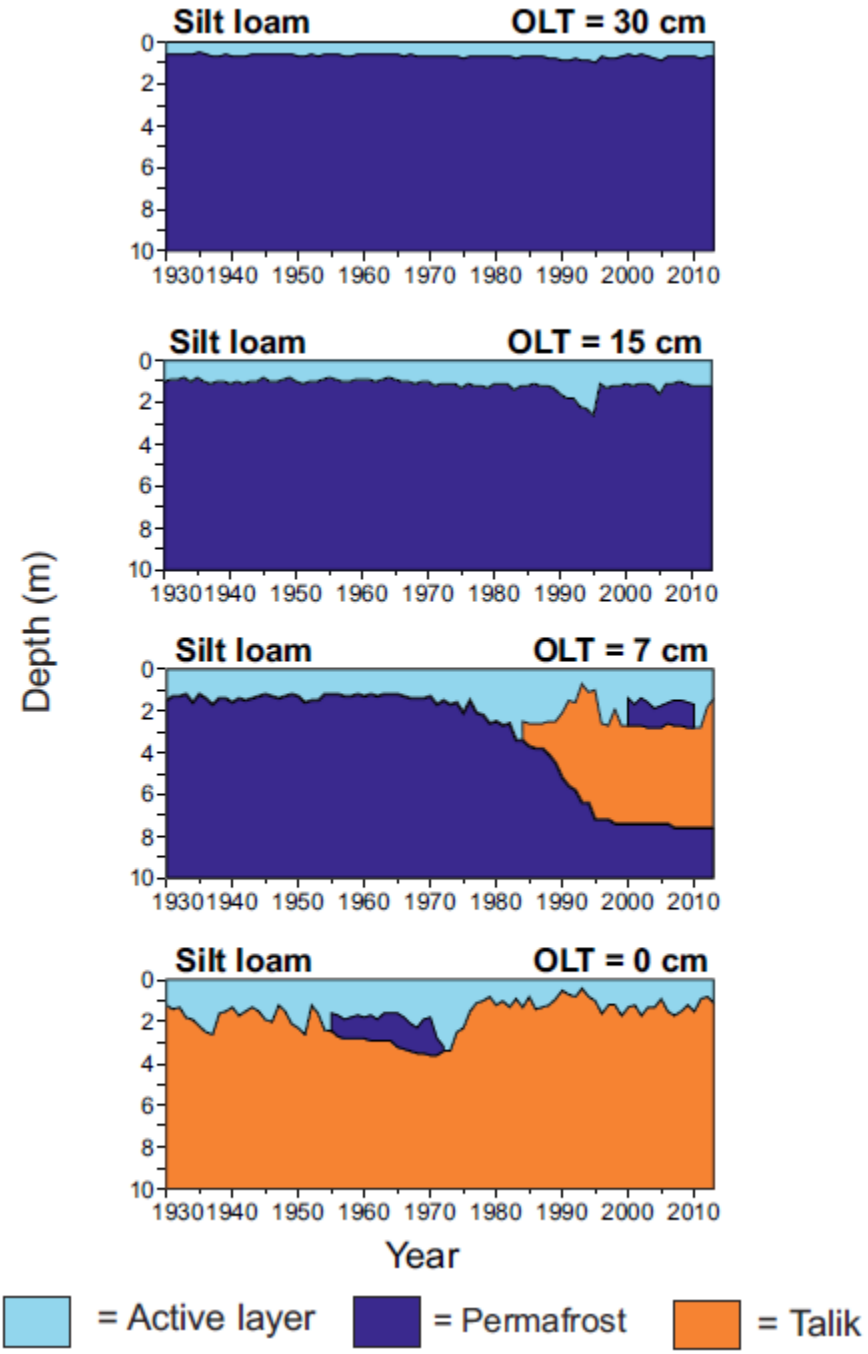

Figure 27. Simulated active layer, permafrost, and talik depths from 1930 - 2013 in silt loam-dominated sites with varying levels of organic layer thickness (OLT).

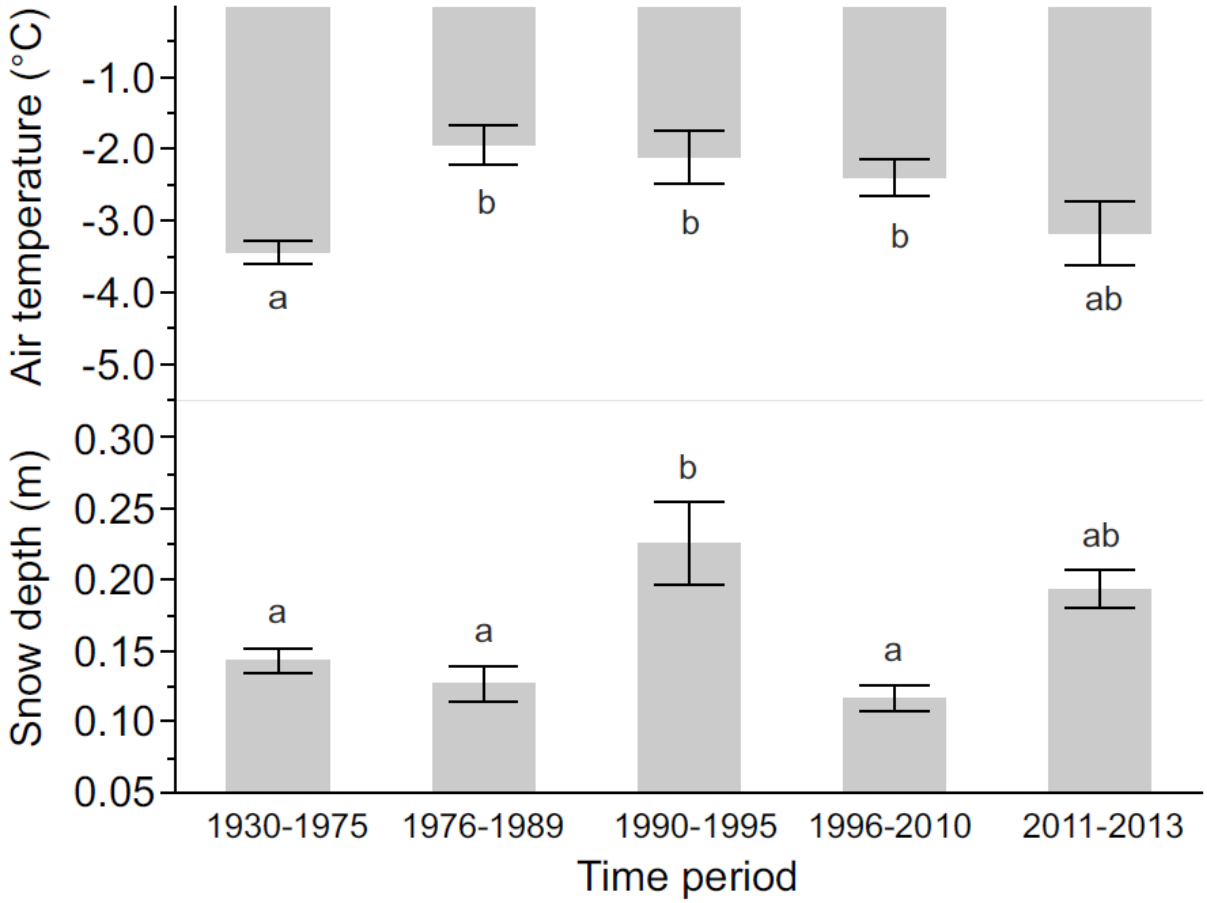

Figure 28. Mean annual air temperature and snow depth by time period. Time periods were chosen to represent dominant patterns in simulated permafrost dynamics. Values are means ± SE and significant differences are depicted by lettering.

5.2.2 Discussion

5.2.1.1 Heterogeneity of soils and vegetation

Our field monitoring of the response of permafrost to fire across a chronosequence of fire scars found that the 2001 and 2010 fires caused substantial permafrost thaw, whereas the older fires had relatively stable permafrost. Assessing the response to fire, however, was complicated by heterogeneous soil conditions, which limited the utility of the chronosequence design. The soil thermal patterns observed among burn ages appeared to be more closely related to organic layer thickness, soil moisture, and mineral soil texture than time since fire. Overall, the observed soil physical and thermal patterns could be broadly grouped by the dominant soil characteristics: the older peaty sites (1930 and 1988 fires), the younger silty sites (2001 and 2010 fires), and the sandy site (1975 fire).

The older peaty sites were characterized by organic layers typically over 1 m thick and moist soils. Radiocarbon dating indicated that the peat had accumulated over the course of at least 2,000-3,000 years. Thaw depths were shallow in these sites due to the insulating upper organic layers, and thus, much of the organic material is frozen as permafrost and protected from combustion. The soil thermal regimes of the peaty sites were all similar, with currently stable but

warm (-1.0 – -0.4˚C) permafrost. The cryostratigraphy of the 1988 peaty sites suggests that permafrost thawed after fire and subsequently recovered. The younger silty sites had thinner post-fire (and presumably pre-fire) organic layers (0 – 15 cm) underlain by thick layers of moist to saturated silt loams. The relatively thin organic layers corresponded to relatively thick active layers in these soils, which are still changing in response to the recent fires. Several of the young silty sites showed potential talik development, with minimum soil temperatures constrained at 0˚C suggesting the presence of unfrozen water year-round. Such talik development buffers the underlying soils from freezing air temperatures and can cause a positive feedback to permafrost thawing (Osterkamp and Burn 2003). The 1975 burn scar was distinct with the presence of sandy loams or sands near the surface and low soil moisture content. Consequently, the dry soils with thin organic layers had a high amplitude of soil temperatures, with early and deep thawing, rapid freezing, and thick active layers.

Plant community composition among the burn scars was correlated with stand age, but the differences in dominant species among the fire scars indicated that the sites did not all represent stages of the same successional sequence. Vegetation composition was closely related to soil moisture, which is associated with soil texture, but not to other soil physical characteristics such as organic layer thickness or thaw depth. Birch forests (1988) and spruce forests (~1930) alike were underlain by thick peats and thin active layers. The most recently burned black spruce stands (2001 and 2010) had early successional vegetation and thawing permafrost in most cases. The mixed forest (1975) with dry sandy soils, a thin organic layer, and thick active layer had unique soil thermal regimes.

The observed heterogeneity in soil conditions within the Tanana Flats reflects the legacy of complex environmental histories. The temporal variation in historic floodplain abandonment has left a legacy of fluvial and eolian sediment deposition that manifests in spatial heterogeneity of mineral soil stratigraphy and subsequent soil development. With vegetation establishment occurs the accumulation of soil organic material, which reduces soil heat flux. In fine-grained soils with high soil moisture, this cooling results in the aggradation of ice-rich permafrost and the uplift of peat plateaus, upon which forested ecosystems continue to develop. In our peaty sites, historic permafrost degradation and thaw settlement led to the conversion of forests to aquatic systems. Subsequent peat accumulation and re-aggradation of ice-rich permafrost reformed peat plateaus which returned to a forested state. The long-term history of sediment deposition, permafrost aggradation and degradation, hydrology, and organic accumulation thus created heterogeneous soil environments within current forests in this lowland. Other lowland areas exhibit similar inherent patchiness resulting from dynamic interactions of these long-term processes, complicating generalizations and predictions in these landscapes (Jorgenson et al., 2013a; Kanevskiy et al., 2014).

5.2.1.2 Thaw settlement, feedbacks, and wetland expansion

Minor differences in elevation are related to major differences in hydrology, permafrost, vegetation, and ecosystem properties in the lowlands (Jorgenson et al., 2001a). The Tanana Flats landscape is a mosaic of forest, scrub, and meadow ecosystems interrupted by numerous collapse-scar bogs and fens. Moderate changes in microtopography due to the thawing of ice-rich permafrost in forests and subsequent collapse of the soil surface can result in major changes in hydrology. Water impoundment greatly alters the surface energy balance, and can cause a strong positive feedback to permafrost degradation, in addition to altering vegetation composition and

ecosystem function (Camill et al., 2001; Jorgenson et al., 2001b; Myers-Smith et al., 2008; Jorgenson et al., 2010).

We found that the upper permafrost (within 3 m of soil surface) within the Tanana Flats study area was generally ice-rich (55-79% vol), and that the thawing of this permafrost could cause up to 0.9 m of thaw settlement, resulting in the soil surface collapsing on average to 0.1 m below the water level of the adjacent collapse-scar bogs. This minimization of relative elevations between forest and bog suggests the potential for water impoundment through collapse-scar expansion or the creation of new thermokarst depressions at many of our sites. Thaw settlement and lateral collapse-scar bog expansion were observed after the 2001 and 2010 fires. The effects of the 2010 fire were particularly notable for the rapid collapse of some of the ground surface in the burned forest to below the water level, with up to 0.5 m of subsidence recorded between 2011 and 2014. The magnitude of permafrost thawing was typically greatest along the forest-bog interface, suggesting the importance of hydrologic feedbacks to fire-initiated permafrost thaw. In the absence of fire, collapse-scar bogs in this region have expanded at rates of 0.1 - 0.5 m/year (Jorgenson et al., 2001a, b), whereas lateral expansion averaged 2 m/year in the first 3 years after the 2001 fire (Myers-Smith et al., 2008). The interaction between fire, ground ice, and hydrology may therefore be a significant mechanism accelerating the decline in forested ecosystems and the expansion of collapse-scar bogs in this landscape.

These results support the first hypothesis we presented in this section, that the initial (i.e. within 1-3 years) response of permafrost lowland landscapes to fire includes a measurable decrease in organic layer thickness, an increase in seasonal thaw depths, an increase in surface soil temperatures, and a change in the areal extent of thawed bogs. These processes lead to substantial permafrost thaw, ground surface collapse (thermokarst), and water impoundment in recently disturbed (burned) areas. The dramatic changes evident in the seasonal thaw depth probing, in our soil temperature measurements, and in the repeat ground elevation surveys support this hypothesis.

5.2.1.4 Permafrost dynamics after fire

To evaluate the effects of fire severity and climate on permafrost dynamics, we supplemented our field studies with simulations using the GIPL permafrost thermal model. The models were calibrated using the observed stratigraphy of silt loam sites, and were run from 1930-2013 with measured air temperature and snow depth as forcing data. We analyzed the sensitivity of thaw depths to varied organic layer thicknesses to infer the effects of different levels of fire.

The simulations in the silt loam sites suggested vulnerability to talik formation and deep permafrost thawing with OLT reduction. The relatively shallow permafrost tables (mean = 0.7 m) at the 30 cm-level of OLT declined sharply to 4.4 - >10 m with talik development. Talik onset occurred when thaw depth exceeded 2.7 m in this soil type. The ability of soils to refreeze beyond this depth is limited by high moisture content, which delays freezing and slows frost penetration.

The simulations also suggest that there are thresholds of OLT below which permafrost will destabilize, but the thresholds vary over time in response to climate. With the complete removal of the organic layer, permafrost could not be sustained within the upper 10 m of soil. With the OLT reduced to 7 cm, a deep talik developed, the upper portion of which refroze temporarily as permafrost. The original permafrost table eventually stabilized beneath the talik at ~7 m depth.

The patterns and timing of permafrost degradation, talik formation, and subsequent permafrost aggradation over the 1930–2013 period also underscore the importance of multi-year

to multi-decadal fluctuations in climate in mediating the effects of fire on permafrost. The vulnerability of permafrost to degradation after fire increased sharply in the 1970s, coincident with multi-decadal increases in air temperatures after a major shift in the Pacific Decadal Oscillation in 1976 (Hartmann and Wendler, 2005). Since the 1970s, permafrost appeared to be sensitive to short-term variations in snow accumulation. The pronounced thawing of permafrost from 1990-1995 and from 2011-2013 was associated with periods of high snow accumulation, whereas a period of permafrost recovery from 1996-2010 co-occurred with low snow accumulation. These patterns highlight a likely interaction between air temperature and snow depth on post-fire permafrost dynamics.

Although talik formation could signal long-term permafrost degradation (Osterkamp and Burn, 2003; Yoshikawa et al., 2003), our simulations demonstrate that, in the absence of water impoundment, short-term fluctuations in snowfall and air temperature could initiate the refreezing of taliks and permafrost recovery in some soil types in the current day climatic regime. However, under future climate scenarios with projected increases in air temperatures and winter precipitation (IPCC, 2014), the thresholds of OLT needed to protect permafrost would increase (i.e., less severe fires will have larger effects in a warmer climate with increased snowfall), and the likelihood of permafrost recovery will be reduced.

These results support the second hypothesis we had for this aspect of our research, that thermal model results simulating thaw depths following fire mimic field thermal measurements and can be used to predict the relationship between permafrost ice content, disturbance, and thaw subsidence. There was a rapid (within years) response to fire in the thawing of permafrost, subsidence of the local ground, and increase in soil temperatures. This response was captured in our GIPL model simulations.

5.3 Biophysical, geophysical, and airborne measurements of permafrost geomorphology

High-resolution satellite imagery, vegetation determinations, airborne LiDAR imagery (except the 1975 site), dGPS surface elevations, seasonal thaw depths, and ERT measurements from all five fire scar locations are provided in Figures 29-33). Table 7 includes a summary of the ERT locations, lengths, and electrode spacings. The five sites represent a chronosequence of areas burned by wildfires in 1930, 1975, 1988, 2001, and 2010. Below we describe the varying patterns of vegetation, topography, thaw depths, soils, and ERT for each site in the different aged fire scars. We then compare the permafrost distribution across the sites and evaluate relationships among biophysical factors.

Table 7. Electrical resistivity tomography information for the five fire scar field sites in this study.

	Site name (fire year)						
	1930	1975	1988	2001	2001	2010	2010
Geophysical line start (distance in meters along transect)	54	-33	0	-26	180	0	130
Geophysical line end (distance in meters along transect)	219	215	152	140	318	90	200
Electrode spacing (meters)	2	3	2	2	2	1	1
Pixels per unit spacing (horizontal)	1.01	21.89	23.91	1.01	26.33	1.01	1.01
Root mean square error	5.5	12.4	13.8	2.7	10	9.5	9.9

5.3.1 Biophysical Characteristics by site

At the 1930 fire site (Figures 29 and 34), vegetation along the 215 m transect consisted of birch forest (23% of transect), mixed black spruce-birch forest (11%), drowned forest with aquatic forbs (10%), dwarf shrub-sphagnum bog (41%), sedge-sphagnum bog meadow (3%) along the collapsing margins of the forest, and herbaceous fen (12%; Table 8). The thermokarst features in the collapsing margins of the forest were not identifiable in the LiDAR imagery because the small surface water bodies absorbed most of the near infrared LiDAR signals and the data holes they represent were smoothed by hydro-flattening. Mean ground-surface elevations of terrain in the mixed black spruce-birch forest (128.65 m asl) were ~0.6 m higher than those in the herbaceous fen (127.60 m), dwarf shrub-sphagnum bog (128.02 m), or sedge-sphagnum bog meadow (128.00 m) associated with thermokarst terrain. The birch forest with thermokarst pits had intermediate and highly variable elevations (128.30 m). Thaw depths indicated near-surface permafrost (NSP) was present in the mixed black spruce-birch forest (mean = 53.3 cm) and in the birch forest (63.3 cm). Seasonal frost was encountered in the dwarf shrub-sphagnum bog (58.6 cm) and sedge-sphagnum bog meadow (62.4 cm), while NSP was absent in the herbaceous fen (unfrozen to 2.5 m). Soil cores in the mixed black spruce-birch forest (4 m deep core at 200 m distance) and in the birch forest (3 m deep at 65 m distance) were ice rich and provided additional confirmation of permafrost below these vegetation types. Soils at this site include an upper peat layer (averaging 89 cm thick) over a mixture of silt loam, sand, and sandy loam, while gravel was encountered at depths of 2.9 to 3.1 m. The permafrost was dominated by thick layered, braided ice, and pore ice cryostructures. ERT measurements at 2 to 5 m depths across the transect starting at 60 m show irregular mixed values in the birch forest (7,000 to 20,000 Ω-m), low values in the bog (<500 Ω-m), and high values in the mixed black spruce-birch forest (2,000–60,000 Ω-m). The ERT profile shows thaw bulbs extending beneath the thin layers of shallow permafrost near the bog margins. The ERT profile suggests the majority of the bog is thawed to a depth of at least 22 m. We attribute the slightly elevated ERT values at 117 to 122 m elevation to unfrozen gravel found below 124 m elevation.

Table 8. Abundance (% of transect) of ecotypes at the study sites on the Tanana Flats.

Fire Scar Transect ID	1930 (T1)	1970 (TF70)	1988 (TF50)	2001 (TF01)	2010 (TF10)	Overall
Black Spruce Forest	0.0	16.0	0.0	0.0	0.0	4.2
Mixed Spruce-Birch Forest	11.3	0.0	0.0	0.0	0.0	1.9
Mixed Spruce-Aspen Forest	0.0	58.9	0.0	0.0	0.0	15.4
Birch Forest	22.5	0.0	56.2	0.0	0.0	13.0
Grass Meadow	0.0	0.0	12.4	0.0	0.0	2.0
Low Shrub-Tussock (post-burn)	0.0	0.0	0.0	0.0	9.4	1.5
Low Shrub-Grass (post-burn)	0.0	25.1	0.0	53.9	0.0	19.9
Forb Meadow (post burn)	0.0	0.0	0.0	0.0	41.9	6.6
Drowned Forest (post-burn)	0.0	0.0	0.0	10.3	3.4	3.1
Drowned Forest	9.5	0.0	0.0	0.0	0.0	1.6
Herbaceous Fen	12.2	0.0	0.0	0.0	0.0	2.1
Sedge-Sphagnum Bog Meadow	3.2	0.0	31.4	35.7	45.3	21.6
Dwarf shrub-Sphagnum Bog	41.4	0.0	0.0	0.0	0.0	7.1
Total	100.0	100.0	100.0	100.0	100.0	100.0

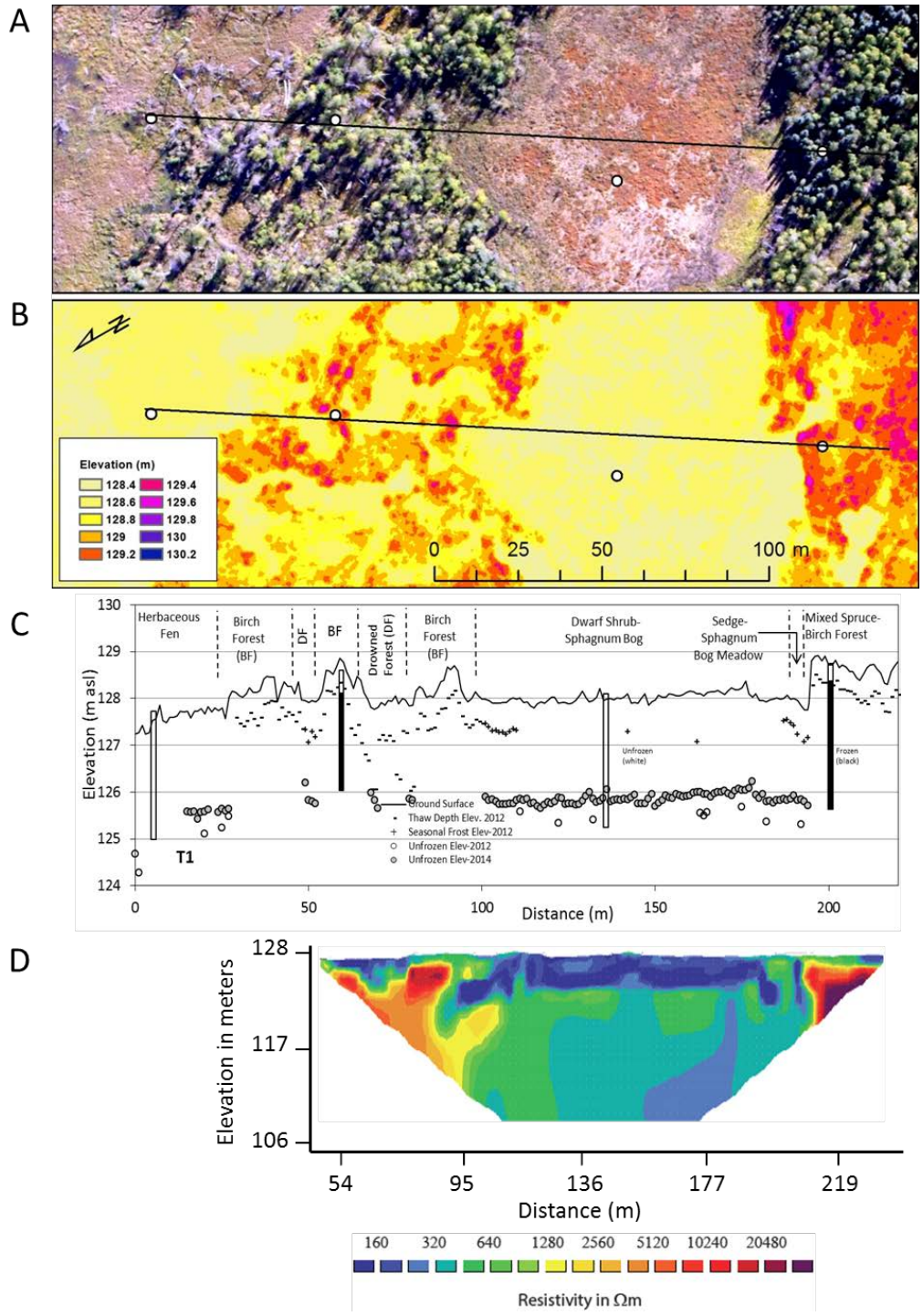

Figure 29. A: An aerial image of the 1930 fire scar. B: airborne LiDAR imagery, shaded by elevation, for the same region presented in the upper panel. The bold line indicates the location and length of the transect at the site while circles denote locations where SIPRE cores were collected. C: A detailed cross section of the vegetation, ground elevation, SIPRE core depths, seasonal thaw depths, and elevations of unfrozen material across the transect. D: electrical resistivity tomography survey results across the transect.

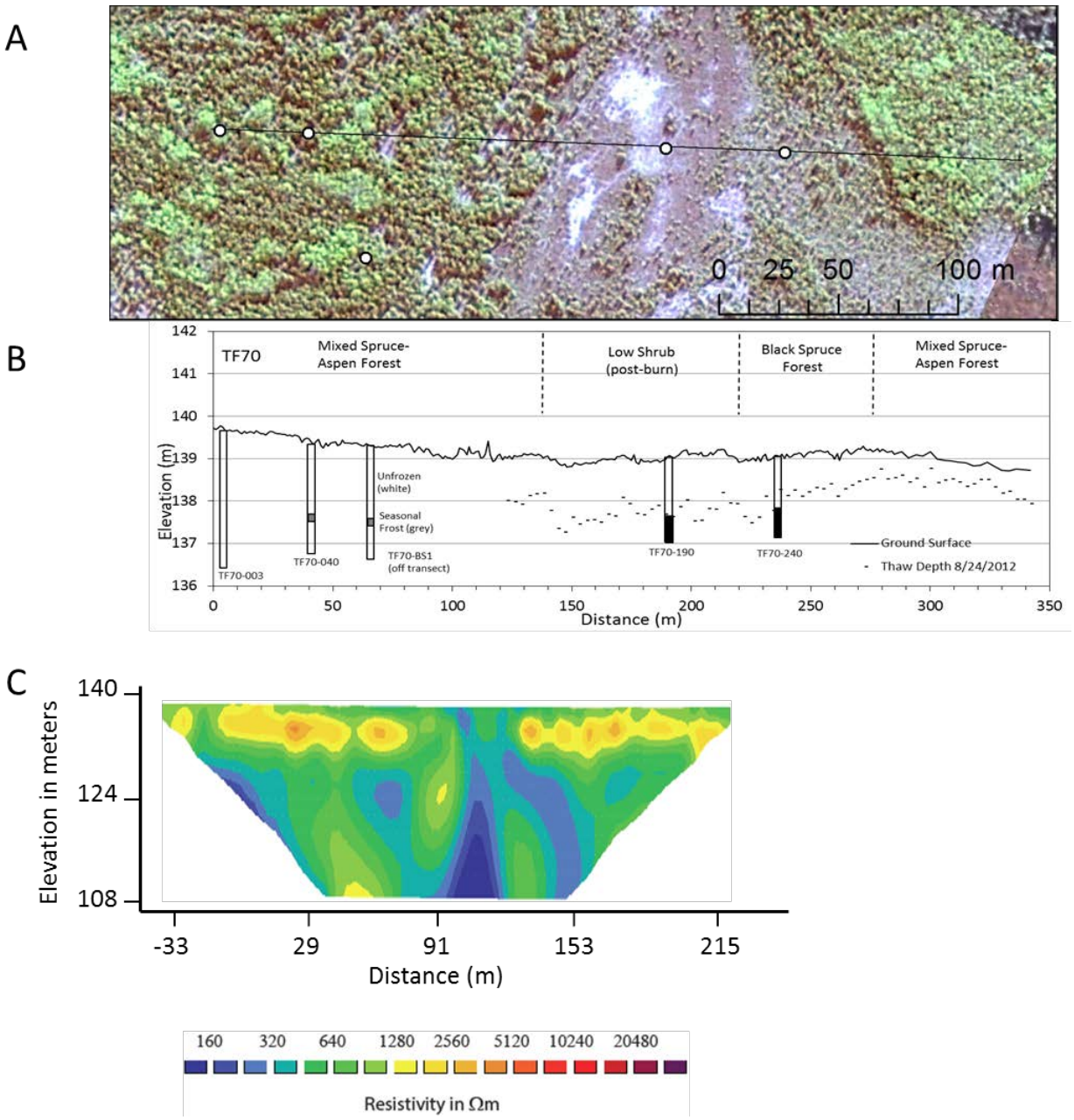

Figure 30. A: An aerial image of the 1975 fire scar. B: airborne LiDAR imagery, shaded by elevation, for the same region presented in the upper panel. The bold line indicates the location and length of the transect at the site while circles denote locations where SIPRE cores were collected. C: A detailed cross section of the vegetation, ground elevation, SIPRE core depths, seasonal thaw depths, and elevations of unfrozen material across the transect. D: electrical resistivity tomography survey results across the transect.

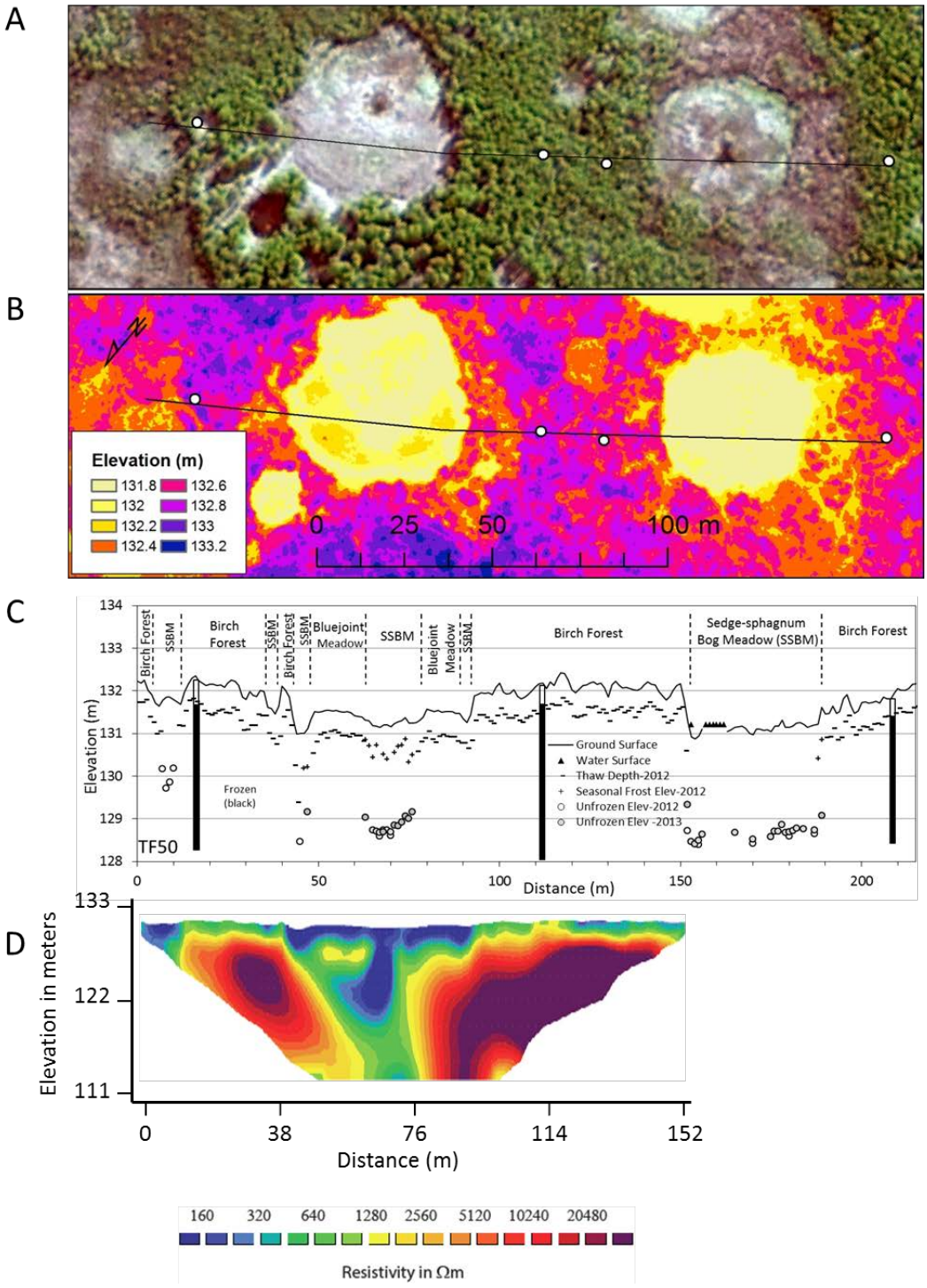

Figure 31. A: An aerial image of the 1988 fire scar. B: airborne LiDAR imagery, shaded by elevation, for the same region presented in the upper panel. The bold line indicates the location and length of the transect at the site while circles denote locations where SIPRE cores were collected. C: A detailed cross section of the vegetation, ground elevation, SIPRE core depths, seasonal thaw depths, and elevations of unfrozen material across the transect. D: electrical resistivity tomography survey results across the transect.

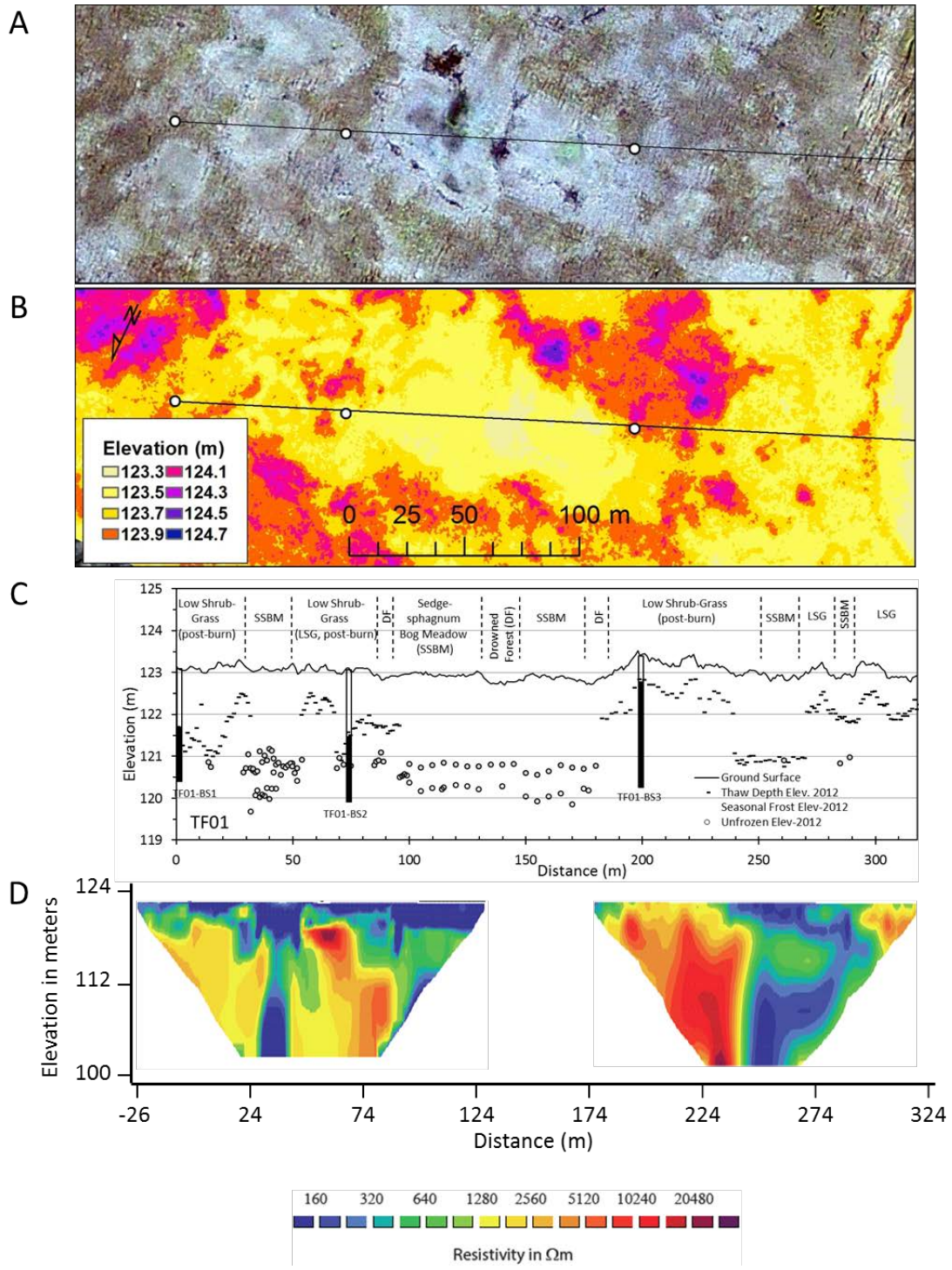

Figure 32. A: An aerial image of the 2001 fire scar. B: airborne LiDAR imagery, shaded by elevation, for the same region presented in the upper panel. The bold line indicates the location and length of the transect at the site while circles denote locations where SIPRE cores were collected. C: A detailed cross section of the vegetation, ground elevation, SIPRE core depths, seasonal thaw depths, and elevations of unfrozen material across the transect. D: electrical resistivity tomography survey results across the transect.

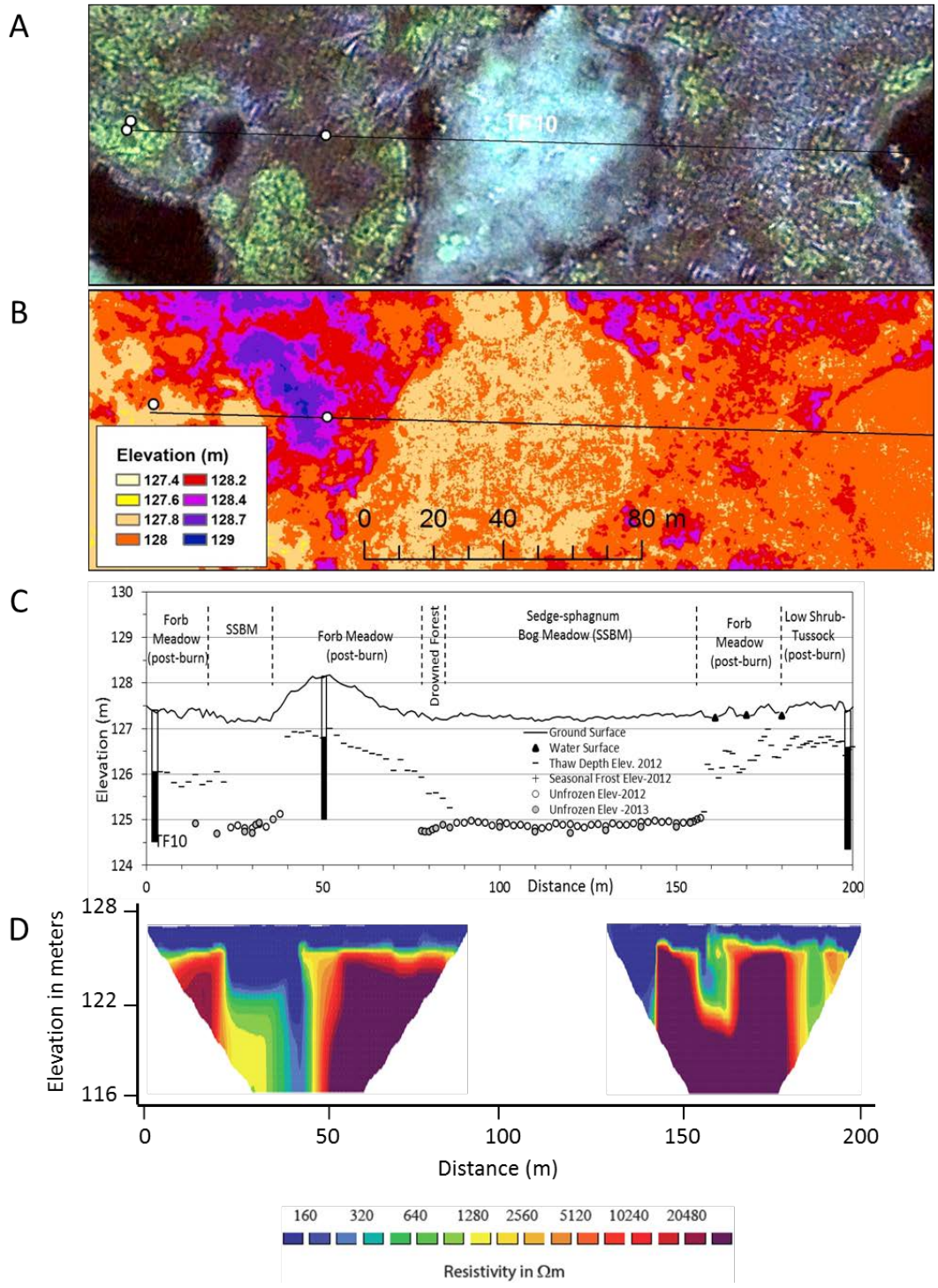

Figure 33. A: An aerial image of the 2010 fire scar. B: airborne LiDAR imagery, shaded by elevation, for the same region presented in the upper panel. The bold line indicates the location and length of the transect at the site while circles denote locations where SIPRE cores were collected. C: A detailed cross section of the vegetation, ground elevation, SIPRE core depths, seasonal thaw depths, and elevations of unfrozen material across the transect. D: electrical resistivity tomography survey results across the transect.

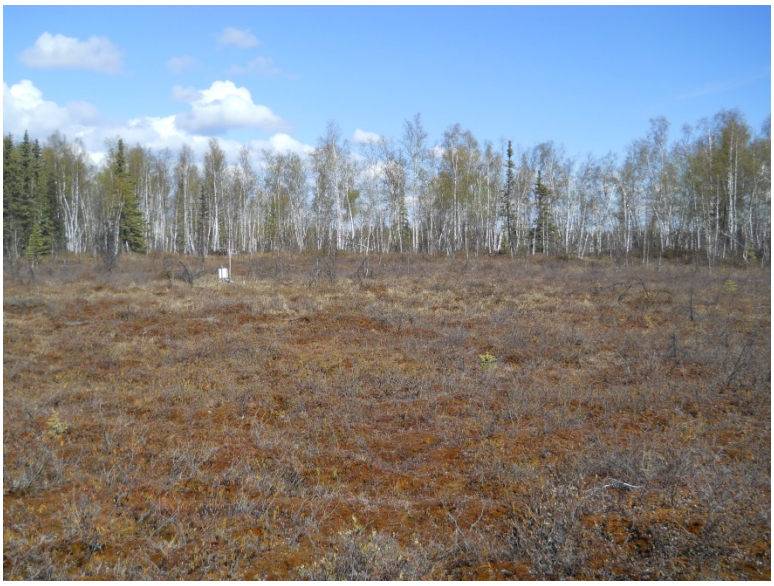

Figure 34. Photos from the 1930 fire scar site. This area has no recent record of fire but the location has been experiencing permafrost degradation since the 1970s. Upper: a dried out open region. Lower: actively degrading permafrost has led to surface water ponding and destruction of birch forest.

At the 1975 fire site (Figures 30 and 35), vegetation along the 342 m transect consisted of mixed black spruce-aspen forest (59%), black spruce forest (16%), and low shrub-grass, post-burn (25%). Elevations ranged from 139.7 m asl in the black spruce forest to 138.8 m in the low shrub-grass, but distinct collapse-scar features were not evident. Relict burned stumps from the 1975 fire still remain.

No LiDAR imagery was available for this location. Frost probe measurements did not conclusively identify permafrost at the site. Some of the silt layers were extremely resistant to the frost probe but SIPRE cores nearby contained unfrozen material. Near-surface soils were sandy loam, sand, or thin silt loam layers underlain by sandy soils, with gravels occurring at depths less than 1 m in the swale located at 150 to 220 m along the transect. Soils in the mixed forest had relatively thin organic layers (averaging 7 cm). In the mixed forest portion of the transect, no permafrost was encountered in the 3.2 m and 2.4 m deep soil cores taken 3 m and 40 m along the transect. In the swale at 190 m along the transect permafrost was found at a depth of 140 cm. In the black spruce forest at 240 m, permafrost was found at a depth of 128 cm. The ERT values were generally below 600 Ω-m, suggesting an absence of permafrost at most of the site. However, some thin horizontal features with ERT values above 1,000 Ω-m were likely indicative of small lenticular bodies of permafrost. They all were more than 3 m below the ground surface so our frost probe and soil coring would not have encountered them. Because our coring and thaw probe measurements could not reach these depths we cannot definitively say whether or not there was permafrost at these locations. However, based on the strong relationship between ERT values >600 Ω-m and permafrost at our sites and in numerous other studies in similar terrains we believe these locations do have small lenses of permafrost at these depths. The permafrost is present under near-surface talik and it is unclear whether this is permafrost that has been thawing to its present extent or whether permafrost is aggrading at these sites.

Figure 35. A photo of the 50 meter mark along the transect at the 1975 fire scar. Note ~50 years of growth of shrubs and birch while the burned stumps from the previous vegetation remain.

At the 1988 fire site (Figures 31 and 36), which also was burned previously around 1950, vegetation along the 215 m transect consisted of birch forest (56%), grass meadow (12%), and sedge-sphagnum bog (31%). Mean surface elevations in the birch forests (131.99 m asl) were ~0.7 m higher than those in the bog (131.28 m), while mean elevations in the grass meadow associated with newly developing permafrost within a collapse-scar bog had intermediate elevations (131.49 m). Mean thaw depths in late August 2012 in the birch forest (58.3 cm) and grass meadow (56.3 cm) were relatively shallow and thus indicative of the presence of permafrost, whereas, the sedge-sphagnum bog had slightly deeper thaw depths (66.4 cm). Soils at this site had a very thick peat layer (averaging 176 cm) on top of a mixture of silt loam and layered sand-silt. Cryostructures in the permafrost soil consisted of organic-matrix ice, lenticular ice, and ataxitic ice. A soil core in the grass meadow (at 60 m) was frozen from 51 to 240 cm, and unfrozen from 240 cm to 350 cm, indicating a new thin layer of permafrost has been aggrading. Gravel was found at 340 cm. The edges and center of the bog yielded the deepest frost probe and lowest ERT values along the transect. In the bog center (65 to 71 m), permafrost was not encountered by frost probing in the upper 2.5 m. The low ERT values in the center of the bog suggest it is thawed to at least 8 m depth. Contact resistance could not be established beyond 152 m because another bog (from 152 to 190 m) had standing water. Some surface water features

are visible in the aerial image but, as with the 1930 site, they are smoothed by the LiDAR hydro-flattening.

Figure 36. A photo of the thermistor installation from transect location 100 meters at the 1988 fire scar site.

At the 2001 fire site (Figures 32 and 37), vegetation along the 320 m transect consisted of low shrub-grass, post burn (54%), sedge-sphagnum bog meadow (36%), and drowned forest, post burn (10%; Table 3). Mean surface elevation of the low shrub-grass, post burn (123.11 m) were only slightly higher than those in the sedge-sphagnum bog meadow (122.95 m), and drowned forest, post burn (122.80 m). The LiDAR imagery from this site exhibit the small (i.e., <1 m) changes in ground surface elevation associated with the changing land surface characteristics from elevated forests to lower elevation bog features. Mean thaw depths in late August 2012 in the low shrub-grass, post burn (117.7 cm) and drowned forest, post burn (114.0 cm) were similar, and slightly deeper in the sedge-sphagnum bog meadow (139.7 cm) but at many locations permafrost was not encountered. Upper mineral soils in the forested sections are fine textured silt loams to depths of approximately 2 m, underlain by sands and gravels with permafrost consisting of layered, braided, and pore ice features. Mean organic layer thickness in the burned forest was 14 cm. At this site there is also an evident correlation between the frost probe depths and the morphology of the subsurface permafrost. For example, from 0 to 30 m the frost probe depths go from >1 m to ~50 cm at the edge of the small bog located from 25 to 55 m

along the transect. Frost probe depths increase for the 5 m on either side of the bog. A collapse scar bog from 100 to 180 m along the transect had an area of standing water from 140 to 180 m into which low contact resistance values could not be established. The ERT cross sections from the two sets of measurements at this site show the large difference in Ω-m values between frozen and thawed material. The low ERT values in the center of the small bog (at about 45 m) indicate it is unfrozen to a ground elevation depth of 100 m. Along the margins of the small bog there appears to be lateral thawing underneath the upper permafrost. The low ERT values in the large bog (from 100–140 m) suggest it is unfrozen to the maximum depths of the ERT measurements. From 180 to 240 m the frost probe depths correspond well with the permafrost surface inferred by ERT. From 238 to 270 m the frost probe depths are close to the maximum we could measure (2.7 m) and a thin horizontal layer with resistivity values between ~700 and 1,000 Ω-m in this area indicate there is a thin (i.e., a few m thick) lens of permafrost. This region is characterized by a small bog feature. The unfrozen zone underlying this bog appears to extend to the area beneath the burned black spruce forest from about 270 to 300 m, but the permafrost beneath the burned black spruce on the other side of the bog remained intact at depth. From 270 to 318 m the frost probe and ERT values again correspond well with one another indicating both methods accurately identified the top of the permafrost table.

Figure 37. Photos of the 2001 fire scar site. Upper: part of the transect (measuring tape extended, roughly 270 to 300 meters along the transect) viewed from the air. Lower: grass and willows emerging in the stand that burned in 2001.

At the 2010 burn site (Figures 33 and 38), vegetation along the 200 m transect consisted of forb meadow, post burn (42%), sedge-sphagnum bog meadow (45%), low shrub-tussock, post-burn (9%), and drown forest, post-burn (3%). Mean surface elevations in the forb meadow, post burn (127.55 m) and low shrub-tussock, post-burn (127.50 m) were only ~0.3 m higher than the sedge-sphagnum bog meadow (127.25 m). Mean thaw depths were much higher in the drown forest, post-burn (169.7 cm) and forb meadow, post burn (115.9 cm), compared to the low shrub-tussock, post-burn (83.3 cm). Permafrost soils typically had a thin organic layer over silt loam, with fluvial sand and gravel found at 2.7 to 3 m depth. Permafrost includes layered, braided, and pore ice features. The ERT measurements were separated into two sections because the middle of the transect had standing water and floating mat vegetation for which low contact resistances could not be established. Low ERT values (<500 Ω-m) from 22 to 45 m is indicates permafrost is absent in the small bog feature. It is possible the permafrost table is present roughly 6 m below the ground surface, as indicated by the elevated ERT values at that depth, but this depth is greater than our frost probe or SIPRE coring could reach so it cannot be verified. From ~50 to 90 m the ERT and frost probe measurements indicated a slowly increasing depth to the top of the permafrost below the sloping ground surface. The collapse-scar bog from 90 to 145 m had low ERT values (~300 Ω-m). A small feature exhibiting elevated ERT measurements, indicative of the presence of a permafrost table, is present from 140 to 155 m but is slightly deeper than the 2.5 m long probe could extend. The permafrost table, as indicated by ERT and frost probe measurements, slowly gained elevation with distance away from the bog (i.e., from 155 to 200 m). The collapse scar features and forested regions at this site are readily visible in the LiDAR imagery.

Figure 38. Photos from site the 2010 fire scar taken in 2011. Upper: note recently burned and downed trees with substantial grass development. This photo is from the beginning (0 meters) of the transect. Lower: researchers standing in the middle of the bog. Photo taken from transect at roughly 100 meter location. We did not detect any permafrost below the bog with frost probing or RES measurements. The bog was present before the fire but the recent fire will likely lead to permafrost degradation along the bog edges.

5.3.2 Permafrost distribution and electrical resistivity tomography

Thaw probing and ERT surveys (Figures 29-33) found permafrost to be sporadic to discontinuous along the transects due to permafrost degradation. The mean (59%) and range (42–75%) of permafrost extent (frequency of occurrence) at 2.5 m depth along our transects based on thaw probing was similar to the permafrost extent of 53% previously estimated for a small area near the 1930 fire site (Jorgenson et al., 2001a) and 48% for the broader Tanana Flats (Osterkamp et al., 2000) based on photo-interpretation. The ERT surveys, however, also provide information on the distribution of deeper permafrost and the morphology of the thawing boundary along the transition zones.

As shown in this and other studies, ERT surveys provide a robust measurement technique for identifying permafrost in the subsurface. This is largely due to the dramatic increase in Ω-m values for frozen versus unfrozen material (Kniesel et al., 2000; Fortier et al., 2008; Lewkowicz et al., 2011; Hubbard et al., 2013; Hauck et al., 2013). In this study, the ERT and thaw probe measurements were consistent with one another in identifying the presence or absence of permafrost within the surface 2.5 m for which the thaw probe could reach (Figure 39). This is similar to coupled measurement campaigns reported for continuous permafrost in the high Arctic (Hubbard et al., 2012) and discontinuous permafrost in the Yukon of Canada (Lewkowicz et al., 2011).

The ERT measurements show a complex distribution of subsurface permafrost resulting from vertical surface thawing and lateral thawing along the margins of thermokarst bogs and fens. While previous studies of thermokarst in peatlands have documented the presence of a thin permafrost shelf and underlying thermal niche along degrading margins (O'Donnell et al., 2012; Jorgenson et al., 2012a), our new ERT data provide much broader and more definitive evidence of this lateral degradation in the subsurface. Information on the geomorphology of these thawed-frozen transitions could be used to support thermal and hydrologic modeling efforts to project the response of permafrost and subsurface groundwater flows to a warming climate. Some of these degradation features will lead to formation of taliks which could then provide a positive feedback to further permafrost thaw when warm surface or shallow subsurface waters interact with the remaining permafrost.

With projected climate warming in Alaska the heterogeneous subsurface matrix of discontinuous permafrost likely will respond in unpredictable ways. The subsurface zones where permafrost thaw are mostly likely to cause topographic and hydrogeologic changes are the transitional margins between frozen and thawed ground. A current limitation in the application of the ERT technique is it is time consuming and requires ground level measurements. A promising extension of ERT measurement capabilities would be a greater application of airborne platforms like airborne electromagnetics (AEM; Minsley et al., 2012). When combined with ground based ERT and thaw probe measurements the AEM technique could allow for the extrapolation of AEM results across a broader spatial scale.

Taken in total, the results from this focus of the study support our hypotheses that the response of permafrost to deep thawing and development of taliks (thawed regions that are deeper than the depth of the winter season freeze) or bogs is controlled by disturbance severity, organic layer thickness, and permafrost geomorphologic properties. This is affirmed through the electrical resistivity measurements, the repeat imagery analyses, the seasonal thaw probing, the surface survey techniques and the core analyses. We would add that time since disturbance is also a key variable not originally addressed in our hypothesis. For example, the response of the 2010 fire to disturbance was far more rapid and provided greater surface soil thermal changes than we expected in a matter of years. This response to disturbance and thaw slows over time (~decades) as the vegetation and surface organic material re-aggrades and provides ecosystem protection once again. This is evident in the survey and thermal measurements at the older fire scars we investigated.

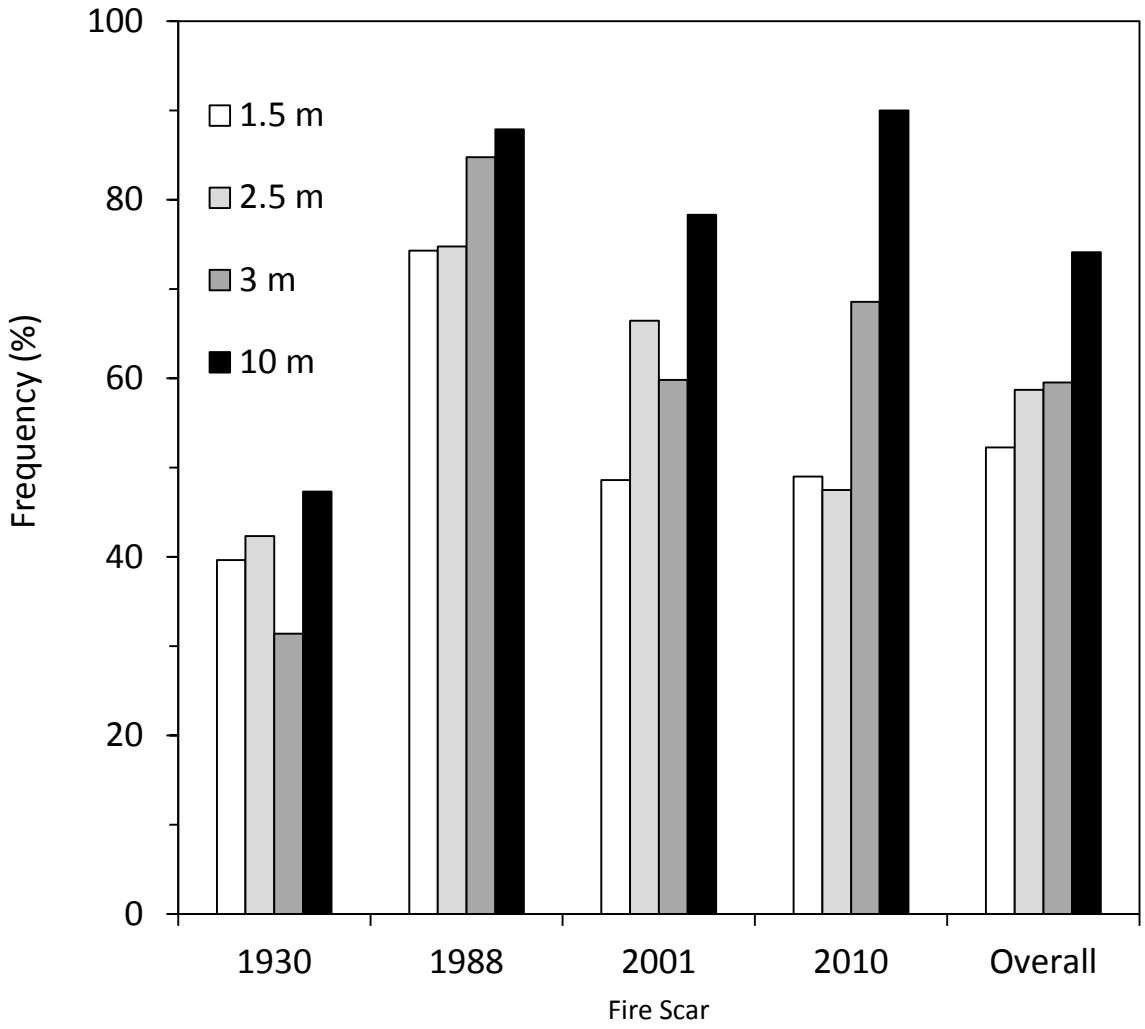

Figure 39. A histogram of permafrost frequency (in percent) for five depths at each fire scar.

5.3.3 Permafrost Distribution

Permafrost abundance at the 1.5 m depth determined from frost probing ranged from 40% to 74% across the 1930, 1988, 2001, and 2010 fire scar sites (Figure 39). Determination of permafrost extent at the 1975 burn site was problematic because of inconsistencies in probing the sandy soils; generally the soils appeared to be free of near-surface permafrost (NSP) but probing was unreliable and the site was excluded from the analyses. Permafrost extent was similar at 2.5 m depth, except at 2001, where NPS increased to 66%, indicating a thin closed talik had developed between the active layer and permafrost along a portion of the transect due to fire and thermokarst.

ERT measurements indicate permafrost degradation is occurring by both vertical thawing from the surface and lateral thawing at the margins of deeper thermokarst features. Thaw probing and ERT measurements indicate vertical thawing and shallow thermokarst pits were present at the 1930, 2001, and 2010 fire scars. At the 1930 fire site there is drowned forest present from 60–80 m distance across the transect (Figure 29). At the 2001 fire site low electric resistivity values from 0–80 and 235–270 m distances (Figure 32) indicate an absence of near surface

permafrost in these areas. At the 2010 fire site (Figure 33) there are low lying areas with low electric resistivity values and no near surface permafrost from 20–40 m and from 150–180 m along the transect. In addition, shallow closed taliks from vertical thawing down to ~2 m depth were evident at the 2001 and 2010 fire sites.

Lateral degradation from subsurface thawing often created thawed "niches" at depths from 2 to 10 m, and frozen "shelves" of NSP where subsurface thawing was more rapid than surface thawing. At the 1930 fire site a thawed niche was evident at ~90 m (~5 m maximum width) and ~200 m (~3 m) distances, based on ERT contours within the 600 to 1,000 Ω-m range. At the 2001 fire site a thawed niche was evident at ~25 m (~6 m), ~50 m distance (~2 m), ~245 m distance (~5 m), and ~300 m distance (~9 m). At the 2010 fire site, a broadly curving niche was evident at ~45 m distance (~3 m).

A comparison between permafrost distribution measured by ERT and by thaw probing at the same location found relatively high agreement in identifying frozen versus unfrozen material among the two methods (Figure 40). For locations determined to be frozen at the 2.5 m depth by probing (left half of Figure 40), ERT indicated permafrost was present at 3 m depth for 81.7% of 487 observations. In contract, at the same locations determined to be frozen at the 2.5 m depth by probing ERT indicated permafrost was (erroneously) present at 3 m depth for 18.3% of 487 observations. For locations determined to be unfrozen at 2.5 m depth by probing (right half of Figure 40), ERT indicated permafrost was present at 81.3% of 246 observations. In contrast, at these same sites ERT indicated permafrost was not present at 18.7% of the observations.

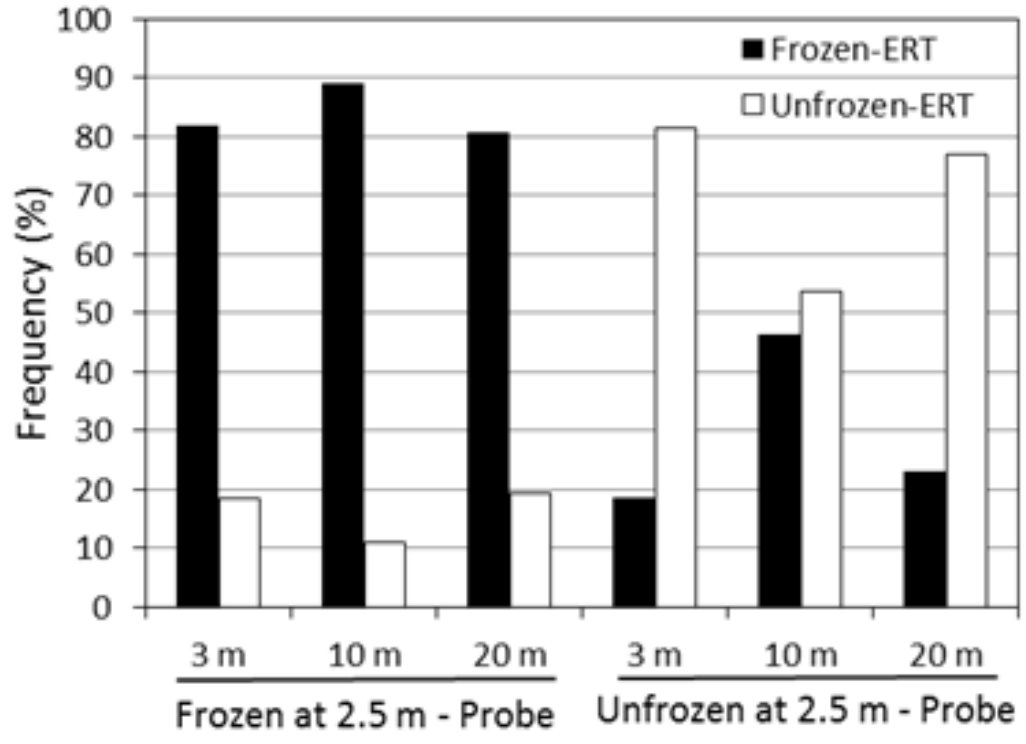

Figure 40. Correlation between permafrost status determined by thaw probing and by ERT across the 1930, 1988, 2001, and 2010 fire scar transects. The frequencies are grouped for locations where soil was frozen or unfrozen at 2.5 m by probing, with frequencies of frozen and unfrozen ground at 3, 10, and 20 m depths as determined by ERT (unfrozen when Ω–m<600, frozen when Ω–m>600).

5.3.4 Permafrost relationships with biophysical factors

Strong associations were found between surface vegetation, topography, thaw depths, and permafrost extent. Across all transects (excluding the 1975 fire site), mean relative heights (based on the mean elevation of bogs at each transect) were consistently higher in forest types (0.58 to 0.65 m) compared to bogs and fens (-0.40 to 0.02 m), while post-burn shrub and meadow ecotypes had intermediate heights (0.07 to 0.30 m). Drowned forests from thermokarst had some of the lowest relative heights (-0.07 to 0.20 m). Mean thaw depths were shallowest in the forest types (53.3 to 59.8 cm) and deepest in the post-burn types (83.3 to 126.8 cm). NSP was generally absent in the bogs, but where it was present along thawing margins the morphology of the margins were highly variable.

Permafrost extent at 2.5 m depth was nearly 100% in the forest type and early successional ecotypes after fire (post-burn), highly variable in drowned forests (25 to 76%), and sporadic in fens and bogs (0 to 16%) where NSP mostly occurred along thawing margins (Figure 41). Permafrost extent was moderately related ($r^2 = 0.52$) to relative elevations (Figure 42), with permafrost nearly always present (93 to 100% of observations) when relative heights of the surface were >5 cm and mostly absent (0 to 25%) when heights were <5 cm. The main exceptions from the trend were for drowned forest type where NPS frequently occurred (25 to 75%) even when heights were <5 cm.

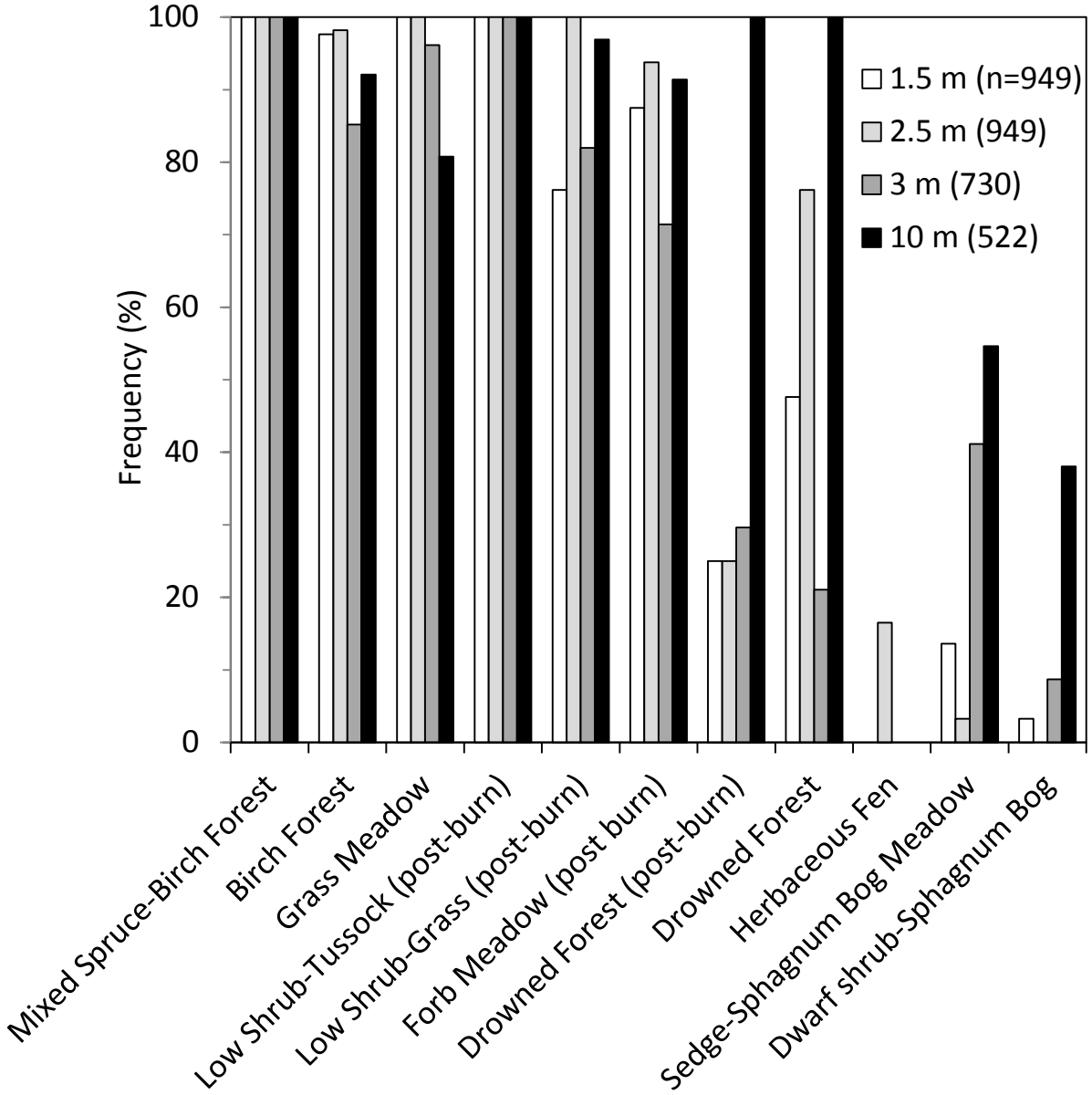

Figure 41. The relationship between the percentage of permafrost extent and the relative elevation.

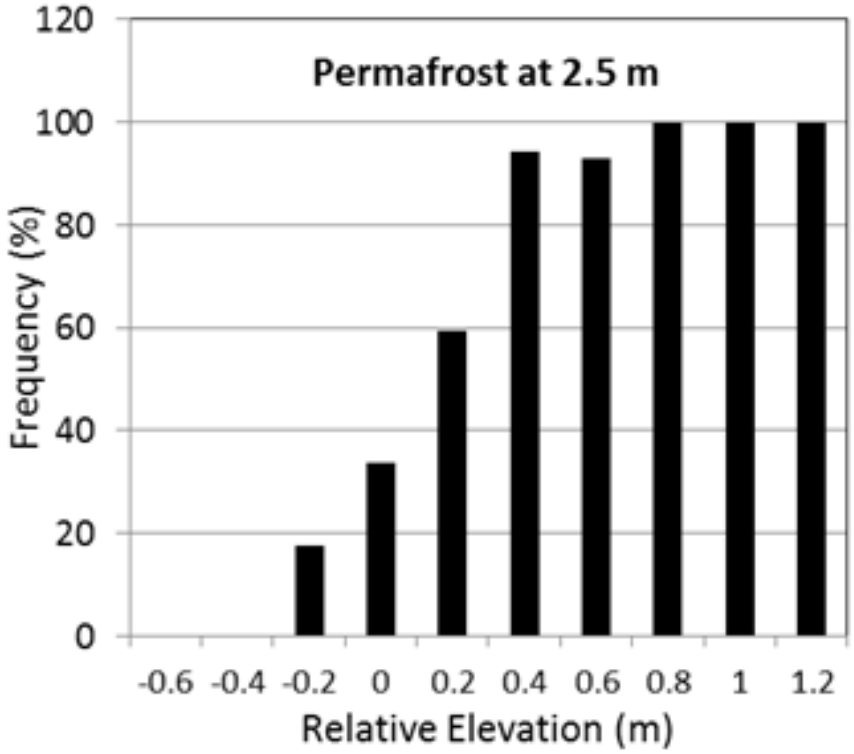

Figure 42. A histogram of the percentage frequency of permafrost extent and the relative elevation across the 11 ecotypes present at the fire scars.

5.3.5 Terrain-Permafrost Relationships

While we found that both vegetation and topography are effective at distinguishing permafrost presence/absence, only ERT is able to definitively map subsurface permafrost distribution. At sites with thawed zones surrounded by permafrost there were strong relationships between permafrost morphology inferred by ERT and the landscape features evident on satellite imagery and determined through by thaw probing. The bog and forest features that characterize the Tanana Flats lowland are easy to identify in both the aerial and LiDAR imagery. At our study sites the bogs occurred in topographic lows surrounded by forests that occurred at higher elevations. Overall, our transects crossed seven bog features that were greater than 10 m across. The distribution of permafrost in collapse-scar bogs was variable, however, and was related to depth and bog age. In one bog at the 1988 site there was a small patch of grass meadow (49-63 m distance), which was underlain by newly aggrading permafrost. One of the three bog features at the 2001 fire scar was found to be underlain by permafrost (from 238 to 270 m), although we suspect the thaw probing that indicated permafrost at depth was not reliable because a single probe in 2014 did not find permafrost. In young sedge-sphagnum bog meadows that form soon after surface thawing, permafrost determinations were inconsistent between probing (16%) and ERT (41%), probably due to both problems with probing and reliability of ERT at shallow depths. In contrast, older dwarf shrub-sphagnum bogs had similarly low permafrost occurrence for both probing (3%) and ERT (9%). We attribute the difference to the time lag for deeper permafrost to thaw under younger bogs.

Vegetation is a strong indicator of permafrost distribution. In our study we found permafrost nearly always present under lowland forest and nearly always absent in herbaceous fens and old sphagnum bogs. Similarly, Jorgenson et al. (1999) found permafrost occurred frequently (>83%)

in lowland needleleaf, mixed, and broadleaf forest but was always absent in lowland bog and meadows (0%). These vegetation indicators appear highly reliable for ice-rich lowland forests where thermokarst lowers the ground surface, increases water saturation, and causes dramatic changes in vegetation type. Vegetation spectral indices and land cover mapping derived from Landsat or SPOT imagery were the primary drivers for mapping permafrost distribution in the Yukon Flats (Pastick et al., 2013) and the Trans-Alaska Pipeline System corridor in central Alaska (Panda et al., 2012).

LiDAR, particularly repeat imagery analysis, has provided valuable information on how and where permafrost landscapes respond to climate warming and disturbance (Aberman et al., 2009; Marsh et al., 2009; Stevens and Wolfe, 2012; Hubbard et al., 2013; Jones, et al., 2013). There is great promise in applying repeat LiDAR to estimating the areal extent of thermokarst development and surface subsidence when permafrost thaws. Being able to map rates of ground surface subsidence along wetland features like bogs, fens, ephemeral and emerging streams, and lake margins would greatly add to our ability to predict how and where surface and shallow subsurface hydrology will respond to climate warming or disturbance. However, an important limiting factor is the collapse of the surface below water level and the poor ability of LiDAR to quantify ground/sediment surface elevations under water. Furthermore, the accurate identification of the water surface in images collected over time is problematic. The LiDAR used in this study was corrected ("hydro-flattened") for streams meeting a minimum width of 15 m and for water bodies $\geq$ 4,000 m^2 in area. The hydro-flattening process eliminates artifacts in the digital terrain model caused by increased variability in ranges or dropouts in laser returns due to the low reflectivity of water. To address this in our study, larger water bodies were flattened to a consistent water level. Near infrared LiDAR (which we used) does not work as well in mapping water bodies, but green wavelength LiDAR has been shown to be a powerful tool for mapping the ground surface beneath small water filled thermokarst features (Collin et al., 2010). LiDAR also is a powerful tool for investigating the relationships between geomorphologic features and landscape processes, particularly where landscape change can be captured by repeat imagery collection. Furthermore, depending on the season, size of smaller scale features, and the presence or absence of snow melt or rainfall in these water features, it could be even more challenging to use LiDAR to estimate areas of landscape change.

While vegetation and topographic characteristics have often been used to infer the presence or absence of permafrost they are less useful for assessing the distribution of deep (i.e. >5 to 10 meters below the ground surface) permafrost distribution. Further, the complex transition boundary morphology between thawed and frozen material reduces our ability to accurately predict how and where permafrost will respond to climate warming or land surface disturbance. This is of particular concern for efforts to predict the fate of carbon stored in permafrost and to predict the spatial and temporal ecosystem or hydrologic processes that will respond to changes in permafrost extent (Turetsky et al., 2002; McGuire et al., 2009; Euskirchen et al., 2010; Jorgenson et al., 2013a; Schuur et al., 2013; Pastick et al., 2014). Many of the regional carbon assessment studies use aerial imagery, particularly repeat imagery, to assess the percent of frozen ground in discontinuous permafrost lowlands. Our results suggest the processes affecting subsurface permafrost distribution are not simple or uniform across the landscape.

The strong relationships we identified between permafrost morphology and cryostratigraphy and terrain biophysical features support our hypothesis that the presence or absence of permafrost beneath lowland landscape features like bogs, thermokarst bodies, and islands of tree stands can be identified and mapped at the ~1 meter scale by combining field measurements,

high resolution GPS measurements, and geophysical surveys. The complex relationships between thawed and frozen material, where permafrost degradation will occur, can be related to quantifiable surficial expressed biophysical measurements like relative elevation, vegetation, soil composition, and ecotype. Our combined geophysical, repeat imagery, and ground survey efforts yielded a consistent result that the presence or absence of permafrost at the local (i.e. meters) scale can be ascertained by looking at biophysical characteristics such as elevation changes and vegetation.

5.4 Permafrost hydrologic modeling in upland catchments

We linked two stand-alone models to develop a capability for simulating streamflow in catchments with varied permafrost extents: the Gridded Surface Subsurface Hydrologic Analysis (GSSHA) model for hydrologic modeling and the Geophysical Institute Permafrost Laboratory (GIPL) soil thermal model. These coupled models allow us to predict where soil thermal, permafrost stability, and hydrologic processes are most likely to respond to change. Details of the theoretical background on coupling and linking GIPL and GSSHA are presented in Pradhan et al. (2013). A detailed Report on how to use the coupled GIPL-GSSHA model is presented in Pradhan et al., (in press as an ERDC-CHL Technical Report for public distribution).

Modeling efforts included: a) preparation of input parameters and variables from the Caribou/Poker Creeks Research Watershed (CPCRW) site; b) building of a hydrology model using the GSSHA pre-processing tools; and c) recommendations in what equations to implement into GSSHA in order to link GIPL outputs to the GSSHA domain.

5.4.1 GIPL

To assess the effects of snow, surface, and subsurface soil properties on ground temperatures, we used the stand alone Geophysical Institute Permafrost Laboratory (GIPL) model, which simulates soil temperature dynamics and the depth of seasonal freezing and thawing by solving a one-dimensional nonlinear heat equation with phase transition (Marchenko et al., 2008). In this model, the phase change (water to ice or vice versa) occurs within a range of temperatures below 0 degree C. This phase change process is characterized by an unfrozen water content curve, which is specific for each soil layer. The model simulates soil temperature and liquid water content fields for the entire depth of soil column with hourly or daily time resolution. The depth resolution is 1 cm for the upper 1 m of soil with lower resolution for the deeper layers. The computation was performed for soil column of 100 m depth.

Ground temperature measurements of a very high quality (precision generally at 0.01°C) in shallow boreholes were used for initial model validation. More than 15 shallow boreholes (1-1.2 m in depth) across Alaska from north to south were available for validation (Romanovsky et al., 2010, Smith et al., 2010). The temperature measurements in the shallow holes performed with vertical spacing of 0.08-0.15 m. At most of these sites, soil water content and snow depth also were recorded. In addition, more than 25 relatively deep boreholes from 29 m to 89 m in depth (Osterkamp, 2003; Osterkamp and Romanovsky, 1999) along the same transect were available for the model validation in terms of permafrost temperature profiles and permafrost thickness (Figure 43).

Different earth materials have varying thermal properties. The soil thermal conductivity and heat capacity vary within the different soil layers as well as during the thawing/freezing cycles and depend on the unfrozen water content that is a certain function of temperature. The method of obtaining these properties is based on numerical solution for a coefficient inverse problem and on minimization locally the misfit between measured and modeled temperatures by changing thermal properties along the direction of the steepest descent. The method used and its limitations are described in more detail elsewhere (Nicolsky et al., 2007).

There are two basic approaches to the calibration of modeled permafrost temperatures against the observed data, which can be distinguished by their use of temporal or spatial relationships. With the temporal approach, the quality of the modeling series is assessed by time series regression against measured data. The quantitative relationship between simulated and measured data is then determined for a ‘‘calibration’’ period with some instrumental data withheld to assess the veracity of the relationship with independent data. We used a variety of landscape settings (black spruce, shrubland, and tundra) to calibrate the model for these specific ecosystems in

interior Alaska. An example from a black spruce forest is given in Figure 44 and Table 9 and an example from a shrubland site is given in Figure 45.

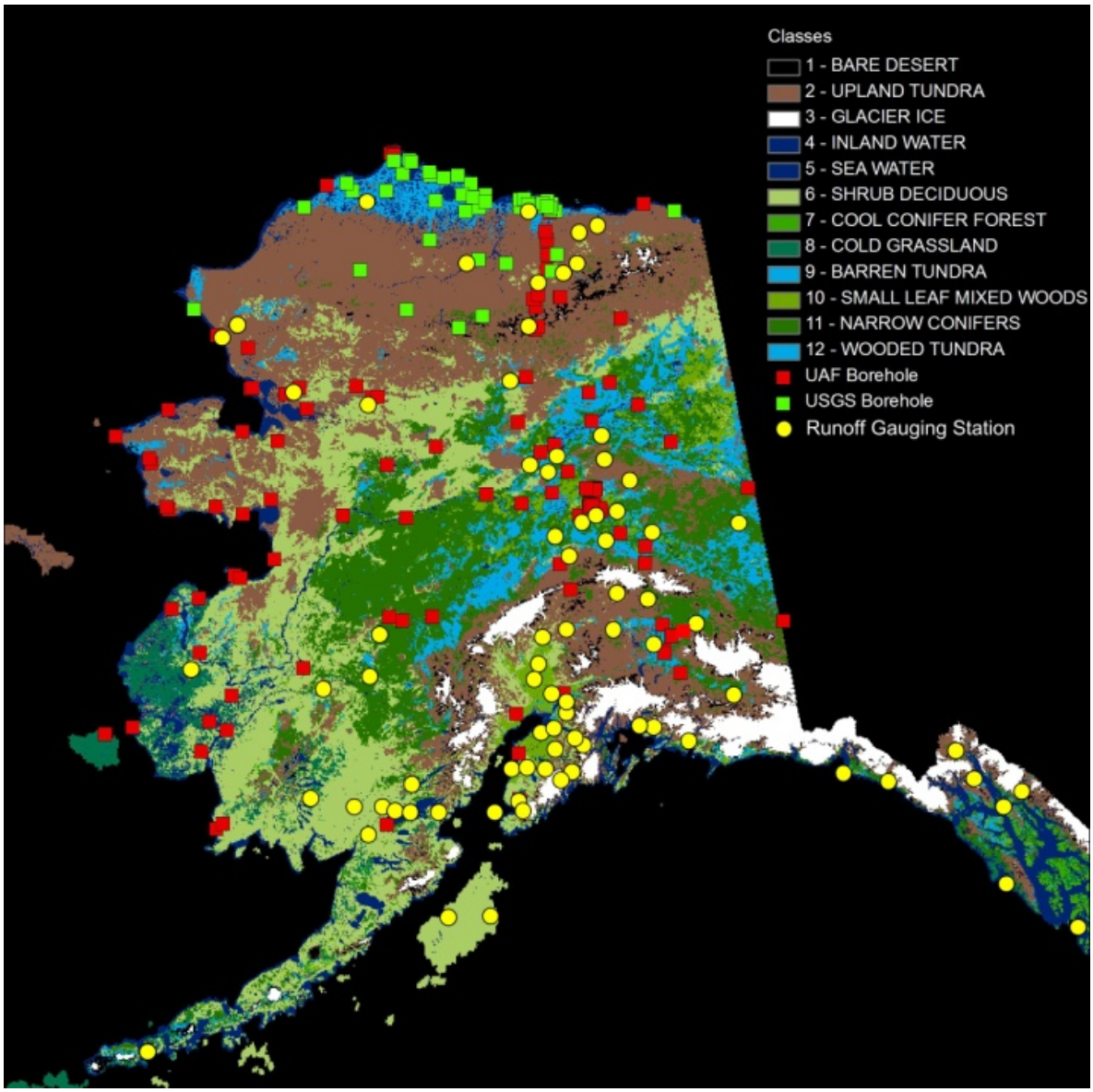

Figure 43. Landscape types and locations of available data used to calibrate the GIPL model.

A B

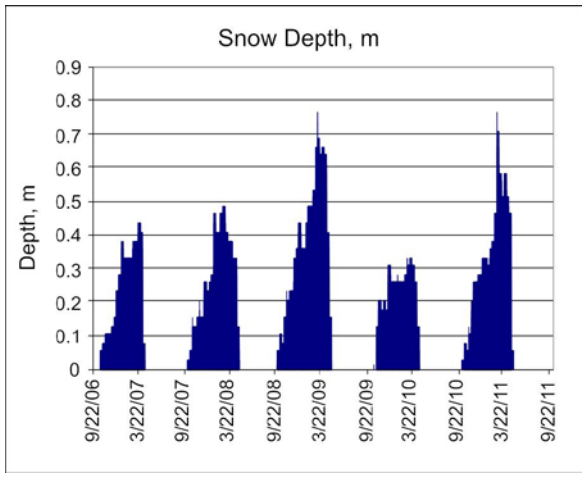

C

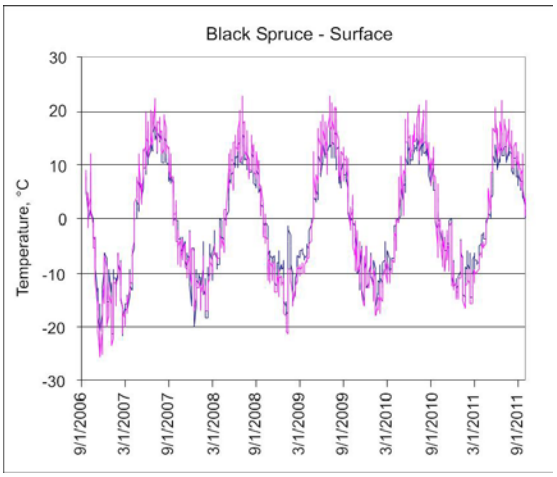

D

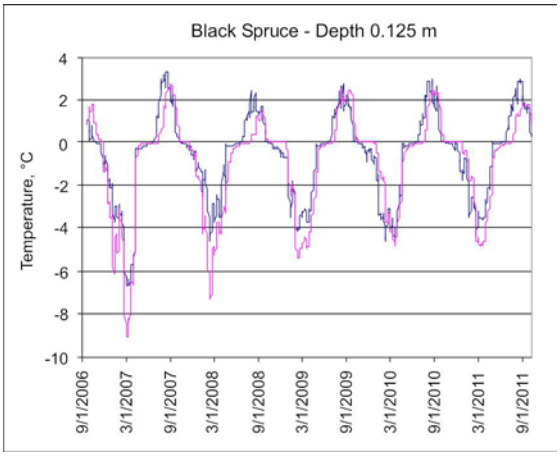

E

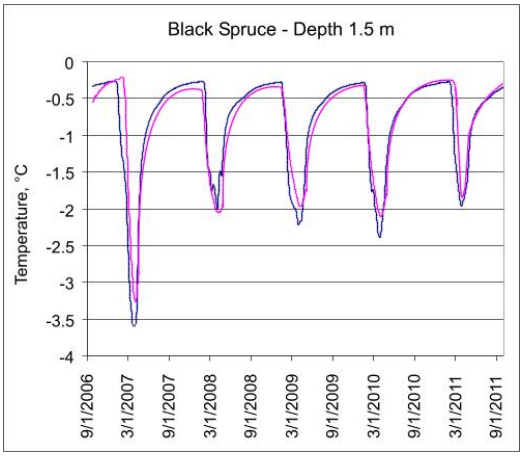

F

Figure 44. Landscape settings (A, B) and examples of the temporal calibration of the GIPL model (C, D, E, F) for one specific site in a black spruce forest interior Alaska. In D, E, and F the blue and pink lines represent measurements from two locations at the site.

Table 9. Soil properties determined as a result of model calibration for a black spruce site with five soil layers.

VWC Fraction of volume	Cap_th J/m3*K	Cap_fr J/m3*K	Cond_th W/m*K	Cond_fr W/m*K	ac	bc	cc	Layer thickness, m
0.65	2.5d6	1.9d6	0.2	0.25	0.05	-0.12	0	0-0.08
0.65	2.5d6	1.8d6	0.3	0.6	0.11	-0.51	0	0.08-0.25
0.39	2.9d6	1.7d6	1	1.4	0.21	-0.22	0	0.25-0.65
0.35	2.9d6	1.7d6	1.1	1.4	0.03	-0.15	0	0.65-4.8
0.12	2.9d6	1.6d6	2.2	2.3	0.09	-0.72	0	4.8-100

VWC – volumetric water content
CAP_th, Cap_fr – heat capacity for thawed and frozen soil
Cond_th, Cond_fr – thermal conductivity for thawed and frozen soil
a, b, c – coefficients for unfrozen water content curve
Unfrozen water (UW) determines as UW=ac*(cc-T)**bc
T – soil temperature.

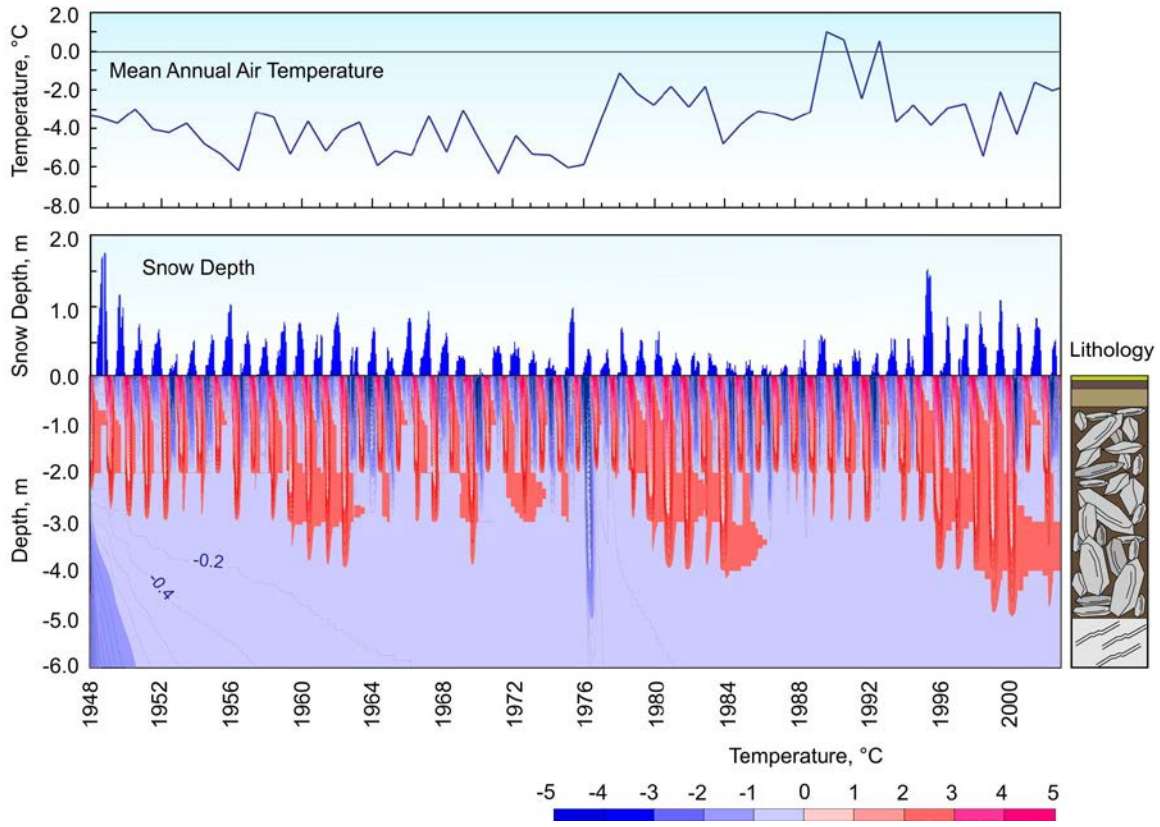

Figure 45. A reconstruction of ground thermal properties (permafrost evolution) from 1948 to 2005 at a shrubland site.

The calibrated model can then be applied to the entire period of meteorological records at this station, producing a time series of permafrost temperature changes. The same calibrated model can be applied for retrospective analysis and for predictions of the future permafrost dynamics when some future climate change scenario is used as input data. In the permafrost temperature reanalysis method that was developed at the Permafrost Lab of the Geophysical Institute, University of Alaska Fairbanks, variations in the air temperature and snow cover (thickness and thermal properties) are the driving forces of the permafrost temperature dynamics. The model is calibrated for a specific site using measured permafrost and active layer temperatures (usually several years of available data are used) and data from the closest meteorological station for the same time interval.

5.4.2 the Caribou/Poker Creeks Research Watershed site

The CPCRW site (Figure 46) is a 104 km^2 basin located in the Yukon-Tanana Uplands of the Northern Plateaus Physiographic Province centered on 65˚10' N latitude and 147˚30' W longitude. The entrance to the site is located off of Steese Highway about 31 miles from Fairbanks, Alaska. The area lies above the Chatanika River floodplain and is characterized by rounded hilltops with gentle slopes and alluvium-floored valleys having minimal relief (Wahrhaftig, 1965) underlaid by a mica schist of the Birch Creek formation (Rieger et al., 1972). The climate region is a cold continental climate characterized by short warm summers and long cold winters. The basin is divided into sub-watersheds shown in Figure 46. A long-term hydrologic simulation is proposed in the C2 and C3 sub-watersheds as part of an effort to couple the Gridded Surface Subsurface Hydrologic Analysis (GSSHA) model with the soil thermal regime model (Marchenko et al., 2008) from the Geophysical Institute Permafrost Lab (GIPL). The sub-watersheds were chosen for their disparate expanses of permafrost in order to better understand the effects of frozen soils within the model. The C2 sub-basin is a 5 km^2 basin nearly free of permafrost whereas the C3 basin is 5.4 km^2 with a large expanse of permafrost. Parameters from C2 & C3 models are used to populate the larger CPCRW model.

Hydrometeorological (HMET) parameters are recorded on an hourly basis throughout the research watershed. Meteorological stations are situated at elevations from about 800 ft. at CRREL up to 2,537 ft. at Caribou Peak. Stream flow is recorded with flumes at both sub-watershed outlets.

The GSSHA model (Downer and Ogden, 2006) is used for the long term simulation. GSSHA is a physically-based spatially distributed numerical model used to simulate important stream flow processes (Downer and Ogden 2004a). GSSHA is used to evaluate flood inundation (Sharif et al., 2010) soil moisture (Downer and Ogden, 2003), and constituent fate and transport (Downer, 2009).

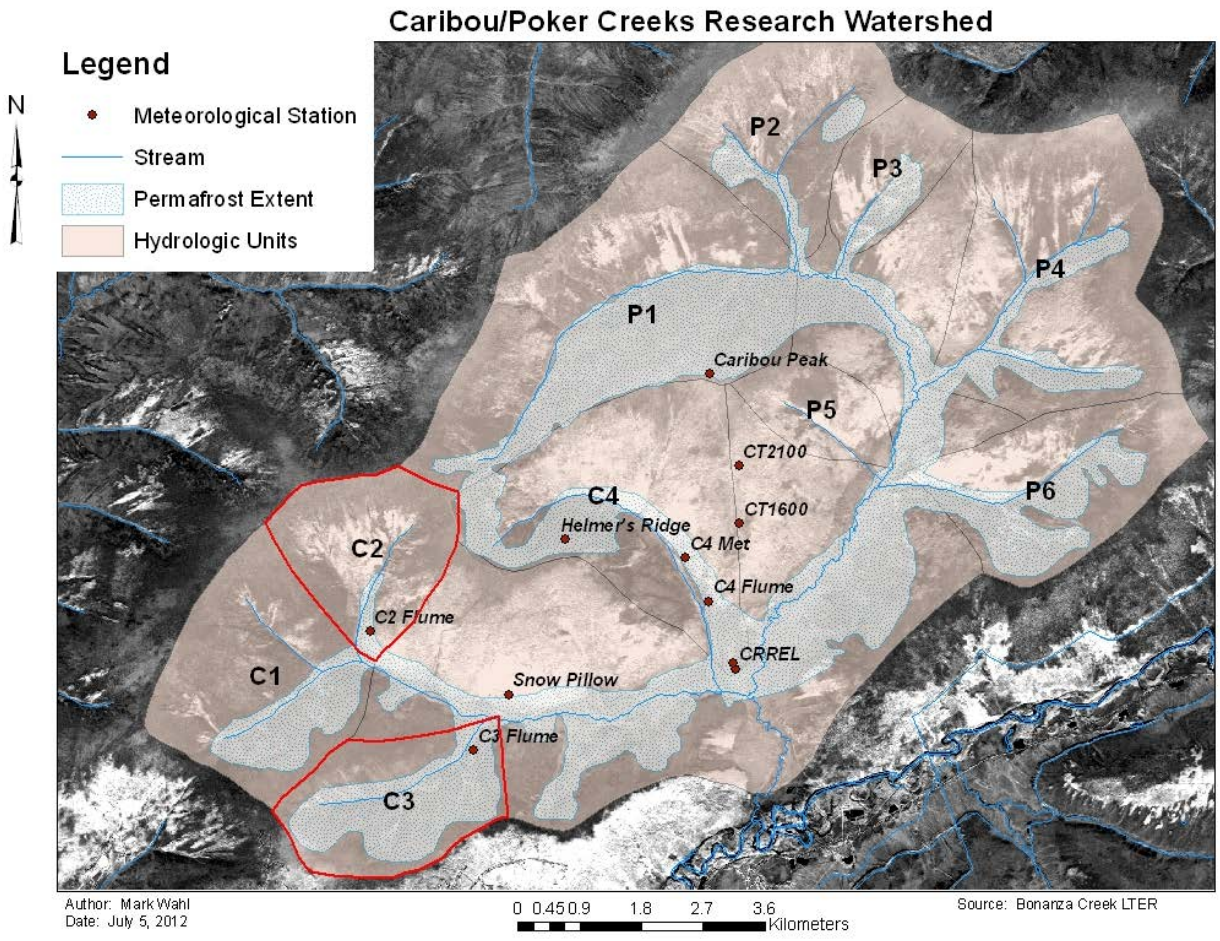

Figure 46. Hydrologic units of the Caribou/Poker Creeks Research Watershed (CPCRW) with locations of hydrometeorological stations and permafrost extents indicated (Chapin and Hollingsworth 2010a; b). Models of the C2 and C3 sub-watersheds compare the hydrologic effects from disparate expanses of permafrost.

A land cover map of the CPCRW is provided in Figure 47 The area is largely coniferous forest with deciduous stands and some shrubs interspersed. A portion of the watershed was affected by the Boundary Fire that burned through the summer of 2004. A shapefile courtesy of the Alaska Interagency Coordination Center provides the areal extents of the Boundary Fire. Fire is expected to alter hydrology in the watershed as a result of thinner vegetation and a reduction in the thickness of the organic material on the forest floor. The fire affects the organic mat variably according to local severity. For modeling purposes, a more simplistic approach is used to estimate the impact. Therefore, a 20% reduction in the organic mat thickness was applied uniformly to the areas affected by fire based on a study of the effects in an adjacent upland area around Nome Creek (Nossov et al., 2013). Post-fire land cover in areas affected by the fire is reduced to tall shrubs in the post-2004 model.

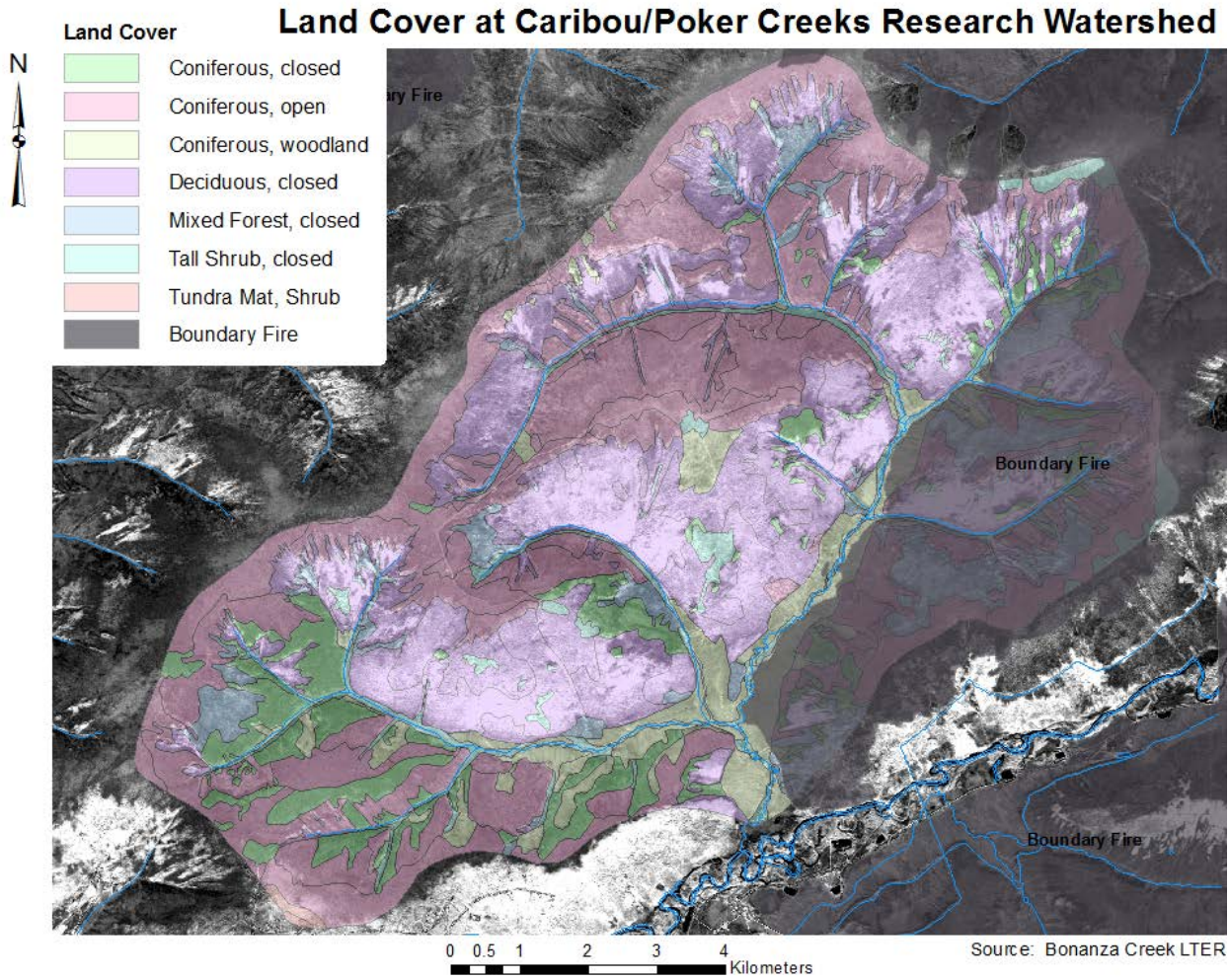

Figure 47. Land cover map of the Caribou/Poker Creek Research Watershed including extents of the 2004 Boundary Fire. Open and closed designations refer to canopy density. An open canopy permits a view of the sky through it.

Soil characteristics are assigned according to information provided by Rieger (1979) and informed by various sources (NCSS Staff, 2014; Rieger et al., 1963). Soils in the watershed are predominately silt loam underlaid by shallow fractured bedrock. In some instances, a thick layer of live sphagnum moss and fine peat covers the ground surface. A restrictive layer of permafrost is found on north facing slopes. A map of CPCRW soils is provided in Figure 48.

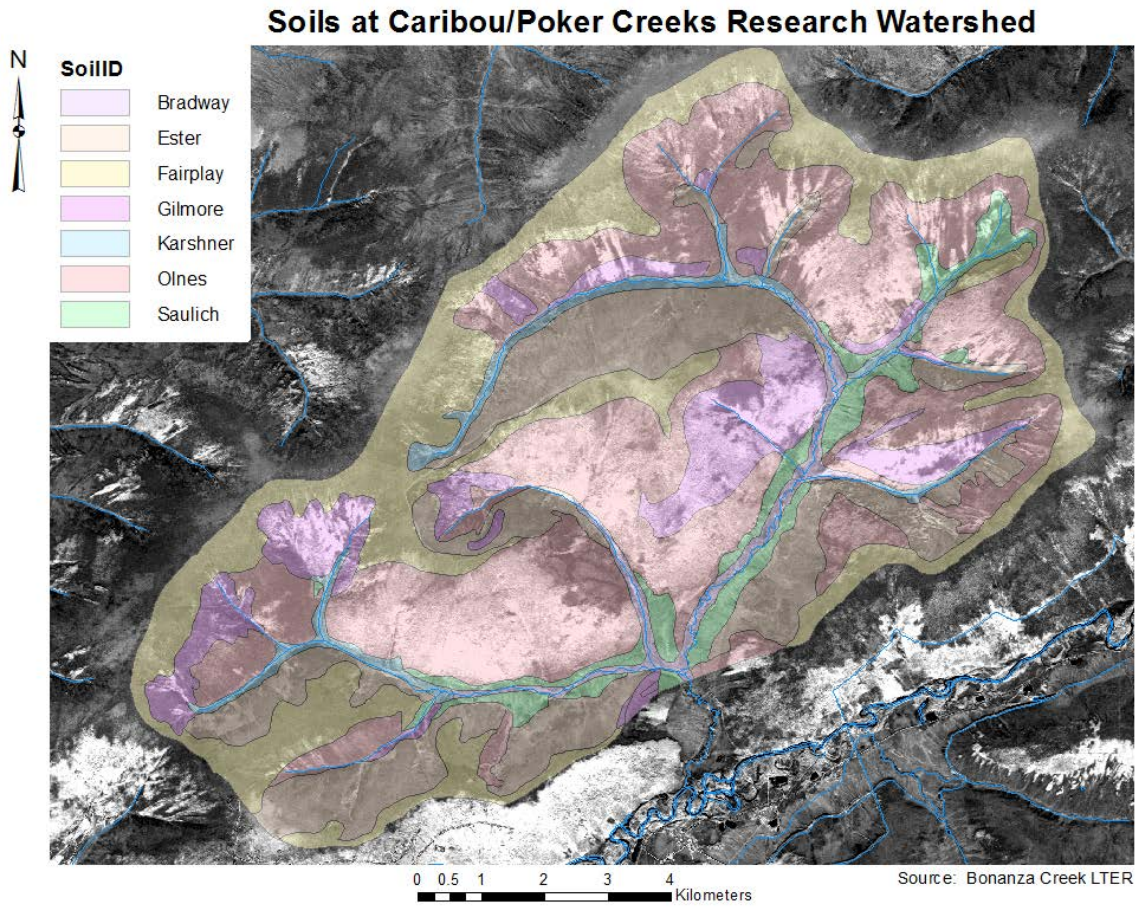

Figure 48. A soil map based on Reiger (1972) at the Caribou/Poker Creek Research Watershed.

Subsurface characteristics were again based primarily on the Rieger (1972) report along with National Cooperative Soil Survey (NCSS) data since detailed information about the underlying geology was not available. The NCSS data (2014) indicates typical depths to the paralithic restrictive layer for several CPCRW soils. This depth to the restrictive layer was subtracted from the ground surface elevations to map the aquifer bottom. Depths to the restrictive layer for soils not contained in the NCSS dataset were inferred based on the Rieger (1972) soil profiles.

Water table elevations were not readily available so preliminary water table elevations were inferred again from the Rieger (1972) descriptions. The water table was assumed to be near the surface for poorly drained soils and was assumed to be near the aquifer bottom or perched just above the permafrost layer for well drained soils. An intermediate depth was assumed for all other soils based on results from flowpath studies in the watersheds (MacLean et al., 1999; Petrone et al., 2006). These assumptions resulted in abrupt changes in the water table at boundaries between soil types. This is addressed through an initialization period where the water table and soil moisture is allowed to stabilize. The final state at the end of the initialization period provides more realistic starting conditions for simulations going forward. The assumed aquifer bottom was adjusted at the end of the initialization period to accommodate the initialized water table.

Long term simulations in GSSHA require inputs for hourly precipitation, temperature, pressure, humidity, wind speed, cloud cover, and solar radiation. Over ten years of nearly continuous hourly hydrometeorological (HMET) data were available from a combination of

stations at CPCRW. Historical HMET records were compiled to produce the necessary input files for the long-term simulation from the available data indicated in Table 10. Records were compiled as described below to produce GSSHA gage files (.gag) and HMET files (.hmt) required for the long-term simulation.

Table 10. Summary of the available hydrometeorological parameters required for a long term simulation at Caribou-Poker Creek Research Watershed (Chapin and Ruess 2003a; b, 2005a, 2006; Van Cleve et al. 2003; Hollingsworth 2007).

HMET Parameters	Units	CPCRW Stations with Available Records
Precipitation	mm	CRREL, CPeak, CT1600, CT2100, Helmers, CARSNOW
Air Temperature	˚F	CRREL, C4, CPeak, CT1600, CT2100, Helmers, CARSNOW
Barometric Pressure	in Hg	CRREL
Wind Speed	knots	CRREL, C4, CPeak
Relative Humidity	%	CRREL, C4, CPeak, CT1600, CT2100, Helmers, CARSNOW
Total Sky Cover	8ths	Fairbanks International Airport
Direct Radiation	W/m^2	None
Global Radiation	W/m^2	CRREL, C4, CPeak

Sky cover information is not recorded at any CPCRW meteorological stations. The nearest location with hourly sky cover information is at the Fairbanks International Airport. Thus, an hourly dataset courtesy of the National Climatic Data Center (NCDC) is used in the long term for sky cover information.

Barometric pressure is recorded only at the main CRREL meteorological station. No records could be identified prior to July 23, 2000. As a result, the ten year simulation period must commence on, or after, this date. Barometric pressure was originally provided in hectopascals and then later converted to inches of mercury.

Historical records of relative humidity are available from nearly all the CPCRW meteorological stations for various time periods. The near-continuous records span 19 years at the CRREL site. These were included in the forcing data for the simulation period.

Historical sky cover information is not available at CPCRW. The nearest instrument recording cloud cover is operated at the Poker Flat Research Range just a few kilometers from the CPCRW.

The next closest hourly sky cover records are recorded by a National Weather Service Station at Fairbanks International Airport (Air Force Catalog Station No. 702610, NCDC WBAN No. 26411). This station is approximately thirty miles from CPCRW. Data for hourly sky cover at the Fairbanks station was provided by the National Climatic Data Center (NCDC) for the period from January 2000 to July 2012. This format provides hourly sky cover in the tiered data structure used for simulations.

Wind speed is primarily measured at the CRREL station and on Caribou Peak at various heights above ground. Additional wind speed records exist for a period at the C4 station. Records from the CRREL site were given precedence since those were the most complete. Gaps were supplemented with data from C4 since Caribou Peak may be less representative of the overall area. Only readings taken below 3 m were used as forcing data. Wind speed was originally recorded in meters per second and later converted to knots.

Historical records of air temperature are available from nearly all the CPCRW meteorological stations. Near-continuous data from the CRREL site spanning 19 years was given precedence while several gaps exist in the record which sometimes span several months. Separate temperature records are available at C4, Helmers Ridge, Caribou Peak, and Caribou Trail 1600 & 2100 for

various time periods. These records could be used to supplement gaps in the CRREL record. Caution is urged here since elevation strongly influences temperature readings while winter temperature inversions pose a challenge in correcting for elevation. Temperatures originally published in degrees Celsius were converted into Fahrenheit for use with GSSHA model.

Solar radiation data is measured at two CPCRW met stations (CRREL and C4). Both measure upwelling and downwelling shortwave and longwave irradiance along with a wind correction factor for net calculations. GSSHA uses global and direct solar radiation values for ET and snowmelt calculations. The downwelling shortwave measurement represents a total hemispheric (i.e. global) value encompassing direct and diffuse components. The instruments deployed at CPCRW do not discriminate between direct and diffuse radiation so direct values are not discerned. Furthermore, global measurements are intermittent, especially during winter months when measuring equipment is obstructed by snow accumulation. In the absence of explicit values, GSSHA calculates the missing radiation values internally based on date, time, and latitude.

Hourly incremental precipitation is available throughout the proposed simulation period (Chapin and Ruess, 2003a). A complete record of snowfall is not available since records relating to winter precipitation from the CARSNOW and Caribou Peak meteorological stations both commence in 2008 (Chapin and Ruess, 2009a; b). Two additional stations, CT1600 and CT2100, had weighing gages capable of measuring year-round precipitation. Records at these locations are available from January 2000 through 2003. The tipping bucket gages found at the other meteorological stations only measure liquid precipitation. Thus, no winter precipitation records are available from January 2004 to May of 2008.

The Watershed Modeling System (WMS 9.1) is used for watershed delineation. Flow directions and accumulations were computed using the Topographic Parameterization Program (TOPAZ) method. This information, along with spatial data pertaining to terrain, soils, land cover and temporal data related to HMET data, are fed to GSSHA.

5.4.3 Processes Modeled

5.4.3.1Overland flow

Overland flow is described in the model with the alternating direction explicit (ADE) method. Overland roughness values were assigned according to land cover within the range suggested by (Senarath and Ogden, 2000). Retention storage is accounted for in soils with heavy forest litter. Overland flow is routed through snowpack using Darcy's law.

5.4.3.2 Channel Routing

A one-dimensional diffusive wave channel routing scheme is used to simulate stream flow. Uniform trapezoidal channel cross-sections are assumed.

5.4.3.3 Infiltration

Infiltration is modeled using the Richards Equation for the movement of water in unsaturated soils (Richards, 1931; van Genuchten, 1980). The GSSHA model uses a one-dimensional finite-difference solution to the Richards Equation in order to describe the movement of water through an unsaturated soil (Downer and Ogden 2006). The Richards Equation is solved iteratively within this framework. Vertical discretization is a critical factor to the accuracy of the solution. Downer and Ogden (2004b) conducted a spatial convergence study and found that small vertical cells are required near the surface to simulate hydrologic fluxes accurately while modest increases in the vertical cell size may be appropriate at greater depths to reduce the computational load without compromising accuracy. A similar convergence study was performed on the soils of CPCRW to identify appropriate sizes of vertical cells for each soil layer. An iterative solution is often

necessary when saturated cells exist within the unsaturated zone due to differences in soil properties between layers (Downer and Ogden, 2006). Accommodations for up to ten iterations were allowed since soil properties vary considerably between the various layers (e.g. sphagnum moss, silt loam, and permafrost). Results of the convergence study varied from one soil type to the next, but generally the upper most soil layer had a vertical cells less than 1 cm while cell sizes for the subsequent layers increased from 1 to 3 cm in most cases.

5.4.3.4 Groundwater Interactions

A two-dimensional simulation of saturated groundwater flow is included in the model. Sub-surface stream losses and gains are governed by a river flux boundary condition.

5.4.3.5 Evapotranspiration

Evapotranspiration (ET), a critical component of the seasonal water balance, is necessary for simulating soil wetting and drying. The Penman method was specified within GSSHA to calculate ET. The required model parameters were assigned according to the vegetation map. Surface albedo values are based on recommended values from the GSSHA user manual (Downer and Ogden, 2006). Canopy transmission coefficients were assigned according to light interception studies for deciduous (Hutchison and Matt, 1977) and coniferous (Gholz and Vogel, 1991) forests. Canopy stomatal resistance was based on two published studies (Eliáš, 1979; Verma and Baldocchi, 1986). The Penman method is fairly sensitive to stomatal resistance (Lemeur and Zhang, 1990) so considerable attention should be given to stomatal resistance during calibration. Hydrometeorological data described below is also used in ET calculations.

5.4.4 Model Initialization and validation analysis

Assumptions about the water table and initial soil moisture conditions based strictly on the soil descriptions result in improbably abrupt changes at boundaries between soil types. To mitigate this, the simulation was initialized over a two year period. Initialization allows soil moisture and groundwater to equilibrate. At the end of each initialization period, the final state is fed back into the model as new initial conditions. The two year simulation was subsequently repeated until the final state roughly matched the starting conditions.

The computational load associated with Richards Equation resulted in prohibitively long runtimes for this extended initialization period. The multi-layer Green and Ampt solution was specified during the initialization period instead to reduce the runtime making the two-year run more feasible. The two-year simulation was repeated until the final state closely matched the initial state. This process provides the initial groundwater table and soil moistures for the study.

Each time the two-year simulation was run the final state more closely resembled the starting conditions. The assumed water table inferred the Rieger (1972) soil report proved low in some areas and high in other as evidenced increases in the groundwater head in certain grid cells and decreases in others. Changes in the groundwater elevations over each initialization run are shown in Figure 49. Bi-annual differences were minimal after three initialization runs.

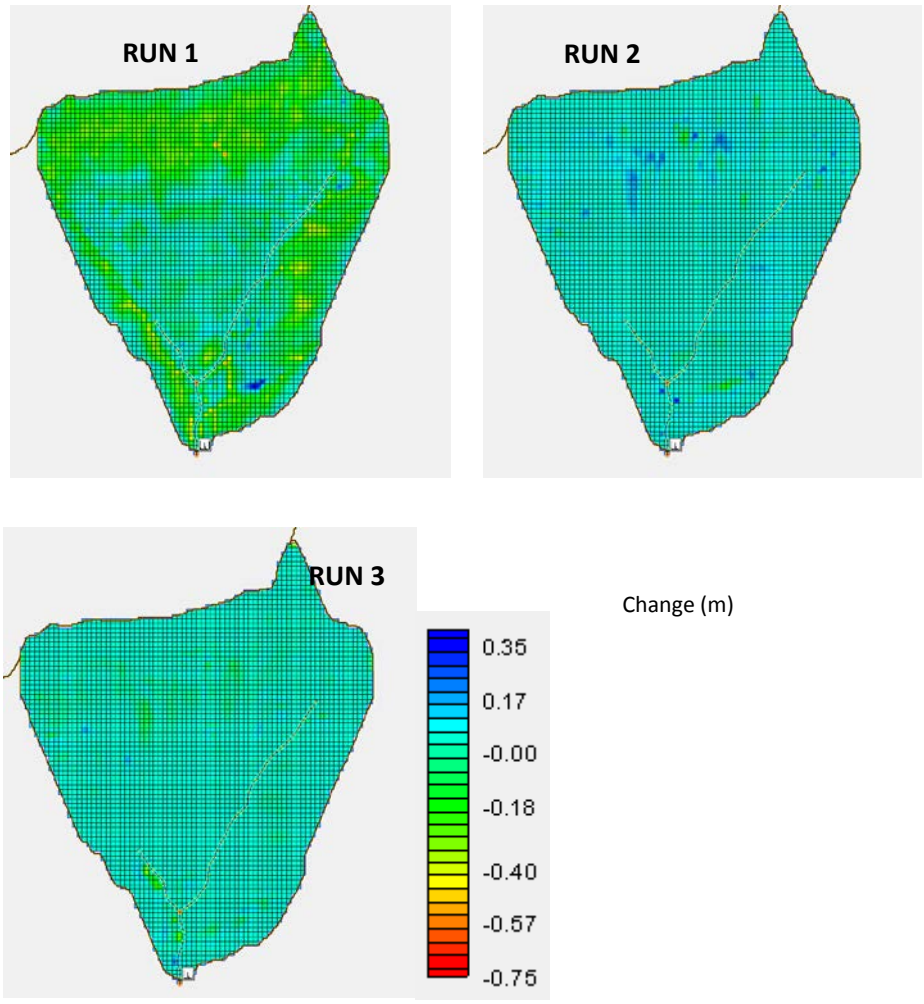

Figure 49. Changes in ground water table during each two-year initialization run.

Runoff is measured with flumes at the outlets of the C2 and C3 sub-watersheds. A continuous record of hourly or sub-hourly flow is available through 2011.
Baseflow was calibrated by adjusting the groundwater hydraulic conductivity and depth to confining layer. Results are shown in Figures 50 and 51.

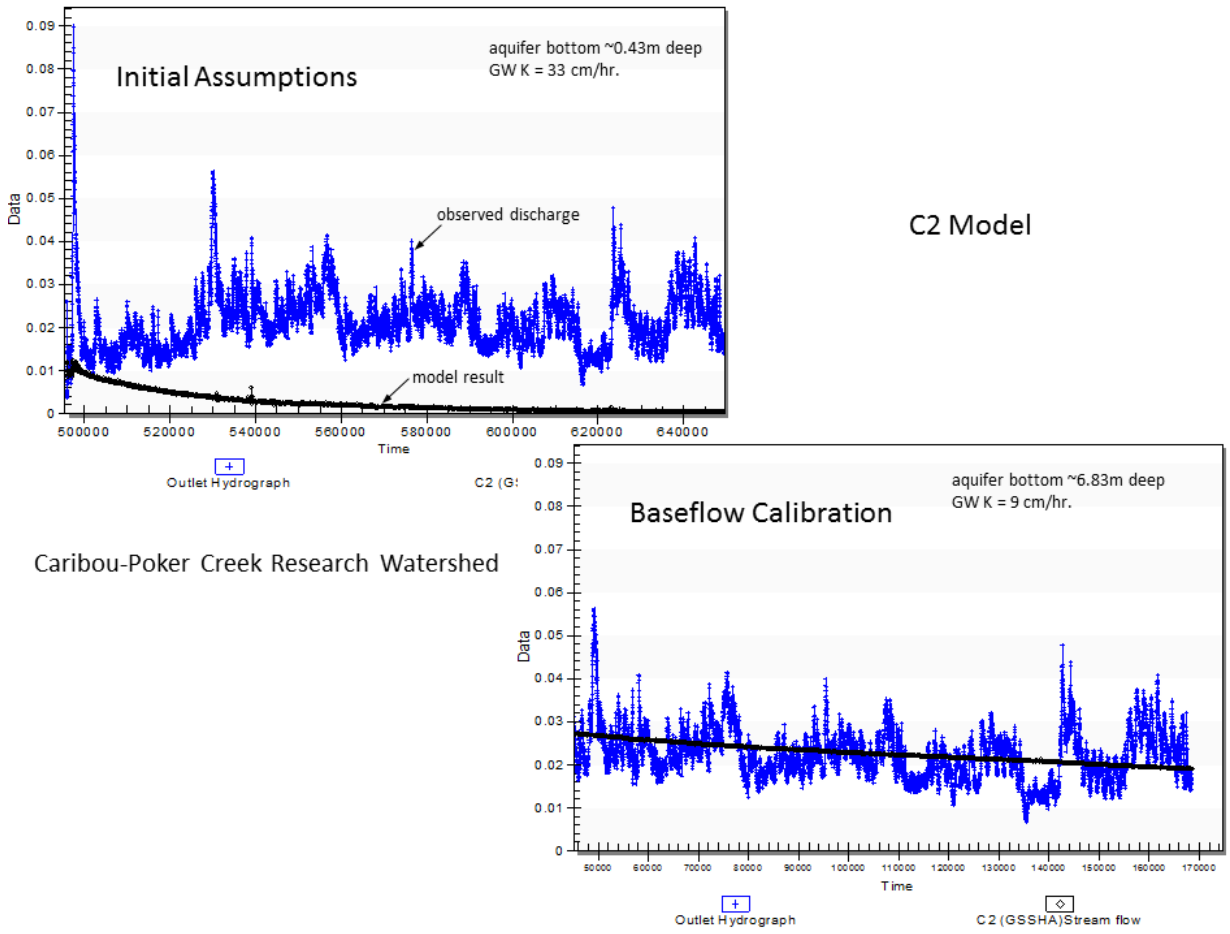

Figure 50. Example baseflow calibration results from the C2 sub basin.

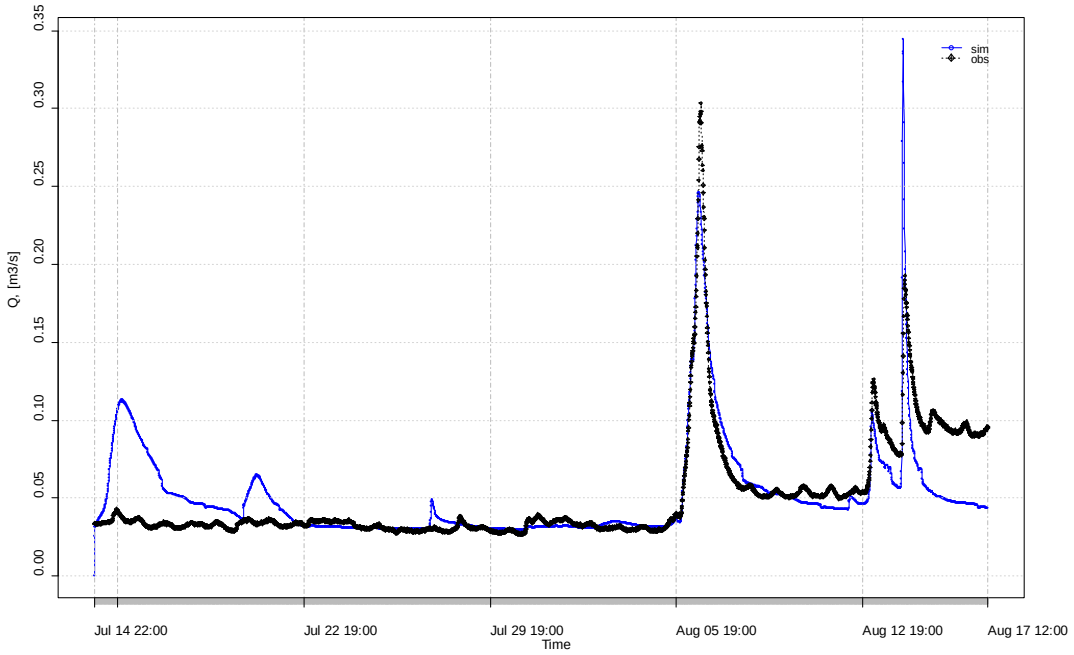

Figure 51. An example validation period for the C2 sub-basin discharge provides a comparison of simulated flow (blue line) with observed discharge over a month long period

Hourly snow accumulation records commence in late 2006 at the CARSNOW met station. Snow pack snow water equivalent (SWE) is measured along with snow pillow observations. These observations are accompanied by incremental precipitation readings. An example of measured and simulated snow pack depth values are presented in Figures 52 while a simulation of basin wide SWE is given in Figure 53.

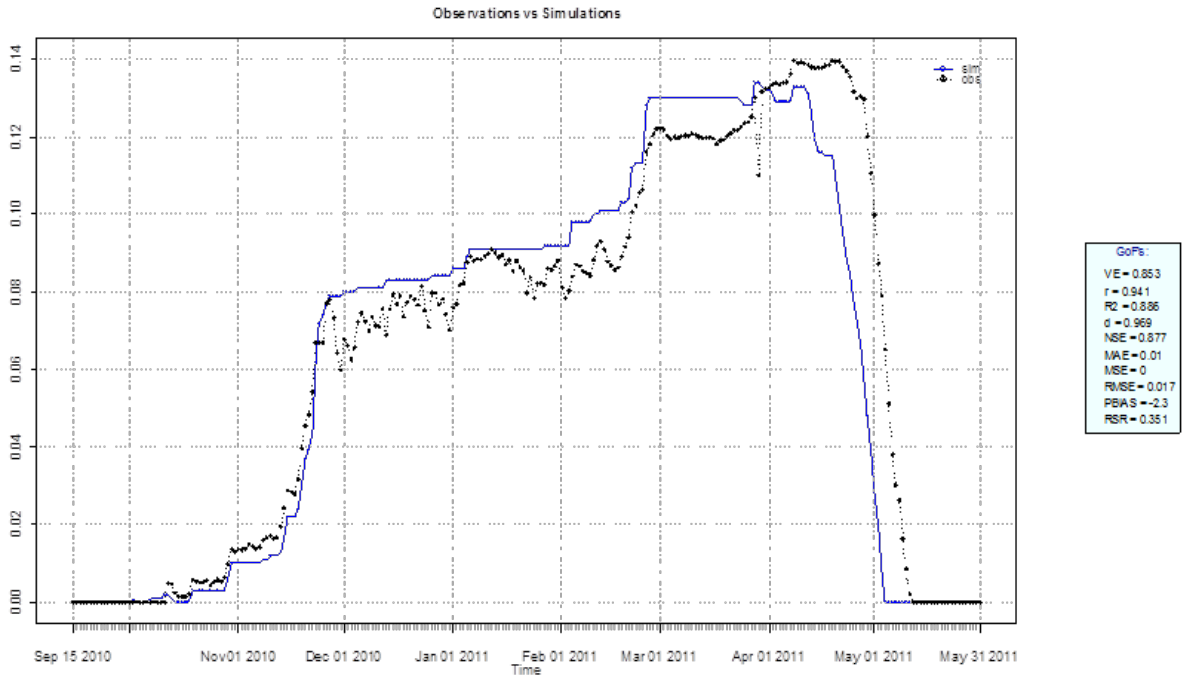

Figure 52. Simulated snow pack (blue line) at CPCRW compared with observed (black line) snow accumulation and snowmelt from 2011. The y-axis is snow water equivalent in centimeters.

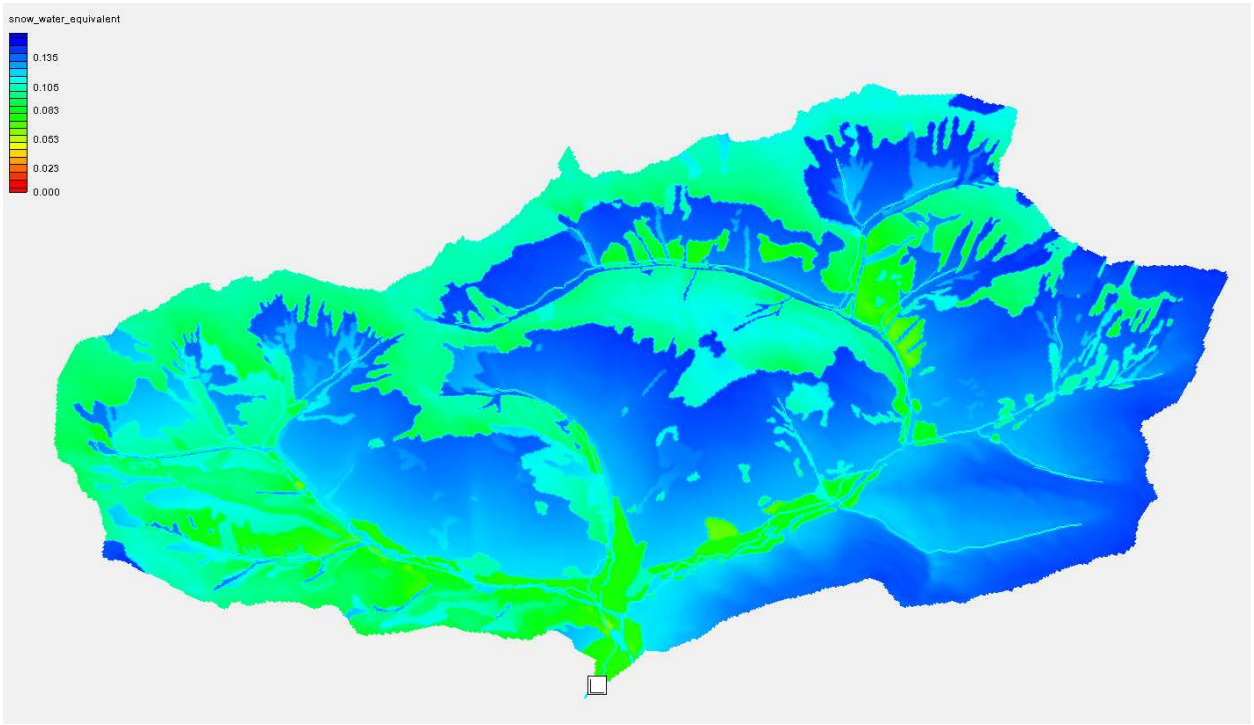

Figure 53. Simulated SWE distribution on 4 April 2011 at the Caribou-Poker Creek Research Watershed.

5.4.5 Permafrost modeling in GSSHA

The GIPL numerical model solves the Stefan problem with phase change which is the problem of thawing or freezing via conduction of heat. In the GSSHA model, the two-dimensional finite-

difference representation of saturated groundwater flow (Downer and Ogden, 2004) is fully coupled to surface flows using a 1-D implicit finite difference solution of Richards (1931) equation. In GSSHA, the soil-freezing characteristic, the relationship between unfrozen water content and temperature, is represented by GIPL numerical model.

Originally, the Geophysical Institute Permafrost Lab (GIPL) permafrost model was coded in FORTRAN. This FORTRAN source code was converted to stand alone C/C++ source code. Originally, GIPL parameters are uni-dimensional in the soil vertical profile but are lumped in the horizontal spatial extent of application. Significant effort has been done to make all the GIPL state variables and parameters distributed as grid based and or permafrost soil type based before merging the C/C++ version of GIPL into GSSHA. Thus, all the uni-dimensional limitation of GIPL is enhanced into multi-dimensional distributed applicability in GSSHA distributed modeling framework.

Originally, the GIPL numerical model of heat transport used a daily and above time step. GIPL coupled into the GSSHA modeling framework has an option for multiple smaller scale (i.e. hourly) time steps. Several thermo-hydrodynamic formulations and modeling concepts are implemented to link and exchange the information back and forth the GIPL and GSSHA numerical schemes. Figure 54 illustrates how the two models have been linked.

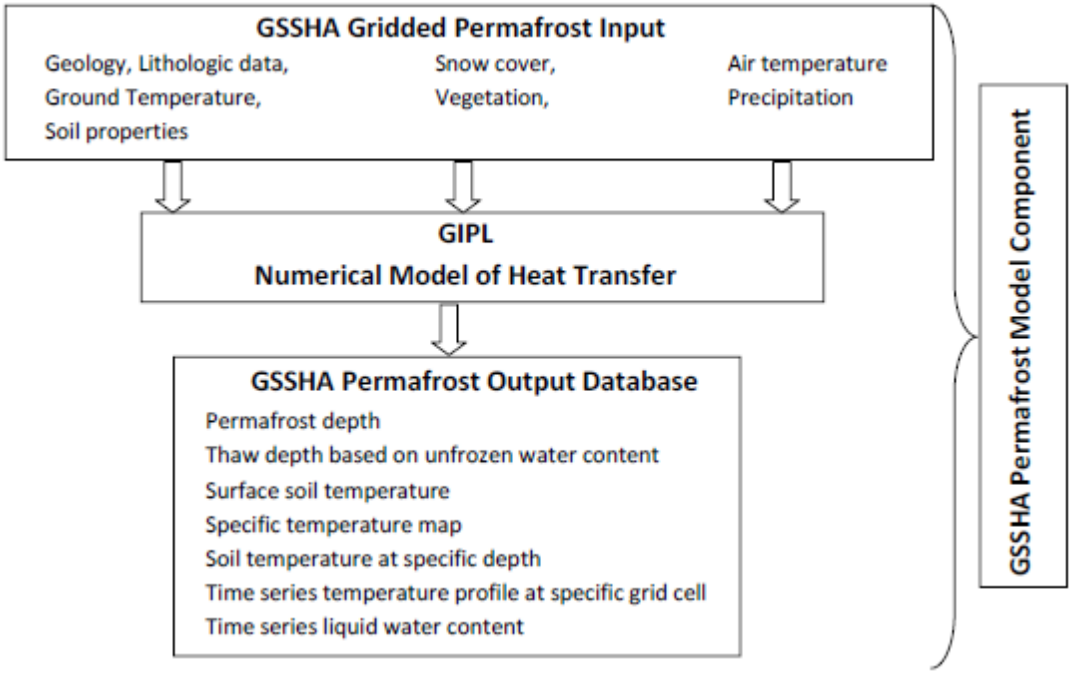

Figure 54. GIPL as a permafrost component in GSSHA.

5.4.5.1 Project file

In *GSSHA*, the model simulation is controlled by a "card based file" (i.e. a character string, or name of a given input) called the project file, with the extension *.prj*. The mapping table file has the extension '.cmt'.

Table 11 shows the card required in the project file for permafrost modeling.

Table 11. Card Required for GIPL Simulation.

Card	Input	Description
PERMAFROST	Filename - *.msp	File containing permafrost mask map info
GIPL_TIMESTEP	Numerical value	GSSHA permafrost model user defined numerical heat transfer time step in sec

The permafrost mask file defines the boundary of the permafrost active zone with id 1. Outside the boundary is 0.

5.4.5.2 Mapping Table file

Table 12 shows the card required in the mapping table file for permafrost modeling.

Table 12. Card required for GIPL grid based parameter input in the mapping table.

Card	Input	Description
PERMAFROST_LAYER_SOIL	**Referenced Filename - *.idx	File containing permafrost soil id map info

**Referenced Filename is the filename that is referred at INDEX_MAP.

If there is PERMAFROST_LAYER_SOIL card in the mapping table, a series of other cards follows as shown in Table 13.

Table 13. Permafrost mapping table inputs that follow the card PERMAFROST_LAYER_SOIL.

Card	Input	Description
NUM_IDS	Numerical value	Total number of permafrost soil ids
MAX_NUMBER_LAYERS	Numerical value	Maximum number of soil layers in the permafrost active grid
DN_INIT_MAX	Numerical value	Maximum number of grid points in the vertical grid for initial conditions
Dn_max	Numerical value	Maximum number of nodes in the depth
INIT_TEMP_FILE	Filename- *.txt	Initial temperature of soil profile. Format is: Each soil id number followed by the depth and temperature for that soil id.
DEP_NODE_FILE	Filename- *.txt	Computational node depth file. Format is: Each soil id number followed by the computational node depth for that soil id.
OUT_NODE_FILE	Filename- *.txt	Time series state variable output node depth. Format is: Each row and column followed by the computational node depth / depths for that grid.

Table 14 shows the required parameters.

Table 14. Permafrost parameters.

Item	Description	unit
ID	Permafrost soil id	-
LAYERNUMS	Total number of soil layers in a soil id type	-
Dn_init	Number of initial temperature inputs in the vertical soil profile	-
Dn	Total number of computational nodes	-
Dn_out	Total number of permafrost state variable output.	-
thick	Thickness of soil layer	m
tfr	Temperature of phase change	Degree Celsius
wvol	Volumetric soil water content	Fraction of 1
wunf	Volume of unfrozen water	Fraction of 1
aclv	A-parameter of unfrozen water	-
bclv	B parameter of unfrozen water	-
cclv	C parameter of unfrozen water	-
Cond_th	Soil thermal conductivity thawed	$W\ m^{-1}\ k^{-1}$
Cond_fr	Soil thermal conductivity frozen	$W\ m^{-1}\ k^{-1}$
cvol	Volumetric heat capacity	$Jm^{-1}m^{-1}m^{-1}k^{-1}$

5.4.5.3 Illustration of modeling in GSSHA

The example illustrates modeling permafrost active area with GIPL coupled in GSSHA. This example project includes surface subsurface runoff where infiltration and groundwater component is turned on. The soil moisture and soil physical state is defined by Richards Equation. Figure 55 shows simulated soil temperature profile extracted from the time series while Figure 56 shows the soil temperature at various depths.

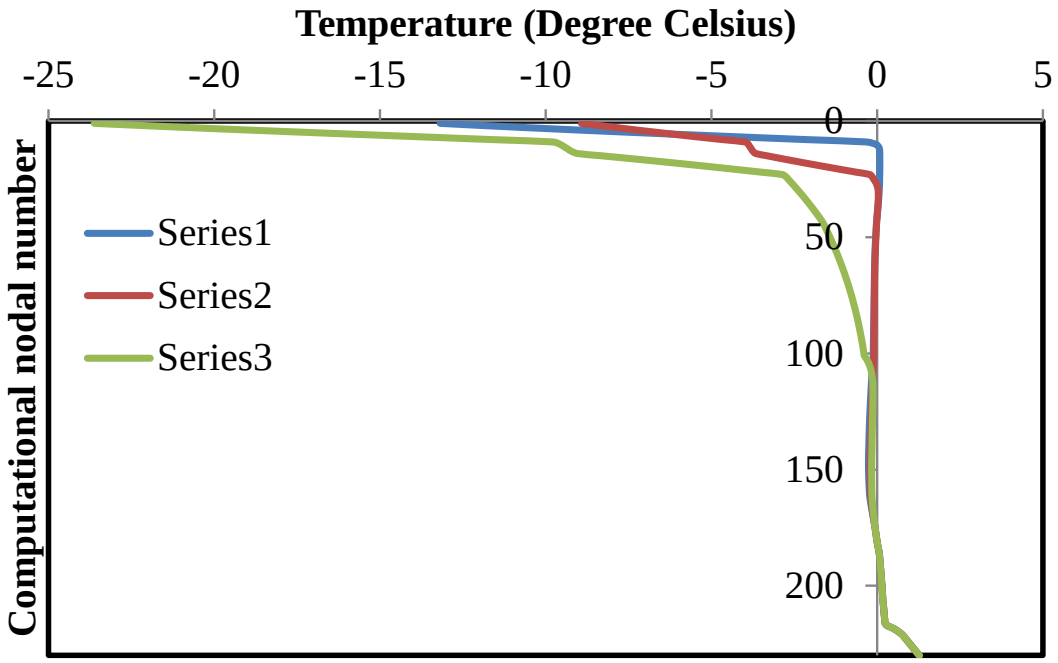

Figure 55. Soil temperature profiles.

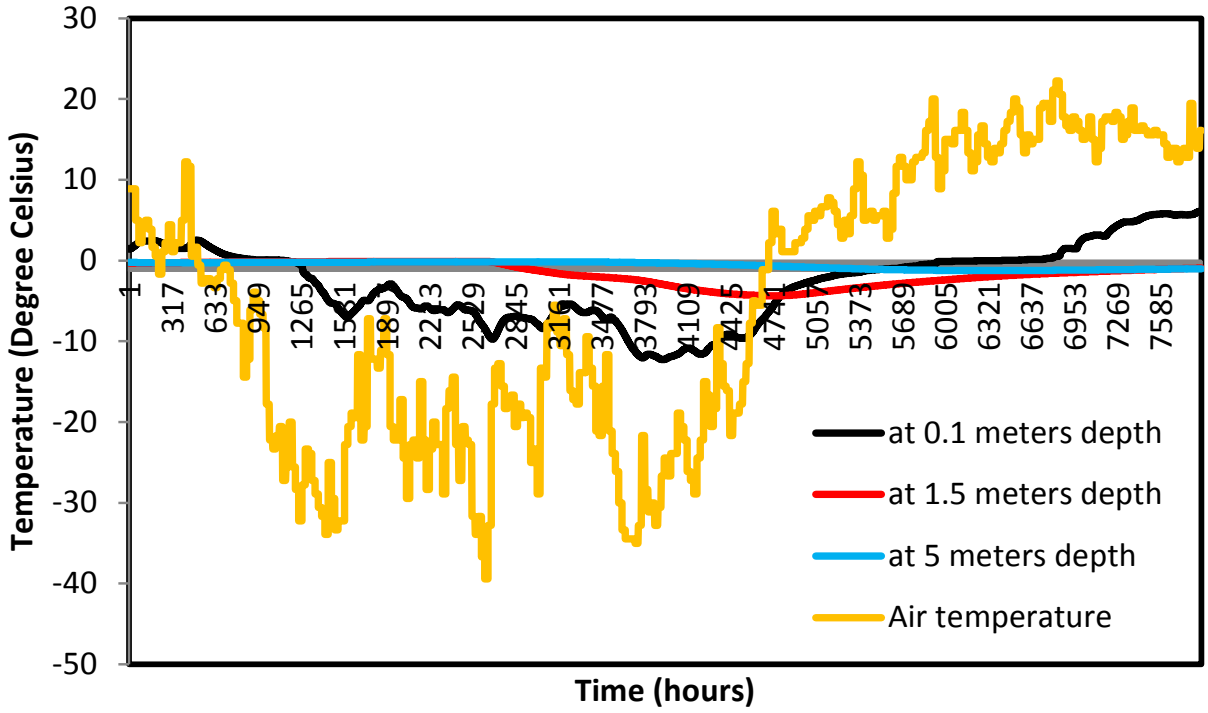

Figure 56.Time series of temperature at various depths.

Figure 57 shows the comparison of GSSHA simulated discharge with and without permafrost incorporated into the model.

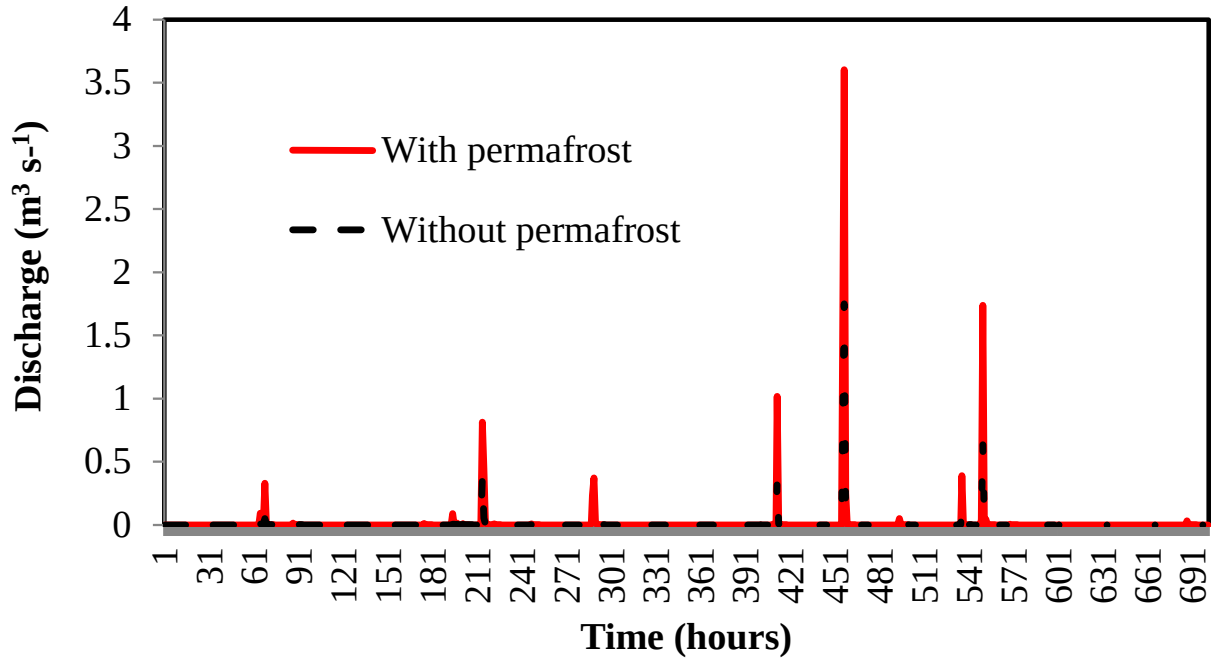

Figure 57. Hydrograph with and without active permafrost.

It is apparent that the increased coverage of permafrost in the High permafrost basin leads to less soil pore water storage and a flashier response precipitation events. Loss of permafrost in interior Alaska will likely lead to enhanced connectivity between the surface and ground water storage regimes. Streams will likely become less flashy with increased connectivity and deeper flow paths. This, in turn, could lead to longer water-rock and water-soil interaction times. The effects of this on watershed nutrient availability and fluxes is not well known.

These results support two hypothesis addressed in this part of the research. First, that a coupled framework explicitly simulating soil moisture effects of soil thermal conductivity and heat capacity and its effects on hydrological response can project how hydrologic flows in permafrost terrains will be altered in a warmer future climate. Second, that the model results will simulate field measurements in catchments of varied permafrost extent. Specifically, warmer soils and decreased permafrost extent are associated with longer flow paths and a larger baseflow component while colder soils and increased permafrost extent lead to a more rapid stream response to precipitation events and a decrease in baseflow and storage. The coupled GIPL-GSSHA model accurately simulated actual measurements of soil temperature dynamics and seasonal freezing and thawing in permafrost terrains at the Caribou-Poker Creek Research Watershed. Model simulation results were similar to discharge measurements made at the site. At locations where precipitation, discharge, soil composition, and permafrost characteristic measurements are available this model could be used to project how a future warmer climate may affect permafrost extent and hydrogeology.

5.5 Ecosystem transition modeling to identify landscape change

5.5.1 Ecotype Changes

Overall, 56.8% (n=2000) of the region had changes in ecotypes over the entire 55–62 yr period. During the first period from 1949–1952 to 1978–1980, 39.7% of the study area changed ecotype, while in the second period to 2006–2011 36.7% experienced change. When comparing ecotypes, the largest gains in area over the entire period occurred for Upland Moist Mixed Forest (7.8% of total area), Upland Moist Needleleaf Forest (1.6%), Lowland Wet Needleleaf Forest (4.5%), Lowland Wet Mixed Forest (1.6%) and Lowland Wet Broadleaf Forest (1.9%) (Figure 58). The largest decreases in area occurred for Upland Moist Broadleaf Forest (-6.2%), Upland Moist Scrub-Disturbed (-4.6%), Lowland Wet Low Scrub (-5.8), Lowland Low Scrub Fire-Disturbed (-4.2%), and Riverine Gravelly Barrens (-0.8%).

Relative change (based on initial area of each ecotype) provides a measure of how much each ecotype changed independent of overall area. The largest relative gains occurred for Riverine Gravelly Low and Tall Scrub (650%), Riverine Gravelly Dry Meadow (500%), Upland Moist Tall and Low Scrub (217%), Upland Moist Mixed Forest (187%), and Upland Wet Needleleaf Forest (136%). The largest relative losses were for Upland Rocky Dry Low Scrub (-100%), Riverine Gravelly Dry Broadleaf Forest (-92%), Upland Moist Broadleaf Forest (-63%), Upland Moist Scrub-Disturbed (-60%), and Riverine Gravelly Barrens (-55%).

5.5.2 Ecological Drivers

The ecological processes driving the changes in the early period (1949-1978) were dominated by post-fire succession (27.5%) and fire (10.1%), while riverine primary succession (0.5%), thermokarst (0.4%), river erosion (0.3%) and deposition (0.2%) caused small changes (Figures 59 and 60). The second period (1978-2007) was slightly more affected by fire (13.7% compared to 10.1%) and less affected by post-fire succession (19.4% compared to 27.5%). Areas affected by thermokarst (0.8%), and fire and thermokarst combined (0.4%), increased nearly three-fold in the second period. Areas affected by human activity (gravel fill, road, trails) increased from 0.0% to 0.2% over the two periods.

Fires at the grid points were identified to have occurred in 20 different years, plus there were large areas of early successional vegetation evident on the early airphotos that persisted from fires before 1949. The early successional vegetation (low and tall scrub) was readily identifiable adjacent to unburned forest stringers within the burned areas. Before 1950, 84% of the landscape was in an early-mid successional state after fire, with most of the area affected by fire around 1920 (61%). In between the early and middle photography years, fires occurred in 8 years and affected 16% of the area. Many of the fires we documented on our grids were not in the database of historical fires. In the recent period from 1978–1980 to 2006–2011, there were fires in 9 years, covering 23% of the area, with negligible area affected by the large fire year in 2004.

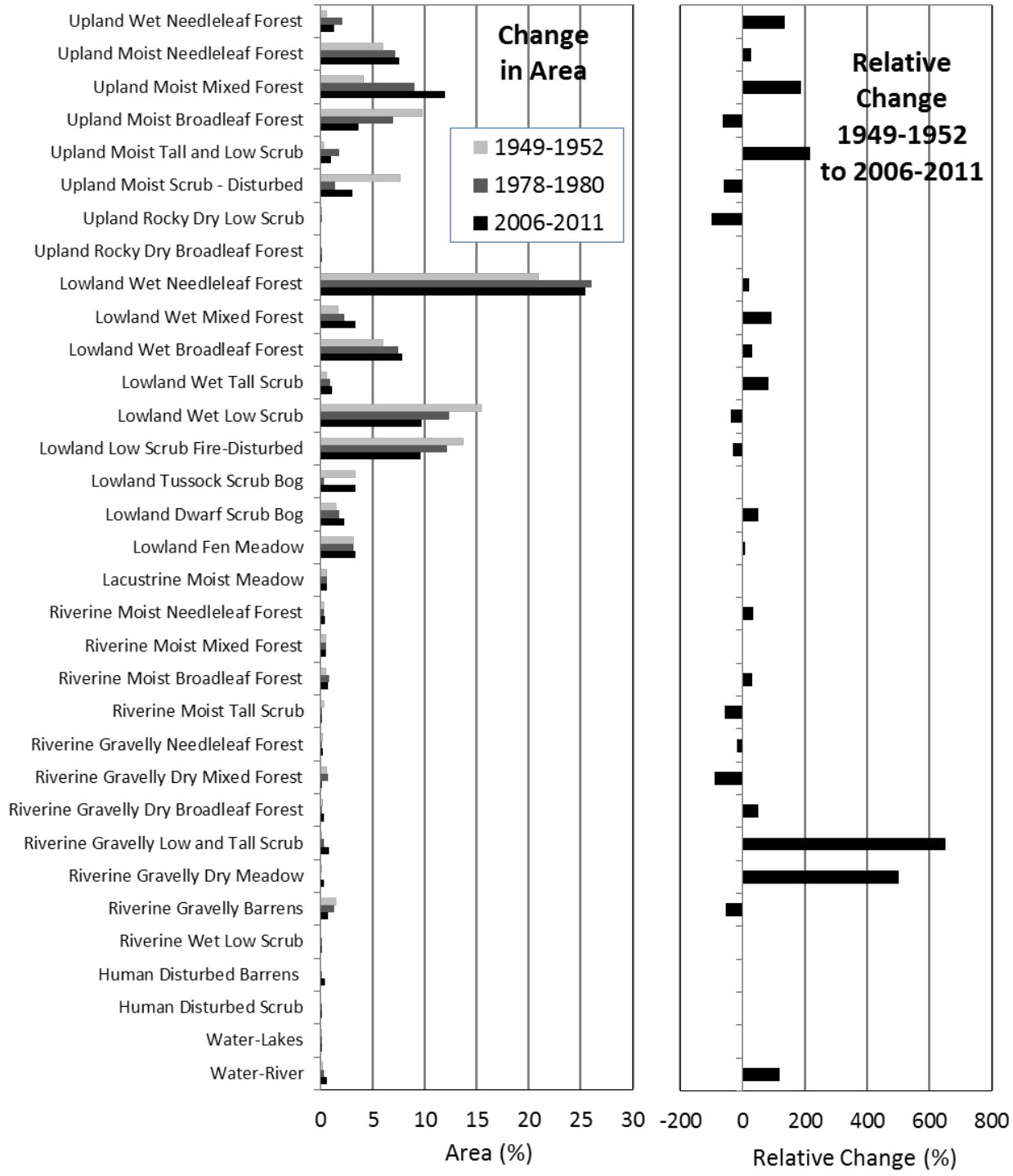

Figure 58. Changes in area (%) of ecotypes from 1949–1952 to 2006–2011.

Figure 59. Photographs illustrating ecological processes affecting change, including thermokarst, fire, post-fire succession, river erosion and deposition, land clearing, and trail development.

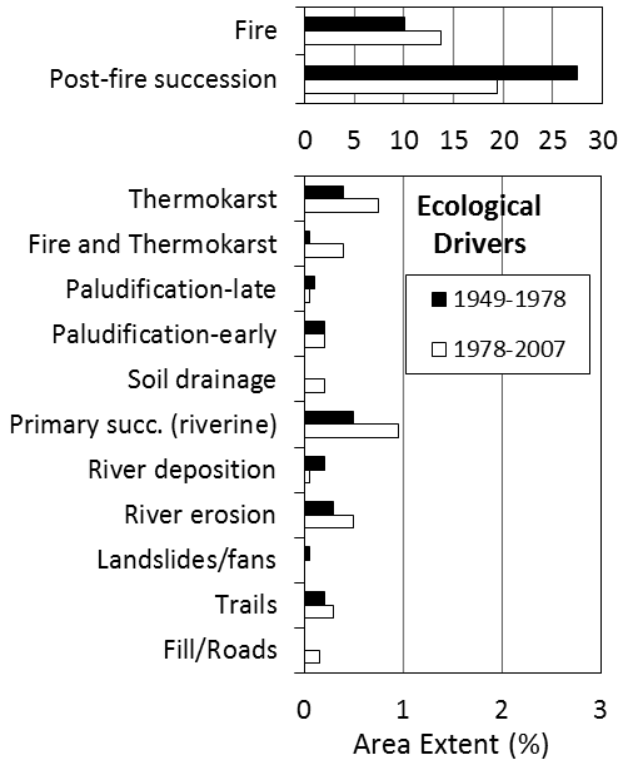

Figure 60. Comparison of the areal extent affected by 13 drivers of ecotype changes. Note difference in scales between charts.

When comparing ecoregions, there were large differences in changes between the Yukon-Tanana Uplands (25% of study area) and the Tanana-Kuskokwim Lowlands (75%). In the Yukon-Tanana Uplands, mainly around the Yukon Training Area, overall change was 56.4% over the two periods, with most change driven by post-fire succession (52.4%), while the area affected by fire (1.4%) was relatively small. This region also had the most human activity, primarily fill (0.6%) and trails (1.0%). In the Tanana-Kuskokwim Lowlands, overall change was 56.9%, with most change driven by both post-fire succession (38.9%) and fire (12.3%). Thermokarst affected more area in the lowlands (2.1%) compared to the uplands (0%). Similarly, the combined area affected by river erosion, deposition, and primary succession on floodplains was substantial in the Tanana-Kuskokwim Lowlands (2.7%) and negligible in the Yukon-Tanana Uplands (0%).

5.5.3 Accuracy Assessment

The overall accuracy of the photo-interpretation was 60% based on 128 ground determinations for 16 classes. Most of the confusion was due to: photo-interpreted Lowland Wet Broadleaf Forest being found to be Lowland Tussock Scrub Bog (3) and Lowland Wet Needleleaf Forest (3); Upland Moist Broadleaf Forest being Lowland Needleleaf Forest (2) and Upland Moist Mixed Forest (3); Upland Moist Mixed Forest being Upland Moist Broadleaf Forest (5); and Upland Moist Needleleaf Forest being Upland Moist Mixed Forest (4). Agreement between the field ecotype determined in the field (assigned to aggregated map ecotypes) and after review of field data by the lead photo-interpreter was 77%, with most of the error resulting from confusion between Lowland Wet Low Scrub vs Lowland Tussock Scrub Bog (3), Upland vs Lowland Low Scrub-Disturbed (5), and Upland vs Lowland Needleleaf Forest (3, and Upland vs Lowland Mixed Forest (4). Overall, the main problems were distinguishing upland vs lowland physiography in

gently sloping terrain and canopy coverage among broadleaf, mixed, and needleleaf forests, where the understory and overstory trees led to confusion. The problem exists both for confusion among ground observers with the same data, and in the photo-interpretation.

5.5.4 Discussion

Boreal ecosystems form a diverse mosaic in central Alaska in response to a wide variety of biophysical drivers. The systematic assessment identified 33 ecotypes within the sampling area, compared to the more comprehensive survey of 44 ecotypes identified in the ecological land survey for Fort Wainwright (Jorgenson et al., 1999), which involved more effort to distinguish rocky and gravelly ecotypes that were combined in this study. The relative abundance of ecotypes, however, was similar with the dominant ecotypes in the Fort Wainwright study: Lowland Wet Needleleaf Forest (20.9%), Lowland Wet Low Scrub (11.4%), Upland Moist Mixed Forest (9.1%), and Upland Moist Broadleaf Forest (6.2%). This indicates that the systematic grid was broadly representative of the terrain conditions quantified through intensive mapping.

Fire was by far the largest driver of landscape change, affecting 24.3% of the region overall from 1949–1952 to 2006–2011. This resulted in ecotypes transitioning from forest types to post-fire early successional types, and from early successional types back to forest. In the early period, early successional types that developed after fire were much more abundant than areas with new fires (13.7%), indicating the region was greatly affected by large fires in the early part of the 1900s. Based on the typical age (10–30 yrs) of early successional tall and low shrub that develop after fire, we estimate that ~60% of the region experience fires around the 1920s. As this was a period of extensive settlement, gold exploration, and steamboat traffic we speculate that human activity contributed to these widespread fires. A large fire on the Tanana Flats reportedly occurred in 1941 (Randi Jandt, pers. comm.). The large extent of early fires and the decrease in recent periods is at odds with recent analyses of fire history that indicate that fire frequency and extent have substantially increased since the 1980s, while the proportion of human-caused fires has remained relative low in the last few decades (Kasischke et al., 2006, 2010).

Thermokarst is typically associated with ice-rich permafrost, especially in lowland environments that frequently have organic-rich silty soils (Jorgenson et al., 2008b). In our study, thermokarst affected only 0.8% of the overall area by 2006–2011, but was much more extensive in the broader Tanana-Kuskokwim Lowlands (2.1%), and within the Tanana Flats portion (4.4%) of the Tanana-Kuskokwim Lowlands. This regional estimate is much lower than the thermokarst extent of 47% estimated for a small area near the 1930 burn site (Jorgenson et al., 2001a) and 41% for the broader Tanana Flats (Osterkamp et al., 2006) based on photo-interpretation. We attribute this large discrepancy in large part to the random selection of 4 of 9 grids being located on the higher elevations of the flats with continuous permafrost, and to a lesser extent to the mapping approach used by Osterkamp et al. (2006) that incorporated substantial areas with permafrost soils as inclusions within the mapped thermokarst polygons.

Fluvial processes create highly dynamic environments associated with channel erosion and deposition, overbank flooding, and primary succession (Viereck et al., 1993, Van Cleve et al., 1996). In our study, riverine ecotypes covered 5.1% of the total area and nearly one-third of riverine ecotypes (1.5% of the total area) were affected by changes associated with river erosion, deposition, and primary succession, indicating the floodplains were highly dynamic. Interestingly, most of the change resulted from loss of mid- to late-successional riverine gravelly broadleaf, mixed, and needleleaf forests (-0.8% combined) due to river erosion on braided floodplains near the mountains, and the conversion of gravelly barrens (-0.8%) to early successional meadow and scrub (1.0%). This is consistent with observations by Nossov et al. (2011) of a large increase in floodplain deposition/silt bar creation between 1949 and the 1970s and the establishment of tall

shrubs (alder) on the new silt bars by the mid-1990s. We speculate that the loss of highly disturbed gravelly barrens and the increase in early successional vegetation are related to changes in the discharge of glacial rivers or recovery from past large flood events.

These results support our initial hypothesis that a time-series analysis of historical airphotos and recent satellite images can be used to identify and quantify changes in local-scale ecosystems (ecotypes) through photo-interpretation of points systematically distributed across a variety of ecotypes. We were able to identify rates of ecotype change over our two different time periods and we identified the ecological drivers of change across the landscape.

The limited accuracy (60%) of the photo-interpretation affects the interpretation of the change assessment. For example, we found large increases in Upland Moist Mixed Forest (7.8% of total area) and Upland Moist Needleleaf Forest (1.6%), and a large decrease in Upland Moist Broadleaf Forest (-6.2%), yet changes in these ecotypes were subject to substantial photo-interpretation error. In the worst case scenario, the relative changes could be off by ~40%, but as the errors occurred in both directions the errors were likely to be partially compensating and, thus, likely to substantially reduce the effect of the error. This problem also applies to the observed increases in Lowland Wet Mixed Forest. However, the substantial error associated with differentiating upland from lowland ecotypes with similar vegetation structure (e.g., Upland vs Lowland Mixed Forest) does not affect the photo-interpreted results because the lowland or upland physiography designated for a point did not change during interpretation. The confusion between upland and lowland physiography is one of the biggest limitations of the ecological classification system.

Knowledge of the magnitude and direction of landscape changes can help inform land management decisions on military lands. Fire is by far the most prevalent driver of change and is the subject of intensive fire-fighting and land management decisions statewide. Fire is a natural process that is essential to maintaining the diversity and health of boreal ecosystems (Chapin et al. 2006), but also has the risk of damaging human infrastructure. Current land management strategies are directed toward allowing man-made and natural fires to burn on military lands, unless they endanger military facilities and private lands adjacent to military lands. Thermokarst has been expanding in response to longer-term climate warming since the Little Ice Age (Jorgenson et al., 2001b) and to recent anthropogenic-induced warming (Grosse et al., 2011). While land management strategies can do little to affect ongoing thermokarst, activities on ice-rich permafrost can be avoided or minimized during training exercises and infrastructure development. In contrast, land use on floodplains is less of a concern because much of the floodplain has early successional vegetation that can more easily recover after human disturbance, and disturbance already is abundant on these dynamic ecosystems.

5.6 Development of a GIS based geospatial decision support tool

The GISMO tool was designed to help U.S. Army Alaska land managers identify when and where a projected future warmer climate will affect two critical aspects of training land ecological, hydrological, and cryospheric processes- seasonal meteorology and the thermal state of soils, including permafrost. Results from the studies that comprise this research project have shown clearly that fire and human disturbance can dramatically affect the ground thermal regime and thus permafrost stability. Further, changes in permafrost extent, whether through disturbance or projected climate warming, will undoubtedly lead to altered surface water and groundwater regimes. This is expected to change wetland status and will undoubtedly feed back on permafrost and soil thermal processes.

Through numerous meetings with a variety of collaborators, land users, and Federal, State, and Local agencies we assembled the most up to date database of GIS layers for the area encompassing interior Alaska DoD training ranges and cantonments (Table 15). Based on our stakeholder meetings, the scientific results from this project, and the research results from hundreds of studies referenced herein and elsewhere we seek to provide training range managers with scientifically based decision support information to help them determine where and when projected climate warming will impact current and planned infrastructure and training activities.

The information presented in GISMO is provided in the most fine scales available for each dataset but they vary (Table 15). For example, the digital elevation information used to develop terrain elevation information is at scales ranging from 7 to 60 meters while climate projection information is at 771 meter resolution. Many site locations are points on the map and are presented as such.

What follows is some background information on the base layers and climate projection model results that are provided in GISMO and some screenshots of various maps and queries that can be created and performed in GISMO. However, the best way to experience what can be done in GISMO is to access it and follow the user interface to perform unique queries.

GISMO can be accessed at the following web location:

https://www.cemml.colostate.edu/gismo-dss-ak

At the prompt for User and Password input the following:

User: CRREL
Password: Permafro$t1

Figures 61 to 68 present historical and projected data on temperature and precipitation during summer and winter in interior Alaska from 1910 to 2039 to include some climatic information presented in GISMO. Climate projections in GISMO run to 2100 but here we present the range of years that are most critical for recent and currently planned infrastructure development (i.e. for the next 25 years).

Figures 61 and 65 present historical temperature measurements. Data are from the Scenarios Network for Alaska and Arctic Planning (SNAP; http://www.snap.uaf.edu) historical dataset, which is derived from downscaled climate data largely contributed from Parameter-elevation Regressions on Independent Slopes Model (PRISM; http://prism.oregonstate.edu) and Climate Research Unit (CRU; http://www.cru.uea.ac.uk) datasets.

Figures 62 and 66 present projected summer and winter season temperatures, respectively. Data are from the Scenarios Network for Alaska and Arctic Planning projected dataset which is derived from downscaled climate model simulations averaged from five climate models that

perform well in Alaska (General Circulation Model version 3.1, European Centre Hamburg Model 5, Coupled Climate Model 2.1, Coupled Model 3.0, and Model for Interdisciplinary Research on Climate-medium resolution). B1, A1B, and A2 scenarios represent relatively low, intermediate, and high CO_2 emission futures (IPCC, 2007).

Historical precipitation for the summer (Figure 63) and winter (Figure 67) are from the Scenarios Network for Alaska and Arctic Planning historical dataset derived from downscaled climate data from the Parameter-elevation Regressions on Independent Slopes Model (PRISM; http://prism.oregonstate.edu) and Climate Research Unit (CRU; http://www.cru.uea.ac.uk) datasets.

Projected summer (Figure 64) and winter (Figure 68) precipitation data are from the Scenarios Network for Alaska and Arctic Planning projected dataset which is derived from downscaled climate model simulations averaged from five climate models that perform well in Alaska (General Circulation Model version 3.1, European Centre Hamburg Model 5, Coupled Climate Model 2.1, Coupled Model 3.0, and Model for Interdisciplinary Research on Climate-medium resolution). B1, A1B, and A2 scenarios represent relatively low, intermediate, and high CO_2 emission futures (IPCC, 2007).

Mean summer temperatures (June-August; Figure 61) show decadal variability and dramatic warming since 1990. Lowland regions have warmed more than the surrounding hills or mountains of the Alaska Range. Though some climate scenarios predict greater rates of warming than others for interior Alaska the general trend is increasing air temperatures in the future (Figure 62).

There was a large amount of interdecadal variability in summer precipitation (1906-2006; Figure 63) but no significant trends in interior Alaska (Wendler and Shulski, 2009). Modeling scenarios for future summer precipitation in the area (Figure 64) result in decadal variability in precipitation with the IPCC B1 and A1B scenarios predicting slightly wetter conditions and the IPCC A2 scenario predicting an overall drying. In general, the climate of interior Alaska is dry, receiving 29 cm of annual precipitation (Jorgenson et al., 2001a; Wendler and Shulski, 2009). As a consequence, a few large convective summer storms can have a substantial impact on any season's precipitation total.

Figure 65 depicts historical decadal mean winter temperatures for interior Alaska. The results show a general trend of increasing winter time temperatures since 1910. Wendler and Shulski (2009) report the greatest winter time warming in the months of December and January for their 1906 to 2006 records from a station near Fairbanks. The mean December-February warming since 2006 is 1.3°C (Wendler and Shulski, 2009). Future climate scenarios predict an increase in December to February temperatures with consistent agreement across three IPCC model scenarios (Figure 66).

Winter season precipitation has decreased from 1910 to 2009 (Figure 67). The future winter season is expected to be shorter based on modeling efforts that simulate snow accumulation and melt over 30 years (1979-2009; Liston and Hiemstra, 2011). For interior Alaska, simulated results indicate a 4 cm decrease in precipitation and a 0.5 °C drop in temperature during the snow-covered seasons. Forty percent of the annual precipitation arrived as snow in 2009 compared with forty-five percent in 1979. Over that 30 year period, snow arrived 8 days later and melted 9 days earlier, leading to a shortened snow season of ~17 days. Predictions of future precipitation in the area based on the IPCC model scenarios suggest winter precipitation totals are expected to be slightly lower while summer precipitation is not expected to change much (Figure 68). This trend is in contrast to the fact that General Climate Models (GCMs) typically assume warmer temperatures lead to greater moisture in the atmosphere and, as a consequence, increased precipitation rates (Räisänen, 2008; Walsh, 2008).

Table 15. A list of the GIS layers we have accumulated for training range land management applications in GISMO.

Theme	Name	Resolution	Tanana Flats	Yukon Training Area	Donnelley Training Area	Fort Greely	Date	Source
Digital Elevation Models (DEMs)	USGS NED Data, 1/3 Arc Sec (Dec. 2012)	7 m	-66%	X	X	X	Dec-12	USGS, National Elevation Dataset
	USGS NED data 1 Arc Sec(July 2012)	42 m	X	X	X	X	Jul-12	USGS, National Elevation Dataset
	USGS NED data 2 Arc Sec(July 2012)	30 m	X (~66%)	X	X	X	Jul-12	USGS, National Elevation Dataset
	DTA Unknown DEM (30m)	30 m			X	x	May-12	CEMML, FT Wainwright
	YTA Unknown DEM (60 m)	60 m		X			May-12	CEMML, FT Wainwright
	FWA Unknown DEM (40 m)	39.6 m	X	X			May-12	CEMML, FT Wainwright
Permafrost	2008 Permafrost Characteristics of Alaska	10-20 km	X	X	X	X	Dec. 2008	Torre Jorgensen et al., 2008
	Permafrost Map produced by Torre	~30 m	X				1998	Torre Jorgensen
	Permafrost Map produced by Torre	~30 m		X			1998	Torre Jorgensen
Soils	NRCS Soils SSURGO Data	1:25,000	X	X	X	X	Feb-12	National Resource Conservation Service
Hydrology	Surface Water (Streams, Lakes, Ice)	1:24,000	X	X	X	X	Dec-12	National Hydrography Dataset
Wetlands	National Wetlands Inventory		Incomplete	Incomplete	Incomplete	Incomplete	Jan-13	US Fish and Wildlife Service
Land Cover	2001 NLCD data for Alaska	30 m	X	X	X	X	2008	USGS National Land Cover Data
	US Army Alaska Habitat Map		X	X	X	X	Unknown	CEMML, FT Wainwright

Table 15 (continued). A list of the GIS layers we have accumulated for training range land management applications in GISMO.

Theme	Name	Resolution	Tanana Flats	Yukon Training Area	Donnelley Training Area	Fort Greely	Date	Source
Normalized Difference Vegetation Index (NDVI	AVHRR-Derived, GIMMS3g	8 km	X		X	X	1982-2010	NASA, Goddard Space Flight Center
	eMODIS, March 2000-2010	250 m	X	X	X	X	2000-2010	GINA, U Alaska Fairbanks
	MODIS NDVI Data March 2000-present	250 m	X	X	X	X	2000-present	MODIS; NASA
Imagery	IKONOS, Quickbird 2, WorldView 2 Satellite imagery	0.5-4 m	100+	100+	100+	100+	2002-present	National Geospatial Intelligence-Agency
	Landsat (1979-present)	30 m	X	X	X	X	1979-present	United States Geological Survey
Fire	Alaska Fire Service Burned Areas from 1946-2011		X	X	X	X	Feb-12	Alaska Fire Service
Lightning	Alaska Fire Service Lightning Detection	point data	X	X	X	X	Feb-12	Alaska Fire Service
	5 km radius strike density from lighting data	500 m	X	X	X	X	Mar-12	Calculated from Alaska Fire Service Data
Climate Projections	SNAP Climate History and Projections for Temp. and Precip.	771 m	X	X	X	X	Mar-12	University of Alaska Fairbanks
Roads	Alaska DOT Road System		X	X	X	X	Jan-12	Alaska DOT
Towns	Alaska Placenames	point data					Oct-10	Alaska DOT
Boundaries	Military Installation Boundaries		X	X	X	X	Feb-12	CEMML, FT Wainwright

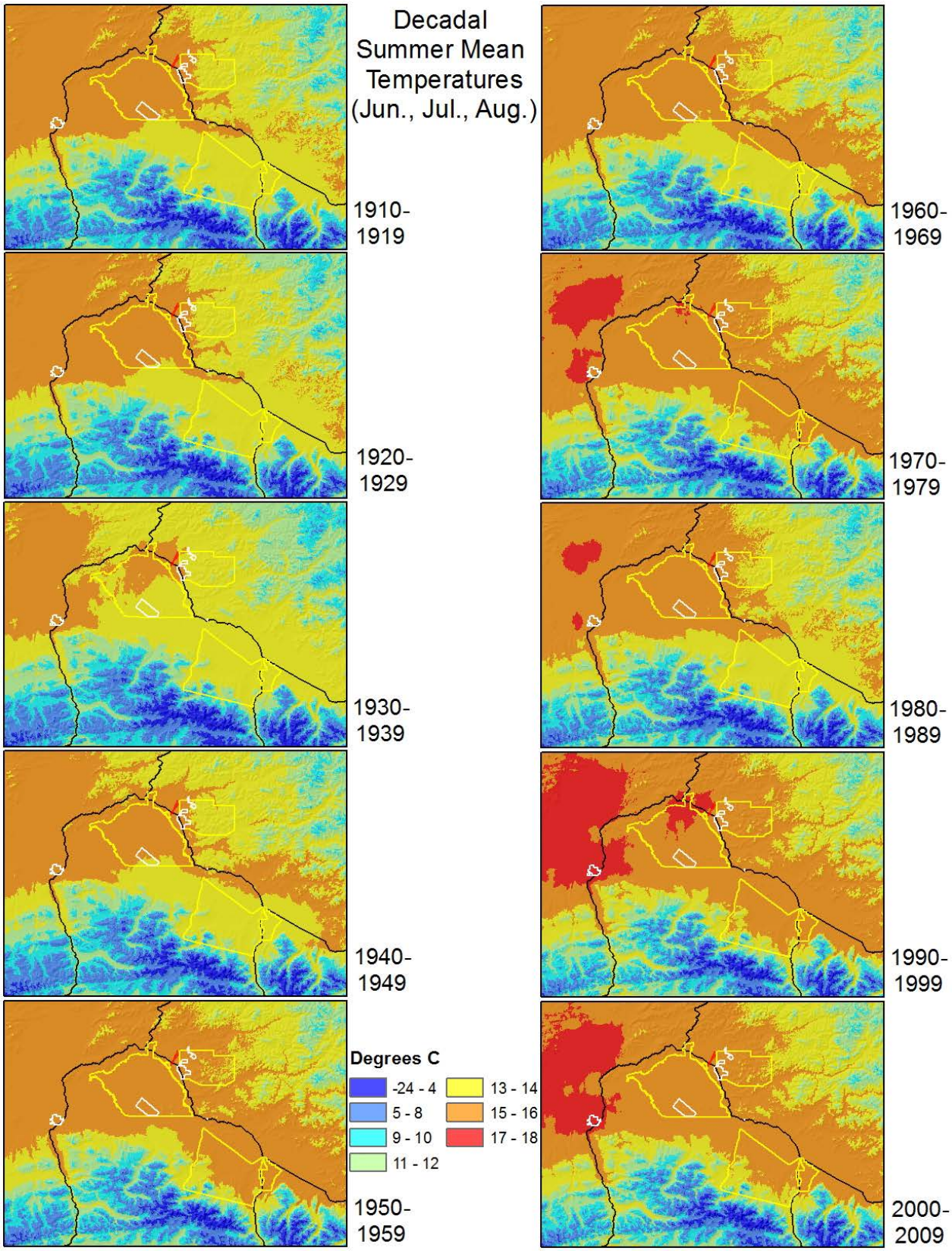

Figure 61. Decadal summer (June-August) mean temperatures. U.S. Army Corps of Engineers project lands are outlined in red, Army lands are delineated by yellow, and Air Force lands are marked by white.

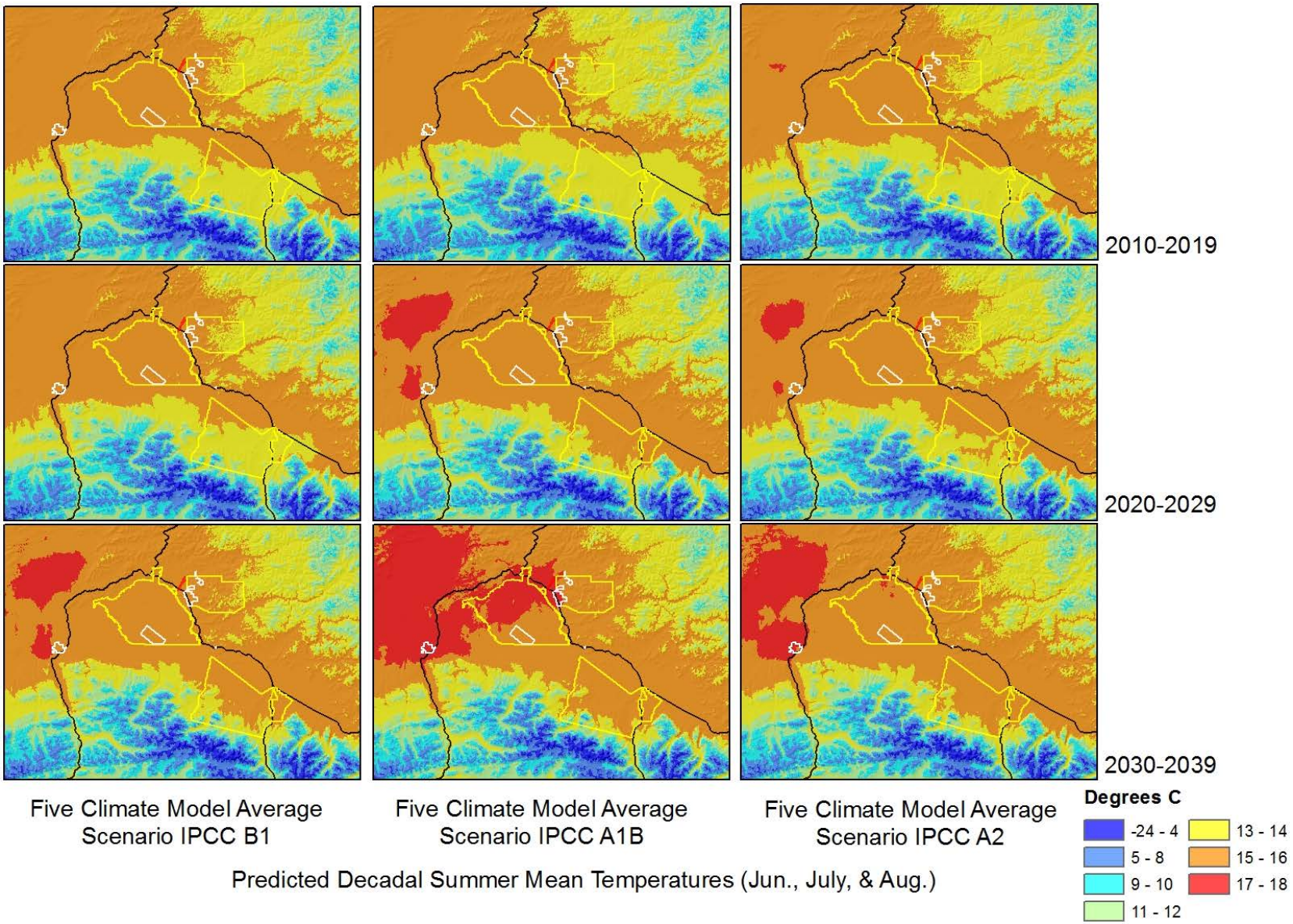

Figure 62. Downscaled projected decadal summer (June-August) mean temperatures for interior Alaska. U.S. Army Corps of Engineers project lands are outlined in red, Army lands are delineated by yellow, and Air Force lands are marked by white.

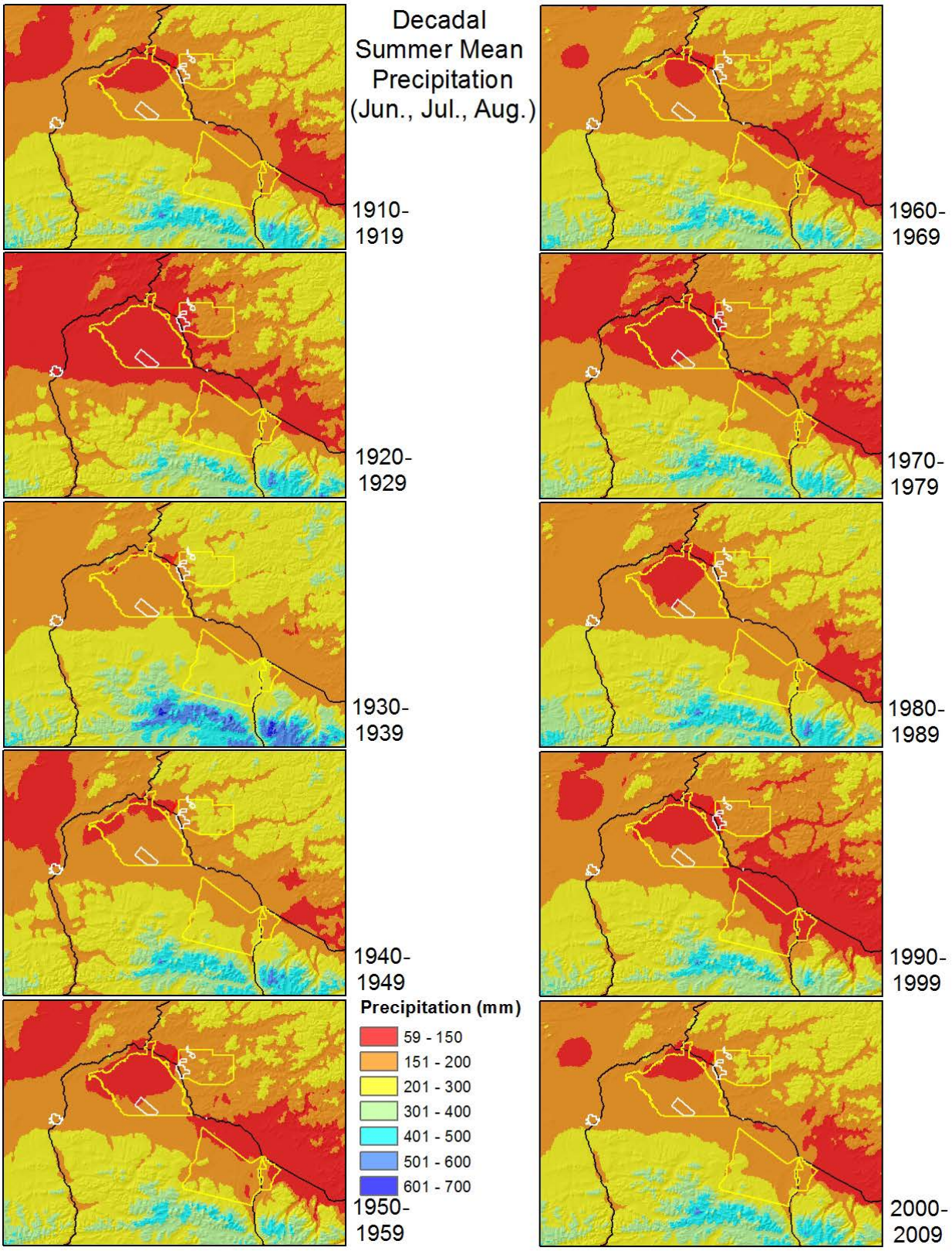

Figure 63. Decadal summer (June-August) total precipitation shows a general increase decrease from one decade to another for interior Alaska. U.S. Army Corps of Engineers project lands are outlined in red, Army lands are delineated by yellow, and Air Force lands are marked by white.

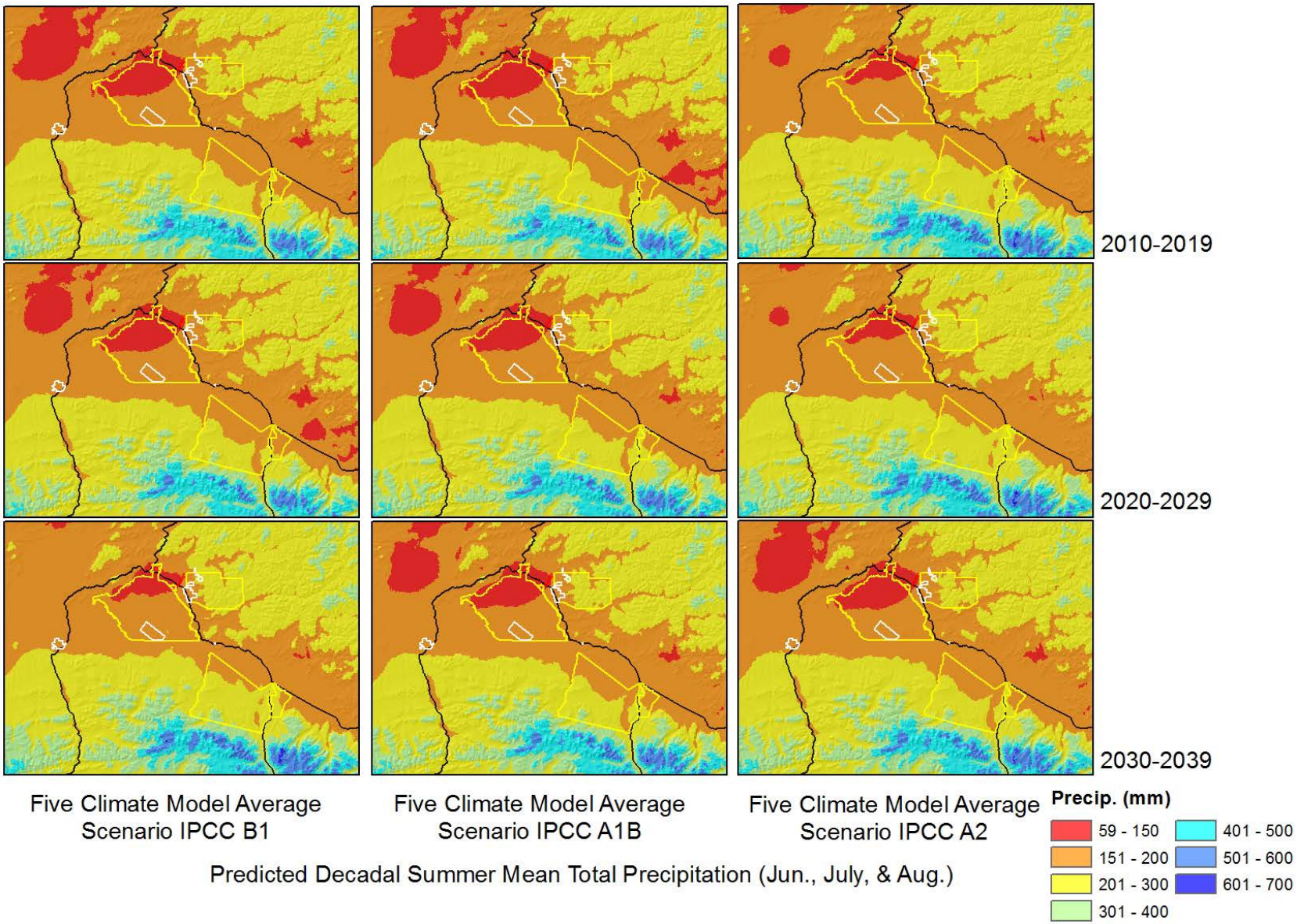

Figure 64. Downscaled projected decadal summer (June-August) average total precipitation for interior Alaska. U.S. Army Corps of Engineers project lands are outlined in red, Army lands are delineated by yellow, and Air Force lands are marked by white.

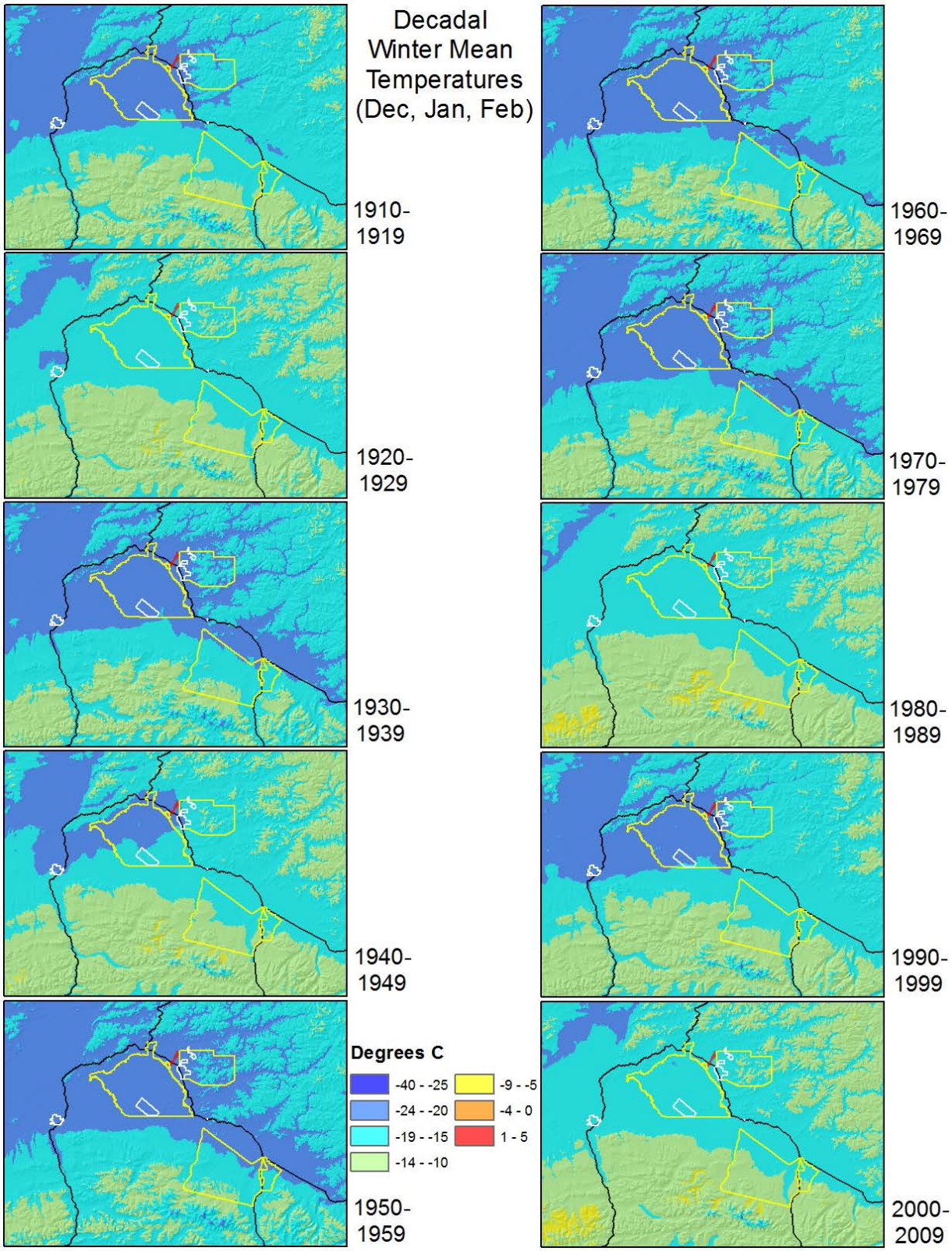

Figure 65. Decadal winter (December-February) mean temperatures show variability from one decade to another. U.S. Army Corps of Engineers project lands are outlined in red, Army lands are delineated by yellow, and Air Force lands are marked by white.

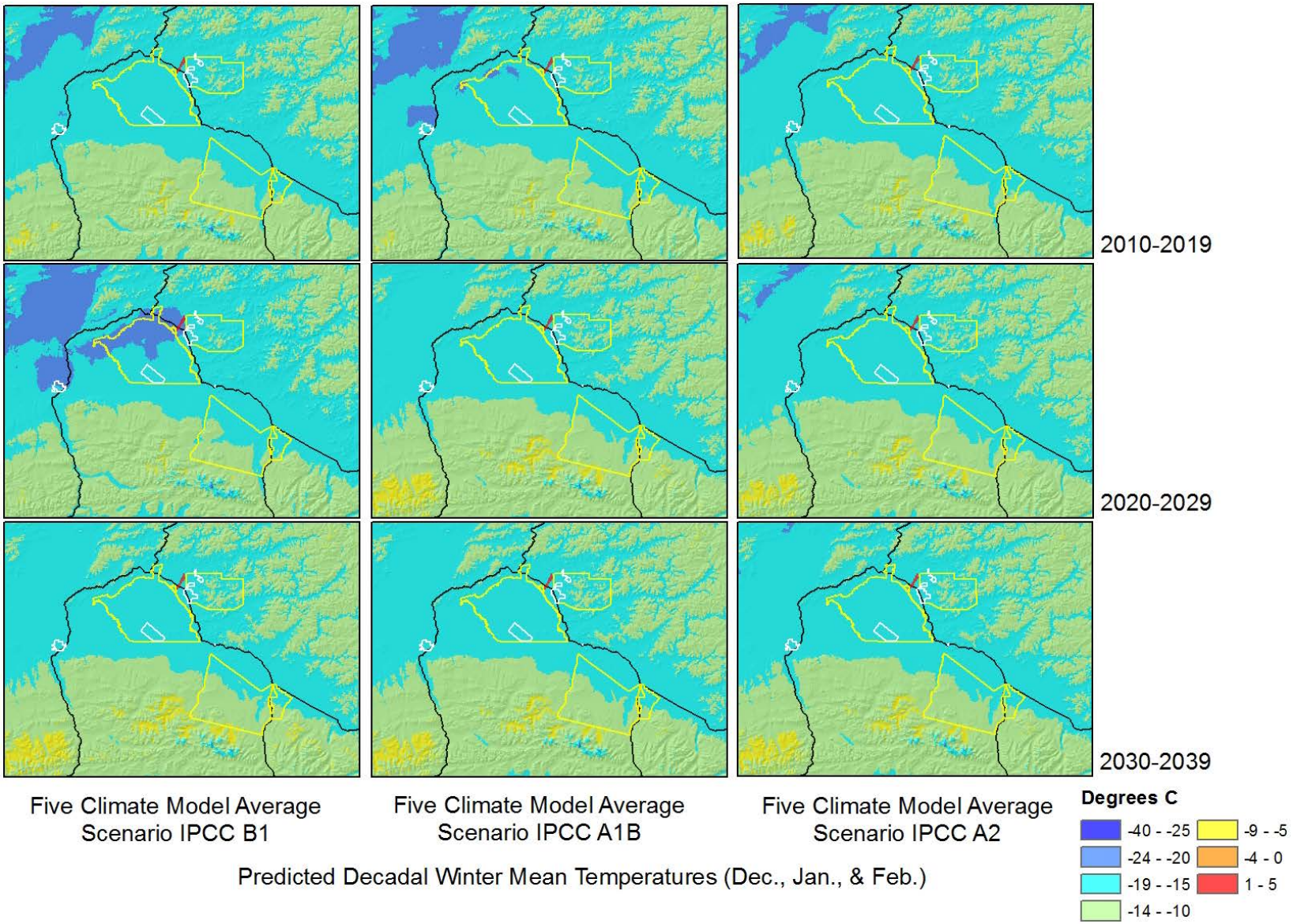

Figure 66. Downscaled projected decadal winter (December-February) mean temperatures for interior Alaska. U.S. Army Corps of Engineers project lands are outlined in red, Army lands are delineated by yellow, and Air Force lands are marked by white.

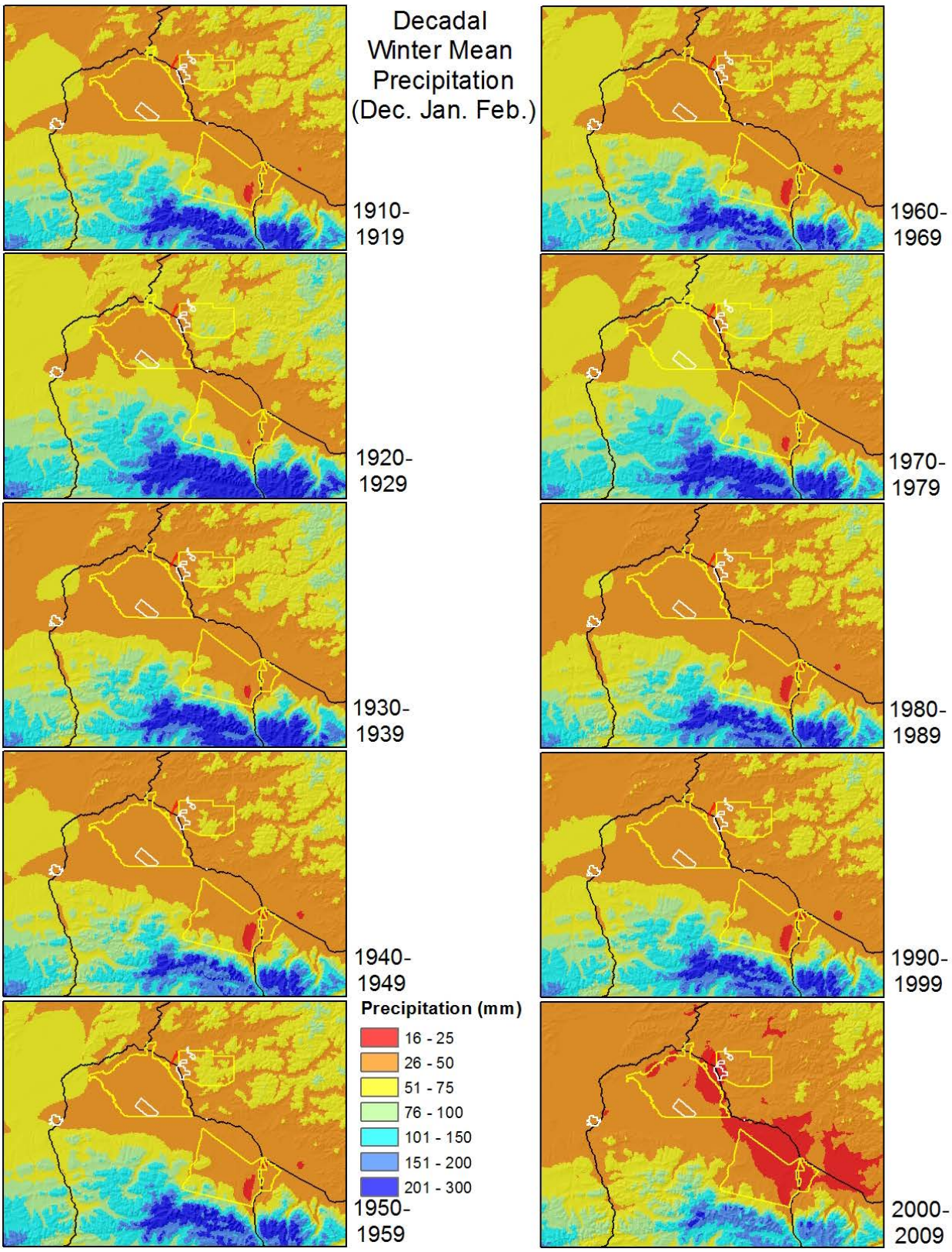

Figure 67. Decadal winter (December-February) total precipitation for interior Alaska shows a general decline from one decade to another. U.S. Army Corps of Engineers project lands are outlined in red, Army lands are delineated by yellow, and Air Force lands are marked by white.

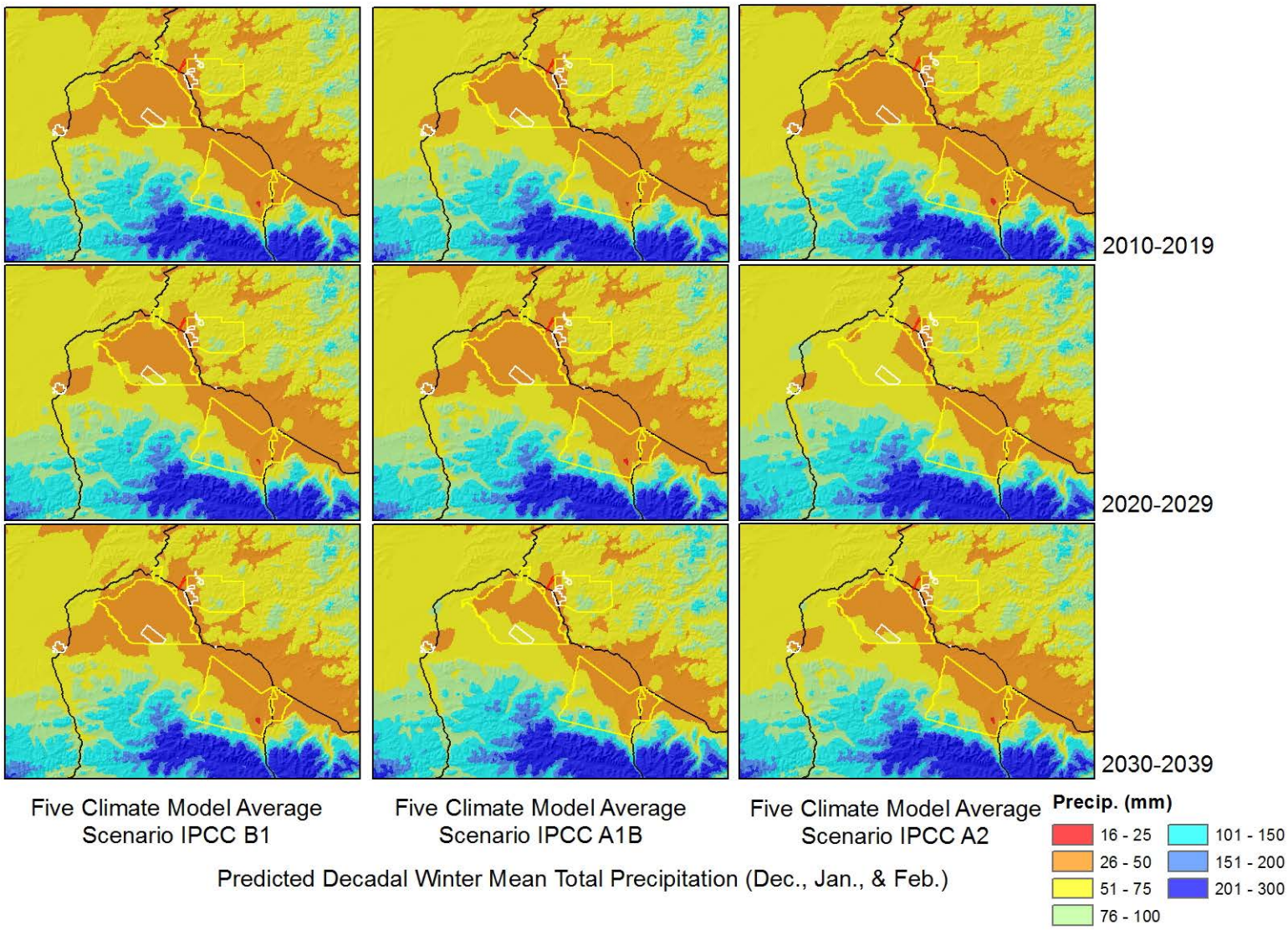

Figure 68. Downscaled projected decadal winter (December-February) average total precipitation for interior Alaska. U.S. Army Corps of Engineers project lands are outlined in red, Army lands are delineated by yellow, and Air Force lands are marked by white.

Following are some screenshots from GISMO to illustrate some of the decision support tools available to users. One of the most powerful modules in GISMO is the "analysis" command bar from which the user can specify start and end dates to see where historical and projected climate information changes over an almost 200 year total record. Figure 69 includes a screenshot of the Analysis command bar. Figures 70 and 71 provide examples from Analysis runs. The user is allowed to select from among Representative Concentration Pathway (RCP) greenhouse gas concentration trajectories they wish among either 4.5, 6.0, or 8.5 (IPCC, 2013). The RCP scenario drives the future climate response which is projected to 2100.

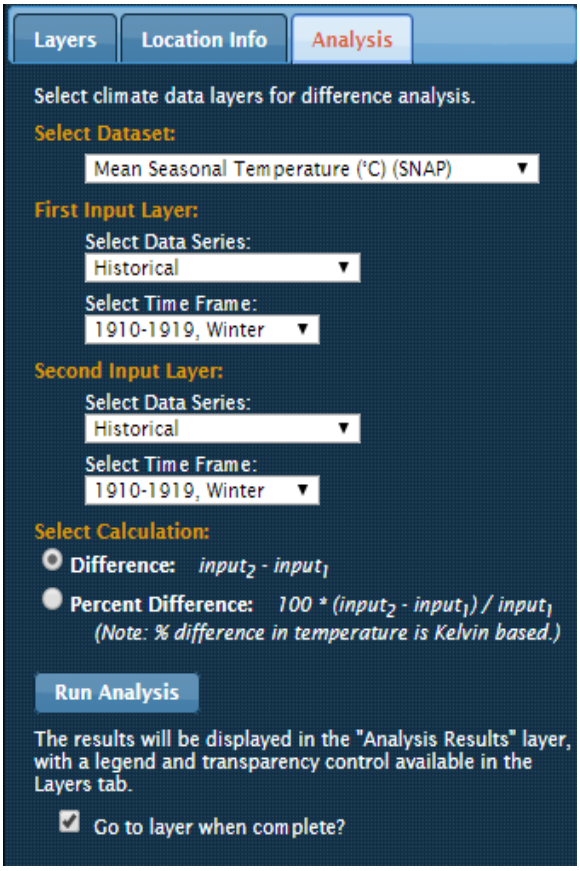

Figure 69. A screenshot from GISMO illustrating the "Analysis" command bar.

In Figure 70 the user has calculated the difference in mean annual ground temperature at 1 meter depth projected to 2100 minus the historically calculated value for 1980. The result is a color coded map indicating where and at what value ground temperatures at m1 meter will increase by the next century.

Figure 71 includes analysis results from a comparison between projected 2090-2099 mean winter season temperatures and mean winter season temperatures from the historical dataset (1910-1919) using RCP scenario 6.0. The difference values plotted are the degrees of warming over the 100 year time span.

Figure 72 includes data of lightning strike density from 1986 to 2013. Note the uplands, particularly in the Stewart Creek Impact Area, have the highest prevalence of lightning strikes. Since lightning is the most common natural cause of wildfire the ability to track strikes and

identify locations of highest risk for lightning can help training range managers manage fire susceptibility and fuels on the training ranges. By keying the lightning susceptibility to where fires have or have not occurred managers can identify potential high risk situations for wildfire.

Figure 73 provides information on mapped wetlands in the Tanana Flats Training Area while Figure 74 illustrates the transparency tool in GISMO. The upper and lower images are both of land cover but the lower image is 80% transparent so the training area boundaries (or whatever other user defined layers) are more readily visible. Figures 75 and 76 provide examples of the wildfire information available in GISMO. Figure 77 shows a GIPL climate modeling output in GISMO showing mean annual ground temperatures at 1 meter depth in 2010 from GIPL compared to projected mean annual ground temperatures at 1 meter depth in 2100.

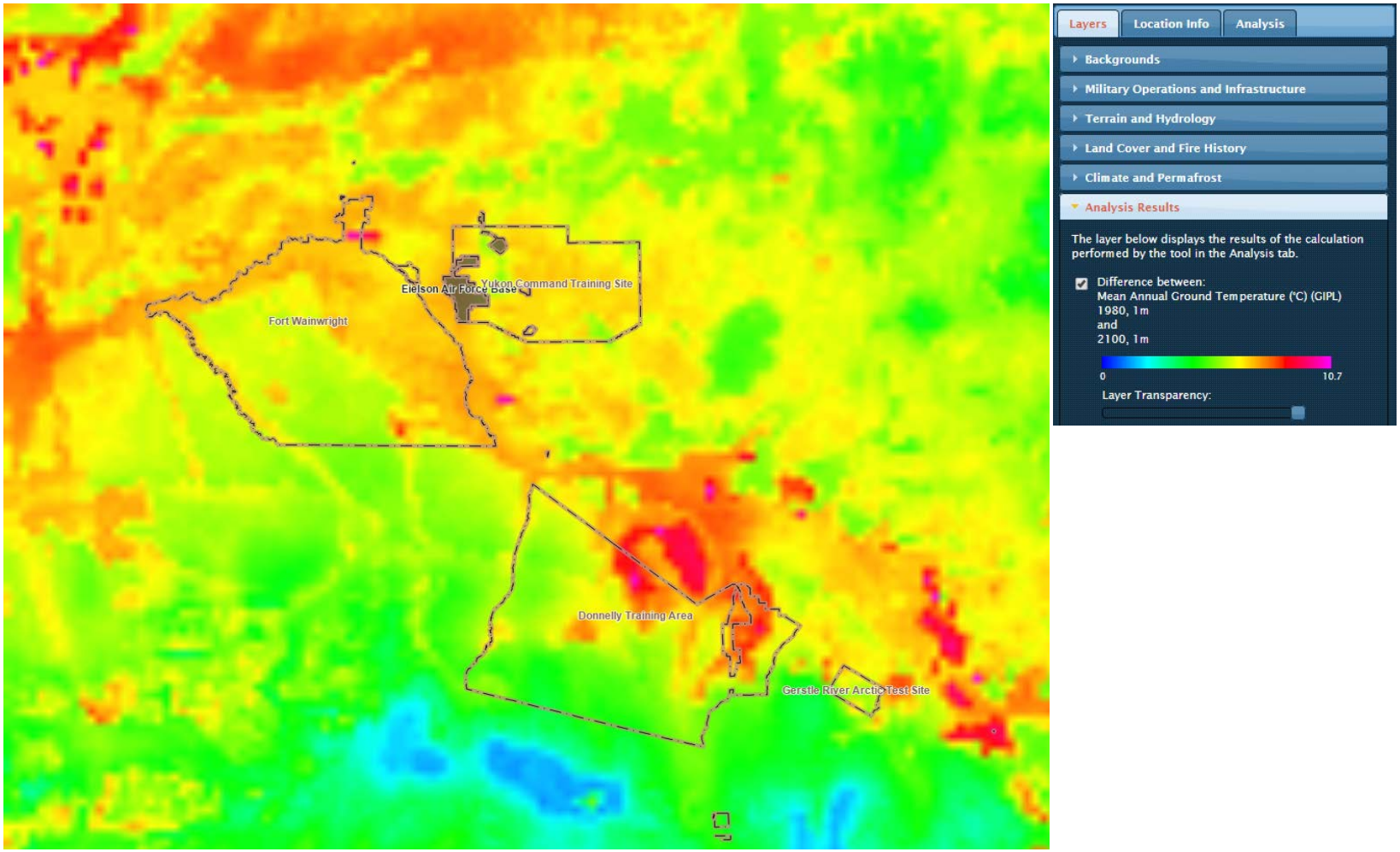

Figure 70. A comparison of mean annual ground temperature at 1 meter calculated for 1980 to projected mean annual ground temperatures in 2100 at 1 m depth. The resulting information shows the projected amount of warming from 1980 to 2100. Note that upland regions are projected to experience the greatest increase in ground temperatures (up to 10ºC).

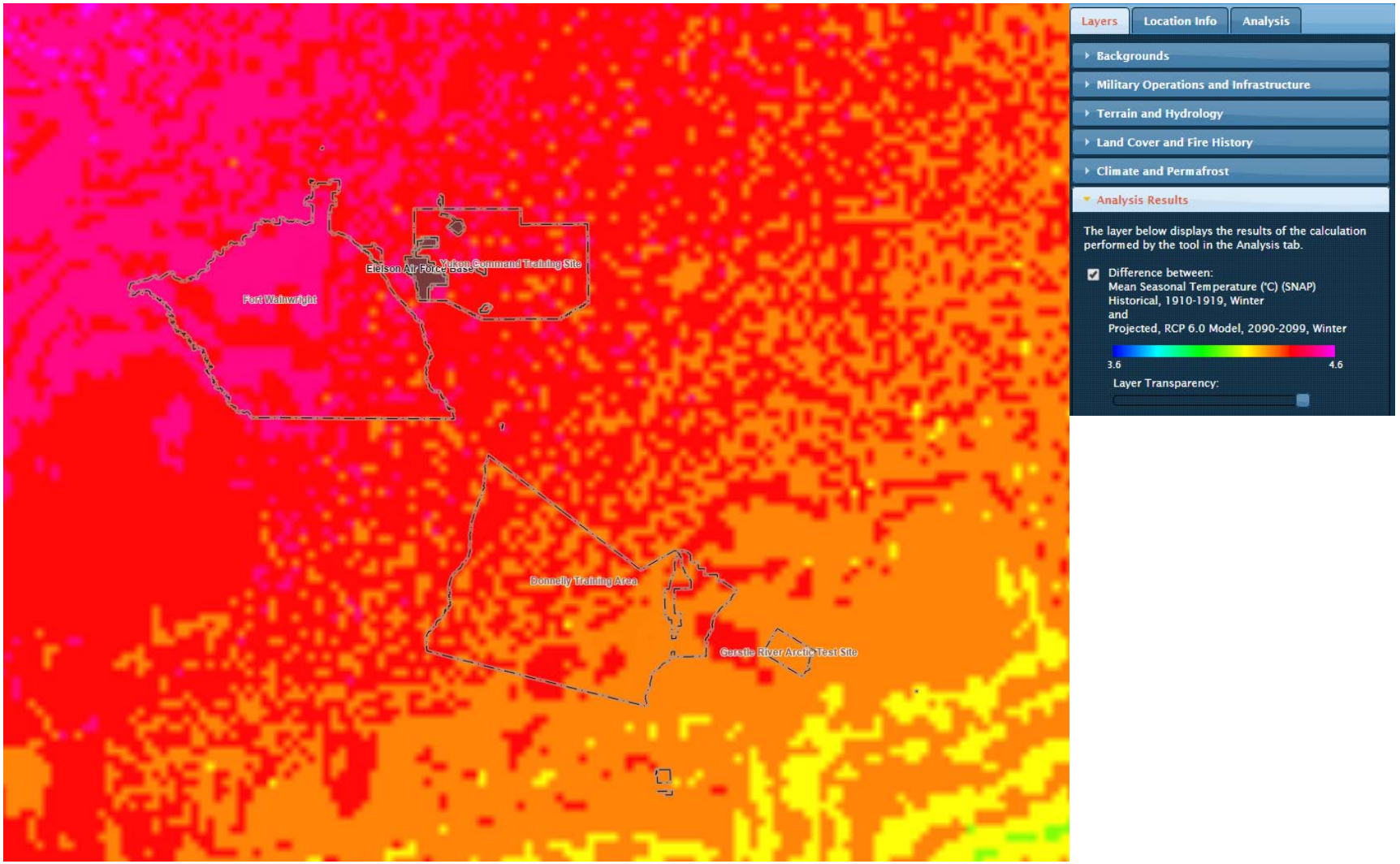

Figure 71. A comparison between mean winter season temperatures from the historical dataset (1910-1919) compared to projected 2090-2099 values using RCP scenario 6.0. The difference values plotted here are the degrees of warming for the interior Alaska training range domain

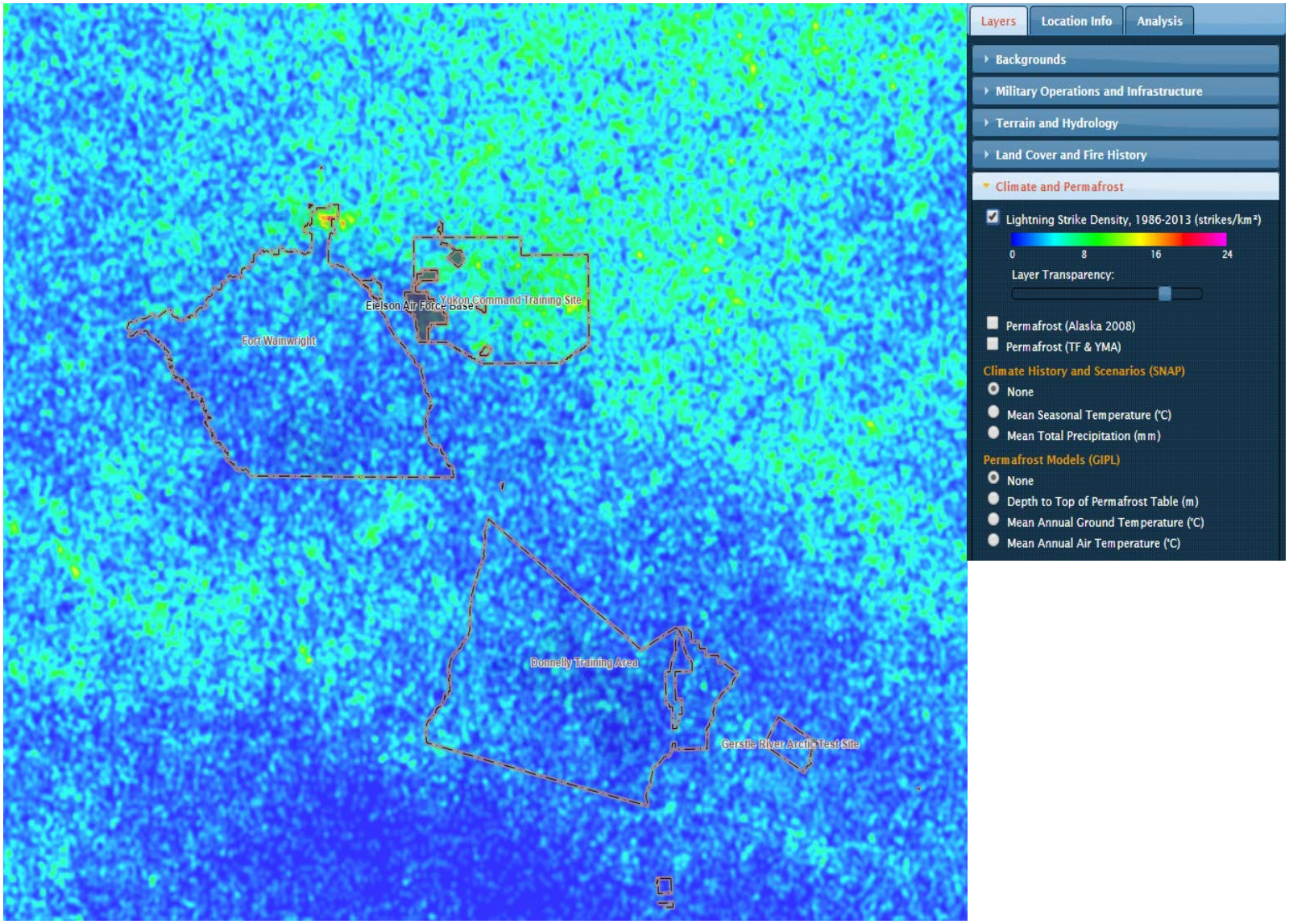

Figure 72. Lightning strike density from 1986 to 2013.

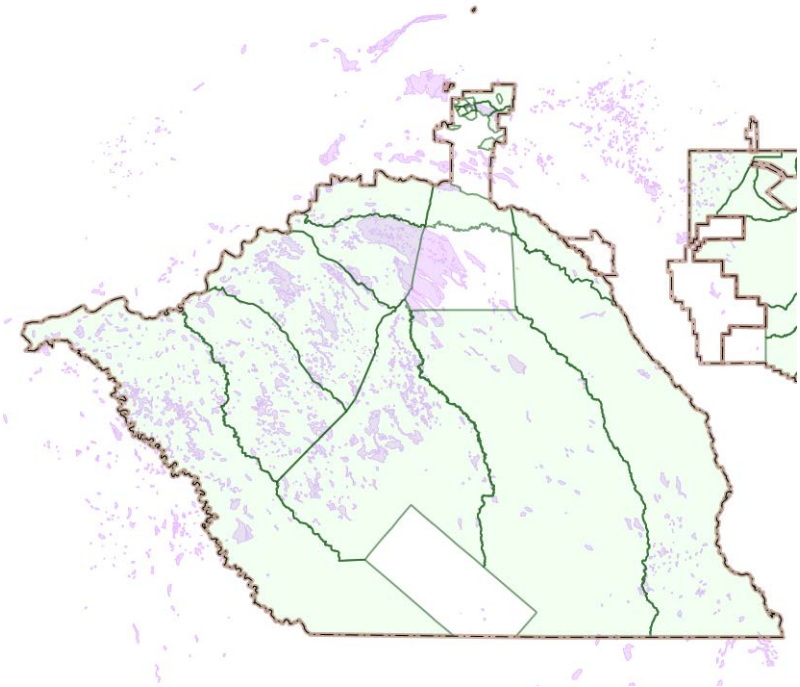

Figure 73. A screenshot from GISMO showing the Tanana Flats Training area with wetland areas mapped in purple.

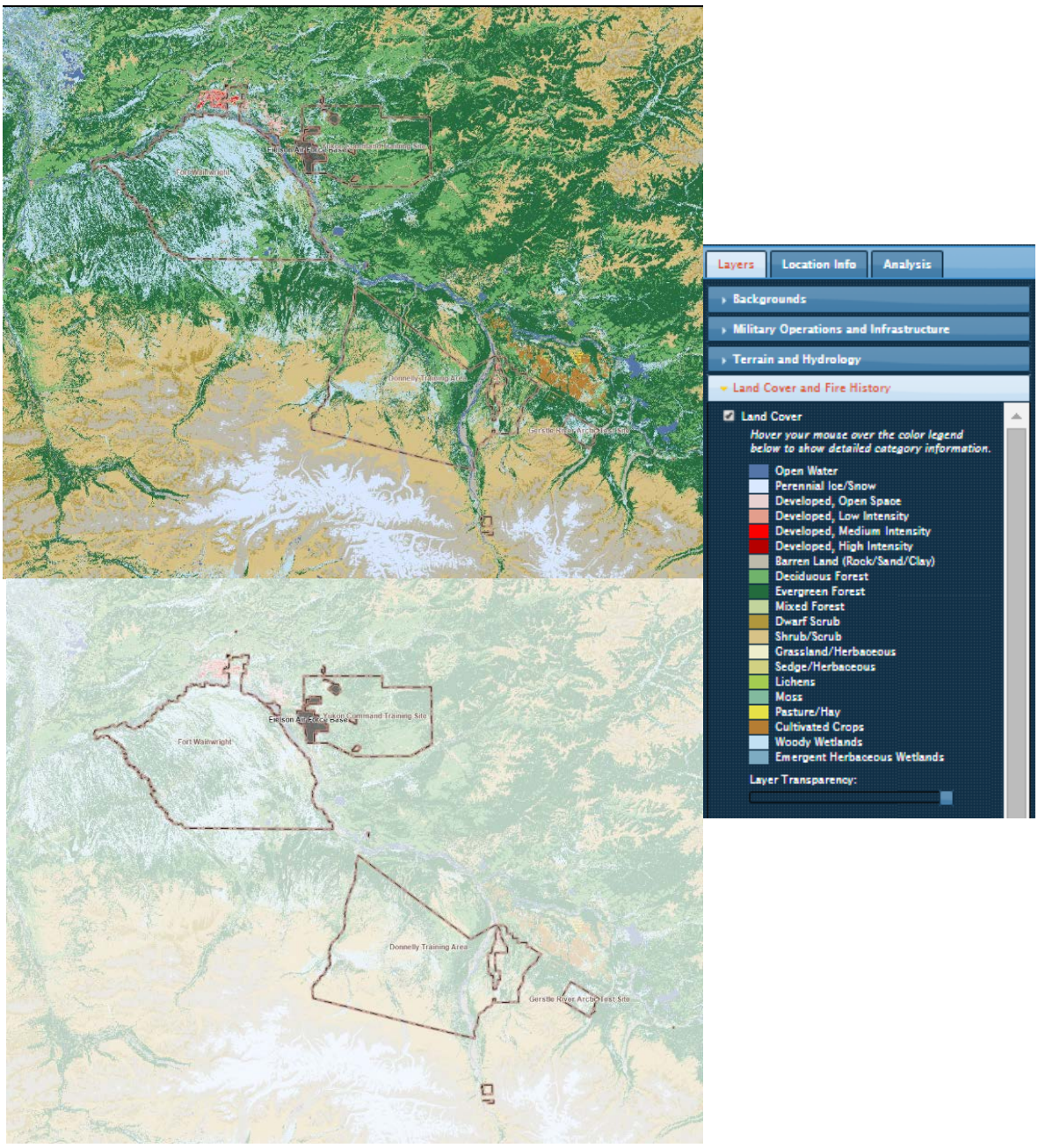

Figure 74. A pair of land cover images to illustrate the transparency tool in GISMO. Top: land cover for the interior Alaska training ranges. Bottom: the same image as the top image but with 80% transparency to better facilitate identification of other map layer information.

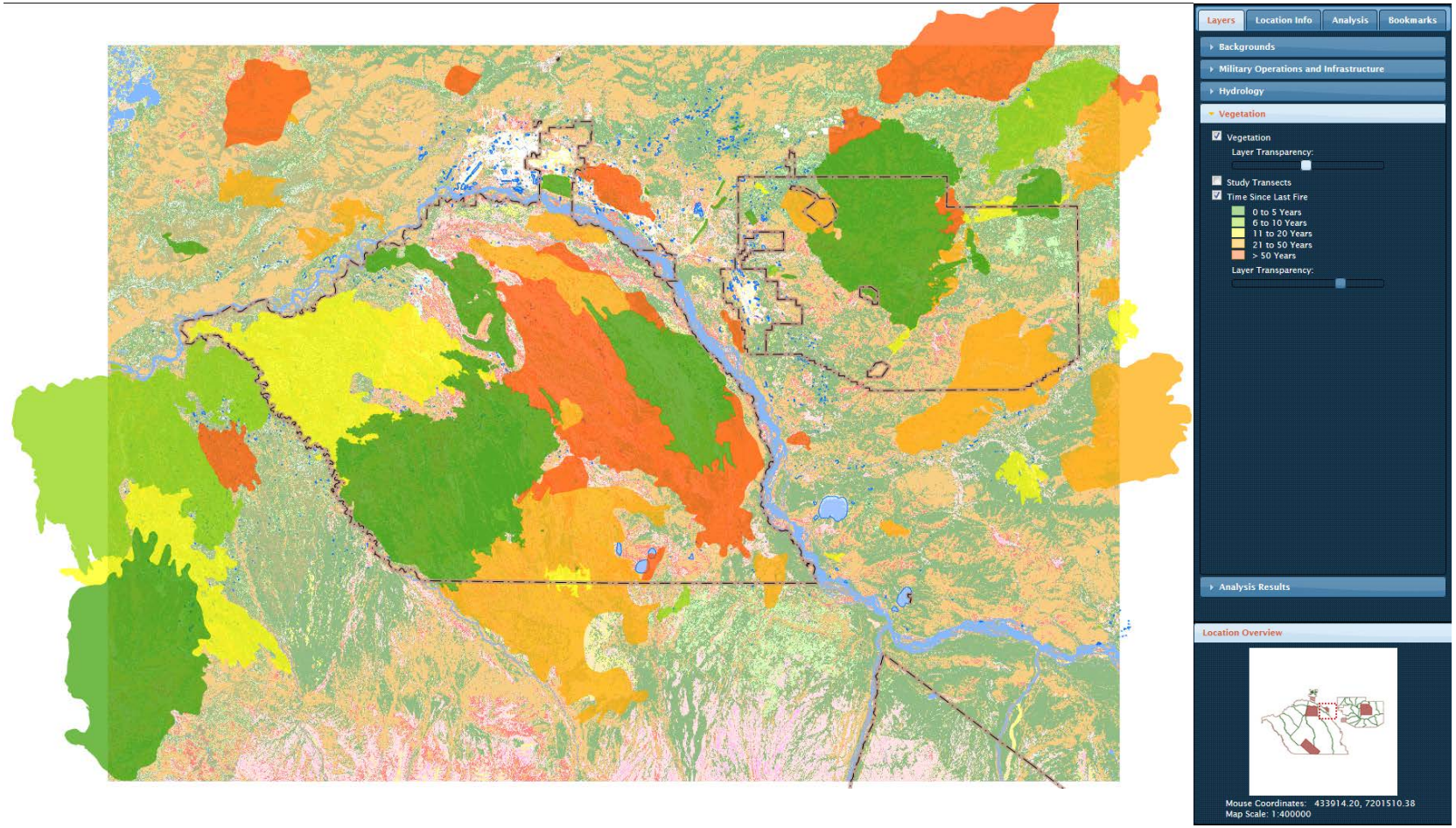

Figure 75. A screenshot from GISMO depicting the fire historical record in time since last fire for interior Alaska training ranges.

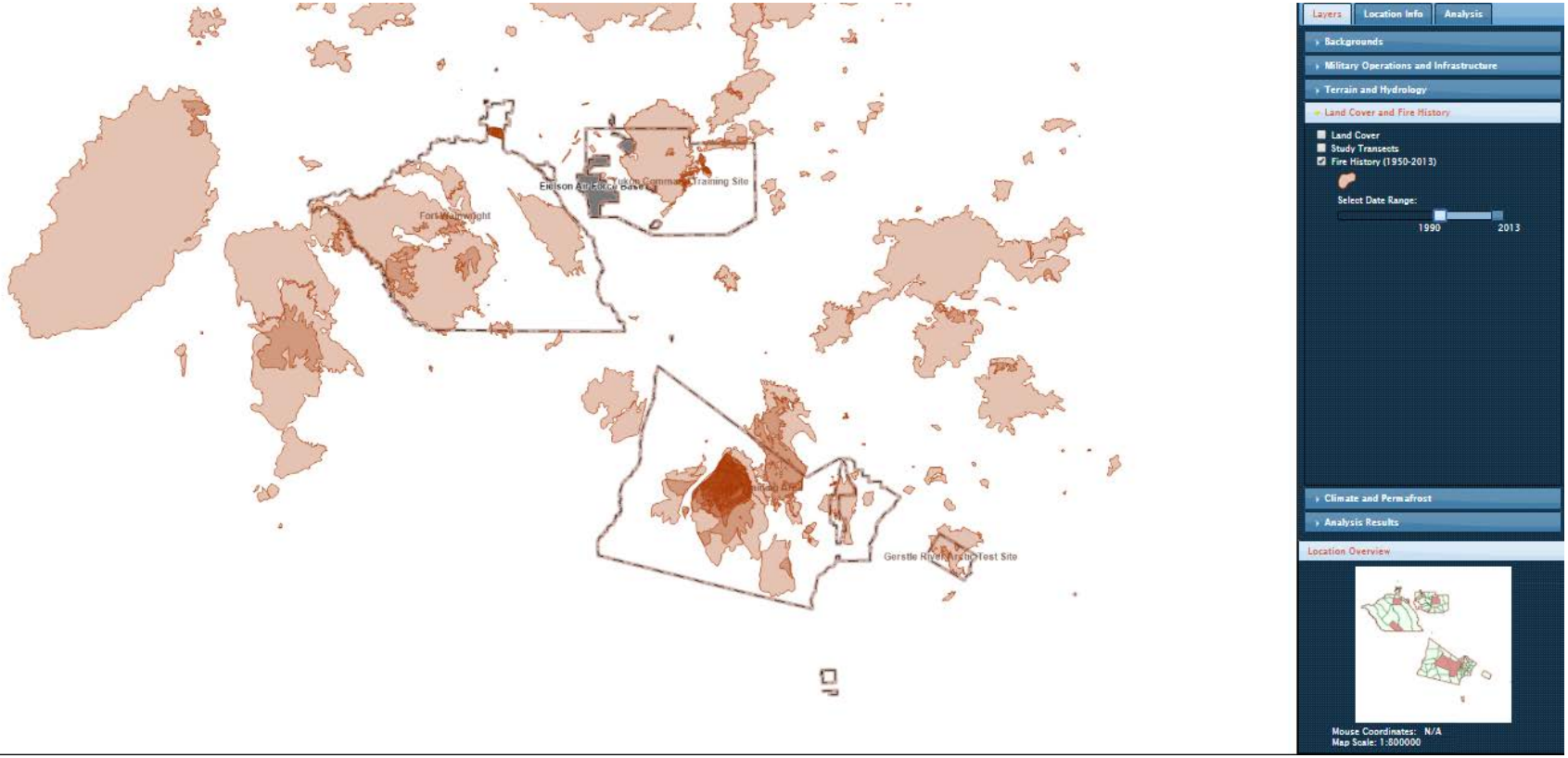

Figure 76. The fire history analysis tool allows the user to specify what time (from 1950 to 2013) to initiate plotting of all fires in the record. In the example here all fire perimeters from 1990 to 2013 are plotted.

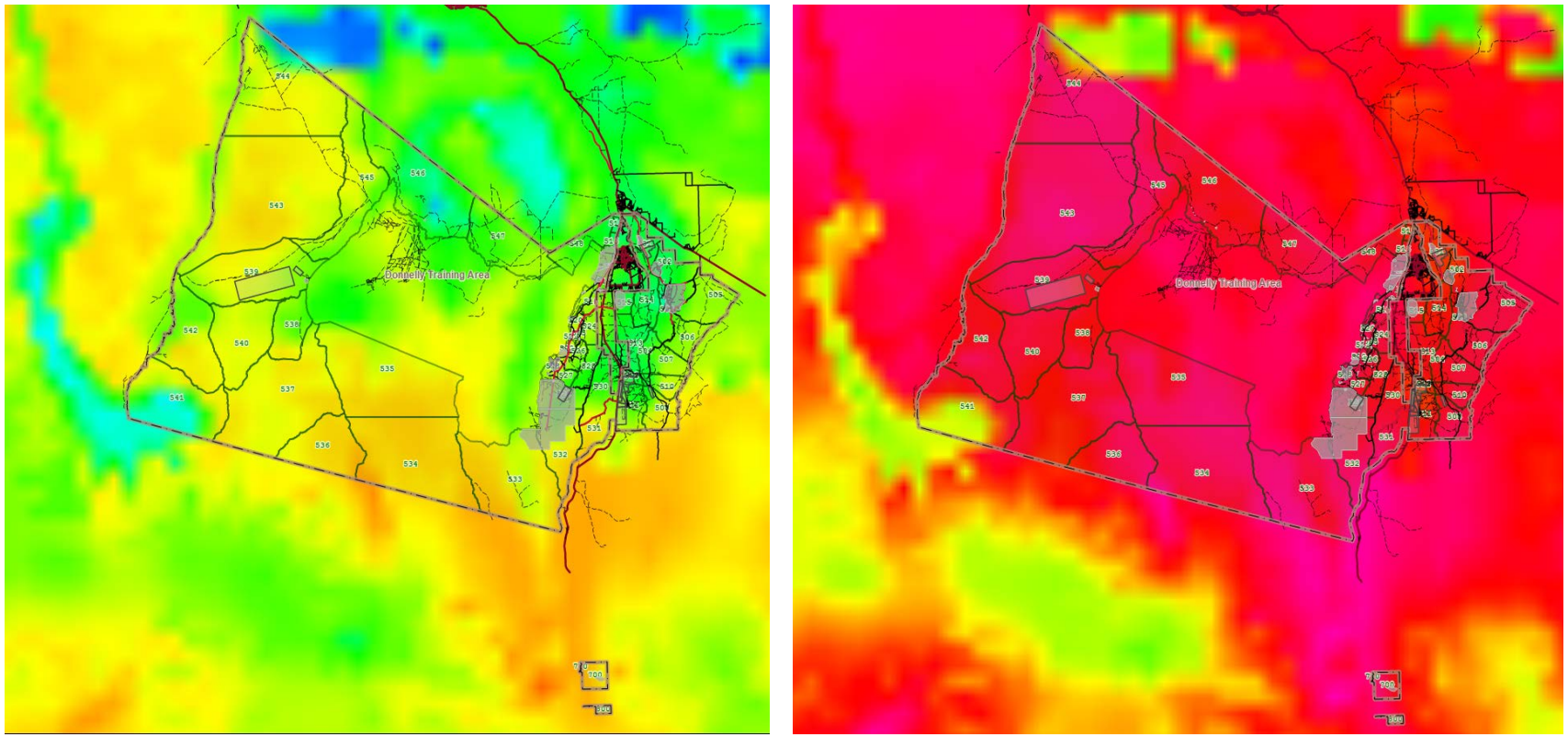

Figure 77. An example of the GIPL climate modeling outputs in GISMO. On the left is a plot of mean annual ground temperatures at 1 meter depth in 2010 as calculated by GIPL using meteorological information. On the right is a plot of projected mean annual ground temperatures at 1 meter depth in 2100. The view in this Figure is of Donnelly Training Area West and East.

6. CONCLUSIONS AND IMPLICATIONS FOR FUTURE RESEARCH/IMPLEMENTATION

6.1 Introduction

Knowledge of the magnitude and directions of landscape change can help inform land management decisions on military lands. In interior Alaska mean annual temperatures are projected to increase and the precipitation regime is expected to change between now and 2100. Increases in mean annual temperatures are also projected for much of the Arctic and for all of Arctic Alaska (Serreze et al., 2011). This will undoubtedly alter the critical interactions between disturbance, the permafrost thermal regime, ecosystem processes, and hydrology. The objective of this research project was to identify how and where changes in ecosystem processes (through climate warming or disturbance) could provide challenges for training range and infrastructure management. This goal was accomplished through our five research subtasks and through development of the GIS based decision support tool GISMO which has been delivered to U.S. Army Alaska land managers. Though the focus region of our research comprised boreal biome ecosystems in interior Alaska many of the results from this study can provide insight into permafrost-vegetation-disturbance feedbacks in other lowland boreal regions such as the Yukon-Kuskokwim and Minto Flats lowlands of Alaska and lowlands of Canada and Russic. Our research results can also be applicable to studying the response of permafrost to disturbance at locations in the high Arctic. Of particular relevance are our measurements of how, where, and at what rates the thermal regime of permafrost soils are affected by disturbance such as fire or anthropogenic activities.

Based on the results from this study, from related and collaborative activities, and from our synthesis of the data and conclusions from other studies we anticipate four main ecological responses to climate warming that will have the most profound influences on DoD training land management in interior Alaska over the next 100 years: 1) climate driven permafrost degradation will radically reorganize upland and lowland hydrogeology and vegetation, 2) surface hydrologic changes from permafrost degradation will lead to wetting and flooding of lowland landscapes and drying of upland landscapes, 3) changing permafrost extent and hydrology and the projected increased growing season will favor some species over others and the vegetation shifts will favor some vegetation and wildlife species over others, 4) decreased soil moisture and humidity will increase fire and the potential for insect disturbance. These four main conclusions are discussed in further detail below.

6.1.1 Climate driven permafrost degradation

We found strong relationships between vegetation type, topography measured with dGPS and LiDAR, and permafrost extent at our fire scar chronosequence sites. Permafrost was nearly always present under forest types, had highly variable thaw depths and occasional thin closed taliks in recently burned areas, and permafrost was nearly always absent in old collapse-scar bogs. In young collapse-scar bogs or actively collapsing margins in older bogs the ERT data indicated permafrost was often present at depth. Permafrost also was strongly related to topography with permafrost nearly always present in areas that were >0.2 m higher than the bogs and fens, and usually absent in the lower-lying bogs. These relationships indicate that remote sensing of vegetation characteristics and LiDAR can be useful for monitoring the surficial and seasonal thaw depth response of permafrost to fire, human disturbance, or climate warming. At the 1-2 meter depth scale the remotely sensed biophysical and landscape geomorphology

relationships are sound. Our results may be applicable to the response of permafrost to fire disturbance in the high Arctic as well. For example, a recent paper by Jones et al. (2015) illustrated, through repeat LiDAR and ground survey measurements, that surface subsidence in tuccosk tundra following fire can occur in a matter of years.

We found through ground survey and ERT measurements that the lateral margins of thawing collapse-scar bogs and fens had complex irregularities. Permafrost distribution was more variable with increasing depth. Some thawed zones had gently sloping walls, some were lacking permafrost in the upper ~5 m but had permafrost at depth, and some areas had small horizontal lenses of permafrost at depth. As a consequence, simple estimates of permafrost extent from airborne or surface survey measurements likely do not adequately "map" the presence of permafrost in the subsurface. As a consequence, surface characteristics are not adequate for assessing permafrost extent, morphology, or for tracking changes over time at depths greater than ~2 meters. The best way to address this problem is to combine geophysical, biophysical, and remotely sensed measurements across a broader set of landscape terrains and vegetation types and at greater depths to better identify what landscape patterns are optimal for mapping permafrost.

Through thermal modeling coupled with field measurements we found permafrost appeared to be sensitive to short-term variations in snow accumulation. In the absence of water impoundment, short-term fluctuations in snowfall and air temperature could initiate the refreezing of taliks and permafrost recovery in some soil types in the current day climatic regime. Snow is generally understudied in the area despite its role in spring melt runoff and in controlling the winter time thermal regime. Long term permafrost monitoring networks should include snow depth and snow water equivalence information.

6.1.2 Surface hydrologic changes

The hydrology of interior Alaska is largely controlled by permafrost distribution. Permafrost acts as a confining bed that reduces soil water storage capacity and constrains subsurface flow (Hinzman et al., 1991; 1998; Kane et al., 1991; Woo, 2000). Changes in surface water extent due to permafrost degradation are linked to local ground subsidence either when near-surface ice-rich permafrost thaws (the area may still be underlain by continuous permafrost) or when permafrost is degraded and a connection develops between surface and sub-permafrost water. In the latter case local hydraulic gradients determine whether or not the area becomes drained or flooded. This is a fundamental aspect of permafrost hydrology that determines which regions become drier and which ones become wetter (Woo, 2000; Marsh and Neumann, 2001). As a consequence, permafrost extent also largely controls the vegetation regime.

We found the upper permafrost (within 3 m of the soil surface) within our Tanana Flats study area was generally ice-rich (55-79% vol) and that the thawing of this permafrost could cause up to 0.9 m of thaw settlement, resulting in the soil surface collapsing on average to 0.1 m below the water level of the adjacent collapse-scar bogs. This would lead to major changes in surface and shallow subsurface water routing.

The soil-freezing characteristic, the relationship between unfrozen water content and temperature, is relevant for any mass transfer processes in frozen porous media. To understand the long term effect of climate warming on hydrogeology, especially in the higher latitudes, interaction of soil thermal state and hydrological dynamics is significant. The coupled GIPL-GSSHA model has shown it can reproduce stream flow in an upland catchment. However, its application should be tested in other catchments, preferably including low gradient streams and

fens. With enhanced ground survey and hydrologic flow information the GIPL-GSSHA model information could be applied toward the Tanana Flats fen systems or to other low gradient stream systems. We also would encourage application of the combined GIPL-GSSHA model to locations with more gradient and to watersheds in the tundra biome. For example, the Toolik Lake area north of the Brooks Range in Alaska has long term discharge measurements in a set of stream networks. In addition, future climate simulations and the projected permafrost response is expected to lead to changes in stream channel morphology and shallow subsurface flow routing. The coupled GIPL-GSSHA model could be used to simulate changes in permafrost extent at locations identified as at risk for permafrost thaw based projected permafrost mapping in GISMO.

Climate driven permafrost degradation will radically reorganize upland and lowland hydrology and vegetation by altering soil flow paths and changing subsurface flow by reorganizing the permafrost aquiclude. This will lead to wetting and flooding of lowland landscapes and drying of upland landscapes and will alter vegetation dynamics and succession rates. Changes in the soil thermal regime will significantly alter the lateral and vertical distribution of permafrost. Groundwater recharge, runoff and water storage will be altered considerably and this will increase the fraction of subsurface flow in annual river runoff. This will change the seasonality and biogeochemistry of Alaskan river discharge by increasing its winter portion and, in some locations, may increase total discharge as well (Peterson et al., 2002). There are few locations on any of the DoD training ranges where surface water discharge is monitored year round. There are also few wells that can access shallow subsurface flow or groundwater. Adding measurement stations for this key hydrologic information is recommended at locations representing a subset of the major terrain types. Further development and refinement of modeling tools is also recommended, particularly from measurements made on the training ranges. Of particular note would be application of the hydrogeologic modeling done by a companion project (RC-2111; Walvoord et al. 2015) to interior Alaska DoD lands.

6.1.3 Changes in species and ecosystem processes and characteristics

Alaska has diverse boreal ecosystems that have developed in response to heterogeneous terrain conditions and to a wide range of biological and geomorphic processes that drive disturbance and successional patterns. We found that across Army lands on Fort Wainwright, the Yukon Training Area, and Fort Greely 56.8% of the region had changes in ecotypes over the 55–62 yr period of repeat aerial photographic records. Most of the changes resulted from increases in upland and lowland forest types with an accompanying decrease in upland and lowland scrub types as post-fire succession led to late-successional stages. Knowledge of the patterns and processes affecting ecosystems and their trajectories of change will aid in ecological management of Army lands and other locations where permafrost or seasonally frozen and thawed soils are affected by disturbance. For example, by identifying which changes can be affected by land management activities, such as fire and facility development, and by identifying ecotypes that are susceptible to impacts from climate change, such as from degrading permafrost, where activities should be avoided or minimized. The remote nature of many of the training ranges and of the corridors for planned linear infrastructure (roads, bridges, and rail) necessitate the application of geospatial tools, remote sensing platforms, and targeted field measurements to provide the information land managers need to prioritize their limited resources. The extreme seasonality of ecosystem characteristics (cold, dark and snow covered winter versus light, warm,

and boggy wetland terrains in summer) also provides a major challenge in identifying where (and when) to apply resources to support the DoD training mission in Alaska.

A projected longer growing season in the future (Høye et al., 2007) will favor some species over others and this will alter vegetation (Wolken et al., 2011) and soils (Grosse et al., 2011). Geospatial tools that track and project vegetation cover, soil composition, and forest succession trajectories would strongly support land management. The resulting information could be used to monitor wetland status, track threatened and endangered species habitats, and help identify where human caused disturbance (especially infrastructure) could negatively affect key species.

6.1.4 A changing fire regime

Decreased soil moisture contents and humidity are expected to increase the number, areal extent and severity of fires across the boreal and tundra biomes and this will alter vegetation and be the prime control on permafrost in/stability. In agreement with previous studies we found that fire is by far the most rapid and wide scale driver of ecosystem change on the training areas. For example, the effects of the 2010 fire were particularly notable for the rapid collapse of some of the ground surface in the burned forest to below the water level, with up to 0.5 m of subsidence recorded between 2011 and 2014. The magnitude of permafrost thawing was typically greatest along the forest-bog interface, suggesting the importance of hydrologic feedbacks to fire-initiated permafrost thaw.

The DoD in Alaska does not have the resources required to manage or fight fires at the large scales of their training range lands. Fire management typically comprises small focused controlled burns in drop zones and in some ipact areas. Current land management strategies are directed toward allowing man-made and natural fires to burn on military lands unless they endanger military facilities and private lands adjacent to military lands.

The amount of organic soil combusted is controlled by the nature of the fuel available and the severity of the fire. Numerous studies have shown that the most severe fires burn the forest down to the mineral soil and this affects the type of forest that regrows following fire. As a consequence, fire management activities should be focused toward encouraging light to medium severity fires to preserve permafrost thermal stability and reduce fuels that could lead to larger, uncontrollable fires. Fire mapping programs are active and provide land managers with adequate information to identify what areas have burned and when. However, the re-accumulation of organic material following fire is largely untracked. Where possible, we recommend actively promoting forest succession following disturbance (fire, road building, installation development, training range construction) in areas where this type of management can occur. This will help prevent permafrost degradation.

Future research efforts on fire and fuels should include combined field and remotely sensed measurements to catalog fine and bulk fuel loads on interior Alaska DoD training ranges. These measurements should include the heterogeneous fuels, forest types, organic material, and geomorphologies on upland and lowland terrains. A series of GIS-based decision support tools could then be developed to identify what locations are most susceptible to high severity fires, what management actions to take, and where to apply limited resources. This would identify locations with reduced potential ignition risks for the use of live fire training with explosives and pyrotechnics. Increasingly, reburn of areas from live fire training is providing a challenge for managing the fire ignition risk associated with training. This particularly of concern in the large impact areas on Donnelly Training Area West. More of a focus on fire severity measurements and vegetation regrowth rates should be applied in these high risk areas.

6.2 Ramifications for training land management

The hydrological and ecological shifts we identified above will have large consequences on USARAK training in Alaska. Unfortunately, change will not come uniformly across the landscape. As a consequence, installation planning will require a better knowledge of locations where change is expected to occur. In addition, decision support tools are needed to help decide where to construct or modify existing facilities, how well terrain can support winter and summer vehicle traffic, where to develop future training ranges, how contaminants may interact with soils, and where to apply focused management actions (such as prescribed burns or invasive species management strategies).

A few conclusions, focused on specific training areas or terrain types, are given below.

- The Tanana Flats (lowland) ecosystem is susceptible to major surface hydrological, vegetation and permafrost changes with climate warming. Due to the intricate feedbacks between permafrost, soils, hydrology, and climate change many of these changes are difficult to predict and thus are not easily integrated into future planning scenarios. The most probable ecosystem shifts could be identified by starting with current ecotypes and predicting their most likely expected response(s) to climate warming.

- The Yukon Training Area (upland) ecosystem is expected to incur increased fire frequency (disturbance) and a general reduction in black and white spruce forests, drying of south-facing slopes, and a loss of permafrost on north-facing slopes as a response to climate warming (Woo, 2000).

- The Donnelly Training Area will likely experience varied effects from climate change because of its mixture of upland and lowland ecosystems. Rocky moraines may be affected by increased fire frequency and this could lead to the reduction of white spruce forests while loess deposits are vulnerable to collapse due to the thawing of ice-rich permafrost (Toniolo et al., 2009). With warming, permafrost degradation, and the likely drying of the Tanana Flats fire will play a major role in controlling forest succession of these ecosystems.

- The estimated recovery times for disturbance (as required in Environmental Impact Statements and in future planning scenarios) are likely to become less predictive in the future. It is difficult to predict how and where disturbance will affect recovery across the wide variety of physiographic, landscape, and ecosystem types present but this will challenge the flexibility and adaptability of Army training plans and infrastructure development.

- Where disturbance activities such as airboat travel, road clearing, infrastructure development, or prescribed burns occur, we encourage minimizing the rapid draining or horizontal movement of water across the surface. The most optimal way to do this is via repeat satellite analyses. If/when vegetation has been degraded or channelization is evident it is recommended that activities causing disturbance be limited for a few years to allow the vegetation to regrow. Channeling, draining, or ponding water destroys the

thermal balance of the surface and subsurface and this can lead to permafrost degradation and thermokarst.

- We recommend establishing a series of long term monitoring sites representing a varied amount of time since disturbance and diverse levels of disturbance to follow landscape succession and soil processes over time. The most likely candidate locations for this work would be areas of similar landscape and ecosystem type that burned at different times/decades. This would allow a comparison across time since disturbance. Repeat imagery analysis and remote sensing tools could help to identify and measure change over time at long term sites. There are a variety of remote sensing measurements that could be used to help manage fire and human disturbance and to predict where permafrost degradation could have the largest impacts on soil thermal and hydrologic stability. The difficulty in gaining access to field sites and the wide variety of landscape and ecological processes occurring in interior Alaska are likely best addressed through remote sensing and repeat imagery analyses.

- More studies are needed during the two major seasonal transitions (spring melt to summer and summer to winter freeze up). The spring melt period is associated with what is typically the largest yearly redistribution of water (snow melt) across the landscape and this can occur in a period of days to weeks. The fall to winter transition is a key part of soil and vegetation dynamics in the boreal forest as the ground initiates freeze and snow starts to cover the landscape. It is expected that the timing of these seasonal transitions will change in the future and it is likely that soil, vegetation, and hydrology will respond to the changing seasonality and the expected longer growing season.

6.3 Implementing Permafrost measurements

Based on the results from this and other studies in the discontinuous permafrost zone, including the other two SERDP supported projects that were active with this one (Walvoord et al., 2015; Schuur et al., (RC-2109, ongoing), there are some clear requirements for implementing a comprehensive permafrost monitoring program.

1) Transect based field plots, augmented by small study plot areas to focus on vegetation soils, or other potentially destructive sampling activities, are the most effective way of establishing measurements across a variety of terrain types.
2) The most optimal sites are transects that cross a variety of terrain, vegetation, and soil types. They are most rapidly accessed and measurements can be made repeatedly with the least amount of surveying, flagging, etc.
3) The sites should be road accessible in all seasons to facilitate repeat measurements, to lower costs, and to support collaborative research activities. In general, when a study site can provide long term measurements and data other research projects will find ways to capitalize on the data availability.
4) Airborne LiDAR, hyperspectral measurements, and repeat color imagery, if available, greatly enhance the identification of ground features in the terrain. See Figure 78 for an example transect where airborne LiDAR is available. Also see Figures 29-33 in this Report. These airborne measurements can be used to identify where to site transects and to "scale up" the field measurements to other similar locations.
5) The sites should comprise a variety of terrain types that are most common in the area. For interior Alaska ecosystems and terrains examples include birch forest, mixed hardwood forest, spruce forest, tussock tundra, shrublands, wetlands, and some upland terrains- typically with mosses, tussocks, or forest varieties.
6) Upland and lowland terrains should be represented because they comprise the two main terrain types in interior Alaska and their hydrogeologic processes are markedly different.
7) Seasonal thaw depth measurements should be made at least once per year at the end of the summer season. It would be preferred to have three to five measurements of seasonal thaw at the sites during the growing season to provide information on the rate and location of changes in seasonal thaw over time. See Figures 79 and 80 for examples of this. Note in Figure 79 how different vegetation types are associated with different seasonal thaw depths. The thaw at disturbance locations (in this case small cleared trails) is also evident.
8) The locations of the seasonal thaw depth measurements should be repeatable such that trends in the downward thaw can be ascertained not by vegetation or elevation but by actual repeated measurements at the same exact locations on the transects. In tussocks it is difficult to produce repeat measurements unless the areas to be probed are flagged. For example, if the tussocks are 50 cm high and the areas between tussocks have a 50 cm seasonal thaw whether one probes through a tussock or between tussocks may lead to a value that is up to 100% off.
9) Soil thermal measurements should be made continuously at a variety of depths throughout the year. This information supports modeling efforts, links to the seasonal thaw depth measurements, and provides information on the role of soil moisture and

water in the seasonal thaw process. Figure 81 gives an example of soil temperatures with depth in a permafrost landscape.

10) Measurements of snow temperature (Figure 82), snow depth (Figure 83), and snow water equivalent across the sites should be done 1-3 times per winter- preferably in early, mid and late season. This information is critical in understanding the relationships between vegetation, snow and the thermal regimes at the site. Figure 83 shows an example of how snow depth is controlled by vegetation type.
11) Electrical resistivity tomography and ground penetrating radar measurements should be made across the site transects. This information can be used to infer subsurface conditions. See Figures 29-33 for examples of this.
12) Cores should be collected to represent the variety of terrains and soil types at the site. This information is critical in understanding cryostratigraphy like volumetric ice content and in identifying massive ice features or the presence of other ice features. Cores can also be used to identify what the geophysical measurements are relating to, and can be used to identify sedimentological changes with depth.
13) A series of surveyed benchmarks should be installed to establish site elevations so that long term (yearly for at least a decade) subsidence, thermokarst features, and other surface elevation changes can be adequately measured to the centimeter scale. Shiklomonov et al., (2013) provides an example of how surface surveying measurements can be critical in assessing the relationship between seasonal thaw and subsidence. Based on their results, repeat measurements should be at the centimeter scale. High resolution dGPS is not at this accuracy (it is closer to 3-5 cm. scale) but laser level surveying with benchmarks is.
14) Detailed vegetation and soil classifications should be made at the sites. Soil organic matter composition and nutrient information should be quantified.
15) Surface hydrology, where quantifiable, should be measured. Preferably the study transects cross a hydrologic boundary like a stream or fen with extreme seasonality. This could support hydrologic modeling efforts.
16) All of the aforementioned data should be archived yearly onto web-accessible platforms that are suitable for the type of data. For example, seasonal thaw depth measurements should be provided to the Circumpolar Active Layer Monitoring network (CALM; http://www.gwu.edu/~calm/). Survey information, coordinates, metadata, soil thermal measurements, and other numerically based data should be archived into a platform built for these types of data such as the ACADIS Gateway Arctic Data Repository (https://www.aoncadis.org/home.html). Satellite imagery and other photographic imagery could be archived at the National Snow and Ice Data Center Data Portal (https://nsidc.org/data) or with the National Oceanographic and Atmospheric Administration (NOAA)'s Office of Satellite and Product Operations (http://www.ospo.noaa.gov/Products/imagery/). GISMO, as an open platform, web accessible geospatial tool, could also be configured to host these data.

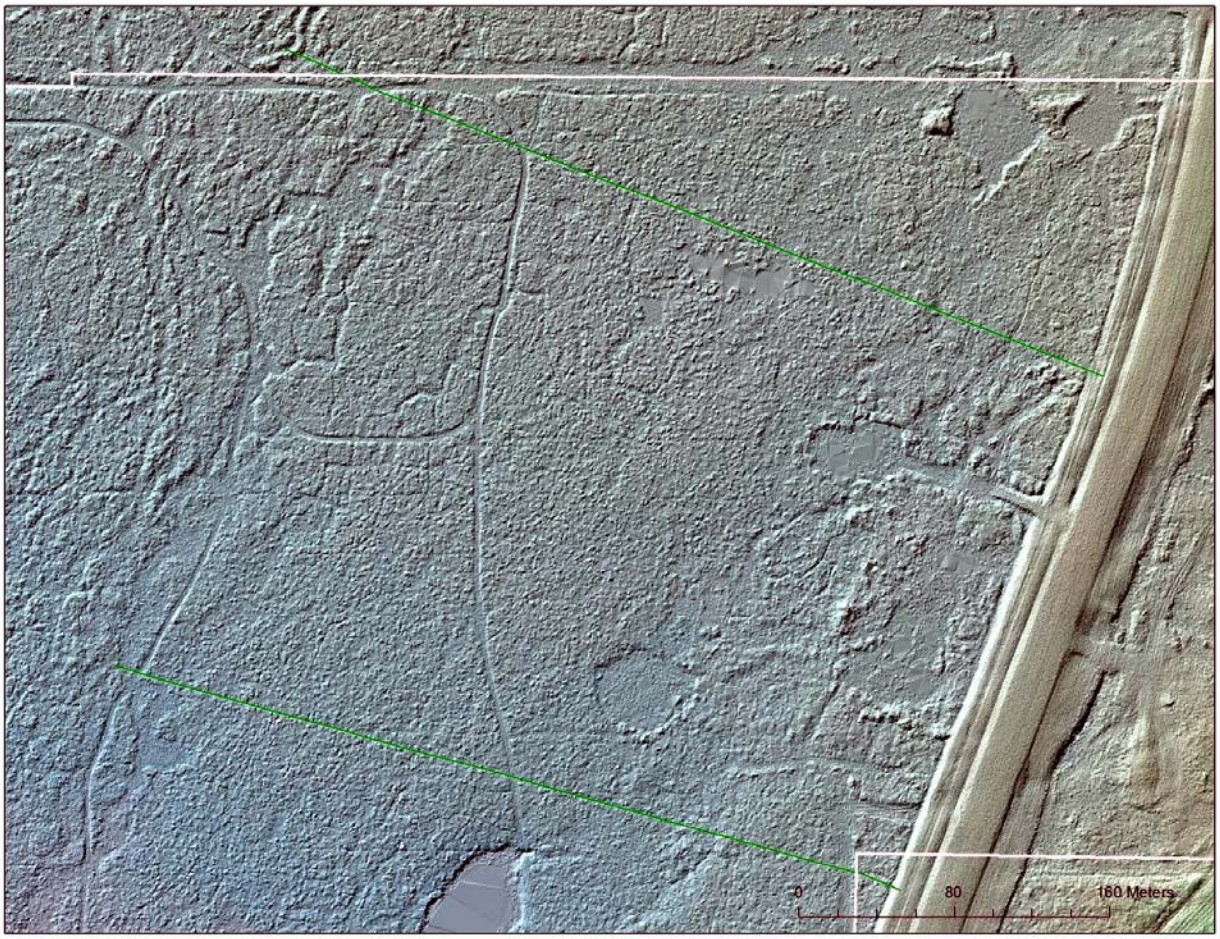

Figure 78. Airborne LiDAR at a permafrost monitoring transect near Fairbanks, Alaska.

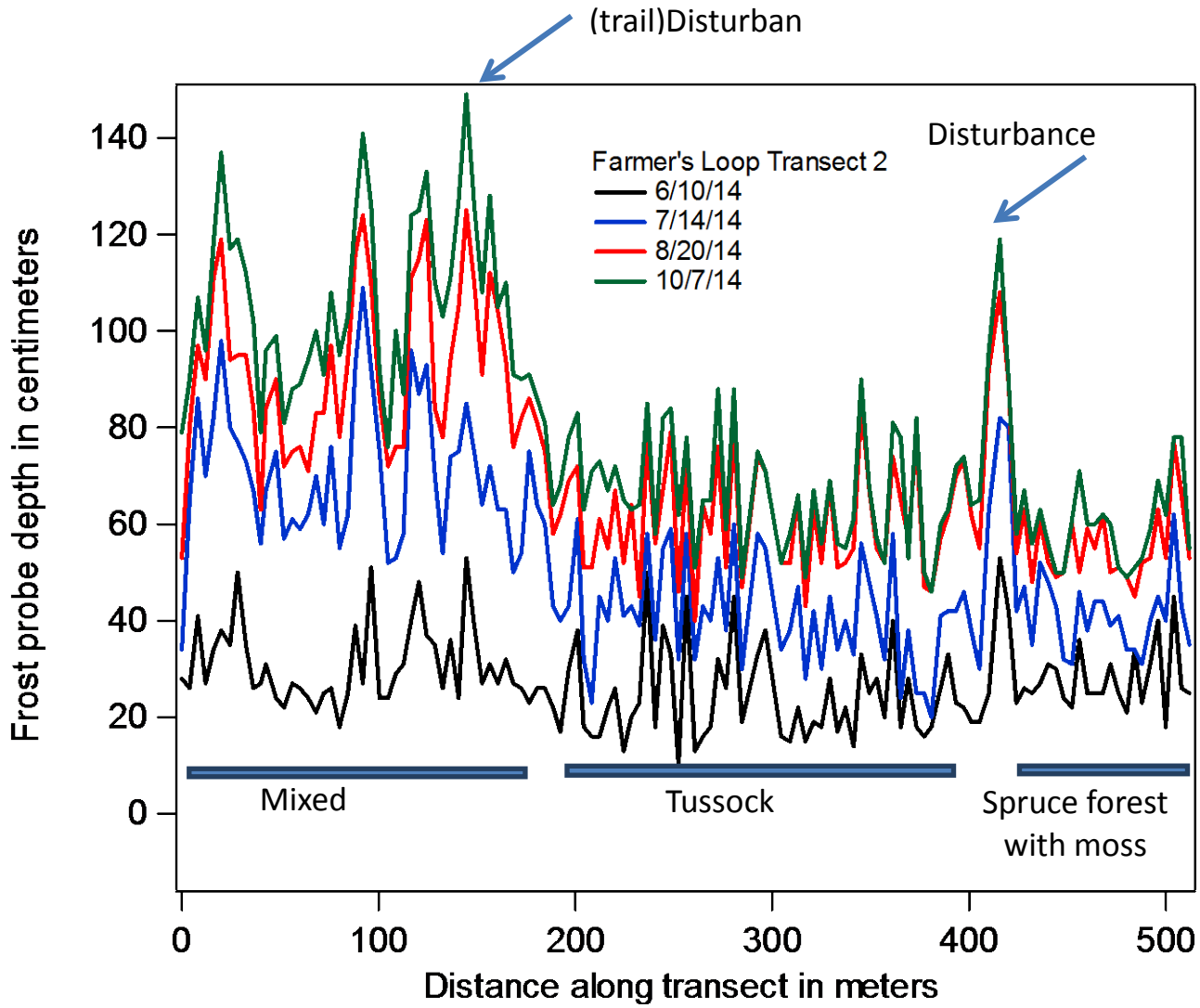

Figure 79. Repeat seasonal thaw depth measurements at a permafrost monitoring transect near Fairbanks, Alaska. Note the downward movement of the seasonal thaw (i.e. increasing depth values) over time. Also note the relationship between vegetation cover and seasonal thaw. The two locations where disturbance is noted are trails that have been cleared of vegetation and this has caused extensive seasonal thaw.

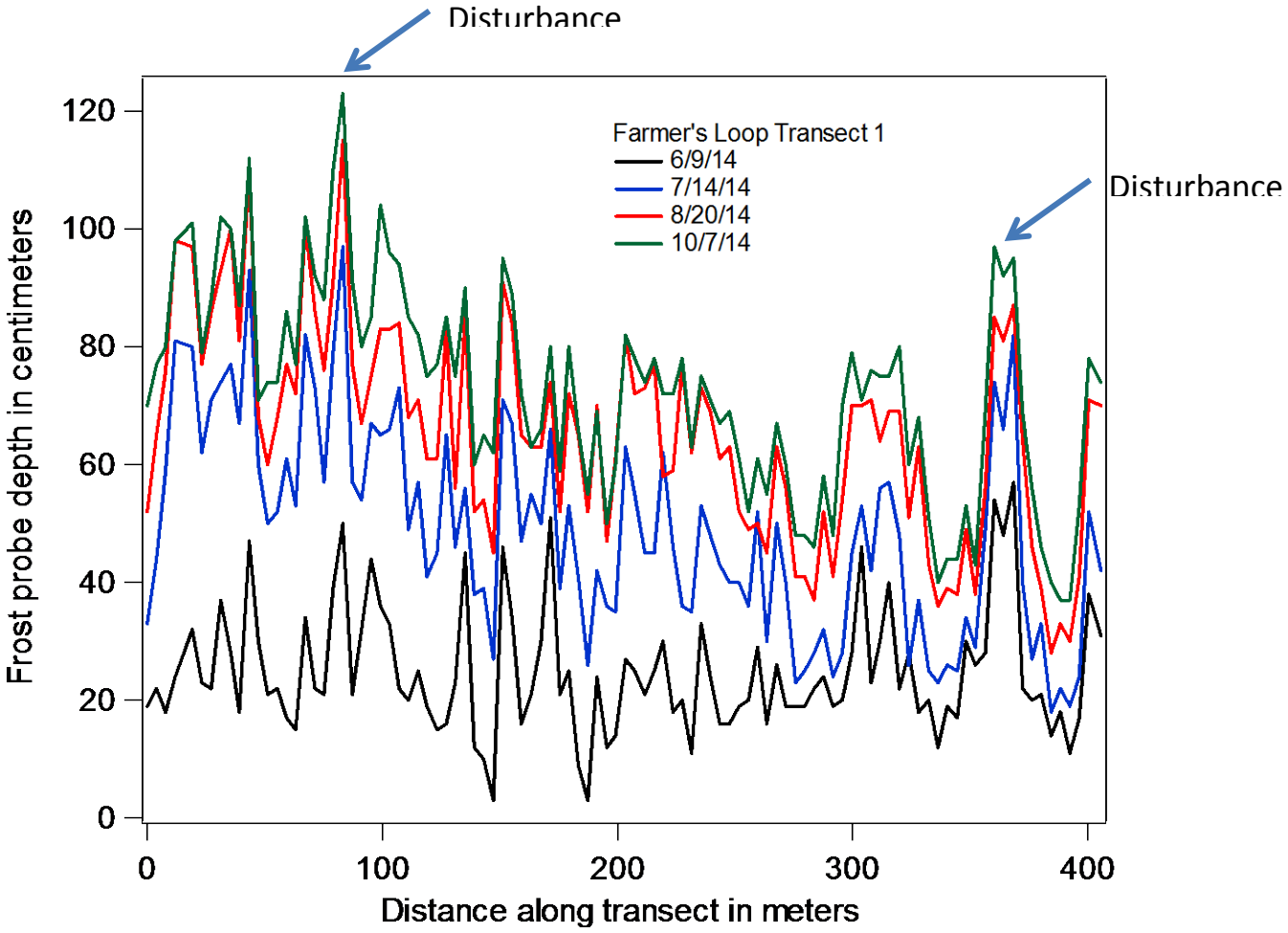

Figure 80. Repeat seasonal thaw depth measurements at a permafrost monitoring transect near Fairbanks, Alaska. Note the downward movement of the seasonal thaw (i.e. increasing depth values) over time. The two locations where disturbance is noted are trails that have been cleared of vegetation and this has caused extensive seasonal thaw.

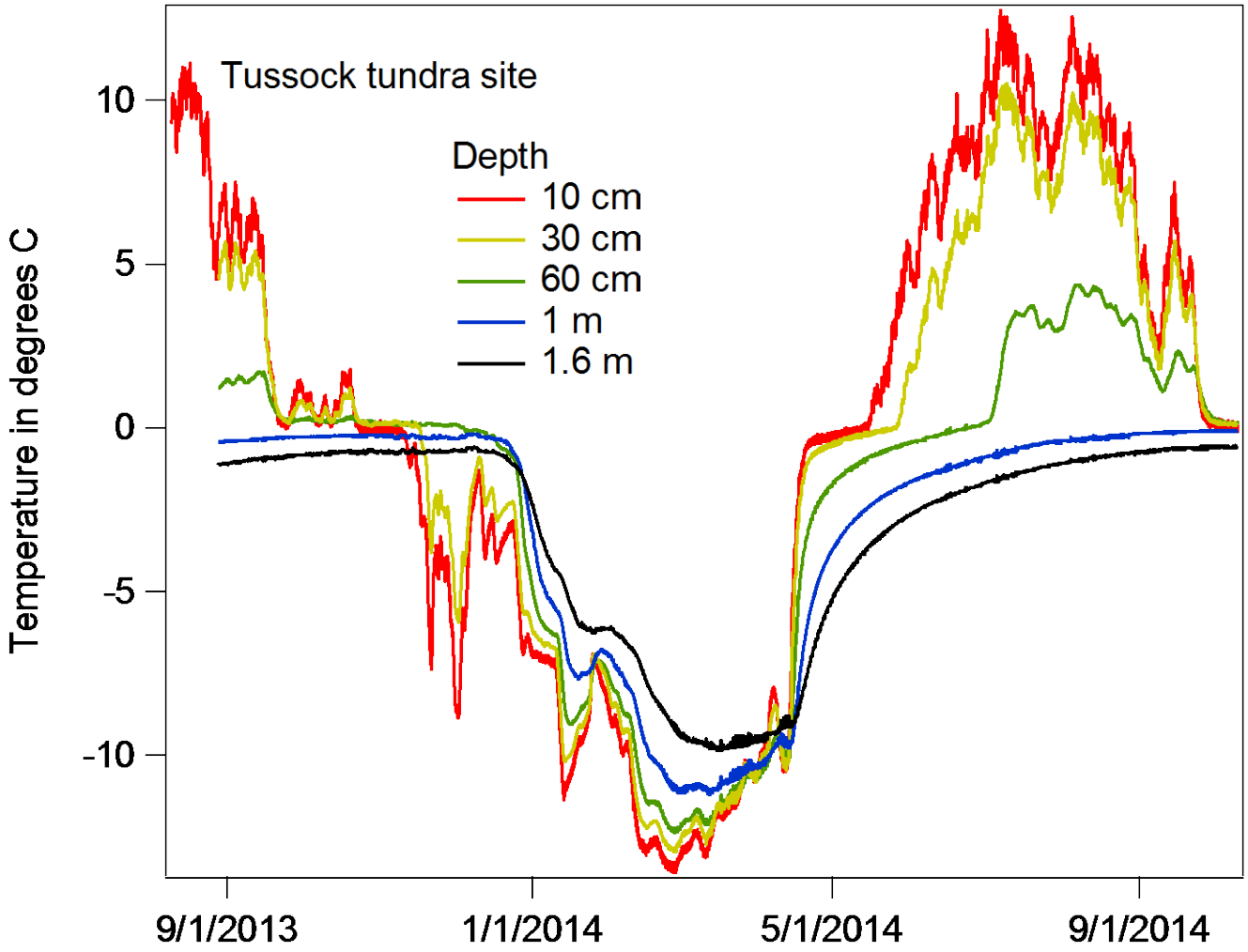

Figure 81. A full year of soil temperatures with depth measured at a permafrost monitoring transect near Fairbanks, Alaska. Seasonal thaw depths at this location is about 80 cm.

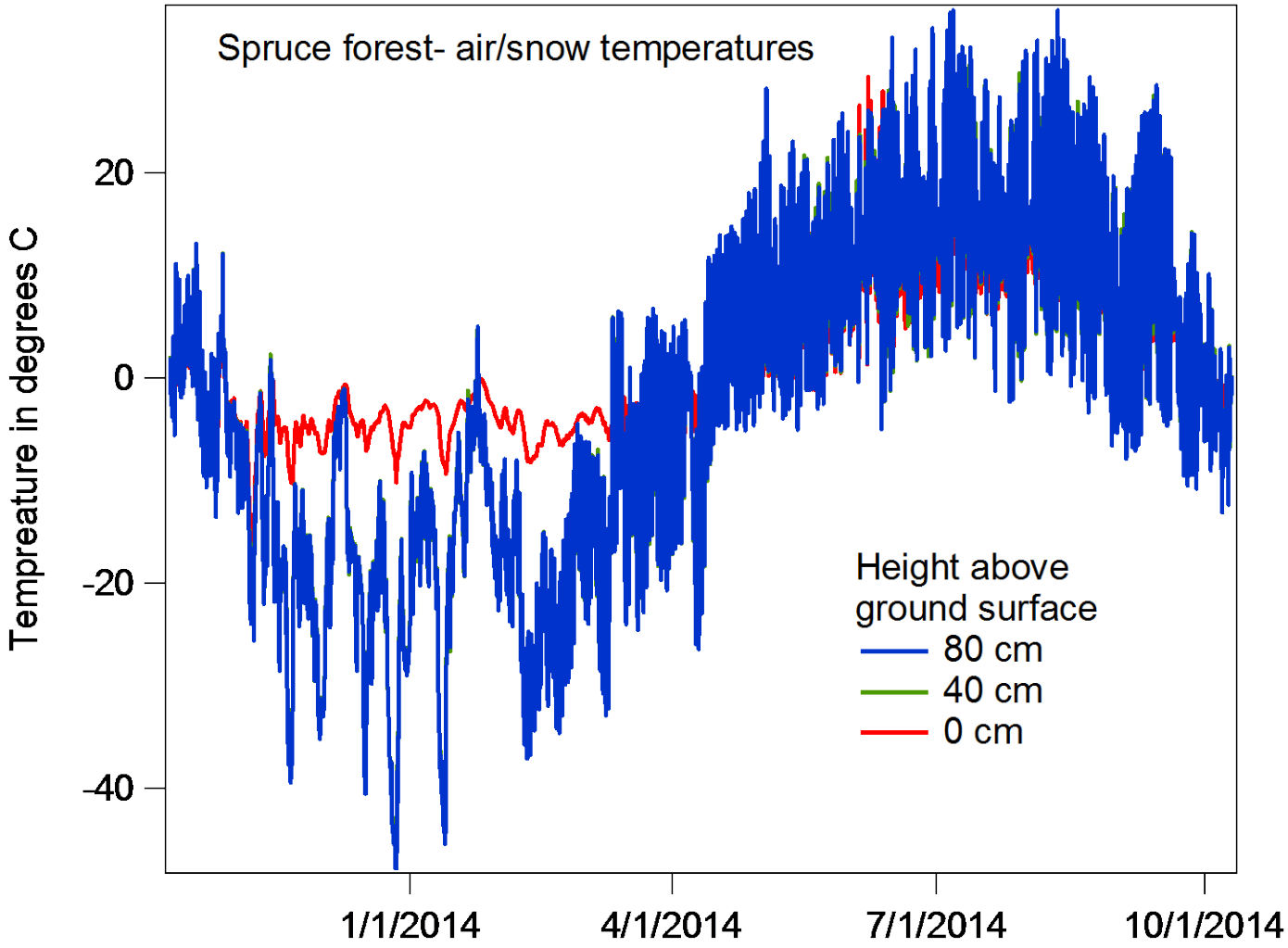

Figure 82. A full year of air and snow temperature measurements at a permafrost monitoring transect near Fairbanks, Alaska. The measurements are made from a rod extending above the ground surface. When there is no snow the measurements are of ambient air. When the snow reaches the height of the thermistor location on the rod the snowpack temperature is measured at that depth.

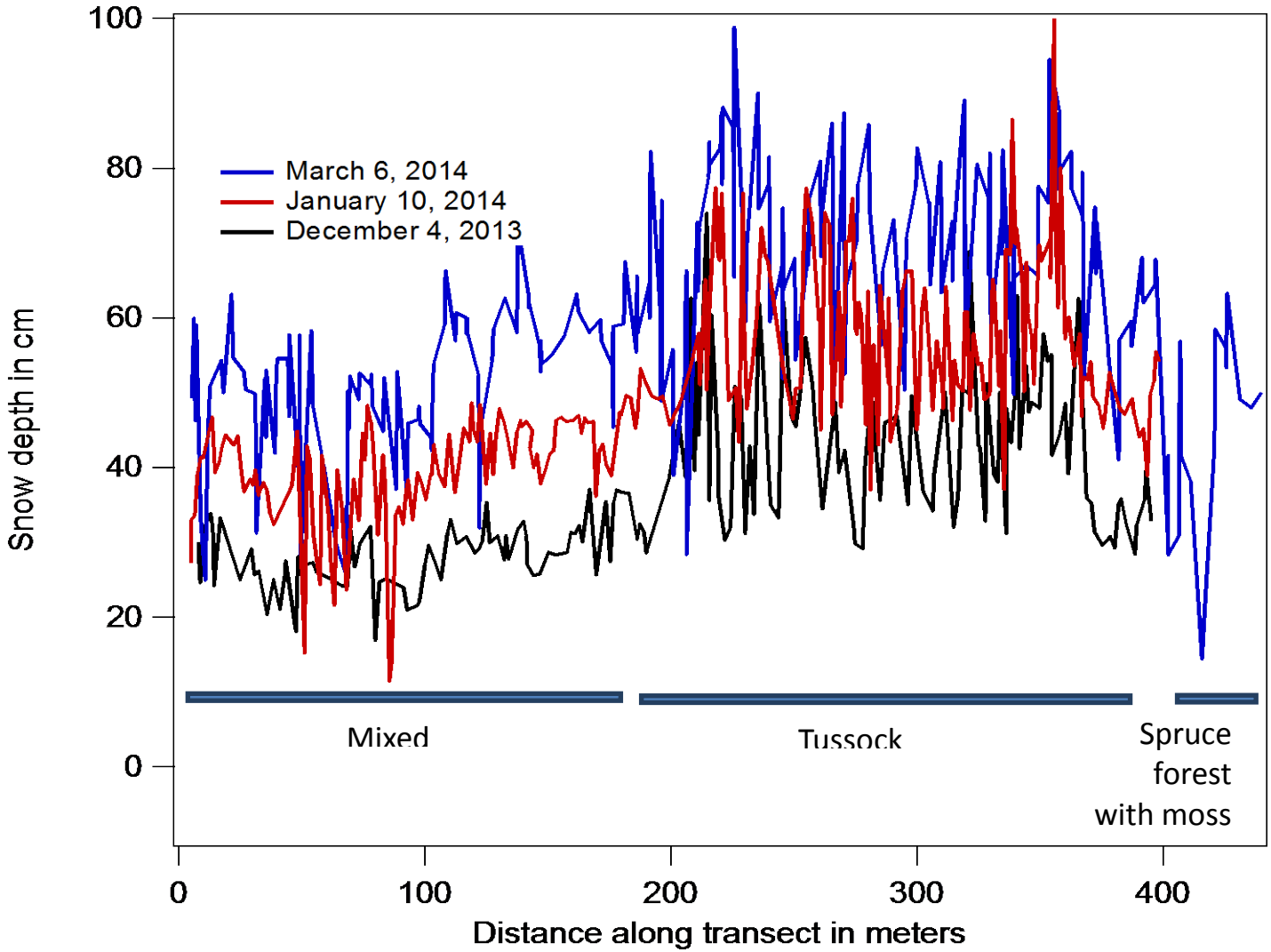

Figure 83. Repeat snow depth measurements at a permafrost monitoring transect near Fairbanks, Alaska. Note the strong relationship to vegetation cover.

7. LITERATURE CITED

Abermann, J., Fischer, A. Lambrecht, A., Geist, T., 2009, Multi-temporal airborne LIDAR-DEMs for glacier and permafrost mapping and monitoring. The Cryosphere Discussions 3, 383-414.

Alaska Climate Research Center. 2013. Climate normals for interior Alaska.

Alaska Climate Research Center. 2014. ACIS Daily Data Browser.

Alexiades, V., and A. D. Solomon. Mathematical Modeling of Melting and Freezing Processes. 1993. Washington DC: Hemisphere.

Anderson, G.S. (1970) Hydrological reconnaissance of the Tanana Basin, central Alaska. U.S. Geological survey Hydrological Investigations Atlas, HA-319. Scale: 1:1,000,000.

Arctic Climate Impact Assessment (ACIA) (2005), Arctic Climate Impact Assessment, 1042 pp., Cambridge Univ. Press, Cambridge, U. K.

Bagard M, Chabaux, F, Pokrovsky OS, Viers J, Prokushkin AS, et al. 2011. Seasonal variability of element fluxes in two Central Siberian rivers draining high latitude permafrost dominated areas. Geochim Cosmochim Acta 75(12): 3335-3357.

Ball BA, Kominoski JS, Adams HE, Jones SE, Kane ES, Loecke TD, Mahaney WM, Martina JP, Prather CM, Robinson TMP, Solomon CT. 2010. Direct and terrestrial vegetation-mediated effects of environmental change on aquatic ecosystem processes. BioScience 60 (8): 590-601.

Barker AJ, Douglas TA, Jacobson AD, McClelland JW, Ilgen AG, Khosh MS, Lehn GO, Trainor TP. 2014. Late season mobilization of trace metals in two small Alaskan Arctic watersheds as a proxy for landscape scale permafrost active layer dynamics. Chemical Geology 381: 180-193

Brabets, T. P., Wang, B., and Meade, R. H., 2000, Environmental and hydrologic overview of the Yukon River Basin, Alaska and Canada: U.S. Department of the Interior, US Geological Survey Report 99-4204.

Billings W, Peterson K. 1980. Vegetational change and ice-wedge polygons through the thaw-lake cycle in Arctic Alaska. Arct Alp Res 413-432.

Britton ME. 1957. Vegetation of the arctic tundra. Oregon State University Press.

Burn, C. R. 1998. The response (1958-1997) of permafrost and near-surface ground temperatures to forest fire, Takhini River valley, southern Yukon Territory. Canadian Journal of Earth Sciences 35:184-199.

Cai Y, Guo L, Douglas TA. 2008a. Temporal variations in organic carbon species and fluxes from the Chena River, Alaska. Limnol Oceanogr 53(4): 1408.

Cai Y, Guo L, Douglas TA, Whitledge TE. 2008b. Seasonal variations in nutrient concentrations and speciation in the Chena River, Alaska. 113(G3).

Camill, P. and J. S. Clark. 2000. Long-term perspectives on lagged ecosystem responses to climate change: Permafrost in boreal peatlands and the grassland/woodland boundary. Ecosystems 3:534-544.

Camill, P., J. A. Lynch, J. S. Clark, J. B. Adams, and B. Jordan. 2001. Changes in Biomass, Aboveground Net Primary Production, and Peat Accumulation following Permafrost Thaw in the Boreal Peatlands of Manitoba, Canada. Ecosystems 4:461-478.

Carey SK. 2003. Dissolved organic carbon fluxes in a discontinuous permafrost subarctic alpine catchment. Permafrost Periglacial Process 14(2): 161-171.

Carey S, Quinton W. 2005. Evaluating runoff generation during summer using hydrometric, stable isotope and hydrochemical methods in a discontinuous permafrost alpine catchment. Hydrol Process 19(1): 95-114.

Chacho, E., Arcone, S., and Delaney, A., 1995, Blair Lakes target facility permafrost and groundwater study: US Army Cold Regions Research and Engineering Laboratory Technical Report, Hanover, NH. 30 p.

Chahine, M.T. (1992) The hydrologic cycle and its influence on climate. Nature 359: 373–380.

Chapin III FS, McGuire A, Randerson J, Pielke R, Baldocchi D, et al. 2000. Arctic and boreal ecosystems of western North America as components of the climate system. Global Change Biol 6(S1): 211-223.

Chapin, F. S. S., and Ruess, R. W. (2003a). "Caribou-Poker Creeks Research Watershed: Hourly Precipitation data, 1998 to Present, Bonanza Creek LTER." University of Alaska Fairbanks, Fairbanks, Alaska.

Chapin, F. S. S., and Ruess, R. W. (2003b). "Caribou-Poker Creeks Research Watershed: Hourly Air Temperature (mean, min, max) from 1995 to Present, Bonanza Creek LTER." University of Alaska Fairbanks, Fairbanks, Alaska.

Chapin, F. S. S., and Ruess, R. W. (2005a). "Caribou-Poker Creeks Research Watershed: Barometric Pressure, 2000 - Present, Bonanza Creek LTER." University of Alaska Fairbanks, Fairbanks, Alaska.

Chapin III, F. S., M. W. Oswood, K. Van Cleve, L. A. Viereck and D. L. Verbyla. 2006. Alaska's Changing Boreal Forest. Oxford University Press, New York. 354 p.

Chapin, F. S. S., and Ruess, R. W. (2009a). "Caribou-Poker Creeks Research Watershed: Hourly Snow Depth Measurements, Bonanza Creek LTER." University of Alaska Fairbanks, Fairbanks, Alaska.

Chapin, F. S. S., and Ruess, R. W. (2009b). "Caribou-Poker Creeks Research Watershed: Hourly Precipitation Weighing Bucket Measurements, Bonanza Creek LTER." University of Alaska Fairbanks, Fairbanks, Alaska.

Collin, Antoine, Bernard Long, and Phillippe Archambault. Salt-marsh characterization, zonation assessment and mapping through a dual-wavelength LiDAR. Remote Sensing of Environment 114, no. 3 (2010): 520-530.

Crory, F. E. 1973. Settlement associated with the thawing of permafrost. Pages 599-607 Proceedings 2nd International Conference on Permafrost, Yakutsk, U.S.S.R., North American Contribution. National Academy of Sciences, Washington, D.C.

Douglas, T.A., Jorgenson, M.T., Kanevskiy, M.Z., Romanovsky, V.E., Shur, Y., Yoshikawa, K., (2008) Permafrost dynamics at the Fairbanks Permafrost Experimental Station near Fairbanks, Alaska. In: Proceedings of the Ninth International Conference on Permafrost, Kane D.L., Hinkel, K.M. (eds). Institute of Northern Engineering University of Alaska Fairbanks: Fairbanks, Alaska, 373–378.

Douglas, T. A., Fortier, D., Shur, Y. I., Kanevskiy, M. Z., Guo, L., Cai, Y., and Bray, M. 2011, Geomorphic and geochemical characteristics of thermokarst-cave ice in the CRREL Permafrost Tunnel, Alaska: Permafrost and Periglacial Processes, 22, 2, 120-128.

Douglas, T. A., Blum, J. D., Guo, L., Keller, K., and Gleason, J. D., 2013, Hydrogeochemistry of seasonal flow regimes in the Chena River, a subarctic watershed draining discontinuous permafrost in interior Alaska (USA): Chemical Geology, 335, 48-62.

Douglas, T.A., Jones, M. C., Hiemstra, C. A., and Arnold, J., 2014, Sources and sinks of carbon in boreal ecosystems of Interior Alaska: Current and future perspectives for land managers: Elementa: Science of the Anthropocene, 2, 39 pages, doi: 10.12952/journal.elementa.000032#sthash.j8pzVjml.dpuf.

Douglas, T.A., Jorgenson, M.T., Brown, D.R.N., Campbell, S.W., Hiemstra, C.A., Saari, S.P., Bjella, K., Liljedahl, A.K. 2015. Degrading permafrost mapped with electrical resistivity tomography, airborne imagery and LiDAR, and seasonal thaw measurements. Geophysics 81(1), 15 pages, doi: 10.1190/GEO2015-0149.1.

Downer, C. W., and Ogden, F. L. (2003). "Prediction of runoff and soil moistures at the watershed scale: Effects of model complexity and parameter assignment." Water Resources Research, 39(3), n/a–n/a.

Downer, C.W., Ogden, F.L., 2004. Appropriate vertical discretization of Richards' equation for two-dimensional watershed-scale modelling. Hydrological Processes 18, 1–22 (2004). DOI: 10.1002/hyp.1306.

Downer, C. W., and Ogden, F. L. (2006). Gridded Surface Subsurface Hydrologic Analysis (GSSHA) User's Manual; Version 1.43 for Watershed Modeling System 6.1. US Army Corps of Engineers, Engineer Research and Development Center,, Vicksburg, MS, 207.

Dyrness C, Viereck L, Van Cleve K. 1986. Fire in taiga communities of interior Alaska, in: Forest ecosystems in the Alaskan taiga Springer, pp. 74-86.

Eliáš, P. (1979). "Leaf diffusion resistance pattern in an oak-hornbeam forest." Biologia Plantarum, 21(1), 1–8.

Eugster, W., W. R. Rouse, R. A. Pielke Sr., J. P. McFadden, D. D. Baldocchi, T. G. F. Kittel, I. Chapin, F.S., G. E. Liston, P. L. Vidale, E. Vaganov, and S. Chambers. 2000. Land-atmosphere energy exchange in Arctic tundra and boreal forest: available data and feedbacks to climate. Global Change Biology 6:84-115.

Euskirchen, E., McGuire, A., Chapin, F.S., Rupp, T., 2010, The changing effects of Alaska's boreal forests on the climate system. Canadian Journal of Forest Research, 40, 7, 1336–1346.

Fan Z, McGuire AD, Turetsky MR, Harden JW, Waddington JM, Kane ES. 2013. The response of soil organic carbon of a rich fen peatland in interior Alaska to projected climate change. Global Change Biology 19(2): 604-620.

Farouki, O. T. 1981. Thermal properties of soils. DTIC Document.

Fortier, R., LeBlanc, A.-M., Allard, M., Buteau, S., and Calmels, F. 2008, Internal structure and conditions of permafrost mounds at Umiujaq in Nunavik, Canada, inferred from field investigation and electrical resistivity tomography: Canadian Journal of Earth Sciences, 45, 367–387.

French, H. M. and Y. Shur. 2010. The principles of cryostratigraphy. Earth-Science Reviews 101: 190-206.

Frey, K. E., and Smith, L. C., 2005, Amplified carbon release from vast West Siberian peatlands by 2100: Geophysical Research Letters, 32, 9.

Frey KE, Siegel DI, Smith LC. 2007. Geochemistry of west Siberian streams and their potential response to permafrost degradation. Water Resour Res 43(3).

Frey KE, McClelland JW. 2009. Impacts of permafrost degradation on arctic river biogeochemistry. Hydrol Process 23(1): 169-182.

Gholz, H., and Vogel, S. (1991). "Dynamics of canopy structure and light interception in Pinus elliottii stands, north Florida." cological Monographs, 61(1), 33–51.

Gillett, N. P., A. J. Weaver, F. W. Zwiers, and M. D. Flannigan. 2004. Detecting the effect of climate change on Canadian forest fires. Geophysical Research Letters 31:L18211.

Grosse, G., and fifteen others (2011) Vulnerability of high-latitude soil organic carbon in North America to disturbance. Journal of Geophysical Research 116(G00K06), doi: 10.1029/2010JG001507.

Hamilton, T.D., Ager, T.A., Robinson, S.W. (1983) Late Holocene ice wedges near Fairbanks, Alaska, U.S.A.: Environmental setting and history of growth. Arctic and Alpine Research 15(2): 157-168.

Harada, K., and Yoshikawa, K., 1996, Permafrost age and thickness near Adventfjorden, Spitsbergen: Polar Geography 20, 4, 267-281.

Harden JW, Manies KL, Turetsky MR, Neff JC. 2006. Effects of wildfire and permafrost on soil organic matter and soil climate in interior Alaska. Global Change Biol 12(12): 2391-2403.

Harvey, L.D.D. (1988) On the role of high latitude ice, snow, and vegetative feedbacks in the climatic response to external forcing changes. Climate Change. 13:191–224.

Hartmann, B. and G. Wendler. 2005. The significance of the 1976 Pacific climate shift in the climatology of Alaska. Journal of Climate 18:4824-4839.

Hauck, C., and Kneisel, C., 2008, Applied geophysics in periglacial environments. Cambridge: Cambridge University Press.

Hauck, C. 2013, New Concepts in Geophysical Surveying and Data Interpretation for Permafrost Terrain: Permafrost and Periglacial Processes, 24(2), 131-137.

Hinzman, L.D., Kane, D.L., Gieck, R.E., Everett, K.R. (1991) Hydrologic and thermal properties of the active layer in the Alaskan Arctic. Cold Regions Science and Technology 19(2): 95-110.

Hinzman, L., Kane, D.L., Benson, C.S., Everett, K.R. (1996) Energy balance and hydrological processes in an Arctic watershed. Ecological Studies 131-154

Hinzman, L.D., Goering, D.J., Kane, D.L. (1998) A Distributed Thermal Model for Calculating Temperature Profiles and Depth of Thaw in Permafrost Regions. Journal of Geophysical Research - Atmospheres. 103(D22):28,975- 28,991.

Hinzman, L.D., Kane, D.L., Yoshikawa, K., Carr, A., Bolton, W.R., Fraver, M. (2003) Hydrological variations among watersheds with varying degrees of permafrost. Proceedings of the 8th International Conference on Permafrost, 21-25 July 2003, Zurich, Switzerland

Hinzman, L.D., Bettez, N.D., Bolton, W.R., Chapin, F.S., Dyurgerov, M.B., Fastie, C.L., Griffith, B., Hollister, R.D., Hope, A., Huntington, H.P., Jensen, A.M., Gensuo, J.J., Jorgenson, M.T., Kane, D.L., Klein, D.R., Kofinas, G., Lynch, A.H. Lloyd, A.J., McGuire, A.D., Nelson, F.E., Oechel, W.C., Osterkamp, T.E., Racine, C.H., Romanovsky, V.E., Stone, R.S., Stow, D.A., Sturm, M., Tweedie, C.E., Vourlitis, G.L., Walker, M.D., Walker, D.A., Webber, P.J., Welker, J.M., Winker, K.W., Yoshikawa, K. (2005) Evidence and implications of recent climate change in northern Alaska and other arctic regions. Climatic Change 72: 251-298.

Hoekstra, P., and McNeill, D., 1973, Electromagnetic probing of permafrost. National Academy of Sciences, National Research Council: Proceedings of Permafrost: North American contribution to the Second International Conference, 517-526.

Homer, C., Dewitz, J., Fry, J., Coan, M., Hossain, N., Larson, C., Herold, N., McKerrow, A., VanDriel, J. N., Wickham, J. (2007) Completion of the 2001 National Land Cover Database for the conterminous United States. Photogrammetric Engineering and Remote Sensing 73:337-341.

Hollingsworth, J. (2007). "Caribou-Poker Creeks Research Watershed Radiation Measurements: Net Radiation, Up and Down Shortwave/Longwave Radiation, Bonanza Creek LTER." University of Alaska Fairbanks, Fairbanks.

Hopkins, D.M., Karlstrom, T.N.V. (1955) Permafrost and ground water in Alaska. U.S. Geological Survey Professional Paper 264: 113-146.

Høye, T.T., Post, E., Meltofte, H., Schmidt, N.M., Forchhammer, M.C. (2007) Rapid advancement of spring in the High Arctic. Current Biology17(12), R449-R451, doi: 10.1016/j.cub.2007.04.047.

Hubbard, S. S., Gangodagamage, C., Dafflon, B., Wainwright, H., Peterson, J., Gusmeroli, A., Ulrich , C., Wu, Y., Wilson, C., Rowland, J., Tweedie, C., and Wullscheleger, S. D., 2013, Quantifying and relating land-surface and subsurface variability in permafrost environments using LiDAR and surface geophysical datasets: Hydrogeology Journal, 21, 1, 149-169.

Hutchison, B. A., and Matt, D. R. (1977). "The distribution of solar radiation within a deciduous forest." Ecological Monographs, 47(2), 185–207.

Intergovernmental Panel on Climate Change (2007) Climate Change 2007: The Physical Science Basis, Solomon, S., D. Qin, M. Manning, Z. Chen, M. Marquis, K.B. Averyt, M. Tignor and H.L. Miller (eds.), Cambridge University Press, Cambridge, United Kingdom and New York, NY, USA, 996 pp.

IPCC AR5 WG1 (2013), Stocker, T.F., et al., ed., Climate Change 2013: The Physical Science Basis. Working Group 1 (WG1) Contribution to the Intergovernmental Panel on Climate Change (IPCC) 5th Assessment Report (AR5), Cambridge University Press.

Jafarov, E. E., Marchenko, S. S., and V. E. Romanovsky, 2012. Numerical modeling of permafrost dynamics in Alaska using a high spatial resolution dataset. The Cryosphere Discuss., 6, 89–124.

Jafarov, E. E., V. E. Romanovsky, H. Genet, A. D. McGuire, and S. S. Marchenko. 2013. The effects of fire on the thermal stability of permafrost in lowland and upland black spruce forests of interior Alaska in a changing climate. Environmental Research Letters 8:035030.

Johnson, K.D., Harden, J., McGuire, A.D., Bliss, N.B., Bockheim, J.G., Clark, M., Nettleton-Hollingsworth, T., Jorgenson, M.T., Kane, E.S., Mack, M., O'Donnell, J., Ping, C.L., Schuur, E.A.G., Turetsky, M.R., Valentine, D.W. (2011) Soil carbon distribution in Alaska in relation to soil-forming factors. Geoderma 167-168: 71-84.

Johnson, K. D., J. W. Harden, A. David McGuire, M. Clark, F. Yuan, and A. O. Finley. 2013. Permafrost and organic layer interactions over a climate gradient in a discontinuous permafrost zone. Environmental Research Letters 8:035028.

Johnstone JF, Kasischke ES. 2005. Stand-level effects of soil burn severity on postfire regeneration in a recently burned black spruce forest. Can J Forest Res 35(9): 2151-2163.

Johnstone JF, Chapin III FS. 2006. Effects of soil burn severity on post-fire tree recruitment in boreal forest. Ecosystems 9(1): 14-31.

Johnstone, J. F., F. S. Chapin, III, T. N. Hollingsworth, M. C. Mack, V. Romanovsky, and M. Turetsky. 2010. Fire, climate change, and forest resilience in interior Alaska. Canadian Journal of Forest Research 40:1302-1312.

Jones, B.M., Stoker, J.M. Gibbs, A.E., Grosse, G., Romanovsky, V.E., Douglas, T.A., Kinsman, N.E.M., Richmond, B.M., 2013, Quantifying landscape change in an arctic coastal lowland using repeat airborne LiDAR. Environmental Research Letters, 8, 045025 doi:10.1088/1748-9326/8/4/045025.

Jones MC, Booth RK, Yu Z, Ferry P. 2013. A 2200-year record of permafrost dynamics and carbon cycling in a collapse-scar bog, interior Alaska. Ecosystems 16(1): 1-19.

Jones BM, Grosse G, Arp CD, Miller E, Liu L, Hayes DJ, Larsen CF. Recent Arctic tundra fire initiates widespread thermokarst development. Scientific reports. 2015;5.

Jorgenson, M. T., J. E. Roth, M. Raynolds, M. D. Smith, W. Lentz, and others. 1999. An ecological land survey for Fort Wainwright, Alaska. U.S. Army Cold Regions Research and Engineering Laboratory, Hanover, NH. CRREL Report 99-9, 83 p.

Jorgenson, M. T., J. E. Roth, M. D. Smith, S. Schlentner, W. Lentz, and others. 2001a. An ecological land survey for Fort Greely, Alaska. U.S. Army Cold Regions Research and Engineering Laboratory, Hanover, NH. ERDC/CRREL TR-01-04., 85 p.

Jorgenson, M. T., C. H. Racine, J. C. Walters, and T. E. Osterkamp. 2001b. Permafrost degradation and ecological changes associated with a warming climate in central Alaska. Climatic Change 48:551-579.

Jorgenson, M. T. and T. E. Osterkamp. 2005. Response of boreal ecosystems to varying modes of permafrost degradation. Canadian Journal of Forest Research 35:2100-2111.

Jorgenson, M. T., Shur, Y. L. Pullman, E.R. 2006. Abrupt increase in permafrost degradation in Arctic Alaska. Geophysical Research Letters 33: L02503, 02510.01029/02005GL024960.

Jorgenson, M.T., and Shur, Y. 2007. Evolution of lakes and basins in northern Alaska and discussion of the thaw lake cycle. Journal of Geophysical Research 112(F02S17), doi:10.1029/2006JF000531.

Jorgenson, T., Yoshikawa, K., Kanevskiy, M., Shur, Y., Romanovsky, V., Marchenko, S., Grosse, G., Brown, J., Jones, B. 2008a. Permafrost Characteristics of Alaska - A new permafrost map of Alaska. Ninth International Conference on Permafrost.

Jorgenson, M. T., Y. L. Shur and T. E. Osterkamp. 2008b. Thermokarst in Alaska. In D. L. Kane and K. M. Hinkel, eds., Proceedings Ninth International Conference on Permafrost. Institute of Northern Engineering, University of Alaska, Fairbanks, AK. pp. 869-876.

Jorgenson, M. T., V. Romanovsky, J. Harden, Y. Shur, J. O'Donnell, E. A. G. Schuur, M. Kanevskiy, and S. Marchenko. 2010. Resilience and vulnerability of permafrost to climate change. Canadian Journal of Forest Research 40:1219-1236.

Jorgenson, M. T. 2012a. Conceptual models of landscape change. In J. H. Reynolds and H. V. Wiggins, eds., Shared Science Needs: Report from the Western Alaska Landscape Conservation Cooperative Science Workshop. Western Alaska Landscape Conservation Cooperative, Anchorage, AK. pp. 21-32

Jorgenson, M. T., M. Kanevskiy, Y. Shur, T. Osterkamp, D. Fortier, and others. 2012b. Thermokarst Lake and Shore Fen Development in Boreal Alaska. In: K. Hinkel, eds., Proceedings of the Tenth International Conference on Permafrost. The Northern Publisher, Tyumen, Russia, Salekhard, Russia. Vol. 1, pp. 179-184.

Jorgenson, M. T., J. Harden, M. Kanevskiy, J. O'Donnell, K. Wickland, S. Ewing, K. Manies, Q. Zhuang, Y. Shur, R. Striegl, and J. Koch. 2013a. Reorganization of vegetation, hydrology and soil carbon after permafrost degradation across heterogeneous boreal landscapes. Environmental Research Letters 8:035017.

Jorgenson, M. T. 2013b. Thermokarst Terrains. In J. Schroeder, eds., Treatise on Geomorphology. Elsevier, pp. 8.28.

Jorgenson, M.T., Marcot, B.G., Swanson, D.K., Jorgenson, J.C., and DeGance, A.R. (2015) Projected changes in diverse ecosystems from climate warming and biophysical drivers in northwest Alaska. Climatic Change, DOI 10.1007/s10584-014-1302-1, 13 pages.

Kane K, Slaughter C. 1973. "Recharge of a central Alaska lake by subpermafrost groundwater", International Conference on Permafrost, 2d, Yakutsk, Siberia, 1973. Papers.

Kane, D.L., Hinzman, L.D., Zarling, J.P. (1991) Thermal response of the active layer to climatic warming in a permafrost environment. Cold Regions Science and Technology 19(2): 111-122.

Kane EZ, Turetsky MR, Harden JW, McGuire AD, Waddington JM. 2010. Seasonal ice and hydrologic controls on dissolved organic carbon and nitrogen concentrations in a boreal-rich fen. Journal of Geophysical Research: Biogeosciences (2005–2012) 115(G04012), doi: 10.1029/2010JG001366.

Kanevskiy, M., T. Jorgenson, Y. Shur, J. A. O'Donnell, J. W. Harden, Q. Zhuang, and D. Fortier. 2014. Cryostratigraphy and Permafrost Evolution in the Lacustrine Lowlands of West-Central Alaska. Permafrost and Periglacial Processes 25:14-34.

Kasischke, E. S., French, N. H., O'Neill, K. P., Richter, D. D., Bourgeau-Chavez, L. L., and Harrell, P. A. 2000a, Influence of fire on long-term patterns of forest succession in Alaskan boreal forests: Fire, Climate Change, and Carbon Cycling in the Boreal Forest, Springer, pp. 214-235.

Kasischke, E. S., O'Neill, K. P., French, N. H., and Bourgeau-Chavez, L. L., 2000b, Controls on patterns of biomass burning in Alaskan boreal forests, in: Fire, climate change, and carbon cycling in the boreal forest Springer, pp. 173-196.

Kasischke ES, Johnstone JF. 2005. Variation in postfire organic layer thickness in a black spruce forest complex in interior Alaska and its effects on soil temperature and moisture. Can J For Res 35(9): 2164-2177.

Kasischke, E. S. and M. R. Turetsky. 2006. Recent changes in the fire regime across the North American boreal region- spatial and temporal patterns of burning across Canada and Alaska. Geophysical Research Letters 33:L09703.

Kasischke, E. S., D. L. Verbyla, T. S. Rupp, A. D. McGuire, K. A. Murphy, R. Jandt, J. L. Barnes, E. E. Hoy, P. A. Duffy, M. Calef, and M. R. Turetsky. 2010. Alaska's changing fire regime — implications for the vulnerability of its boreal forests. Canadian Journal of Forest Research 40:1313-1324.

Kneisel, C., 2006, Assessment of subsurface lithology in mountain environments using 2D resistivity imaging: Geomorphology. 80, 1, 2006, 32-44.

Kneisel, C., Emmert, A., and Kästl, J., 2014, Application of 3D electrical resistivity imaging for mapping frozen ground conditions exemplified by three case studies: Geomorphology, 210, 71-82.

Kreig, R. A. and R. D. Reger. 1982. Air-photo analysis and summary of landform soil properties along the route of the Trans-Alaska Pipeline System. Alaska Div. of Geological and Geophysical Surveys, Fairbanks, AK. Geologic Report 66. 149 p.

Kuhry, P. 1994. The role of fire in the development of Sphagnum-dominated peatlands in western boreal Canada. Journal of Ecology 82:899-910.

Lawson, D. E., J. C. Strasser, J. D. Strasser, S. A. Arcone, A. J. Delaney, and others. 1996. Geological and geophysical investigations of the hydrogeology of Fort Wainwright, Alaska, Part I: Canol Road area. U.S. Army Cold Regions Research and Engineering Laboratory, Hanover, NH. CRREL Report 96-4, p.

Lemeur, R., and Zhang, L. (1990). "Evaluation of three evapotranspiration models in terms of their applicability for an arid region." Journal of hydrology, 114(3-4), 395–411.

Lewkowicz, A. G., Etzelmüller, B., and Smith, S. L., 2011, Characteristics of discontinuous permafrost based on ground temperature measurements and electrical resistivity tomography, southern Yukon, Canada: Permafrost and Periglacial Processes, 22, 4, 320-342.

Liston, G.E., Hiemstra, C.A. (2011) The changing cryosphere: Pan-Arctic snow trends (1979−2009). Journal of Climate 24: 5691–5712.

Loke, M. H., and Barker, R. D., 1996, Rapid least-squares inversion of apparent resistivity pseudosections by a quasi-Newton method: Geophysical Prospecting 44, 1, 131-152.

Loke, M.H., Acworth, I. and Dahlin, T., 2003. A comparison of smooth and blocky inversion methods in 2D electrical imaging surveys. Exploration Geophysics, 34, 182-187.

Mackay, J. R. 1995. Active layer changes (1968 to 1993) following the forest-tundra fire near Inuvik, N.W.T.,Canada. Arctic and Alpine Research 27:323-336.

MacLean R.O., Oswood M.W., Irons I J.G., McDowell W.H. The effect of permafrost on stream biogeochemistry: a case study of two streams in the Alaskan (USA) taiga. Biogeochemistry. 1999 Dec 1;47(3):239-67.

Marchenko, S., Romanovsky, V., and Tipenko, G., 2008. Numerical modeling of spatial permafrost dynamics in Alaska, in: In Proceedings of the Eighth International Conference on Permafrost, 190–204, Willey, Institute of Northern Engineering, University of Alaska, Fairbanks, 2008. 91, 95.

Marsh, P., Neumann, N.N. (2001) Processes controlling the rapid drainage of two ice-rich permafrost-dammed lakes in NW Canada. Hydrological Processes 15(8): 3433-3446.

Marsh P., Russell, M., Pohl, S., Haywood, H., Onclin, C., 2009, Changes in thaw lake drainage in the Western Canadian Arctic from 1950 to 2000 Hydrological Processes, 23, 145–58.

McClymont, A. F., Hayashi, M., Bentley, L. R., and Christensen, B. S. 2013, Geophysical imaging and thermal modeling of subsurface morphology and thaw evolution of discontinuous permafrost: Journal of Geophysical Research: Earth Surface, 118, 3, 1826-1837.

McGuire, A. D., Anderson, L. G., Christensen, T. R., Dallimore, S., Guo, L., et al, 2009, Sensitivity of the carbon cycle in the Arctic to climate change: Ecological Monographs, 79, 4, 523-555.

McCune, B. and J. B. Grace. 2002. Analysis of Ecological Communities. MjM Software Design, Gleneden Beach,OR, USA.

McCune, B. and M. J. Mefford. 2011. PC-ORD. Multivariate Analysis of Ecological Data. Version 6.0. MjM Software, Gleneden Beach, Oregon, USA.

Minsley, B. J., J. D. Abraham, B. D. Smith, J. C. Cannia, C. I. Voss, and others. 2012. Airborne electromagnetic imaging of discontinuous permafrost. Geophysical Research Letters 39, L02503.

Myers-Smith, I. H., J. W. Harden, M. Wilmking, C. C. Fuller, A. D. McGuire, and F. S. Chapin, III. 2008. Wetland succession in a permafrost collapse: interactions between fire and thermokarst. Biogeosciences 5:1273-1286.

NCSS Staff. (2014). "National Cooperative Soil Survey, Natural Resources Conservation Service, United States Department of Agriculture. Web Soil Survey." National Cooperative Soil Characterization Database, <http://ncsslabdatamart.sc.egov.usda.gov> (Mar. 21, 2014).

Nelson, D. W. and L. E. Sommers. 1996. Total carbon, organic carbon, and organic matter. Pages 963-977 in J. M. Bartels, editor. Methods of Soil Analysis. Soil Science Society of America, American Society of Agronomy, Madison, Wisconsin.

Nicolsky, D.J., Romanovsky, V.E. & Tipenko, G.S. 2007. Estimation of thermal properties of saturated soils using in-situ temperature measurements. The Cryosphere, 1, 41–58, 2007.

Nossov, D. R., T. N. Hollingsworth, R. W. Ruess and K. Kielland. 2011. Development of Alnus tenuifolia stands on an Alaskan floodplain: patterns of recruitment, disease and succession. Journal of Ecology 99: 621-633.

Nossov, D. R., M. T. Jorgenson, K. Kielland, and M. Z. Kanevskiy. 2013. Edaphic and microclimatic controls over permafrost response to fire in interior Alaska. Environmental Research Letters 8:035013.

O'Donnell JA, Jones JB. 2006. Nitrogen retention in the riparian zone of catchments underlain by discontinuous permafrost. Freshwat Biol 51(5): 854-864.

O'Donnell, J. A., V. E. Romanovsky, J. W. Harden, and A. D. McGuire. 2009. The effect of moisture content on the thermal conductivity of moss and organic soil horizons from black spruce ecosystems in interior Alaska. Soil Science 174:646-651.

O'Donnell, J. A., Jorgenson, M.,T., Harden, J. W., McGuire, A. D., Kanevskiy, M. Z., et al. 2012, The effects of permafrost thaw on soil hydrologic, thermal, and carbon dynamics in an Alaskan peatland: Ecosystems, 15(2), 213–229.

Ogden, F. L., Pradhan, N.R., Downer C.W., Zahner, J.A. 2011. Relative importance of impervious area, drainage density, width function, and sub-surface storm drainage on flood runoff from an urbanized catchment. Water Resources Research, 47, W12503, doi: 10.1029/2011WR010550.

O'Neill, K. P., Kasischke, E. S., and Richter, D. D., 2002, Environmental controls on soil CO2 flux following fire in black spruce, white spruce, and aspen stands of interior Alaska: Canadian Journal of Forest Research, 32, 9, 1525-1541.

O'Neill, K. P., Kasischke, E. S, and Richter, D. D., 2003, Seasonal and decadal patterns of soil carbon uptake and emission along an age sequence of burned black spruce stands in interior Alaska: Journal of Geophysical Research Atmospheres, 108, D1.

Osterkamp, T. E., Jurick, R. W., Gislason, G. A., and Akasofu. S-I. 1980, Electrical resistivity measurements in permafrost terrain at the Engineer Creek road cut, Fairbanks, Alaska: Cold Regions Science and Technology, 3(4), 277-286.

Osterkamp, T.E. & Romanovsky, V.E. 1999. Evidence for Warming and Thawing of Discontinuous Permafrost in Alaska. Permafrost and Periglacial Processes, 10: 17-37.

Osterkamp, T., Viereck, L., Shur, Y., Jorgenson, M., Racine, C., et al, 2000, Observations of thermokarst and its impact on boreal forests in Alaska, USA: Arctic, Antarctic and Alpine Research, 32, 3, 303-315.

Osterkamp, T.E. 2003. Establishing Long-term Permafrost Observatories for Active-layer and Permafrost Investigations in Alaska: 1977–2002. Permafrost and Periglacial Processes. 14: 331–342.

Osterkamp, T. E. and C. R. Burn. 2003. Permafrost. Pages 1717-1729 in J. R. Holton, J. Pyle, and J. A. Curry, editors. Encyclopedia of Atmospheric Sciences. Academic Press, Oxford, U.K.

Osterkamp, T.E., Jorgenson, J.C. (2006) Warming of Permafrost in the Arctic National Wildlife Refuge, Alaska. Permafrost and Periglacial Processes 17: 65–69. DOI: 10.1002/ppp.538

Osterkamp, T.E. (2007) Characteristics of the recent warming of permafrost in Alaska. Journal of Geophysica Research 112, F02S02, doi:10.1029/2006JF000578.

Osterkamp, T., Jorgenson, M., Schuur, E., Shur, Y., Kanevskiy, M., et al., 2009, Physical and ecological changes associated with warming permafrost and thermokarst in interior Alaska: Permafrost and Periglacial Processes, 20, 3, 235-256.

Parmentier, F.J.W., van der Molen, M.K., van Huissteden, J., Karnasaev, S.A., Kononov, A.V., Suzdalov, D.A., Maximov, T.C., Dolman, A.J. (2011) Longer growing seasons do not increase net carbon uptake in the northeastern Siberian tundra. Journal of Geophysical Research 116(G04013), doi: 10.1029/2011JG001653.

Panda, S. K., Prakash, A., Jorgenson, M. T., and Solie D. N. 2012, Near-surface permafrost distribution mapping using logistic regression and remote sensing in Interior Alaska: GIScience & Remote Sensing, 49(3), 346-363.

Pastick, N. J., M. T. Jorgenson, B. K. Wylie, J. R. Rose, M. Rigge, and M. A. Walvoord. 2014. Spatial variability and landscape controls of near-surface permafrost within the Alaskan Yukon River Basin. Journal of Geophysical Research: Biogeosciences 119:1244-1265.

Peterson, B.J., Holmes, R.M., McClelland, J.W., Vorosmarty, C.J., Lammers, R.B., Shiklomanov, A.I., Shiklomanov, I.A., Rahmstorf, S. (2002) Increasing river discharge to the Arctic Ocean. Science 298(5601): 2171-2173.

Petrone KC, Jones JB, Hinzman LD, Boone RD. 2006. Seasonal export of carbon, nitrogen, and major solutes from Alaskan catchments with discontinuous permafrost. J Geophys Res Biogeosci 111(G2).

Petrone KC, Hinzman LD, Shibata H, Jones JB, Boone RD. (2007) The influence of fire and permafrost on sub-arctic stream chemistry during storms. Hydrological Processes 21(4): 423-434.

Pradhan, N.R., Ogden, F.L. and Downer, C.W. 2009. Uncertainty in tile drain locations: implications for hydrologic modelling of agricultural watersheds. Transactions of the American Geophysical Union, 90, 52.

Pradhan, N.R., Downer, C.W., Marchenko, S., Liljedahl, A., Douglas, T.A., and Byrd, A. (2013) Development of a Coupled Framework for Simulating Interactive Effects of Frozen Soil Hydrological Dynamics in Permafrost Region. ERDC-TR-13-15, 30 pages.

Pullman, E. R., M. Torre Jorgenson, and Y. Shur. 2007. Thaw Settlement in Soils of the Arctic Coastal Plain, Alaska. Arctic, Antarctic, and Alpine Research 39:468-476.

Racine, C. H. and J. C. Walters. 1991. Groundwater-discharge wetlands in the Tanana Flats, interior Alaska. CRREL Report 91-14. U.S. Army Cold Regions Research and Engineering Laboratory, Hanover, New Hampshire.

Racine, C.H., Walters, J.C. (1994) Groundwater-discharge fens in the Tanana Lowlands, interior Alaska, U.S.A. Arctic and Alpine Research 26(4): 418-426.

Racine, C. H., M. T. Jorgenson and J. C. Walters. 1998. Thermokarst vegetation in lowland birch forests on the Tanana Flats, interior Alaska, U.S.A. In A. G. Lewkowicz and M. Allard, eds., Proceedings of Seventh International Conference on Permafrost. Universite Laval, Sainte-Foy, Quebec. Collection Nordicana (57), pp. 927-933.

Räisänen J. 2008. Warmer climate: less or more snow? *Clim Dyn* **30**(2-3): 307-319.

Richards LA. 1931. Capillary conduction of liquids in porous mediums. Physics 1: 318–333.

Rieger, S., Dement, J. A., and Sanders, D. (1963). Soil survey of Fairbanks area, Alaska. Washington, DC.

Rieger, S., Furbush, C. E., Schoephorster, D. B., Summerfield Jr., H., and Geiger, L. C. (1972). Soils of the Caribou-Poker Creeks Research Watershed, Interior Alaska. Hanover, New Hampshire.

Rieger, S., Schoephorster, D. B., and Furbush, C. E. (1979). Exploratory soil survey of Alaska. USDA Soil Conservation Service, 213.

Riordan B, Verbyla D, McGuire AD. 2006. Shrinking ponds in subarctic Alaska based on 1950–2002 remotely sensed images. J Geophys Res Biogeosci 111(G4).

Roach J, Griffith B, Verbyla DJones, J. 2011. Mechanisms influencing changes in lake area in Alaskan boreal forest. Global Change Biol 17(8): 2567-2583.

Rober AR, Wyatt KH, Stevenson RJ, Turetsky MR. 2014. Spatial and temporal variability of algal community dynamics and productivity in floodplain wetlands along the Tanana River, Alaska. Freshwater Science 33(3):765–777.

Romanovsky, V. E. and T. E. Osterkamp. 2000. Effects of unfrozen water on heat and mass transport processes in the active layer and permafrost. Permafrost and Periglacial Processes 11:219-239.

Romanovsky, VE, Smith, SL, and Christiansen, HH. 2010. Permafrost Thermal State in the Polar Northern Hemisphere during the International Polar Year 2007–2009: a Synthesis. Permafrost and Periglac. Process. 21: 106–116 (2010). DOI: 10.1002/ppp.689

Romanovsky VE, Smith SL, Christiansen HH, Shiklomanov NI, Streletskiy DA, Drozdov DS, Oberman NG, Kholodov AL, Marchenko SS. 2012. Permafrost. Arctic Report Card: Update for 2012. www.arctic.noaa.gov/reportcard.

Roulet, Nigel, T. I. M. Moore, Jill Bubier, and Peter Lafleur. Northern fens: methane flux and climatic change. Tellus B 44, no. 2 (1992): 100-105.

Rover, J, Ji L, Wylie BK, Tieszen LL. 2011. Establishing water body areal extent trends in interior Alaska from multitemporal Landsat data. Remote Sensing Letters 3(7): 595-604.

Schuur EA, Bockheim J, Canadell JG, Euskirchen E, Field CB, et al. 2008. Vulnerability of permafrost carbon to climate change: Implications for the global carbon cycle. Bioscience 58(8): 701-714.

Schuur, E. A. G., B. W. Abbott, W. B. Bowden, V. Brovkin, P. Camill, J. G. Canadell, J. P. Chanton et al., 2013, Expert assessment of vulnerability of permafrost carbon to climate change: Climatic Change, 119, 2, 359-374.

Senarath, S. U. S., and Ogden, F. L. (2000). "On the calibration and verification of two-dimensional, distributed, Hortonian, continuous watershed models." Water Resources Research, 36(6), 1495–1510.

Sergueev, D., G. Tipenko, V. Romanovsky, and N. Romanovskii. 2003. Mountain permafrost thickness evolution under influence of long-term climate fluctuations (results of numerical simulation). Pages 1017-1021 The Seventh International Permafrost Conference, Switzerland.

Serreze MC, Barry RG. Processes and impacts of Arctic amplification: A research synthesis. Global and Planetary Change. 2011 May 31;77(1):85-96.

Shiklomanov, N. I., Streletskiy, D. A., Little, J. D., and Nelson, F. E. 2013, Isotropic thaw subsidence in undisturbed permafrost landscapes: Geophysical Research Letters, 40, 24, 6356-6361.

Shur, Y. L. and M. T. Jorgenson. 2007. Patterns of permafrost formation and degradation in relation to climate and ecosystems. and Periglacial Processes 18:7-19.

Smith LC, Sheng Y, MacDonald GM, Hinzman LD. 2005. Disappearing Arctic lakes. Science 308(5727): 1429. 10.1126/science.1108142.

Smith SL, Romanovsky VE, Lewkowicz AG, Burn CR, Allard M, Clow GD, Yoshikawa K, Throop J. 2010. Thermal state of permafrost in North America: a contribution to the International Polar Year. Permafrost and Periglacial Proceses 21: 117–135. DOI: 10.1002/ppp.690.

Stevens, C.W., Wolfe, SA, 2012, High-Resolution Mapping of Wet Terrain within Discontinuous Permafrost using LiDAR Intensity. Permafrost and Periglacial Processes 23, 4, 334-341.

Symstad AJ, Chapin FS III, Wall DH, Gross KL, Huenneke LF, Mittelbach GG, Peters DPC, Tilman D. 2003. Long-term and large-scale perspectives on the relationship between biodiversity and ecosystem functioning. Bioscience 53(1): 89-98.

Thie, J. 1974. Distribution and thawing of permafrost in the southern part of the discontinuous permafrost zone in Manitoba. Arctic 27:189-200.

Toniolo, H., Kodial, P., Hinzman, L.D., Yoshikawa K. (2009) Spatio-temporal evolution of a thermokarst in Interior Alaska, Cold Regions Science and Technology 56(1): 39-49.

Turetsky, M.R., Wieder, R.K., Vitt, D.H., 2002, Boreal peatland C fluxes under varying permafrost regimes. Soil Biology and Biochemistry, 34, 7, 907–912.

Turetsky MR, Mack MC, Hollingsworth TN, Harden JW. 2010. The role of mosses in ecosystem succession and function in Alaska's boreal forest. Can J For Res. 40(7): 1237-1264.

Turetsky MR, Kane ES, Harden JW, Ottmar RD, Manies KL, et al. 2011. Recent acceleration of biomass burning and carbon losses in Alaskan forests and peatlands. Nature Geosci 4(1): 27-31.

Turetsky MR, and eighteen others. 2014. A synthesis of methane emissions from 71 northern, temperate, and subtroptical wetlands. Glob. Change. Bio. 29(7): 2183-2197.

Van Cleve K, Viereck L. 1983. A comparison of successional sequences following fire on permafrost-dominated and permafrost-free sites in interior Alaska. Permafrost: Fourth International Conference, Proceedings, pp. 1286.

Van Cleve, K., L. A. Viereck and C. T. Dyrness. 1996. State factor control of soils and forest succession along the Tanana River in interior Alaska, USA. Arctic and Alpine Research 28 388-400.

van Genuchten, M. Th. (1980). A-Closed Form Equation for Predicting the Hydraulic Conductivity of Unsaturated Soils. Soil Science Society of America Journal 44 (5): 892–898.

Verdi, C. (1994) Numerical aspects of parabolic free boundary and hysteresis problems. Lecture Notes in Mathematics, New York, Springer-Verlag, 213-284.

Verma, S., and Baldocchi, D. (1986). Eddy fluxes of CO2, water vapor, and sensible heat over a deciduous forest. Boundary-Layer Meteorology, 36(1-2), 71–91.

Viereck, L. A., 1973, Ecological effects of river flooding and forest fires on permafrost in the taiga of Alaska: International Conference on Permafrost, 2d, Yakutsk, Siberia.

Viereck LA. 1982. Effects of fire and firelines on active layer thickness and soil temperatures in interior Alaska. Proceedings of the Fourth Canadian Permafrost Conference. National Research Council of Canada Calgary: Ottawa, Ontario: 123-135.

Viereck, L. A., C. T. Dyrness and M. J. Foote. 1993. An overview of the vegetation and soils of the floodplain ecosystems of the Tanana River, interior Alaska. Canadian Journal of Forest Research 23 (5): 889-898.

Viereck, L. A., N. R. Werdin-Pfisterer, P. C. Adams, and K. Yoshikawa. 2008. Effect of wildfire and fireline construction on the annual depth of thaw in a black spruce permafrost forest in interior Alaska: A 36-year record of recovery. Pages 1845-1850 in Proceedings of the Ninth International Conference on Permafrost, Fairbanks, Alaska.

Vitt, D. H., L. A. Halsey, and S. C. Zoltai. 1994. The bog landforms of continental western Canada in relation to climate and permafrost patterns. Arctic and Alpine Research 26:1-13.

Wahrhaftig, C. (1965). Physiographic divisions of Alaska. Washington, DC, 52.

Walvoord MA, Striegl RG. 2007. Increased groundwater to stream discharge from permafrost thawing in the Yukon River basin: Potential impacts on lateral export of carbon and nitrogen. Geophys Res Lett 34(12).

Walvoord, M. A., C. I. Voss and T. P. Wellman. 2012. Influence of permafrost distribution on groundwater flow in the context of climate-driven permafrost thaw: Example from Yukon Flats Basin, Alaska, United States. Water Resources Journal 48 W07524.

Walvoord, M.A., Day-Lewis, F.D., Lane, J.W., Jr., Striegl, R.G., Voss, C.I., Douglas, T.A. Improved understanding of permafrost controls on hydrology in interior alaska by integration of ground-based geophysical permafrost characterization and numerical modeling. SERDP Project RC-2111 Final Report. May 2015. 123 pages.

Walters, J. C., Racine, C. H., and Jorgenson, M. T., 1998. Characteristics of permafrost in the Tanana Flats, Interior Alaska: Proceedings of the Seventh International Conference on Permafrost, Collection Nordicana, 55, 1109-1114.

Walsh JE, Chapman WL, Romanovsky V, Christensen JH, Stendel M. 2008. Global climate model performance over Alaska and Greenland. *J.Clim.* **21**(23).

Wendler, G., Shulski, M. (2009) A century of climate change for Fairbanks, Alaska. Arctic 62: 295–300.

Wendler, G., Conner, J., Moore, B., Shulski, M., and Stuefer, M., 2011, Climatology of Alaskan wildfires with special emphasis on the extreme year of 2004: Theoretical and Applies Climatology, 104, 3-4, 459-472.

White D, Hinzman, L, Alessa, L, Cassano, J, Chambers, M, et al. 2007. The arctic freshwater system: Changes and impacts. J Geophys Res Biogeosci 112(G4).

Windsor J, Moore TR, Roulet NT. 1992. Episodic fluxes of methane from subarctic fens. Canadian Journal of Soil Science 72(4): 441-452.

Wolken, J.M., Hollingsworth, T.N., Rupp, T.S., Chapin, F.S., III, Trainor, S.F., Barrett, T.M., Sullivan, P.F., McGuire, A.D., Euskirchen, E.S., Hennon, P.E., Beever, E.A., Conn, J.S., Crone, L.K., D'Amore, D.V., Fresco, N., Hanley, T.A., Kielland, K., Kruse, J.J., Patterson, T., Schuur, E.A.G., Verbyla, D.L., Yarie, J. (2011) Evidence and implications of recent and projected climate change in Alaska's forest ecosystems. Ecosphere 2(11): 1-35.

Woo, M.K. (2000) Permafrost and Hydrology. In: The Arctic: Environment, People, Policy, pages 57-96.

Wurtz, T. L., Ott, R. A., and Maisch, J. C., 2006, Timber harvest in interior Alaska. Alaska's Changing Boreal Forest. Oxford University Press, 302-308.

Wyatt KH, Stevenson R, Turetsky MR. 2010.The importance of nutrient co-limitation in regulating algal community composition, productivity and algal-derived DOC in an oligotrophic marsh in interior Alaska. Freshwater Biology 55(9): 1845-1860.

Yarie J. 1981. Forest fire cycles and life tables: a case study from interior Alaska. Can J For Res 11(3): 554-562.

Yoshikawa, K., and Hinzman, L. D., 2003, Shrinking thermokarst ponds and groundwater dynamics in discontinuous permafrost near Council, Alaska. Permafrost Periglacial Process, 14, 2, 151-160.

Yoshikawa, K., W. R. Bolton, V. E. Romanovsky, M. Fukuda, and L. D. Hinzman. 2003. Impacts of wildfire on the permafrost in the boreal forests of Interior Alaska. Journal of Geophysical Research 108:8148.

Yoshikawa, K., Leuschen, C., Ikeda, A., Harada, K., Gogineni, P., Hoekstra, P., Hinzman, L., Sawada, Y., and Matsuoka, N, 2006, Comparison of geophysical investigations for detection of

massive ground ice (pingo ice): Journal of Geophysical Research: Planets (1991–2012) 111, E6, 10 pages.

Zhang, T. 2005. Influence of the seasonal snow cover on the ground thermal regime: An overview. Reviews of Geophysics 43.

Zhuang, Q., McGuire, A. D., Melillo, J., Clein, J., Dargaville R, et al., 2003, Carbon cycling in extratropical terrestrial ecosystems of the Northern Hemisphere during the 20th century: A modeling analysis of the influences of soil thermal dynamics: Tellus B 55(3): 751-776.

Zoltai, S. C. 1993. Cyclic development of permafrost in the peatlands of Northwestern Alberta, Canada. Arctic and Alpine Research 25:240-246.

Appendix A. DELIVERABLES, OUTREACH, AND LEVERAGING EFFORTS

A.1 Conference Presentations and Participation

2011

Department of Defense and Climate Change: Initiating the Dialogue. July 19-21, 2011. Aurora, Colorado. PI Douglas participated in this meeting.

-American Geophysical Union Fall Meeting. December, 2011. San Francisco, California
Douglas, T.A., Liljedahl, A.K., Astley, B., Downer, C., Jorgenson, M.T., Bagley, C., and Burks-Copes, K. (2011) Anticipated impacts of climate warming on ecosystems in interior Alaska. Eos, Transactions of the American Geophysical Union. Volume 92, C41B-0393.

-Astley, B., Douglas, T.A., Campbell, S., Snyder, C., Goggin, E., Saari, S. (2011) Response of Permafrost to Anthropogenic Land Surface Disturbance near Fairbanks, Alaska. Eos, Transactions of the Fall American Geophysical Union Meeting. Volume 92, C41B-0392.

-Pradhan, N.R., Downer, C.W., and Ogden, F.L (2011) Applicability of laboratory scale sediment transport capacity model to watershed scale. Eos, Transactions of the American Geophysical Union. Volume 92, EP41C-0628.

2012

-American Water Resources Association Alaska State Section
Liljedahl, A.K., Ardnet, A., Barnhard, C., Douglas, T.A., Durham, J., Herreid, S., Hock, R., McNabb, E., Wright, W. (2012) Glacier melt: A source for groundwater recharge and streamflow in semi-arid interior Alaska.

-American Geophysical Union Fall Meeting. December, 2012. San Francisco, California
Campbell, S.W., Saari, S.P., Douglas, T.A., Day-Lewis, F.D., Walvoord, M.A., Nolan, J.T. (2012) Shallow Geology and Permafrost Characterization using Ground-Penetrating Radar to infer Hydrological Controls and Landscape Evolution of interior Alaska. This was a collaborative effort with SERDP project RC-2111 “Improved Understanding of Permafrost Controls on Hydrology in interior Alaska by Integration of Ground-Based Geophysical Permafrost Characterization and Numerical Modeling.”

Jorgenson, M. T., Y. Shur, M. Kanevskiy and J. Harden 2012. Role of permafrost in landscape heterogeneity and ecological transitions in boreal and tundra regions. Eos, Transactions of the American Geophysical Union 2012 AGU Fall Meeting, Abstract B52C-04.

-Two additional presentations supported by this project were accepted for presentation but we were unable to attend the meeting:
Douglas, T.A., Jones, M.C., and Hiemstra, C. Changing sources and sinks of carbon in boreal ecosystems of interior Alaska: Current and future perspectives. American Geophysical Union Fall Meeting. San Francisco, California.

Pradhan, N.,R., Downer, C.W., Liljedahl, A.K., Marchenko, S., Douglas, T.A., Wahl, M.D. (2012) Development of a coupled framework for simulating interactive effects of soil thermal and hydrological dynamics in landscapes underlain by permafrost. American Geophysical Union Fall Meeting. San Francisco, California.

-Tenth International Conference on Permafrost. July, 2012. Salekhard, Russia
Douglas, T.A., Liljedahl, A.K., Jorgenson, M.T., Bagley, C., Downer, C., Pradhan, N., Burks-Copes, K. (2012) Effects of a changing permafrost regime on hydrology and ecosystems in interior Alaska. Extended Abstracts of the Tenth International Conference on Permafrost, Salekhard, Russia. Volume 4/1, pages 124-125.

2013
-We presented our project research results at the American Geophysical Union Fall Meeting. December, 2013 in San Francisco, California:
Douglas, T.A., Bjella, K., Campbell, S.W. (2013) What's down below? Current and potential future applications of geophysical techniques to identify subsurface permafrost conditions (Invited). Eos, Transactions of the American Geophysical Union C53C-01.

Campbell, S.W., Kreutz, K.J., Arcone, S.A. (2013) Ground-Penetrating Radar vertical resolution, signal attenuation, and penetration in temperate and polar glaciers: Case studies from North America and Antarctica. Eos, Transactions of the American Geophysical Union NS21C-1575.

Wu, N.L., Campbell, S.W., Douglas, T.A., Osterberg, E.C. (2013) Developing an Ice Volume Estimate of Jarvis Glacier, Alaska, using Ground-Penetrating Radar and High Resolution Satellite Imagery. Eos, Transactions of the American Geophysical Union GC23D-0965.

-We presented our project research results at the Geological society of America Annual Meeting:
Horing, J., Campbell, S., Douglas, T.A., Chipman, J. (2013) Thickness and Extent of Permafrost Determined by Resistivity Profiles Compared to Vegetation Type in Tanana Flats, Alaska. Geological Society of America Annual Meeting. Denver, Colorado.

2014
Nossov, D., Jorgenson, M.T., Kielland, K., Douglas, T.A., Romanovsky, V., Euskirchen, E., Ruess, R. Vulnerability of permafrost to fire-initiated thaw in lowland forests of the Tanana Flats, interior Alaska. Presented at the Alaska Cooperative Fish and Wildlife Research Unit Annual Meeting in March, 2014.

Douglas, T.A., Bjella, K., Newman, S., Hiemstra, C., Deeb, E., Anderson, J. (2014) Throwing it all out there: An attempt at a holistic view of ground ice in discontinuous permafrost near Fairbanks, Alaska. Fourth European conference on Permafrost. Evora, Portugal.

A.2 Peer-reviewed publications

Brown, D.R.N., Jorgenson, M.T., Douglas, T.A., Romanovsky, V., Kielland, K., Euskirchen, E. 2015. Vulnerability of permafrost to fire-initiated thaw in lowland forests of the Tanana Flats, interior Alaska. Journal of Geophysical Research Biogeosciences, 19 pages; doi: 10.1002/2015JG003033.

Douglas, T.A., Jones, M.C., Hiemstra, C.A., and Arnold, J. (2014) Sources and sinks of carbon in boreal ecosystems of Interior Alaska: A Review. Elementa: Science of the Anthropocene; 10.12952/journal.elementa.000032#sthash.j8pzVjml.dpuf.

Douglas, T.A., Jorgenson, M.T., Brown, D.R.N., Campbell, S.W., Hiemstra, C.A., Saari, S.P., Bjella, K., Liljedahl, A.K. 2015. Degrading permafrost mapped with electrical resistivity tomography, airborne imagery and LiDAR, and seasonal thaw measurements. Geophysics 81(1), 15 pages, doi: 10.1190/GEO2015-0149.1.

Jones, B.M., Stoker, J.M., Gibbs, A.E., Grosse, G., Romanovsky, V., Douglas, T.A., Kinsman, N.E.M., Richmond, B.M. (2013) Quantifying landscape change in an arctic coastal lowland using repeat airborne LiDAR. Environmental Research Letters 8 (045025), 10 pages.

Pradhan, N.R., Downer, C.W., Marchenko, S., Liljedahl, A., Douglas, T.A., and Byrd, A. (2013) Development of a Coupled Framework for Simulating Interactive Effects of Frozen Soil Hydrological Dynamics in Permafrost Region. ERDC-TR-13-15, 30 pages.

In preparation for submission

Douglas, T.A., Bjella, K., Hiemstra, C., Newman, S., Anderson, J., Edwards, J., Arcone, S. Wagner, A., Barbato, R., Berkowitz, J., Deeb, E. Integration of geophysical, ground surface, and remote sensing methods to identify ice features in discontinuous permafrost near Fairbanks, Alaska. In preparation for submission to Permafrost and Periglacial Processes.

Jorgenson, M.T., Brown, D.R.N., Douglas, T.A. Patterns and rates of landscape change in central Alaska. In preparation for submission to Ecoscience.

Pradhan, N.R., Downer, C.W., Marchenko, S., Modeling Permafrost in GSSHA with the Geophysical Institute Permafrost Lab Model, GIPL and Use Guidelines. ERDC/CHL Technical Report.

Wahl, M. Caribou/Poker Creeks Research Watershed long-term hydrologic simulation using the coupled GIPL-GSSHA model. In preparation for an ERDC-CHL Technical Report.

A.3 Outreach

-The city of Delta Junction, Alaska (where Fort Greely and the Donnelly Training Area are located). Co-PI Liljedahl has met twice with city planners to discuss Delta Junction and Fort Greely area hydrology and climate change impacts as part of a meeting initiate by the Salcha-Delta SWCD personnel.

-Co-PI Liljedahl participated in The Salcha-Delta Soil Conservation District's "Conservation Camp" at the Lost Lake Boy Scout camp in the summers of 2013 and 2014.

A.4 Leveraging/collaborative activities with related ongoing efforts

1) We have been working with the Salcha Delta Soil and Water Conservation District (SWCD) since spring, 2011 when they started collecting water samples and making discharge measurements in the Jarvis Creek and Granite Creek watersheds near Delta Junction/Fort Greely. Jarvis Creek has a glacial melt flow year round while Granite Creek typically runs dry in the summer. Both are losing streams and represent the beginning of the regional hydrology where snow melt and precipitation leave the mountains and head northward toward the lowlands. Adding Salcha Delta SWCD personnel and interest to this project has allowed us to get more discharge information than we had planned.

2) Dr. Miriam Jones of the University of Alaska Fairbanks, accompanied us in the field on numerous occasions and provided detailed vegetation and ecologic measurements of our field sites.

3) Dr. Teresa Hollingsworth of the U.S. Department of Agriculture Forest Service and the University of Alaska Fairbanks accompanied us to all of our Tanana Flats field sites and provide detailed vegetation, animal browse and ecologic field measurements.

4) We worked with the University of Alaska Fairbanks Glaciology Program and the Salcha Delta SWCD in summer 2011 and 2012 to establish a glacier mass balance campaign on the Jarvis Glacier. This will help us acquire key regional hydrology data for the Jarvis Creek watershed.

5) U.S. Army Alaska has funded CRREL ($425,000 in 2011 and 2012) to collect well water sampled and make geochemical measurements on fort Greely. This has allowed us to gain more insight into the regional flows in the Donnelly Training area. A recently funded project ($75,000 for 2013) will support the development of a groundwater model for the Battle Area Complex-Combined Arms Collective Training Facility (BAX/CACTF) on Donnelly Training area East. This information will help us assess the regional hydrology of the Jarvis Creek watershed.

6) Through a collaboration with SERDP project RC-2109 "Identifying Indicators of State Change and Forecasting Future Vulnerability in Alaskan Boreal Ecosystems" April Melvin (a Postdoctoral Scholar with Ted Schuur's SERDP project group) accompanied us to the field and she collected soil and vegetation samples from our 2010 burn site and from a 2011 site near our 1975 site.

A.5 Interactions with Department of Defense and Other Governmental Endusers

U.S. Army Alaska Directorate of Public Works, Fort Wainwright, Alaska

We have held regular bi-monthly meetings with U.S. Army Alaska (USARAK) personnel to provide an update and to solicit their "end user" needs and suggestions. In May, 2012 PI Douglas and co-PI Liljedahl gave an hour long presentation on the project to identify what topics, goals, and deliverables could assist training range planning efforts. They identified fire prevalence, soil carbon storage, potential threatened and endangered species habitat, invasive species, and spruce bark beetle susceptibility as potential needs. There are no current threatened/endangered species issues or major invasive species issues. However, they foresee future use for a system whereby they can use ecosystem scenarios, climate projections, and decision support tools to address needs as they emerge.

Ms. Maureen Sullivan, Director, Environmental Management, Office of the Deputy UnderSecretary of Defense for Installations and Environment

In April, 2012 PI Douglas had a half day one on one visit with Ms. Sullivan. We toured project sites near Fairbanks, Alaska.

The U.S. Army Corps of Engineers Institute for Water Resources

May, 2012 in Washington, DC

Gave presentation to over 40 Corps employees through a virtual teleconference on some of the project content: "Climate Change and carbon in interior Alaska: Relevant impacts for future USACE and DoD policy development"

The U.S. Army Environmental Command

In August, 2012 PI Douglas visited USAEC in San Antonio and briefed multiple Branch Chiefs, Division Chiefs, and Research Team members on the project.

The U.S. Army Corps of Engineers Geotechnical and Dam Safety Section

In August, 2012 we visited the Moose Creek Dam near Fort Wainwright with 8 members of the U.S. Army Corps of Engineers Geotechnical and Dam Safety Section. They are worried that loss of permafrost from the Moose Creek dam spillway walls and embankment could lead to accelerate piping or seepage of water through the dam. As a consequence, the Chena Dam is a Dam Safety Action Class (DSAC) 1 dam which is the highest level of risk they can assign to a dam facility. Though the current SERDP project does not have a field or mapping or modeling focus at the dam site we were able to provide the dam risk assessors an update on the current and future predicted state of permafrost in the area. We hope to be supported to make some geophysical measurements at the dam site in the summer of 2013 with funding from the Corps Dam Safety Section.

A report to U.S. Army Alaska that was partially supported by this project

Wagner, A.M., Douglas, T.A., Walsh, M.E., Collins, C.M., Gelvin, A.B., Beede, M.C., Saari, S.P. 2013. Water sampling and groundwater modeling in Donnelly Training Area East, Fort Greely Alaska. A Report submitted to U.S. Army Garrison Fort Wainwright. 131 p.

Chief of USACE Bostick
In the spring of 2014 U.S. Army Corps of Engineers Commanding General and Chief of Engineers visited with CRREL researchers and was briefed on this project.

Secretary of Energy Moniz
In the fall of 2014 Secretary of Energy Ernest Moniz visited with CRREL researchers and was briefed on this project.

U.S. Senator Lisa Murkowski
In the fall of 2014 U.S. Senator Lisa Murkowski visited with CRREL researchers and was briefed on this project.